U.S. DEPARTMENT OF DEFENSE

Environmental Security Technology Certification Program (ESTCP)

Final Report

Electrospark Deposition for Depot- and Field-Level Component Repair and Replacement of Hard Chromium Plating

Project WP-0202

September 7, 2006

Environmental Security Technology Certification Program

REPORT DOCUMENTATION PAGE

Form Approved
OMB No. 0704-0188

PLEASE DO NOT RETURN YOUR FORM TO THE ABOVE ORGANIZATION.

1. REPORT DATE *(DD-MM-YYYY)*	2. REPORT TYPE	3. DATES COVERED *(From - To)*
15-09-2006	Final Report	March 2002 - November 2006

4. TITLE AND SUBTITLE

Electrospark Deposition for Depot- and Field-Level Component Repair and Replacement of Hard Chromium Plating

5a. CONTRACT NUMBER

5b. GRANT NUMBER

5c. PROGRAM ELEMENT NUMBER

63851D8Z

6. AUTHOR(S)

Bruce D. Sartwell, Naval Research Laboratory, Washington, DC
Keith O. Legg, Rowan Technology Group, Libertyville, IL
Norma Price, Advanced Surfaces and Processes, Inc., Cornelius, OR
Denise Aylor, Naval Surface Warfare Center, Carderock, MD
Victor Champagne and Marc Pepi, Army Research Lab, Aberdeen, MD
Tony Pollard, Anniston Army Depot, Anniston, AL

5d. PROJECT NUMBER

WP-0202

5e. TASK NUMBER

5f. WORK UNIT NUMBER

61-8353

7. PERFORMING ORGANIZATION NAME(S) AND ADDRESS(ES)

Naval Research Laboratory, Code 6170
4555 Overlook Ave SW
Washington, DC 20375

8. PERFORMING ORGANIZATION REPORT NUMBER

9. SPONSORING/MONITORING AGENCY NAME(S) AND ADDRESS(ES)

Environmental Security Technology Certification Program
901 North Stuart Street, Suite 303
Arlington, VA 22203

10. SPONSOR/MONITOR'S ACRONYM(S)

ESTCP

11. SPONSOR/MONITOR'S REPORT NUMBER(S)

WP-0202-FR

12. DISTRIBUTION/AVAILABILITY STATEMENT

Approved for public release; distribution is unlimited

13. SUPPLEMENTARY NOTES

14. ABSTRACT

Electrospark Deposition (ESD) is a microwelding process capable of depositing a wide variety of metal or ceramic/metal coatings onto components using small, portable equipment. This project investigated ESD repair of different types of weapons components that have been subjected to localized damage such as wear, gouging or corrosion pitting. Currently, there are either no repairs available for such components and they have to be replaced or else the components are completely overhauled using complicated electroplating or thermal spray processes. ESD offers the possibility of performing repairs just on the damaged areas, in some cases without removing the component from the aircraft or ship. Extensive materials studies have been conducted on Inconel 718 in which pre-designed defects have been introduced and then repaired by ESD of similar material. Axial fatigue testing on ESD-treated coupons showed no loss of fatigue strength and wear testing indicated that the ESD-repaired areas demonstrated excellent wear resistance. ESD repairs on actual components from gas turbine engines, tanks and ship components were demonstrated.

15. SUBJECT TERMS

Electrospark deposition; Hard chromium plating; Fatigue; Wear; Corrosion

16. SECURITY CLASSIFICATION OF:			17. LIMITATION OF ABSTRACT	18. NUMBER OF PAGES	19a. NAME OF RESPONSIBLE PERSON
a. REPORT	b. ABSTRACT	c. THIS PAGE			Bruce D. Sartwell
Unclassiified	Unclassified	Unclassified	UL	258	19b. TELEPHONE NUMBER *(Include area code)* 202-767-0722

Reset

Standard Form 298 (Rev. 8/98)
Prescribed by ANSI Std. Z39.18

This page intentionally left blank.

EXECUTIVE SUMMARY

Background: Military components are frequently damaged in service through corrosion, impact or wear. They must be either repaired in the field (O-level repair) or shipped back to the depot. Where a localized repair is possible it is usually done by brush plating of Ni and/or Cr (using a Cr^{6+} solution). Where the component cannot be repaired in the damaged area alone, the entire surface, and any coating on it, must be removed and rebuilt, usually by chrome plating or sulfamate Ni to reclaim dimensions followed by chrome plate for wear. Where chrome plate is damaged the only recourse for a permanent repair is to strip and replate. All of these processes create hazardous waste and expose personnel to toxic materials.

In addition, there are many components that suffer significant damage and for which there is neither a field nor depot-level repair currently available. At present, these components must be condemned, resulting in costs associated both with replacing them and with their demil and disposal.

A technology that could replace brush plating and provide field repair on currently non-repairable parts would reduce waste generation, personnel exposure and cost, while improving readiness by returning components to service more rapidly.

Electrospark deposition (ESD), also known as electrospark alloying (ESA) is a micro-welding technique that has demonstrated capability for filling damaged areas and restoring coating damage. It uses short-duration, high-current electrical pulses to weld a consumable electrode material to a metallic substrate. Since almost any alloy can be deposited the method is ideal for filling damage over small areas, such as localized wear or corrosion, using the same alloy as the parent metal. The heat generated in the process is very small, eliminating thermal distortion and allowing the process to be used on heat-sensitive materials. The equipment is small and portable and can be manually operated with a simple shroud to remove any fumes. The simplicity and cleanliness of the process allows it to be safely used by operators without extensive training, for both D-level overhaul and O-level in-place repair.

The process is used industrially, including its use by Rolls Royce for dimensional restoration of non fatigue critical areas of turbine engine components. It is being used at ASAP for a number of certified aircraft repairs, including:

1. Single crystal turbine blade for two gas turbine engines (FAA approved repair)
2. Second stage gas turbine blade sulfidation corrosion repair (DER repair)
3. Helicopter flap restraint for main rotor (DER approved repair).

Objectives of the Demonstration: The objective was to demonstrate ESD as a technically feasible and commercially viable production-scale process for localized repair of weapons systems components, and to transition ESD repairs for use on DoD components for gas turbine engines, vehicles and ships.

Demonstration sites were Oklahoma City Air Logistics Center (OC-ALC) and Anniston Army Depot (ANAD) (working with the Army Research Laboratory (ARL). ESD units were acquired and placed in each of these facilities, and candidate components identified.

In addition NSWC-CD evaluated the process for repair of submarine components under a parallel program. Because the potential usage was so broad, a complete Demonstration Plan incorporating a Joint Test Protocol (JTP) was developed only for gas turbine engine applications [1], working in conjunction with OC-ALC, to qualify ESD for:

1. localized repair by depositing the same alloy material from which the component is manufactured,
2. localized repair of chrome plating

Regulatory Drivers: The primary ESOH issue is reduction of Cr^{6+} air emissions and waste discharges from processes such as chrome stripping and tank plating, and chrome brush plating. The Cr^{6+} PEL has recently been lowered by an order of magnitude, to 5 $\mu g/m^3$, with an Action Level of 2.5 $\mu g/m^3$. This will affect DoD repair operations, including tank and brush plating. The difficulty and cost of meeting this rule will be substantial and will help to drive the adoption of clean processes.

Component Testing and Qualified Repairs: Specific components investigated for ESD repair under the gas turbine engine Demonstration Plan included:

1. Oklahoma City Air Logistics Center - Air Force Components - TF33 10-12 Stator Segment fabricated from Inconel 718 (non-line of sight)
2. Oklahoma City Air Logistics Center - Air Force Components - TF 39 Shaft fabricated from Inconel 718 (chrome plate repair)
3. Oklahoma City Air Logistics Center - Air Force Components – TF33 #5 Bearing Housing fabricated from 410 stainless steel (dimensional restoration)

Other applications at NSWC-CD and ANAD included:

1. NSWC-CD - Navy components – submarine steering and diving control rods fabricated from K-Monel
2. ANAD/ARL - Army components - Abrams tank M1A1 Cradle fabricated from 4130 steel and helical gear shaft.

A repair was developed, qualified and implemented at ANAD for the M1A1 Abrams tank gun barrel cradle. This process is now being used to recover about 12 cradles per year at an annual saving of about $300,000. This repair was developed by ANAD personnel based on a clear depot need, with minimal process development and operator training. A repair was also developed for an M1A1 turbine engine helical gear shaft. This repair will be qualified on successful completion of a 100 hour engine test. Local process specifications were written for operation and maintenance of the ESD process. Repair specifications were developed to ensure acceptable quality and a reproducible process.

ESD repair of the TF33 #5 bearing housing has been qualified at OC-ALC. TO changes have been made to allow this repair.

Process and equipment development:

During the course of the project various process and equipment developments were made including process optimization, robotic coating (which was compared with manual

operation) and incorporation of Ultrasonic Impact Treatment to impart compressive stress to the ESD coating. The latter was found to improve fatigue and hardness. In addition, two developments made by PNNL were evaluated – force control feedback to the operator and an ultrasonic technique known as Surface Sifting. Neither of these appeared to offer improvements to the process.

Demonstration Results – process development and materials testing:

The substrate alloy used for materials testing was Inconel 718 (IN718). Electrodes of the same material were applied to each of these substrate alloys. In addition, IN718 specimens were prepared with an electrolytic hard chrome (EHC) coating and the ESD electrode material was Inconel 625 (IN625).

ESD was used to fill spherical-bottom holes (divots) and spherical-bottom grooves. The process was characterized for deposition rate and coating quality – hardness, porosity and discontinuities. The following data were obtained for IN718 filled with IN718:

- Bond strength (ASTM C633): As expected for a weld process the bond strength exceeded 10 ksi, with all failures in the glue.
- Deposition rate: Overall deposition rate was 1 to 7 mg/min depending on conditions. This low deposition rate clearly demonstrates that the primary use of the process is localized repair rather than large scale coating deposition.
- Tensile properties: Flat tensile bars with ESD-filled divots had yield and ultimate strengths within 2% of the undamaged material. Reduction in area was about 30% lower and elongation about 40% lower with a filled defect than in the virgin material. This shows that the use of ESD will not degrade the strength of repaired components.
- Residual stress: As with all weld processes, ESD coatings were tensile.
- Fatigue: In general the fatigue curve for repaired material fell between that of the undamaged material and that of the damaged but unrepaired material. Thus the repair added somewhat to the properties of the material and did not degrade the fatigue of the substrate. However, a repair carried out under high spark energy conditions (to achieve a higher deposition rate) did create a fatigue debit below that of the unrepaired material. Thus repairs of fatigue-critical components should not be done under high energy conditions.
- Corrosion (ASTM B117 salt fog, 168 hour, ASTM G48 pitting and crevice corrosion): There was no evidence of corrosion in salt fog testing. In the G48 tests there was minor pitting in the ESD material but not in the substrate. Presumably this is because of the presence of some porosity in the ESD material.
- Wear (pin on disk, and Hamilton-Sundstrand oscillating long stroke and fretting): The ESD-repaired areas wore in essentially the same way as the substrate for dithering wear and about 30% less for long stroke wear. There was no evidence of different wear mechanisms or wear rates in the two materials.
- Repair of chrome plating: When repairing chrome damage in chrome plating there is a tendency for the ESD repair to have a “halo” of porosity around the repaired area. This problem was largely eliminated by depositing the ESD at low

energy.

Cost/Benefit Analysis (CBA): A cursory cost analysis was performed on the M1A1 gun cradle repair to determine the cost savings by implementing ESD for M1A1 cannon cradles. The cost to purchase a new component is $24,636. The reclamation costs have been determined to be $698.50, based on a labor rate of $76.50/manhour for 9 hours and a material cost of $10.00. Annual savings for 15 items were thus estimated as about $360,000.

A detailed cost analysis was made of the following GTE items at OC-ALC: TF33 #5 Bearing Housing, TF39 Compressor Shaft, F100 10-12 Stator Segment. The cost-benefit for the bearing housing depended strongly on the number of lugs needing repair, with a 10-year NPV of $1.3 million and a payback period of 4 months for an average repair of 6 lugs, but a 10-year NPV of -$1 million if an average of 12 lugs need repair. This demonstrates that the cost-effectiveness of the process is best when repairs are limited. The TF39 Compressor Shaft showed a 10-year NPV of $65,000 and a payback of 4 years. The F100 Stator Segment showed a 10-year NPV of -$24,000.

Stakeholder and End-User Issues: ESD technology has demonstrated potential for repair of limited areas for dimensional restoration and salvage of components. With its low cost, simple manual operation, portability and low level of training, it is ideal for use for both D- and O-level repair. However, for engine components, which are some of the most sensitive flight-critical components that DoD overhauls, these characteristics are often disadvantages since they make it difficult to ensure process reproducibility.

It has already been adopted for some vehicle repairs at ANAD. In these cases there is obviously no issue of flight-criticality, and simple repairs can be used to reclaim a variety of expensive or difficult-to-obtain components. It is likely to find additional applications driven by ease of repair and cost-benefit, and the simplicity of developing repairs at the depot level without recourse to extensive engineering and laboratory facilities.

While the tests at NSWC-CD were not as positive, it appears that, with further development and optimization, there is significant potential for the process for D-level and perhaps even O-level in-place repair of components such as diving rods, shafts, and other components that suffer pitting corrosion. In order to find applications in this area, however, the process must be developed to the point where the quality of the repairs on Monels is similar to that seen in Inconels, especially in terms of the adhesion and porosity of the repaired area and its resistance to crevice corrosion.

For aircraft engines the cost of qualifying a repair and instituting the necessary TO changes is so high that the cost-benefit must be clearly demonstrated for it to be worthwhile embarking on the effort. The easiest way to gain acceptance and adoption of the technology for Air Force GTE repair is through the MRB (Materials Review Board) system, which is used whenever a component cannot be repaired by standard TO methods and an MRB engineer reviews the problem to determine whether the component must be condemned. In order to use ESD, MRB engineers must be aware of the capability of the technology, and see it as a method they can draw on for repairs where there are no other qualified repairs already specified in the TO. This is a matter of education and availability of the technology at the repair depot.

TABLE OF CONTENTS

LIST OF FIGURES

LIST OF TABLES

This page intentionally left blank.

LIST OF ACRONYMS AND SYMBOLS

410SS	410 stainless steel
A	ampere(s)
ALC	Air Logistics Center
AISI	American Iron and Steel Institute
AMS	Aerospace Materials Specification
ANAD	Anniston Army Depot
ANSI	American National Standards Institute
ARL	Army Research Laboratory
ASAP	Advanced Surfaces and Processes, Inc.
ASTM	American Society for Testing and Materials
ATDR	arc time deposition rate
CBA	cost/benefit analysis
cfh	cubic feet per hour
CFR	Code of Federal Regulations
DOD	Department of Defense
DOE	design of experiment
ECAM	Environmental Cost Analysis Methodology
E_{corr}	open-circuit corrosion potential
EHC	electrolytic hard chrome
EPA	Environmental Protection Agency
ESA	electrospark alloying
ESD	electrospark deposition
ESOH	environmental, safety and occupational health
ESTCP	Environmental Security Technology Certification Program
EWI	Edison Welding Institute
FPI	fluorescent penetrant inspection
FTE	full-time equivalent
GEAE	GE Aircraft Engines
GTE	gas turbine engine
HAZ	heat-affected zone
HCAT	Hard Chrome Alternatives Team
HEPA	high-efficiency particulate arresting
hex-Cr	hexavalent chromium
H-S	Hamilton Sundstrand
HV	Vickers hardness number
HVOF	high-velocity oxygen-fuel
Hz	hertz (cycles-per-second)

IARC	International Agency for Research on Cancer
ID	internal diameter
IN625	Inconel 625 alloy
IN718	Inconel 718 alloy
IRR	internal rate-of-return
JTP	joint test protocol
kJ	kilojoules
ksi	thousands of pounds per square inch
LCF	low-cycle fatigue
MRB	Materials Review Board
MRO	maintenance, repair and overhaul
MTS	mechanical test system
NADEP-NI	Naval Air Depot North Island (located in San Diego, CA)
NAVAIR	Naval Air Systems Command
NAVSEA	Naval Sea Systems Command
NDE	non-destructive evaluation
NDI	non-destructive inspection
NLOS	non-line-of-sight
NPV	net present value
NSWCCD	Naval Surface Warfare Center Carderock Division
OC-ALC	Oklahoma City Air Logistics Center
OD	outside diameter
OEM	original equipment manufacturer
OMB	Office of Management and Budget
ONR	Office of Naval Research
OSHA	Occupational Safety and Health Administration
P&W	Pratt & Whitney
PDR	production deposition rate
PEL	permissible exposure limit
PEWG	Propulsion Environmental Working Group
PFA	pulse fusion alloying
PFS	pulse fusion surfacing
PNNL	Pacific Northwest National Laboratory
PPE	personal protective equipment
psi	pounds per square inch
PSU	Portland State University
QC	quality control
R	ratio of minimum to maximum stress in fatigue testing
Ra	arithmetic average surface roughness
RC	resistance-capacitance

RH	relative humidity
ROI	return-on-investment
rpm	rotations per minute
SAE	Society of Automotive and Aerospace Engineers
SBIR	Small Business Innovative Research
SEM	scanning electron microscopy
SERDP	Strategic Environmental Research & Development Program
S-N	stress versus number of cycles (for fatigue data plots)
SuSi	Surface Sifter
TACOM	U.S. Army Tank and Automotive Command
TO	technical order
TWA	time-weighted average
µin	microinch(es)
µF	microfarad(s)
UIT	ultrasonic impact treatment
UTRC	United Technologies Research Center
UTS	ultimate tensile strength
V	volt(s)
WPS	welding procedure specification
XRD	X-ray diffraction

ACKNOWLEDGMENTS

The financial and programmatic support of the Environmental Security Technology Certification Program (ESTCP), under the direction of Dr. Jeffrey Marqusee, Director, and Mr. Charles Pellerin, Program Manager for Weapons Systems and Platforms, is gratefully acknowledged. In addition, the financial and programmatic support of the DOD Propulsion Environmental Working Group (PEWG) is gratefully acknowledged. The Naval Surface Warfare Center Carderock Division gratefully acknowledges the financial support of the Office of Naval Research for some of the work presented in this report.

Principal Investigators: Mr. Bruce D. Sartwell
Naval Research Laboratory

Dr. Keith Legg
Rowan Technology Group

1. Background and Introduction

1.1. Background

The removal of components from military systems in the field which have become damaged due to wear, corrosion, impact, etc., their shipment to a depot, and subsequent overhaul and repair all generate either hazardous or industrial waste and represent a significant cost to the Department of Defense (DOD). It is therefore important that field repair of such components be performed whenever possible. Currently, brush plating is the only viable technology for field repair and it has extensive environmental problems. Hard chromium coatings are repaired by brush plating with nickel to rebuild and then finishing with a thin layer of brush-plated chromium which always utilizes a hexavalent chromium (hex-Cr) plating solution. Although nickel solutions are not as hazardous as chromium, Ni is coming under increasing environmental pressure. In general, with brush plating there are significant difficulties ensuring proper containment and minimizing personnel health hazards. There are many applications for which brush plating cannot be used and thus the components are returned to depots for repair where the damaged areas are machined away and the dimensions of the component are restored using electrolytic hard chrome (EHC) plating. If a technology could be validated that would both replace brush plating and provide field repair on currently non-repairable parts, then there would be a reduction in both waste generation and cost, plus readiness would also be affected because weapons systems would be returned to service in a shorter period of time.

Finally, there are many components that suffer significant damage and for which there is neither a field nor depot-level repair currently available. At present, these components must be scrapped, resulting in costs associated both with disposal and loss-of-use.

Electrospark deposition (ESD), also known as electrospark alloying (ESA) is a micro-welding technique that has demonstrated capability for filling damaged areas and restoring coating damage. It uses short-duration, high-current electrical pulses to weld a consumable electrode material to a metallic substrate. Electrode materials may be nearly any electrically conductive metal or ceramic/metal (cermet) mixture capable of being melted in an electric arc. The ESD process is distinguished from other arc welding processes in that the spark duration is limited to a few microseconds and the spark frequency to around 1000 Hz or less. Thus, welding heat is generated during less than 1% of a weld cycle, while heat is dissipated during 99% of the cycle. This provides extremely rapid solidification, resulting in a nanocrystalline structure or, in some cases, an amorphous surface layer. Regardless of the structure that is obtained, the coatings are extremely dense and they are metallurgically bonded to the substrate. The combination of extremely fine grain structure, high density, and high bond strength offer the possibility of achieving substantial corrosion resistance, augmented wear resistance, and enhanced ductility. The low heat input eliminates thermal distortion or changes in metallurgical structure and thus allows the process to be used on heat-sensitive materials. ESD is also advantageous from an environmental and worker safety standpoint. Best manufacturing practice generally recommends that in most applications a simple shroud with vapor exhaust be used to remove any fumes. The use of such a shroud ensures that operator exposure is below permissible exposure limits for any materials being deposited.

Although results were first reported on ESD more than 30 years ago, process improvements developed at organizations such as the Pacific Northwest National Laboratory (PNNL) have led to a maturation of the technology and demonstrations of a wide variety of applications. One of the earliest developed by PNNL was the qualification of ESD chromium carbide coatings for nuclear reactor core components. This application imposed stringent requirements on coating performance in corrosion, thermal cycling, wear, friction and irradiation effects tests. The ESD process was automated and placed in production, replacing the previously used detonation-gun thermal spray coatings. During 10 years of production, there were zero coating rejects and performance exceeded all requirements. There are many other applications in the nuclear field where ESD coatings have been successfully applied. In the aerospace field, ESD coatings have been approved by the FAA and are being applied as a repair process to commercial gas turbine engine components. These include (a) application of corrosion resistant coatings to turbine blade tips where protective diffusion coatings were removed, (b) buildup of nickel-base superalloys to reclaim close-tolerance parts, and (c) repair of chipped or damaged diffusion coatings.

From the examples given above, it is clear that ESD is a technology with sufficient maturity for demonsration/validation on weapons systems components including legacy and out-of-production parts at DOD repair facilities. For either field- or depot-level application, there are several attractive aspects to ESD including low capital cost, ability to be used by hand or robotically, and the ability to deposit the same coating materials as those currently being applied by electroplating or thermal spray (e.g., chrome, nickel, Tribaloys, cermets) and the same metals/alloys that are used as base materials on many functional components (e.g., Ni-base superalloys, stainless steels, Monel, titanium alloys), thus allowing for self-repair. Although there are many deposition parameters that can affect the properties of the coatings and operators must receive appropriate training to ensure uniformity of quality, ESD is still a low complexity technology that is amenable to many different environments, including in-situ repair.

There had been several ongoing relatively small research and development and Small Business Innovation Research (SBIR) efforts examining the technology and a number of potential applications. For example, the Naval Surface Warfare Center Carderock Division (NSWC-CD), began examining ESD coatings under a 6.2/6.3 project funded by the Office of Naval Research (ONR) that was initiated in FY99. Applications that were pursued include: (a) wear and corrosion on submarine steering and diving components; and (b) localized corrosion and wear on main propulsion shaft seals on ships. ESD offers the prospect of in-situ repair with no waste generation for both of these applications.

As another example, tests were completed on ESD repairs to the Hellfire Missile Launch Latch for the Apache Helicopter. This latch is no longer being made and some 13,000 latches no longer function reliably due to wear. The ESD repair, estimated to cost $75, recovers this $350 part. But more importantly, it allows a legacy weapons system to remain in service while providing a repaired part that outlasts a new part by a factor of at least 10.

Based on some the previous work discussed above, there were many DOD repair depots and original equipment manufacturers (OEMs) that were interested in investigating the technology for possible implementation. Since one of the most attractive potential uses

of the technology was the repair of localized damage on gas turbine engine (GTE) components, the Propulsion Environmental Working Group (PEWG) expressed a strong interest in executing a project to demonstrate and validate the ESD process for those applications. As a result, the PEWG collaborated with the DOD Hard Chrome Alternatives Team (HCAT) to submit a proposal to the DOD Environmental Security Technology Certification Program for a four-year project titled, "Electrospark Deposition for Depot- and Field-Level Component Repair and Replacement of Hard Chromium Plating." Although the principal focus of the proposal was repair of GTE components, either self-repair of the base material or repair of hard chrome plating on components, it also included expanding the work being performed by NSWC-CD on ESD repair of ship/submarine components and demonstration/validation on Army tank components. The proposal was accepted by ESTCP, with the project being initiated in March 2002.

1.2. Objectives

The goals of this demonstration/validation project were to demonstrate and validate that ESD is a technically feasible and commercially viable production-scale process that can be used for localized repair of weapons systems components, and to transition ESD repairs for use on gas turbine engine and other types of components.

Two demonstration sites were identified: Oklahoma City Air Logistics Center (OC-ALC) and Anniston Army Depot (ANAD) (working with the Army Research Laboratory (ARL). ESD units were acquired and placed in each of these facilities, and candidate components meeting the above criteria were identified. Because it was impossible within the scope of the project to develop test protocols for all potential applications, a complete Demonstration Plan incorporating a Joint Test Protocol (JTP) was developed only for gas turbine engine applications [1], working in conjunction with OC-ALC, to qualify ESD for:

1. localized repair by depositing the same alloy material from which the component is manufactured,
2. localized repair of chrome plating and thermal spray coatings, and
3. replacement of chrome plating in complex geometries.

Specific components investigated for ESD repair under the gas turbine engine JTP include:

- Oklahoma City Air Logistics Center - Air Force Components - TF33 10-12 Stator Segment fabricated from Inconel 718 (non-line of sight)
- Oklahoma City Air Logistics Center - Air Force Components - TF 39 Shaft fabricated from Inconel 718 (chrome plate repair)
- Oklahoma City Air Logistics Center - Air Force Components – TF33 #5 Bearing Housing fabricated from 410 stainless steel (dimensional restoration)

Other applications that were pursued at NSWC-CD and ANAD included:

- NSWC-CD - Navy components - Steering and Diving Control Rods for Trident Submarine fabricated from K-Monel

- ANAD/ARL - Army components - Abrams tank M1A1 Cradle fabricated from 4130 teel

Individual test plans were developed for the validations being performed at NSWC and ANAD.

Local process specifications were written for operation and maintenance of the ESD process. Repair specifications were developed to ensure acceptable quality and a reproducible process.

1.3. Regulatory Drivers

Environmental, health and safety regulations are driving the search for a replacement for EHC plating. Chromium plating baths contain chromic acid, in which the chromium is in the hexavalent state, with hexavalent chromium (hex-Cr) being a known carcinogen having a level of toxicity greater than arsenic or cadmium. During operation chrome plating tanks emit a hex-Cr mist into the air, which must be ducted away and removed by scrubbers. Wastes generated from plating operations must be disposed of as hazardous waste and plating operations must abide by EPA emissions standards and OSHA permissible exposure limits (PEL).

A significant lowering of the hex-Cr PEL would most likely have the greatest cost impact on military and commercial repair facilities. Such a change has been expected since the mid 1990's. But it was only in 2004 that OSHA began the process to issue a new PEL as a result of a lawsuit filed in 2002 by a citizens group and union that petitioned OSHA to issue a lower PEL, and a subsequent ruling by a Federal District Court upholding the petition. The court ruling required OSHA to publish a new draft hex-Cr PEL in the Federal Register no later than October 2004. Public review and hearings would be conducted in 2005, with a final rule issued in January 2006. In October 2004 OSHA proposed a new PEL of 1 $\mu g/m^3$ with a 0.5 $\mu g/m^3$ action level, which represents almost a two-order-of-magnitude reduction from the current PEL of 52 $\mu g/m^3$. The expected compliance costs in all industries including electroplating, welding, painting and chromate production was estimated to be $226 million. On 28 February 2006 the final rule was promulgated at 5 $\mu g/m^3$, with an action level of 2.5 $\mu g/m^3$. While this is a factor of five higher than the initial proposed rule, it will effectively require that facilities maintain a level close to 1 $\mu g/m^3$ in order to stay below the action level. The difficulty and cost of doing this will be substantial.

As stated above, a change in the hex-Cr PEL has been expected since the mid 1990's. In anticipation of the change, in 1995 a Navy/Industry task group under the coordination of the Naval Sea Systems Command studied the technical and economic impact of a reduction in the hex-Cr PEL [2]. At the time, a reduction in the 8-hour time-weighted average (TWA) from the existing 100 $\mu g/m^3$ to between 0.5 and 5.0 $\mu g/m^3$ was being considered. The Navy/Industry task group performed the following tasks:

- Identified the manufacturing and repair operations, materials and processes that are used in Navy ships, aircraft, other weapons systems and facilities where worker exposure to hex-Cr would be expected
- Developed data on current worker exposure levels to hex-Cr using OSHA Method

215

- Estimated the technical and economic impact of the anticipated reductions in hex-Cr exposure on Navy ships, aircraft, other weapons systems and facilities
- Identified future actions required to comply with the anticipated PEL reductions

The following operations within the Navy were identified as having the potential for exposing workers to hex-Cr:

- Metal cleaning (including abrasive blasting and grinding) of chromate-coated materials
- Electroplating of chromium
- Painting and application of chromate paints and coatings
- Welding, thermal spraying and thermal cutting

The following conclusions were reached by the task group:

1. Regulated areas for hex-Cr would have to be created in much greater numbers than have been required for cadmium or lead exposure
2. Local exhaust ventilation, which is the presently available engineering control, is not completely effective in reducing exposure to below 0.5 $\mu g/m^3$ for many operations or even below 5 $\mu g/m^3$ in some cases
3. The inability of engineering controls to consistently reduce worker exposure below the anticipated PEL levels will significantly increase the use of respirators
4. The costs of reducing the hex-Cr PEL will include costs for training, exposure monitoring, medical surveillance, engineering controls, personal protective equipment, regulated areas, hygiene facilities, housekeeping and maintenance of equipment. There will also be costs due to reduced efficiency of not only the operations involving hex-Cr but adjacent operations and personnel as well.
5. The estimated costs for compliance with a PEL of 0.5 $\mu g/m^3$ at Navy facilities include an initial, one-time cost of about $22,000,000 and annual costs of about $46,000,000 per year.
6. The estimated costs for compliance with a PEL of 5.0 $\mu g/m^3$ at Navy facilities include an initial, one-time cost of about $3,000,000 and annual costs of about $5,000,000 per year
7. In addition to the greatly increased cost that would be associated with chrome plating, turnaround times for processing of components would be significantly increased as well, impacting mission readiness.

Based on the projections of the metal finishing industry and the study conducted by NAVSEA in 1995, it is clear that a reduction of the hex-Cr PEL to 5 $\mu g/m^3$, although higher than the original proposed level, will greatly increase the cost and processing times associated with hard chrome plating within DOD. It is therefore desirable to identify and qualify a technology that would be capable of localized repair to parts rather than the current large-scale overhaul. This would result in considerably reduced plating

operations at repair facilities.

1.4. Stakeholder/End-User Issues

The ESD process, while not a new process, has not been viewed as a welding process to be utilized for critical applications (gas turbine, medical, nuclear etc.) until the recent past and has, therefore, never been wholly embraced. Demonstrating a successful repair of a gas turbine engine component, supported by a detailed welding process specification, was expected to reveal to end users the viability of the ESD process for repairing components. Once the ESD process was embraced, it was anticipated that many applications would become apparent.

The users of the ESD technology may be any user with a need to repair gas turbine engine or other types of components. These users include Navy, Army and Air Force repair depots, and OEMs such as Pratt & Whitney (P&W) and General Electric Aircraft Engines (GEAE). Many air, land or sea components currently plated with EHC could potentially be repaired with the ESD process.

Tri-service and OEM approval authorities are concerned with the functional performance of an ESD coating on aircraft components. ESD coatings need to exhibit functional performance that is equivalent, or superior, to EHC without detrimentally affecting the substrate. Where ESD is used for self-repair (i.e., for a non-coated component, the ESD repair material is the same as the base material), the component must be restored to its original performance. A set of common and extended functional tests were determined for non-flight critical components by the stakeholders (joint services and OEMs) and these were included in the GTE JTP.

Depot concerns related to implementation of ESD are based on workload, operational costs, and reliability/maintainability.

Workload: A concern voiced by the end users is the relatively slow deposition rate of the ESD process, as compared to other welding processes or compared to other coating processes. However, deposition rate alone should not be the basis for selecting ESD as a viable repair. The entire component repair time, including fixturing, masking, post heat treat, post machining, etc. should be included when comparing the ESD process to other processes. To increase productivity, a number of solutions could demonstrate the advantage of the ESD process over other processes. These include purchasing and operating multiple ESD systems. At capital expenses around $50,000 for each unit, the option for increasing productivity by doubling or tripling the amount of equipment is not unreasonable. Also, the ESD equipment lends itself well to automation, and automated turn-key operations could easily be developed for high volume repair needs.

Operational Costs: The initial purchase cost of ESD equipment is very low. Training is generally included in the purchase price. Additional training is available, but extensive operator training is generally not required. Once an operator qualifies on ESD equipment, little follow-on training is ever needed. The operating costs for ESD equipment are very low. No special booth or environmental chamber need be constructed; the equipment can be utilized anywhere there is access to a standard electric outlet. The vapor emitted during the process can easily be removed using a portable shroud with vacuum exhaust. Hazardous wastes are not a by-product of this process.

The UV emitted during the process is insignificant and can be blocked by any standard protective eyewear. Should a cover gas be desired, this would have to be factored into operating costs. However, operating costs for other processes, such as time-consuming masking, may no longer be required when repairing a component with the ESD process.

Reliability / Maintainability: The ESD equipment is robust and extremely reliable and has been demonstrated to have a 100% duty cycle. Preventive and corrective maintenance on the equipment is relatively simple. Most major repairs can be performed on site by the ESD equipment manufacturer, generally in a very short time frame.

1.5. Overview of Final Report

Section 2 of this report provides a description of the ESD technology and equipment.

Section 3 describes enhancements to the ESD process that were developed during the project. This includes automation of the process and development of the ultrasonic impact treatment (UIT) technique which improves the quality of the ESD deposits and increases the net deposition rate.

Section 3.5 describes the procedures for optimizing the ESD process for GTE alloys. Section 4 presents the results of the execution of the GTE Demonstration Plan. Section 4.3 describes the results of the materials tests performed under the JTP, and Section 4.4 describes the development of ESD repairs to actual GTE components.

Section 5 describes the development of ESD repairs on two M1A1 Tank components.

Section 6 describes work performed to qualify ESD as a technique for repair of Navy ship and submarine components.

Section 7 presents cost/benefit analyses performed using the Environmental Cost Analysis Methodology (ECAM) for the application of ESD to repair the three GTE components described in Section 4.3.

Section 8 presents results on evaluation of techniques developed by Pacific Northwest National Laboratory intended to improve the quality control associated with use of ESD and to improve the quality of the ESD deposits.

Section 9 discusses issues associated with implementation of the ESD technology.

Section 10 lists the references cited in the report.

This page intentionally left blank.

2. Technology Description

2.1. History of the development of ESD

ESD is known by a number of names, including electrospark alloying (ESA), spark hardening, spark toughening, pulse fusion surfacing (PFS), and pulse fusion alloying (PFA). The spark deposition phenomenon was first reported by H.S. Rawdon at the U.S. Bureau of Standards in 1924 [3]. Rawdon's research included sparking pure iron with a similar electrode, resulting in a significant hardening of the substrate surface. The sparking led to the formation of martensite (an interesting outcome for a non-carbon containing iron material). The martensite formation resulted from the rapid quenching of the tiny volumes of iron that underwent a very rapid melt/freeze cycle – a form of rapid solidification. Rawdon's observation was repeated and reported by N.C. Welsh in 1957 [4]. Welsh went on to show that very hard surfaces could be deposited on steel by sparking it with electrodes of tungsten carbide and tungsten/titanium carbide. He also hardened the surfaces of copper, brasses, aluminum and titanium.

Starting in the mid 1940's, and continuing on to the present day, many studies of the spark deposition process have been reported by researchers in the former Soviet Union (now Russia and Ukraine). The primary focus of that work appears to be for increasing life of tools and wear-prone machine components.

A moderate amount of work on spark deposition has been reported in the U.S. over the past three decades [5-9]. Much of that work was done at, or in collaboration with, the Battelle Pacific Northwest National Laboratories (PNNL), formerly Westinghouse Hanford Company, in Richland, Washington, and Washington State University (WSU) in Pullman, Washington. Their research has led to the development of high performance coatings on nuclear reactor components, wear and corrosion resistant coatings for coal gasification equipment, and important improvements in spark deposition equipment.

Since 1988, additional improvements in the spark deposition equipment have been made by Advanced Surfaces And Processes, Inc. (ASAP) in Cornelius, Oregon. The improved equipment, controlled by a microprocessor and advanced electronic circuitry, has been utilized by a number of research laboratories, universities, government and military agencies, and private companies.

Research and development on ESD is increasing as the awareness of the capabilities of the process expands, with important work being done and reported by such R&D groups as Edison Welding Institute (EWI), The Welding Institute (TWI in UK), Battelle Pacific NW National Laboratories (PNNL), and the National Institute of Science of Ukraine. Universities presently pursuing ESD development projects include: The University of Waterloo, Ontario, Canada; University of Manitoba, Manitoba Canada; Queens University, Ontario, Canada; Portland State University, Portland, Oregon, and the Oregon Health and Science University, Portland, Oregon.

A number of private U.S. corporations are presently contributing to the expanding knowledge base of ESD Technology as well. Among these are Rolls Royce Corporation, General Electric Aircraft Engines, General Electric Power Systems, Pratt and Whitney, Advanced Surfaces And Processes, Inc., ATK Thiokol, Moog, Hamilton Sundstrand, The

Boeing Company, Honeywell Engines and Systems, American Airlines, Sikorsky and Flight Support, Inc. Foreign companies engaged in ESD development include Pratt and Whitney Canada, MERTEC (Canada), Rolls Royce (UK), and SNECMA (France).

The following is a chronological summary of the development of the ESD technology to date and its potential applications.

- 1924 - Rawdon observes spark-induced martensite formation from rapid solidification in pure iron.
- 1957-1961 - Welsh creates TiC surface by sparking Ti under oil. Welsh & others go on to develop carbide electrodes for ESA carbide coatings.
- 1944-1964 - Lazarenko & others observe spark hardening & material transfer during spark erosion experiments. Results in developing industrial applications of ESA in USSR.
- 1969-1999 - Johnson & others develop automated ESA process for production coating of nuclear components, go on to develop fossil energy & other commercial applications.
- 1988-1999 - Kelley & others develop and identify numerous successful commercial applications for ESA, and develop state-of-the-art ESA equipment.

2.2. ESD Technology Description

2.2.1. General Technology Description

ESD is a micro-welding technique that has demonstrated capability for filling damaged areas and restoring coating damage. It is a pulsed-arc micro-welding process that uses short-duration, high-current electrical pulses to weld a consumable electrode material to a metallic substrate. Micro-volumes of electrode material are melted in the arc plasma of a pulsed current (spark) and fused into the substrate surface forming a metallurgical bond. Over time, many such electrode volumes, or splats, are overlapped on each other to provide a full coverage of new surface material. With additional overlapping passes, the new surface deposition material can build up more and more thickness. Electrode materials may be nearly any electrically conductive metal or ceramic/metal (cermet) mixture capable of being melted in an electric arc.

The ESD process is distinguished from other arc welding processes in that the spark duration is limited to a few microseconds and the spark frequency to around 1000 Hz or less. Thus, welding heat is generated during less than 1% of a weld cycle, while heat is dissipated during 99% of the cycle. This provides extremely rapid solidification, resulting in a nanocrystalline structure or, in some cases, an amorphous surface layer. Regardless of the structure that is obtained, the coatings are extremely dense and they are metallurgically bonded to the substrate. The combination of extremely fine grain structure, high density, and high bond strength offer the possibility of achieving substantial corrosion resistance, augmented wear resistance, and enhanced ductility. The low heat input eliminates thermal distortion or changes in metallurgical structure and thus

allows the process to be used on heat-sensitive materials. Substrates require no special surface preparation and often no post-weld processes such as heat treatments. ESD is also advantageous from an environmental and worker safety standpoint. Best manufacturing practice generally recommends that in most applications a simple shroud with vapor exhaust be used to remove any fumes. ASAP conducted a study in which air samples were collected in the vicinity of the operator for ESD of aluminum onto cadmium plate in which an exhaust shroud was used. The concentration of cadmium was well below the OSHA PEL.

In addition to using ESD for filling damaged areas, ESD has been implemented in many applications as a coating. The ESD coatings have been found to be among the most damage-resistant coatings known and are particularly suitable for use in the severe environments involving high stresses, high temperatures, thermal cycling, irradiation, wear, corrosion, and erosion.

2.2.2. Equipment

ESD equipment consists of two major components; a pulsed, capacitor discharge, power supply, and an applicator head (sometimes called a torch) with an electrical ground cable attached to the work piece to complete the electrical circuit between the electrode and the substrate. The process parameters controlled by the power supply include: voltage; capacitance value; welding current, and pulse frequency. The wave form shape is controlled by the power supply. Control of the electrode motion is also provided by the power supply.

The electrode is held and controlled by the applicator head, and consists of: a collet system for holding various sizes of electrodes; a conductor for supplying the pulsed welding current; a motor for providing rotational and/or oscillatory motion to the electrode, and an insulating sleeve for electrical and heat protection for the operator. The torch manufactured by ASAP has a water cooling system to allow for a 100% duty cycle.

A critical factor in ESD operation, as in conventional electric arc welding, is the need to break the contact between the electrode and the substrate. Without some sort of relative motion the electrode will weld itself to the substrate. Relative motion may be accomplished in a number of ways. Some torches rotate the electrode, others oscillate the electrode, and still others vibrate the electrode (in the axis of the electrode). Each of these torch configurations is available to provide a desired electrode motion effect.

Some ESD torches have an inert gas supply system attached to allow a protective cover gas, such as argon or helium, to flow onto the weld site at all times. The use of a cover gas provides protection from oxidation, furnishes cooling, and influences the physical properties of the arc, thereby affecting the characteristics of the deposit. For example, argon helps provide a smoother deposit and reduce oxide formation with some materials.

Most ESD equipment uses a simple resistance-capacitance (RC) circuit, as shown in Figure 2-1. The electrode is mechanically rotated, vibrated or oscillated to make and break the circuit to the workpiece and generate the spark.

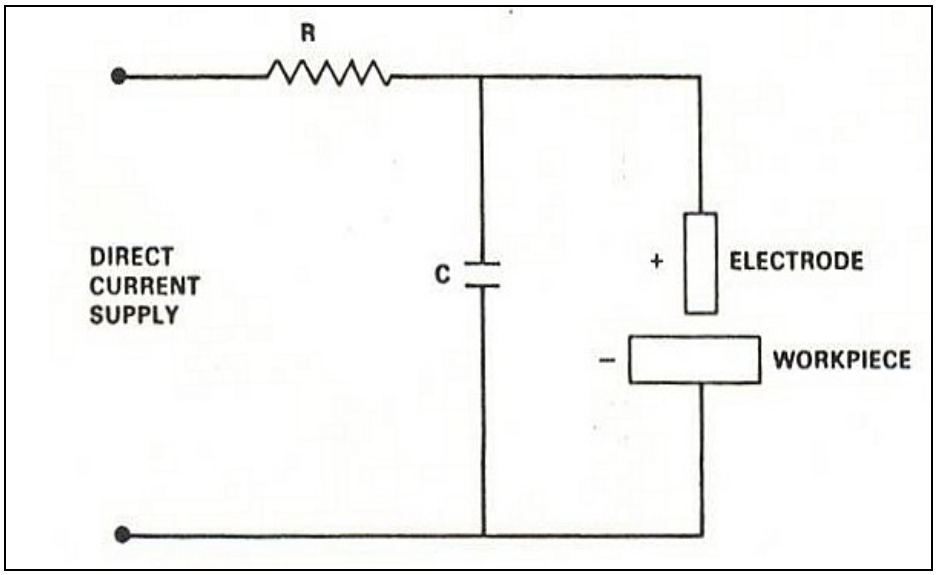

Figure 2-1 RC Circuit in ESD Equipment

The technical data and specifications for the equipment used in this project, manufactured by ASAP, are:

Power Supply (shown in Figure 2-2):

Model: PS98 – MKII

Power Requirements: 115/125 VAC, 50/60 cycle, 20-amp circuit

Parameter Controls: Microprocessor based, Remote computer control ready, LCD 2 Line Display, Key Pad Parameter Entry System

Internal Capacitor Selection: 10, 20, 30, 40, 50, 60 mF

Infinitely Variable Frequency Range: 50 to 4000 Hz

Infinitely Variable Voltage Range: 50 to 250 VDC

Dimensions: 17" x 17" x 9"

Weight: ≈ 70 lbs.

Applicator Head (Torch, shown in Figure 2-3):

Model: AH98 – MKIB

Controls: Patented Programmable Motion Control, Liquid Cooled, Integral Cover Gas Delivery to Electrode/Workpiece

Collet Style Electrode Holders: 1/8" and 3/16" Diameter Electrodes

Dimensions: 1½" Body Diameter, 6" Body Length, 5' Standard Umbilical Length

Weight: ≈ 1½ lb.

Figure 2-2 ESD Power Supply

Figure 2-3 ESD Applicator Head (Torch)

2.2.3. ESD Parameters

Both mechanical and electrical parameters must be controlled in the ESD process. Mechanical parameters are very important for producing quality deposits, and include travel motion of the electrode across the substrate, rotation (or oscillation) velocity of the electrode, step-over of the electrode with each pass to allow some overlap of deposit, and electrode contact force against the substrate. Electrical parameters are also important to produce quality deposits, and are equally significant for avoiding heat damage to the substrate. Electrical parameters include spark voltage, capacitance, pulse frequency, pulse duration (wave form width), pulse current, and circuit inductance. Spark energy, or heat to the substrate, is affected by the voltage, current and capacitance. Higher voltages and currents produce higher spark energy, and a resulting increase in deposition rate and roughness. Larger capacitance produces a wider pulse width, and thus can put more heat into the substrate. If heating of the substrate must be avoided, the ESD should be done with lower total energy values.

2.3. General Applications of ESD

There are many types of applications for which ESD can be used as a surface engineering process. This is primarily due to the wide variety of materials that may be deposited. Nearly all electrically conducting materials with a melting point may be considered for both electrodes and substrates. Surface properties of metallic substrates can therefore be modified to produce a very large number of desired properties.

Two major types of applications receive ESD treatments; surface modification, and build-up repair. The majority of surface modification applications involve enhancement of tribological properties of surfaces. Commonly used electrodes for wear and friction enhancement include sintered carbides, borides, and hard alloys such as Stellite 1, Stellite 6, Tribaloy 700 & 800, and molybdenum. Dynamic coefficient of friction of machine

component surfaces can be reduced from 0.6 to less than 0.2 with an ASAP proprietary process. Corrosion applications frequently are addressed with iron-aluminide and nickel alloys such as IN-625 and Hastelloy C-22.

Figure 2-4 ESD Coating Applications

Wear applications that are commonly treated with ESD include: cutting edges of chipper knives, saw teeth, and mower blades; wear surfaces of slurry pumps, dewatering drums, water treatment valves, and food processing dies; grip surfaces of dental extraction forceps and surgical hemostats and needle holders as shown in Figure 2-4.

Using ESD to make relatively thick deposits for defect repair and dimensional restoration has become more prevalent in the last several years. Most very hard materials, such as carbides, cannot be deposited more than a few thousandths of an inch without stress-induced cracking. But more ductile alloys can be deposited to any desired thickness, and therefore can be used for repair or restoration. Applications for ESD repair include: components of steel, stainless steel, nickel- and cobalt-based superalloys, aluminum, Monel, titanium and magnesium. Examples of such components are turbine blades and vanes, shaft seals, bearing housings, actuator rods, and hydraulic cylinders in aircraft, as well as in aircraft engines, military vehicles, and submarines. Illustrative examples are shown in Figure 2-5.

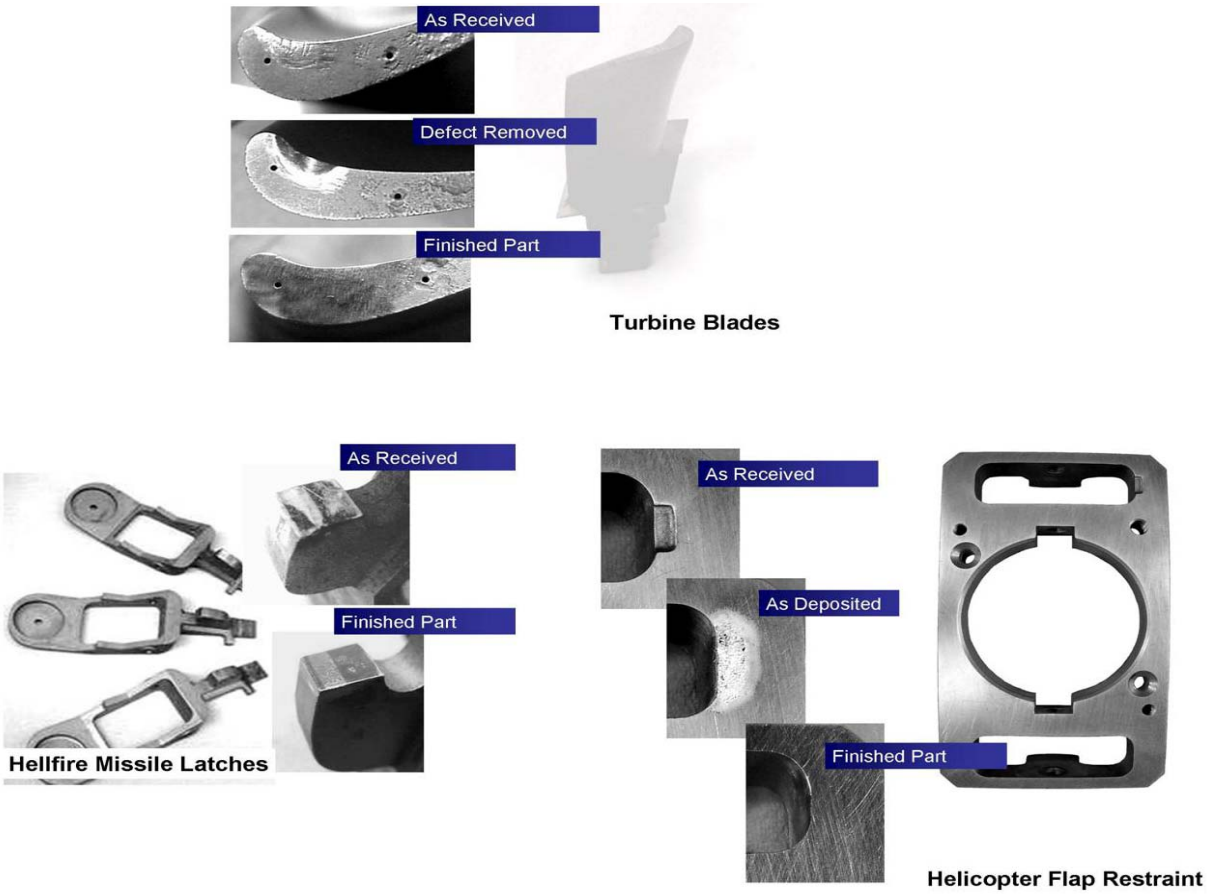

Figure 2-5 ESD Applications for Defect Repair and Dimensional Restoration

2.4. Previous Testing of the Technology

The following are several Government-sponsored projects related to investigating properties of ESD coatings and/or developing ESD applications. Additional information can be obtained by contacting ASAP.

Strategic Environmental Research and Development Program (SERDP) Project: ESD Tungsten Carbide and Co-Based Alloy Coatings for Replacement of Electrolytic Hard Chrome. The objective of this project was to develop and demonstrate a controllable non-line-of-sight (NLOS) process for coatings to replace EHC on military components whose geometry does not allow the use of present alternative processes such as high velocity oxy-fuel (HVOF) coatings. ESD operating parameters for coating 4340 steel with tungsten-carbide/cobalt cermet materials were optimized, and several tests were performed on optimum coatings, with results compared to those for EHC plated on 4340 steel. These tests included: metallography, particle erosion wear, sliding wear, and salt-fog corrosion. ASAP worked with Roger Johnson at PNNL and the findings were published in the Final Report for the SERDP project.

Small Business Innovation Research (SBIR) Project: Repair of Corrosion Coatings of

Cadmium Plating and IVD-Aluminum with ESD. The objective of this project was to explore the feasibility of making repairs of cadmium plating and IVD-aluminum on steel substrates with the ESD process. The project involved the evaluation of ESD-aluminum deposits and applications for repair as well as the ESD applications of cadmium. Since the welding of (or with) cadmium metal may generate toxic vapors and respirable particles, the processes were performed with protective and automated equipment to prevent human exposure.

Army Armament Research & Development Engineering Center (ARDEC) Project: ESD Coating ID of Gun Barrels. The M249 semiautomatic weapon currently employs chrome plating to enhance barrel life. The project, funded by the EPA, investigated the viability of using the ESD process as a replacement for chrome plate. ESD was applied to the interior surface of M249 barrels with a semi-automated, non-line-of-sight process.

NIH STTR Project: Incorporating Bone Minerals into Orthopedic Surfaces by submerged ESD. Phase I of this project was completed in December 2005.

2.5. Factors Affecting Cost and Performance

It is clear that initially the area where ESD can make the most significant impact is repair of relatively expensive components for which no current repair process exists. If the current procedure involves inspection, discarding a component if damage or defects exceed a specified limit, and replacement with a new component, then the acquisition cost of the new component can be saved if ESD can be used to repair the damage. Although this is simple in concept, the actual implementation of such repairs involves a number of factors.

The first relates to the importance of the component to the overall operation of the weapons system. For aircraft, if the component is considered "flight critical," then the qualification of the ESD repair will involve an extensive amount of testing, most likely including both materials and component rig testing. If the component is not "flight critical," then considerably less qualification testing will be required.

A second factor relates to the size or extent of damage that must be repaired. The deposition rate for ESD is quite low, on the order of 0.01 to 0.03 grams-per-minute of material for most alloys. Therefore, if components are large with many areas where the damage is widely dispersed or very deep, then the time, and thus cost, associated with ESD repairs could be prohibitive. On the other hand, if damage is quite localized on components, then ESD repairs become very attractive in terms of time and cost. A good example is a large shaft that rotates against seals where the damage is confined to contact points.

Another factor relates to reproducibility of the process. If repairs must be performed manually, then it is critical that artisans be adequately trained, not only in general use of the ESD equipment, but specifically in deposition of the actual material that will be used for the repair. As has been shown in the studies reported here, it is possible that by adjusting the deposition parameters, poor-quality deposits with high porosity can be produced that would provide inadequate performance. Related to this is whether

designated repairs can be made in which the ESD applicator head can be mounted to a robot and whether ultrasonic impact treatment (described in Section 3) can be used. If they can, then concerns related to manual deposition are mitigated, plus deposition efficiency is increased, lowering the cost of the process.

The primary barrier to the use of the ESD technology for repairs of high-cost, critical components such as gas turbine engine components (shafts, turbine blades, etc.) is the very high cost of qualification testing and, if the testing is successful, the extensive paperwork required for technical order changes and OEM acceptance. If a full engine test is required, the cost can be well in excess of $1 million, making a change practicable only if testing can be piggy-backed onto existing engine tests. In addition, OEM acceptance depends very strongly on whether ESD is defined as a coating, not a weld, since acceptance and qualification of a weld method is much more difficult.

2.6. Advantages and Limitations of ESD

2.6.1. Advantages

The ESD process generally uses a pulsed current of a few hundred Hertz pulse-rate and a very narrow pulse-width to provide low heat input to the substrate while depositing micro-volumes of electrode material. The low heat input results in five of the major benefits of the ESD process - a minimal Heat Affected Zone (HAZ); minimal annealing effect in the substrate; very little dilution, minimal residual stress and low distortion when compared to conventional welding methods. As a result of these benefits, some alloys normally considered to be “un-weldable” due to cracking in the deposit and substrate can be successfully repaired or built-up with ESD. Another benefit of the process is the metallurgical bond between the ESD deposit and the substrate. This very strong bond prevents ESD deposits from chipping or spalling. The rapid solidification of ESD deposits frequently results in enhanced properties, such as increased hardness, increased wear and corrosion resistance, and a reduced friction coefficient. These effects are undoubtedly due to a very fine grain structure formed during rapid quenching, a phenomenon called the Hall-Petch Effect. Grain sizes of 100 nanometers or less are not uncommon, and some materials can actually solidify to an amorphous state.

The ESD process is environmentally benign, easily automated and generally requires no pre or post treatments (masking/thermal treatment). No toxic waste streams are produced. Because the equipment is relatively small, it is field portable and can easily be used for many in-situ applications. Another distinct advantage of the ESD process over other welding or coating processes is its ability to make coatings and repairs in non-line-of-sight applications.

2.6.2. Limitations

Because very small volumes of electrode material are transferred with each electrical pulse the deposition rate is low, especially compared to batch processes such as electroplating or automated thermal spray processes. Therefore the trade-off of benefits versus cost to produce must be made.

The deposition of ESD material typically produces a textured surface of over 100 micro-

inch finish. Applications requiring a super finish may not be good candidates for the ESD process. However, if the ESD deposit is thick enough, fine abrasive grinding or super finishing can remove the as-deposited surface roughness and produce a finish in the 8-16 micro-inch range, depending upon the material being deposited.

3. Development of Automation and UIT

3.1. Introduction

The objective of this portion of the project was for ASAP, working in conjunction with Portland State University (PSU), to demonstrate improvement in quality and production rates of ESD deposition on IN718 through automation and development of a technique designated ultrasonic impact treatment (UIT). This effort was in support of the objective of identifying ESD repairs for gas turbine engine components. This effort was completed in two phases. The results of the first phase were very promising, which led to a second phase of additional investigation and refinement.

The ESD process is usually performed using a hand-held electrode holder assembly. The manual ESD method allows flexibility and the ESD is easily applied. However, automation of the ESD process has proven, in previous testing, to result in higher quality and more consistent deposited material, when compared to a manual ESD application. Automation, operating all day with little human intervention, demonstrates an increase in repair production rates and is essential in situations where enclosed chambers are required, either for a desired atmosphere (i.e. 100% Argon) or environmentally hazardous applications (i.e. cadmium repair). Automation is also critical in non-line-of-sight applications where a hand-held method is not possible or practical. Previous demonstrations of ESD automation include:

- Inside diameters of gun barrels were successfully coated in a non-line-of-sight Army project.
- Integration of 5-axes robotics, ESD equipment and collection devices allowed cadmium repair, via ESD, in a recent Navy SBIR project.
- Pacific Northwest National Lab (PNNL), which has extensive ESD experience, uses an integrated system of ESD equipment, xyz positioner table and control feedback systems to produce consistent results.

ASAP has performed extensive research in improving the quality of ESD using a variety of automated systems. However, the maximum thickness of an ESD deposit appears to be limited due to the formation of a non-uniform (bumpy) surface after a certain number of passes. The nature of ESD tends to accentuate surface geometry which can lead to low quality deposits, specifically the formation of bridging porosity. If the ESD surface could remain smooth and uniform between passes, the thickness of an ESD deposit may be unlimited. It was believed that by incorporating ultrasonic impacting equipment in conjunction with the automated ESD equipment could achieve this type of surface.

Ultrasonic impact technology is based on the conversion of harmonic oscillations of an acoustically tuned body into resonant impulses of ultrasonic frequency. The energy generated from these high frequency impulses is imparted to the treated surface through the contact of specially designed pins. These transfer pins are free to move axially between the resonant body and the treated surface. To couple the ultrasonic generator to the treated surface the pins are impacted upon the surface causing a local plastic deformation similar in appearance to peening. This results in a visibly smoother surface than that of as-deposited ESD. While the primary focus of this investigation was using

UIT equipment to improve surface finish, the effect of the ultrasonic energy imparted by UIT was also measured. This energy penetrates much deeper than the energy attributable to the peening aspect of its application and can be tuned to induce compressive stresses in the substrate to a depth of up to several millimeters.

3.2. Nomenclature

The following ESD terminology is used in this section.

- Splat – An ESD deposit from a single pulse (Figure 3-1)
- Pass – A grouping of ESD splats in a row (Figure 3-2)
- Pass overlap – the width that two sequential passes overlap each other (Figure 3-3)
- Layer – A grouping of passes covering a particular area
- Travel direction – direction of travel in a single pass (Figure 3-4)
- Progression direction – direction of travel in a layer (Figure 3-5)
- Torch leading – torch angle is acute in the direction of progression (Figure 3-5)
- Discontinuities – Voids or foreign material in the coating, defined as four general types:
    - Gas porosity – small spherical voids
    - Laminar porosity – thin void layers
    - Bridging porosity – large, random shaped voids
    - Inclusions – solid foreign material, often oxides

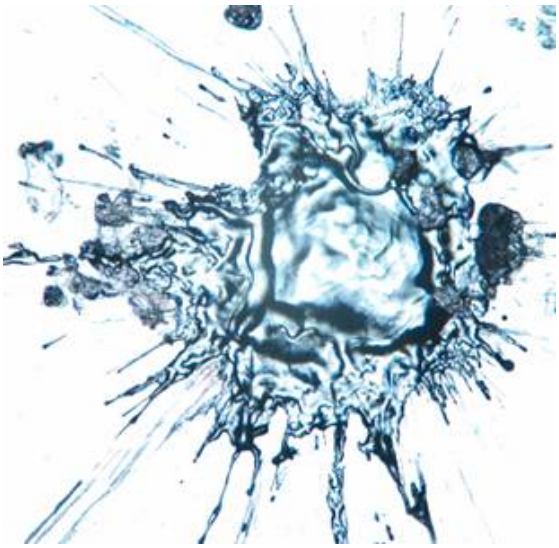

Figure 3-1 Optical Image of a Single Splat From One ESD Pulse. (Splat Size Diameter is Approximately 0.02")

Figure 3-2 ESD Pass. 1.0” Long and 0.085” Wide.

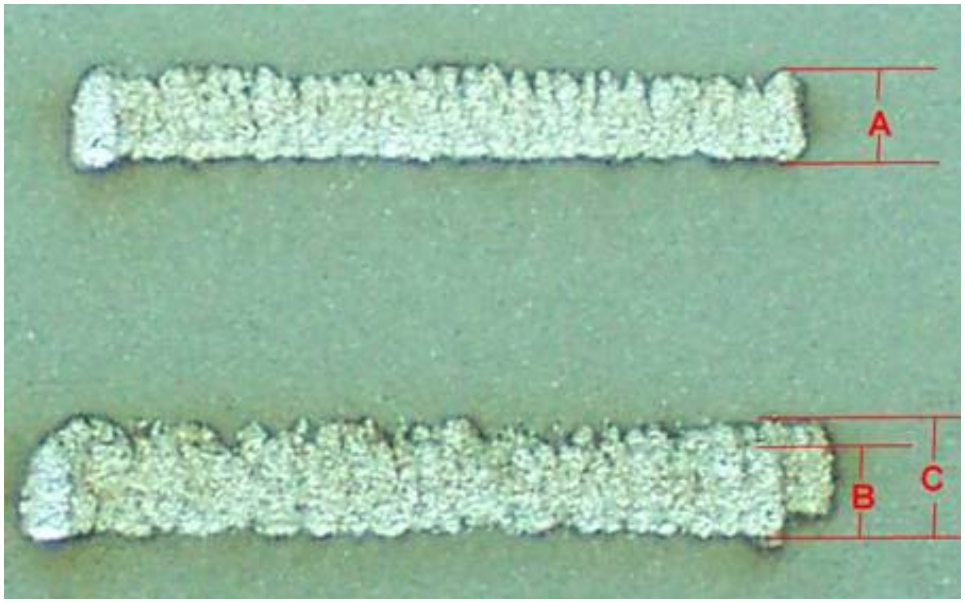

Figure 3-3 Example of Pass Overlap (A and B are 0.085” wide, C is 0.115” wide, resulting in overlap of 0.03”).

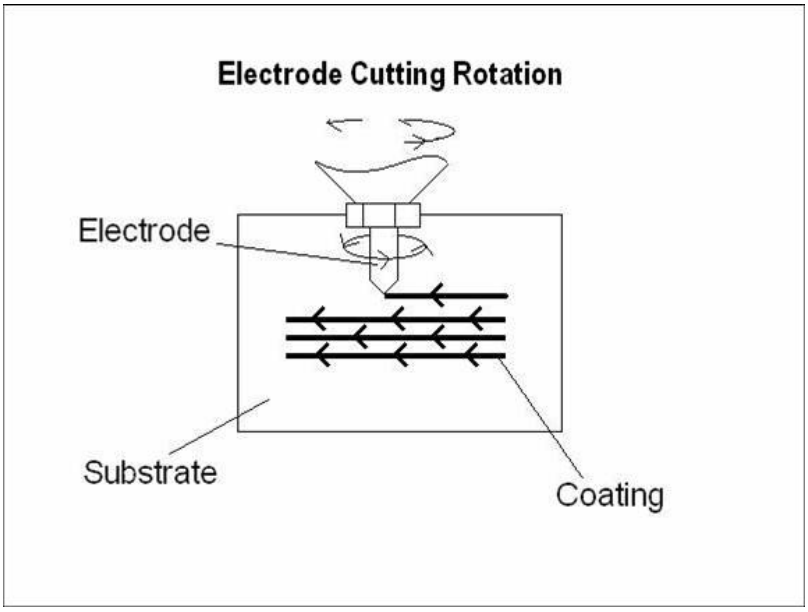

Figure 3-4 Torch head Rotation Direction During Pass Deposit; Cutting Rotation and Single Travel Direction.

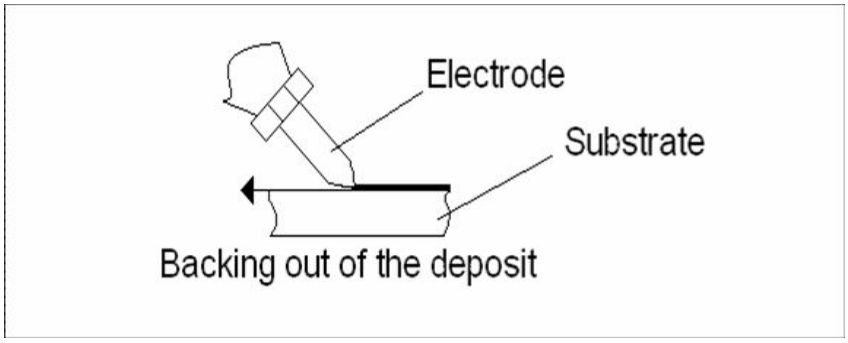

Figure 3-5 Torch-Leading Progression During Deposition of a Layer

3.3. Equipment

3.3.1.ESD and Robotic Equipment

ESD equipment as described in Section 2 was provided by ASAP and a MOTOMAN SV3X robotic system with 6 degrees of freedom was also utilized. The system consists of the robotic arm, the control/programming system and a PushCorp force control unit as shown in Figure 3-6 and Figure 3-7. The MOTOMAN XRC control system supports the arm and supplies power to the arm and ESD machine. This control system is also the programming interface. The ESD torch is connected to the end of the MOTOMAN arm through a PushCorp pneumatic load control system which was used to control the amount of downward force of the electrode tip to the substrate while applying ESD.

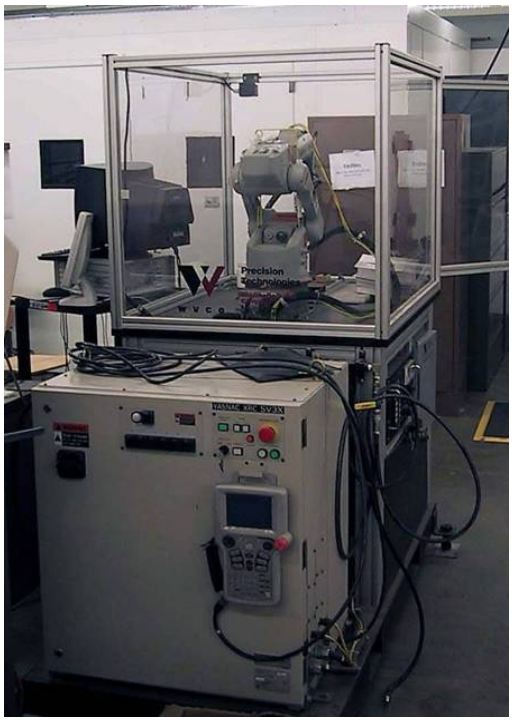

Figure 3-6 MOTOMAN XRC Control System.

Figure 3-7 MOTOMAN SV3X Robot With PushCorp Pneumatic Load Control System

3.3.2. UIT Equipment

The UIT system used consists of three parts as shown in Figure 3-8; the Esonix 3644 control box, a Dynaflux Inc. cooling unit and a UIT gun.

UIT operation consists of manually moving the UIT gun over the area requiring the UIT treatment. The gun must be held so that the impacting pin is perpendicular to the surface being treated. During phase one of this project, this was done manually but for phase two a semi-automated fixturing system was employed. The UIT energy intensity is controlled two ways. The first is by the intensity dial, ranging from 1 to 9 (1 = lowest intensity and 9 = highest) and second by pin diameter, the smaller the diameter the greater the local UIT intensity. Two different pin diameters were used in phase one of this project, 0.125" and 0.25" tool steel pins (Figure 3-9). In phase two the steel pins were replaced with 0.25"-diameter tungsten carbide pins. One was slightly rounded and the other was flat.

Figure 3-8 The UIT System (Cooling Unit, Gun, and Control Unit)

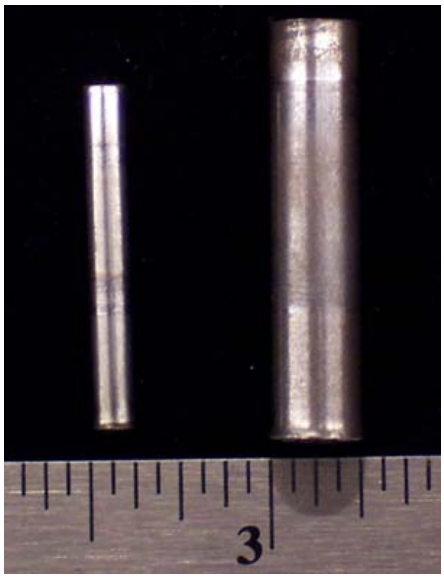

Figure 3-9 UIT Steel 0.125"- and 0.25"-Diameter Pins

3.3.3. X-Y Positioner and UIT Gantry

One of the changes made from phase one to phase two of this project was to better control and quantify the UIT applied. To this end, a rigid support structure to hold the UIT applicator and an X-Y positioner were constructed and integrated into the work station. The X-Y positioner was designed and developed under a separately funded PSU project. The positioner included a base, X axis motor and controller, Y axis manual control, a four-jawed, horizontally oriented chuck, a specimen clamping system and a gantry system to rigidly hold the UIT applicator as shown in Figure 3-10. The positioner was used to hold the specimen under the robot for ESD and then translate it to the UIT applicator for impact treatment. The contact force for the UIT applicator was controlled with the use of a manually adjustable pneumatic cylinder.

The four-jawed chuck permits specimen rotation with each successive ESD layer without reorienting the ESD torch or UIT applicator as shown in Figure 3-11. By providing all necessary degrees of freedom in the specimen holder, it was possible to avoid repositioning the robot arm or UIT applicator.

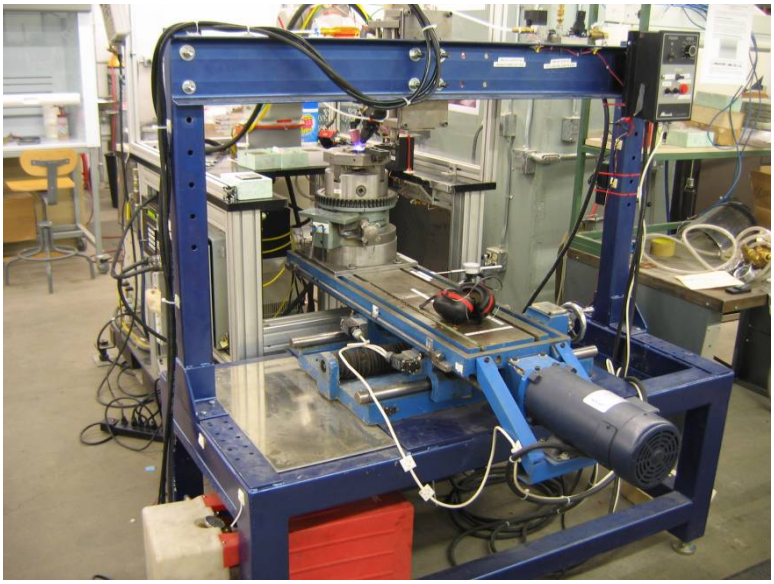

Figure 3-10 X – Y Positioner With UIT Gantry.

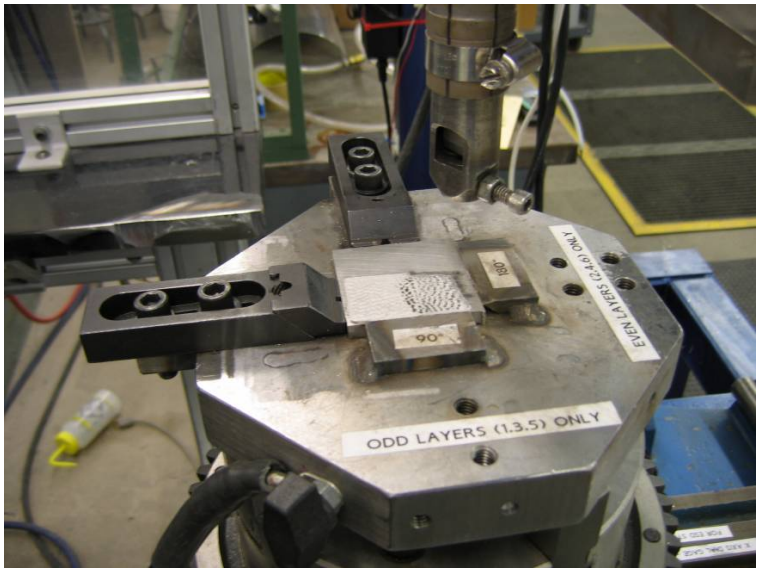

Figure 3-11 Rotating Specimen Chuck Positioned Under UIT Applicator.

3.4. Methodology

Because the project was completed in two distinct phases and the second phase was designed after the completion of the first phase there are many differences between the methodologies for each of the phases. To avoid confusion, the methodologies for each of the phases are presented in order.

3.4.1.Phase One

3.4.1.1. Materials

All coupons used in this project were IN718. The ESD electrodes were also IN718.

3.4.1.2. Robot Methodology

Programming the MOTOMAN robot is performed with a hand held teach pendant. In the teach mode the user moves the arm through desired mechanized steps. Each arm movement is recorded as a line of code that can later be modified, e.g. to change movement velocities. The programming involved for this experiment consisted of creating 75 ESD passes that slightly overlap to create the 1.25" square. The arm then rotates 90° and moves through another 75 ESD passes. After these two ESD layers have been applied the robotic arm moves the torch to a cleaning station were the electrode tip is cleaned. This entire process is repeated through six ESD layers at which time the arm moves to a home position. The coupon is ready to have UIT or other surface preparation performed. This process in repeated until the coupon has reached the desired amount of layers.

3.4.1.3. ESD Torch Motion

ESD is applied with the electrode travel direction and rotation creating a cutting motion. After a pass the electrode was lifted from the surface and returned to the opposite side to begin the next pass. The progression direction was perpendicular to the pass direction with the torch leading. Each pass took approximately 3 seconds with a travel speed of 0.35 inch/sec.

3.4.1.4. Test Matrix

The test matrix used in phase 1 of this project is presented in Table 3-1.

Table 3-1 Phase One Text Matrix of ESD and UIT Conditions

Coupon #		ESD Layers	ESD Thickness (inch)	UIT Pin size (inch)	UIT Intensity H = dial setting of 9 L = dial setting of 4
UIT	T1A	36	0.024	0.25	H
	T1B	36	0.024	0.125	L
	T2A	36	0.024	0.25	H
	T2B	36	0.024	0.125	L
	T3A	24	0.016	0.25	H
	T3B	24	0.016	0.125	L
	T4A	24	0.016	0.25	H
	T4B	24	0.016	0.125	L
	T5A	12	0.008	0.25	H
	T5B	12	0.008	0.125	L
	T6A	12	0.008	0.25	H
	T6B	12	0.008	0.125	L
Abrasively Ground	T7	12	0.008	n/a	n/a
	T8	24	0.016	n/a	n/a
	T9	36	0.024	n/a	n/a
Manual	2 hr	12	0.008	n/a	n/a
	5 hr	24	0.016	n/a	n/a
	8 hr	36	0.024	n/a	n/a
Substrate		n/a	n/a	n/a	n/a

3.4.1.5. Surface Finish Methodology

Two methods of controlling the ESD surface roughness were used: grinding with a paper-backed abrasive and UIT. The grinding used a 4”-diameter paper-backed, 40 grit zirconia wheel. Care was taken to remove only the amount of material to restore the surface to nearly flat condition.

The UIT procedures include two UIT intensity settings and two pin sizes as indicated in Table 3-2. The selected intensities were 9 (maximum) and 4 (mid range). Incorporating both the dial settings and pin sizes allowed for four separate UIT test conditions to be

performed on the ESD surfaces. The coupons received UIT every 6 layers. The deposits were 1.25" by 1.25" and the coupon was divided into three sections as shown in Figure 3-12. The left received high intensity (H UIT), the middle ESD only (ESD), and the right low intensity (L UIT).

Table 3-2 UIT Parameters

Coupon	T1 (36)	T2 (36)	T3 (24)	T4 (24)	T5 (12)	T6 (12)
A	H	H	H	H	H	H
B	L	L	L	L	L	L
Pin Size	0.25 in.	0.125 in.	0.25 in.	0.125 in.	0.25 in.	0.125 in.
Note: H = Dial setting of 9 and L = dial setting of 4.						

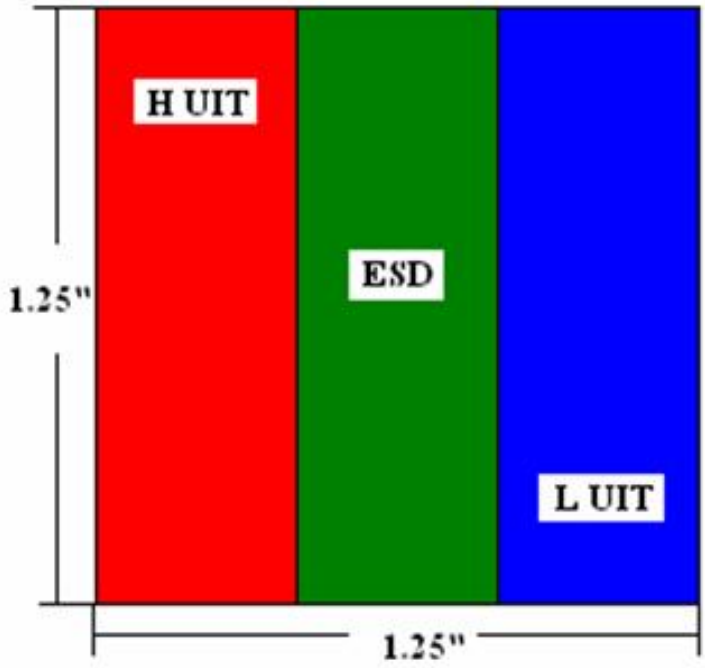

Figure 3-12 Phase One ESD Coupon Layout With UIT Plan. (Red – High Intensity UIT, Green - ESD Only, Blue – Low Intensity UIT)

Each UIT treatment took approximately two minutes to cover the entire ESD area. The larger pin setup had one 0.25 inch diameter pin and the smaller had a 0.125 inch diameter pin. The 0.25" setup is shown in Figure 3-13.

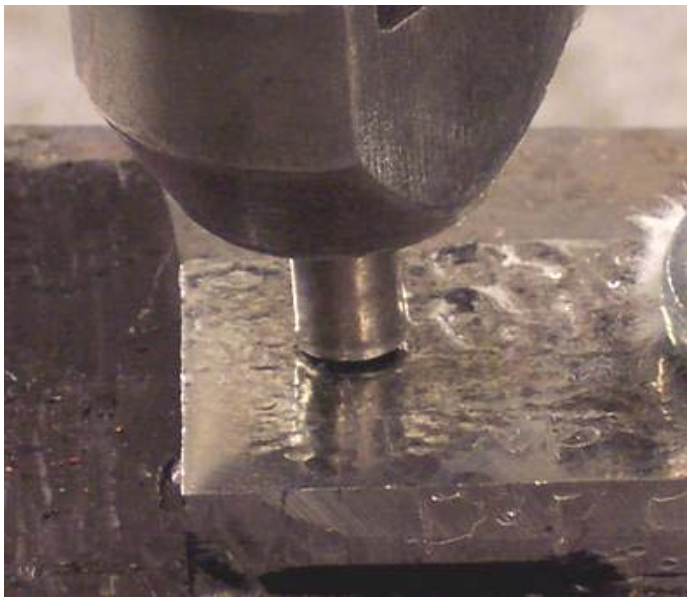

Figure 3-13 UIT Treatment Process With a 0.25" Diameter Pin.

3.4.1.6. ESD Application

A two-step process was used to select the ESD parameters for the deposition rate test matrix. Several preliminary ESD deposits were made and evaluated for quality and deposition rate. After this initial screening, a single set of ESD parameters was selected and used for the actual deposition rate experiments. The ESD parameters used for the deposition rate study are summarized in Table 3-3. The same parameters were used for all automated deposition rate coupons. The electrode tip was cleaned every other layer. Cleaning consisted of moving the electrode tip across a diamond abrasive wheel for approximately 5 seconds. This was done by the robot. Protective argon gas shielding was argon delivered via two plastic nozzles attached to the torch immediately adjacent to the electrode tip. The flow rate was 40 cfh.

Manual application used higher electrode rotation and capacitance and lower voltage and pulse rate parameters than the automated application. Although the electrode was cleaned periodically, no surface treatment was used during the manual ESD application. Argon was delivered to the coupon via one plastic nozzle attached to the torch immediately adjacent to the electrode tip. The flow rate was 25 cfh.

Table 3-3 Phase One ESD Parameters

	Robot	**Manual**
Volts (V)	400	130
Amps (A)	6	5
RPM	700	1500
Pulse Rate (Hz)	800	500
Capacitance (μF)	10	40
Torch: Lead or Lag	Lead	Random
Travel Speed (in/min)	0.35	Variable
Layer Pattern	Alt 90°	Variable
Contact Force (oz)	5	Unknown
Shielding Gas	Localized nozzles	Localized nozzle

3.4.1.7. Surface Finish Evaluation Methods

Two types of surface finish evaluation were used. The first was a visual Gar S-22 Microfinish Comparator gauge and the second was a Mitutoyo SurfTest 301 surface profilometer. The Microfinish Comparator was capable of measuring average surface roughness (Ra) values up to 600 microinches (μin) and the profilometer Ra range was 0-500 μin.

3.4.1.8. Deposit Evaluation Methods

Once prepared, the coupons were cross-sectioned and evaluated which included microscopy, discontinuity quantification and microhardness testing. Optical micrographs were taken at 200 X. Discontinuity quantification was conducted via grey scale image analysis. A series of sections in the ESD were measured for discontinuities and the average was calculated. Knoop microhardness measurements were taken with a 500 g load and a 15 second dwell time. Five hardness indentations were measured and the average was calculated.

3.4.1.9. Deposition Rate Evaluation Methods

Two deposition rates were measured. The first, arc time deposition rate (ATDR), is the amount of material deposited on the surface per arcing time only. The second, production deposition rate (PDR), is the total time elapsed to deposit a given volume of ESD. PDR is meant to take several things into account that are not part of the ATDR like electrode cleaning and equipment adjustments. The coupons were weighed after six ESD layers, before and after UIT (or sanding) and after cleaning. The total weight gained after 36 layers was divided by the time to deposit which, for ATDR, is the time of arcing only, and for PDR is the total time to make the deposits minus the time for tasks not relevant to an industrial situation. For example, the time to clean and weigh the ESD sample, the electrode and the UIT pin would not exist in practice. The time to conduct these steps was deducted from the PDR.

Weight measurements were not taken during the manual ESD application. The PDR of the manual ESD was calculated by measuring the thickness and area of the deposit with a caliper. The deposit volume was calculated with these dimensions, multiplied by the density of IN718 (8.19 g/cm^3) and divided by the total time to deposit the volume of the three samples. The result was a PDR in grams/hour for each sample. Another method of calculating the deposition rate was by deposit thickness instead of weight. This method is included in the deposition rate results. ATDR values were not available for the manually prepared coupons.

Deposition rates were not calculated for the automatically prepared coupons T1 through T9. One coupon was prepared in the initial set up of ESD and UIT parameters and it was from the change in weight and thickness of this coupon and time to prepare that the deposition rates were established.

3.4.2.Phase Two

3.4.2.1. Materials

Preparation of the IN718 specimens was based on compatibility with the robot/UIT/positioner equipment while maximizing the number of specimens for the available material. The welds were made on surface ground plates 2.5" x 2.5" x 0.25"-thick using 0.125"-diameter IN718 electrodes. Four test conditions per plate provided a good combination of welding and UIT accessibility plus ease of post-weld processing such as sectioning, mounting and polishing. Once the specimen parameters were chosen, appropriate plate stock was obtained, sectioned, heat treated and surface ground.

3.4.2.2. Design of Experiments (ESD and UIT Inputs)

The welding parameter matrix was selected based on previous experience and a full factorial Design of Experiment (DOE) analysis. The DOE work was conducted using Minitab™ statistical software. Several matrices were investigated before choosing an experimental matrix with four-inputs and either two or three levels per input. The total number of tests was 36 with no duplicates. Metrics (outputs) included deposition rate, surface roughness, hardness and porosity. Statistical analyses were conducted on the outputs also using Minitab™. Table 3-4 through Table 3-7 list the inputs and levels and Table 3-8 lists the DOE test matrix. The ESD parameters were selected to maximize energy without overloading the equipment so voltage, capacitance and pulse rate were constant at 150 volts, 30 μF and 800 Hz respectively. The electrode rotational speed was 100%, 50% and 25% of the maximum (approximately 1400 rpm).

The experimental test matrix was designed to produce data on surface morphology, weld quality and deposition rates. Initial selection of all experimental parameters was based on previous data and equipment capabilities. Also taken into consideration was how to maximize welding energy while still being able to control surface quality.

Table 3-4 ESD Input Levels in DOE

	ESD Parameters		
Levels	Amps	RPM	Pulse
1	6	25%	800 Hz
2	6	50%	800 Hz
3	6	100%	800 Hz

Table 3-5 UIT Input Levels in DOE

	UIT Parameters (0.25 inch pin)				
Levels	Pin Geometry	Intensity	Travel Speed inch/sec	Table Speed: % of Maximum	Overlap
1	Flat	9	0.11	14%	No Overlap
2	Rounded	6	0.26	16%	0.0625 inch (25%)
3	Rounded	9	0.05	13%	0.125 inch (50%)

Table 3-6 UIT Frequency in DOE

	Number of Layers Between UIT Treatments		
Levels	Layers	Total # of Layers	Total # of UIT Treatments
1	1	6	5
2	2	6	2

Table 3-7 Gas Shielding in DOE

Gas Shielding	
Levels	Type of Gas
1	Argon
2	95% Ar + 5% H2

Table 3-8 DOE Experimental Test Matrix

Run Order	ESD	Number of Layers between UIT	UIT	Shielding Gas
1	2	1	3	1
2	1	2	2	2
3	2	1	3	2
4	2	2	3	2
5	3	1	1	2
6	1	1	1	2
7	2	2	2	1
8	3	1	3	1
9	3	2	3	2
10	2	2	1	2
11	1	1	3	1
12	2	1	2	1
13	3	2	2	2
14	3	1	1	1
15	1	1	1	1
16	1	2	1	1
17	2	2	2	2
18	2	2	3	1

Run Order	ESD	Number of Layers between UIT	UIT	Shielding Gas
19	3	1	2	1
20	1	2	3	2
21	1	1	2	1
22	3	2	3	1
23	3	2	2	1
24	2	1	1	2
25	1	2	2	1
26	2	2	1	1
27	1	1	3	2
28	1	1	2	2
29	3	2	1	2
30	1	2	3	1
31	1	2	1	2
32	2	1	1	1
33	3	1	2	2
34	3	2	1	1
35	2	1	2	2
36	3	1	3	2

3.4.2.3. UIT Quantification

The amount of energy imparted into a surface by UIT has not been quantified. There are several factors involved. Force, in this case downward pressure exerted by the pin, is probably impossible to accurately describe due to its inherently unstable operation. While the applicator is held in place by a relatively stable air cylinder, the actual contact force is controlled by the ultrasonic waves and bouncing impact that occurs during the treatment. Likewise the control panel intensity setting, a unitless number, has no direct energy or force conversion. Overlap describes the amount a previous UIT track retreated by each successive pass. If one-fourth of the previous track is re-treated by the following track, the overlap is 25%. Treatment time is quantified by the travel speed of the pin across the surface. Using these parameters, quantification of UIT can be described as:

$$\text{UIT Number} = \frac{(\text{Dial Intensity})(1+[2][\%\ \text{Overlap}])}{(\text{Travel Speed})(\text{Pin Contact Diameter})}$$

This assumes that if coupling is occurring then the energy or power transferred into the

surface is relatively constant for a given intensity setting. The UIT Number will then be time/area.

3.4.2.4. Gas Shielding

Shielding gases are used in welding technology to protect and/or enhance the melting and solidification processes. Prior to this effort all work with the IN718 alloy had been conducted under an inert atmosphere of argon. Some commercially available welding mixtures include other gases that affect arc physics and the amount of heat generated by an arc. This effort included one of those gases, a mix of argon (95%) plus hydrogen (5%). Traditional welding processes use this combination to increase heat and penetration. Both gas species, mixed and not, were delivered via a flow regulating valve through tubing to a standard gas tungsten arc welding handheld torch. The torch was mounted to the ESD torch fixture on the end of the PushCorp slide as shown in Figure 3-14.

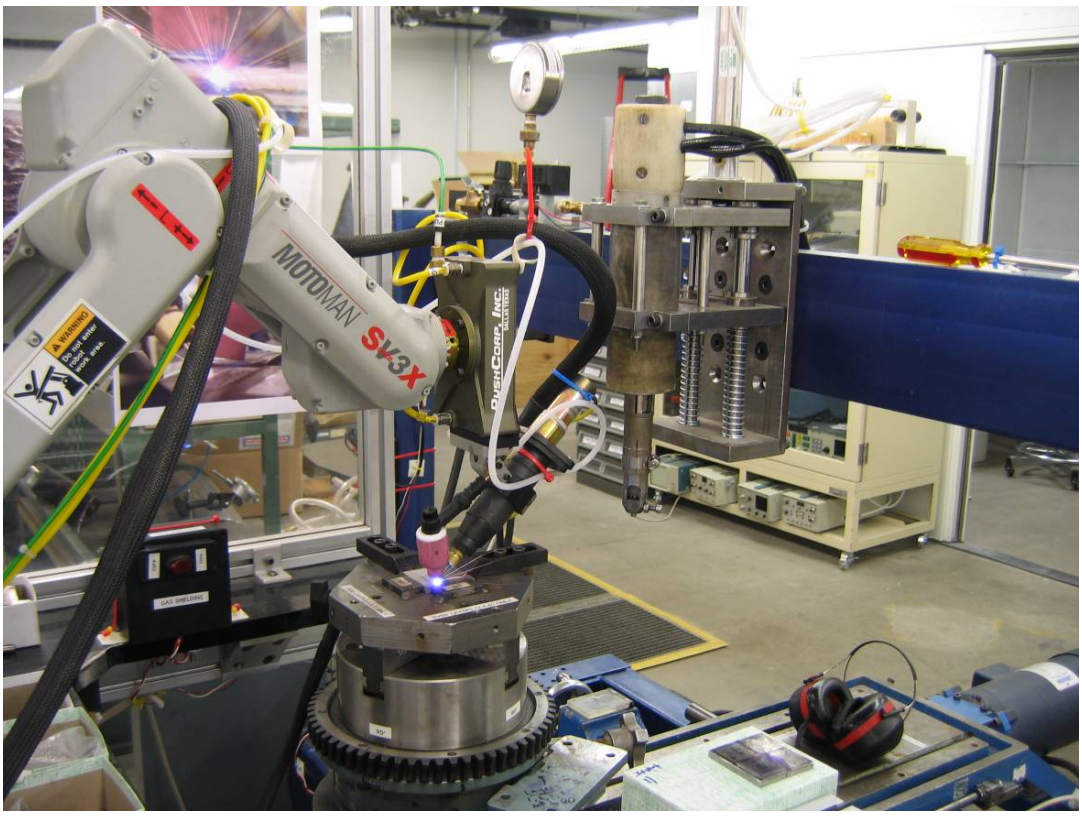

Figure 3-14 Relative Positions of UIT, Specimen Chuck and Welding Robot.

3.4.2.5. UIT Frequency

The last experimental input was the number of ESD layers between UIT treatments. The input was a two-level input. The first level was UIT treatment after every ESD layer and the second was UIT treatment after every other ESD layer.

3.4.2.6. Residual Stress

X-ray diffraction (XRD) is currently one of the most accurate methods to measure

residual stresses in metals. It uses the coherent domains of the metal (grain structure) like a strain gauge which reacts to the stress state existing in the metal. Residual stress and/or applied stress expands or contracts the atomic lattice spacing. The expansion or contraction in the lattice spacing is measured by the XRD technique, and converted to stress values. This analysis was performed by Proto Industries in Ypsilanti, Michigan, and followed SAE Method J784a.

Locations on ESD-repaired specimens were first analyzed on the as-deposited surface, then that spot was chemically etched 0.005" deep, and analyzed again. XRD patterns were thus taken every 0.005" into the specimen to a depth of 0.020". The ESD deposits of IN718 on the IN718 specimens were approximately 0.008" thick. Therefore, two XRD measurements were taken in the ESD deposit, and three in the substrate, to a depth of approximately 0.012".

Ten combinations of ESD and UIT conditions were evaluated, as shown in Table 3-9. The ESD welding parameters were a pulse rate of 600 Hz, capacitance of 500 μF, voltage of 140V with a current of 8A. UIT conditions included a high intensity setting of 9 and a low intensity setting of 4 using a 0.25" pin for 60 seconds. The ESD layers were typically 0.008" thick prior to performing UIT.

Table 3-9 ESD/UIT Combinations Evaluated for Residual Stress

Specimen Designation	Condition
Baseline	IN718 base metal, no ESD or UIT
ESD	ESD deposit only
AH	UIT only, high intensity
AL	UIT only, low intensity
BH	ESD then UIT, high intensity
BL	ESD then UIT, low intensity
CH	UIT then ESD, high intensity
CL	UIT then ESD, low intensity
DH	UIT, ESD then UIT, high intensity
DL	UIT, ESD then UIT, low intensity

3.4.2.7. Metallography

After welding and UIT the specimens were cut (four different specimens per coupon) then sectioned through the center of the deposit. They were mounted so the deposit cross-section was visible and prepared by standard metallographic practice.

Evaluation of the deposits included porosity by image analysis, microhardness and general deposit and fusion zone appearance. The procedures were established in previous projects. It was necessary to etch the samples to distinguish the different layers, especially those having UIT performed on them. Porosity counts were performed prior to etching and consisted of 6 random fields that were averaged.

3.4.2.8. Porosity

Porosity counts were conducted in the same manner as previous projects using an MSQ Image Analysis software program based on gray shades in an image. Six random fields were measured and averaged.

3.4.2.9. Microhardness Testing

Microhardness testing was conducted in two phases. The first phase consisted of vertical traverses that attempted to distinguish among the various layers of UIT and ESD. After it was determined that a distinct hard/soft layer pattern did not exist, hardness readings were taken every 0.05 mm starting at the fusion line and progressing into the deposit. Depending on the deposit thickness, between 4 and 7 total readings were taken per deposit and averaged.

Indentations were made with 500 grams and a dwell time of 15 seconds in accordance with Knoop hardness testing standards. Microhardness, although normally taken in the unetched condition, was done on lightly etched surfaces because it was often not possible to otherwise distinguish the deposits from the substrate otherwise.

3.4.2.10. Surface Morphology

Surface morphology was evaluated with a replica technique. Exaflex putty Type O, a two part vinyl polysiloxane impression material, was mixed and pressed onto the surface. The putty cured in about five minutes and was peeled from the surface. Each sample was cut into five slices perpendicular to any ESD grain and/or to the roughest surface patterns. Cross sections were examined on a metallograph at 50 X and the maximum peak-to-valley distances were measured and recorded. Five measurements were taken per slice and the measurements were averaged. The data were analyzed to compare the results of different UIT levels and also as function of number of layers in one specimen. A total of 146 replicas were taken.

3.4.2.11. Deposition Rate

Deposition rates for most specimens were calculated by weighing the specimens prior to welding and after all the layers had been deposited and any UIT processing had been completed. Two specimens were weighed after each layer to verify uniform deposition as a function of layer number.

3.5. Results

Because the project was completed in two distinct phases and the second phase was designed after the completion of the first phase there are many similar sections of results

between each of the phases (i.e. hardness, porosity, etc.). To avoid confusion, the results for each of the phases will be presented in order.

3.5.1.Phase One

3.5.1.1. Surface Finish Methodology Results

When applying ESD manually, the operator continuously monitors the surface. Whenever the operator judges the finish is impairing further deposition a smoothing operation is performed. A typical method of smoothing high spots is with an abrasive stone or pad on a high speed rotary grinder.

UIT, due to its vibratory nature, is difficult to control manually and tends to wander across the surface being treated. The smaller pin (0.125 inch) flattened high spots more rapidly than did the large (0.25 inch) pin. The small pins were more difficult to direct and the finish was generally rougher than with the larger pin. A single, round-tip, large diameter pin produced the best combination of surface finish, treatment time and controllability. The high intensity setting was more efficient than lower intensities.

3.5.1.2. Surface Finish Results

Surface finish measurement was problematic. Figure 3-15 is the final ESD layer of the manual 2-hour sample. Although these surfaces were the smoothest of all surface treatment conditions, they were rougher than the maximum (600 µin Ra) of the visual comparator gauge. Most tests with the profilometer also exceeded the maximum roughness that could be measured. Thicker manual coupons had rougher surface than the one shown.

For comparison, Figure 3-16 shows automated ESD surfaces, one as-deposited (right) and the other after receiving UIT (left). The as-deposited surface is approximately the maximum roughness that can be effectively corrected with UIT. The surfaces that received UIT had a smoother finish than the as-deposited ones, but were not as smooth as the manual deposits.

The surface of a coupon which received the manual sanding surface treatment is shown in Figure 3-17.

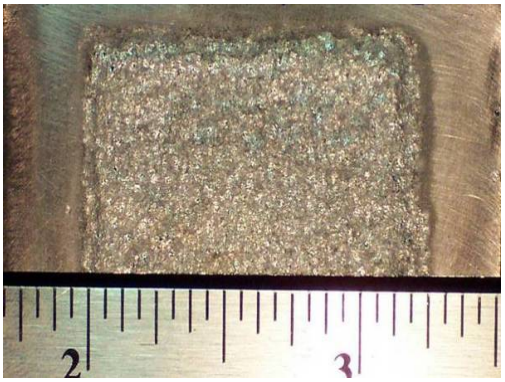

Figure 3-15 Surface of Manual ESD

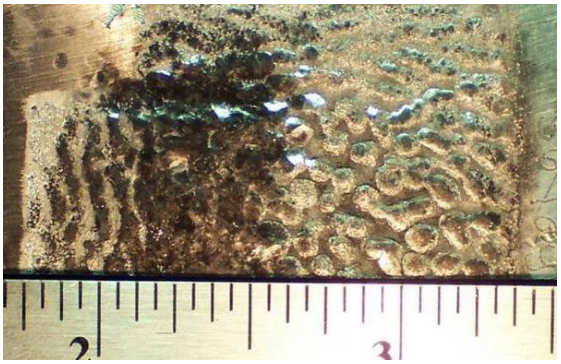

Figure 3-16 Surface of Automated ESD Left Received UIT, Right As-deposited

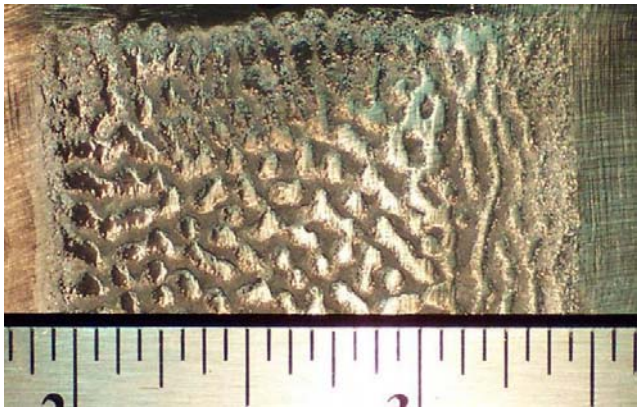

Figure 3-17 Surface of Automated ESD After Manually Sanding

3.5.1.3. Deposit Results

The extent of discontinuities was generally less than 3% as measured in cross sectional analysis for all deposit types as shown in Figure 3-18. The automated deposits had a maximum of approximately 3% and minimums in the range of 0.5%. All three of the manual deposits were about 1.5%. Coupons which received UIT had significantly lower discontinuities than the other two types. However, intensity and pin size of the UIT equipment had variable effects on discontinuity measurements. In some cases the higher intensity resulted in higher percent discontinuities; in other cases the opposite was true. Coupons that received manual sanding instead of UIT had slightly higher discontinuity values. Average discontinuity values are presented in Table 3-10. Micrographs demonstrating typical discontinuities are shown in Figure 3-19.

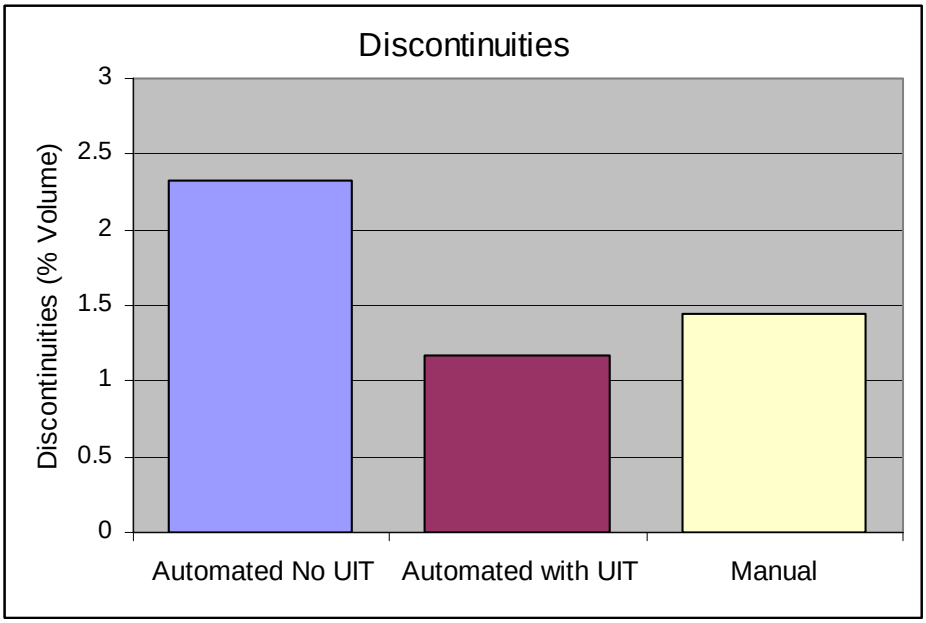

Figure 3-18 Discontinuities as a Volume Percentage for Different Application Procedures

Table 3-10 Discontinuity Values

Coupon #		Average Discontinuity (%)	Standard Deviation
Manual	2hr	1.67	0.90
	5hr	1.45	0.87
	8hr	1.21	0.88
UIT	T1A	1.12	0.51
	T1B	1.62	0.40
	T2A	0.83	0.43
	T2B	0.57	0.48
	T3A	2.95	2.50
	T3B	1.59	0.70
	T4A	0.67	0.42
	T4B	1.35	1.59
	T5A	0.50	0.24
	T5B	1.53	0.99
	T6A	0.62	0.69
	T6B	0.71	0.54
Abrasively Ground	T7	3.09	1.20
	T8	1.04	0.65
	T9	2.82	1.07

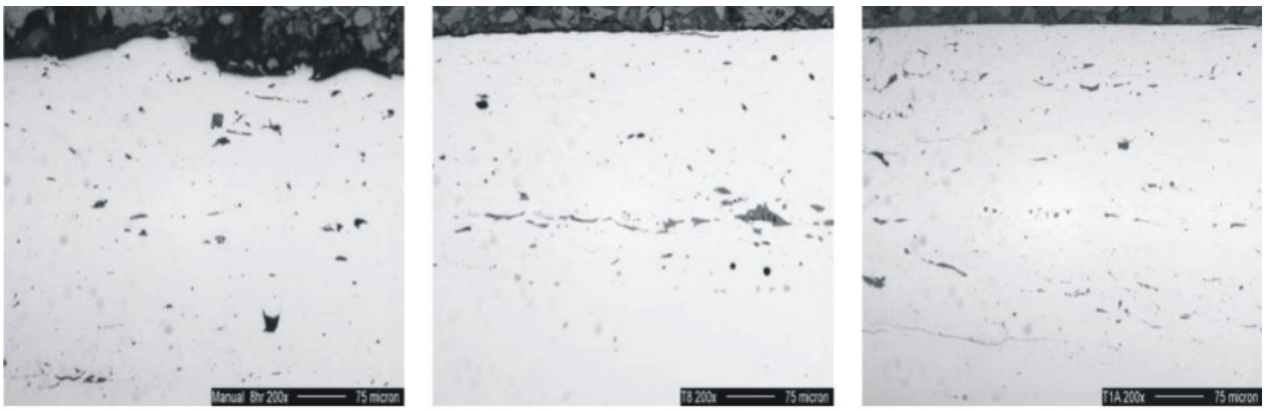

Manually applied Robot applied, no UIT Robot applied with UIT

Figure 3-19 Micrographs of Cross Section of ESD Deposit (200 X)

Microhardness measurements of manually ESD applied IN718 were 336 to 382 Knoop as indicated in Figure 3-20. Coupons which received UIT had hardness measurements ranging from 355 to 575. Coupons that received sanding as a surface finish control had an average hardness of 370 Knoop. Average microhardness measurements are presented in Table 3-11. In all but one case (T4 A and B), the deposit was harder for those that received the high intensity, 0.25" pin UIT. The average hardness increased with increasing deposit thickness. All deposits subjected to UIT were harder than the substrate, with the exception of two that were treated with low intensity and a 0.125" pin.

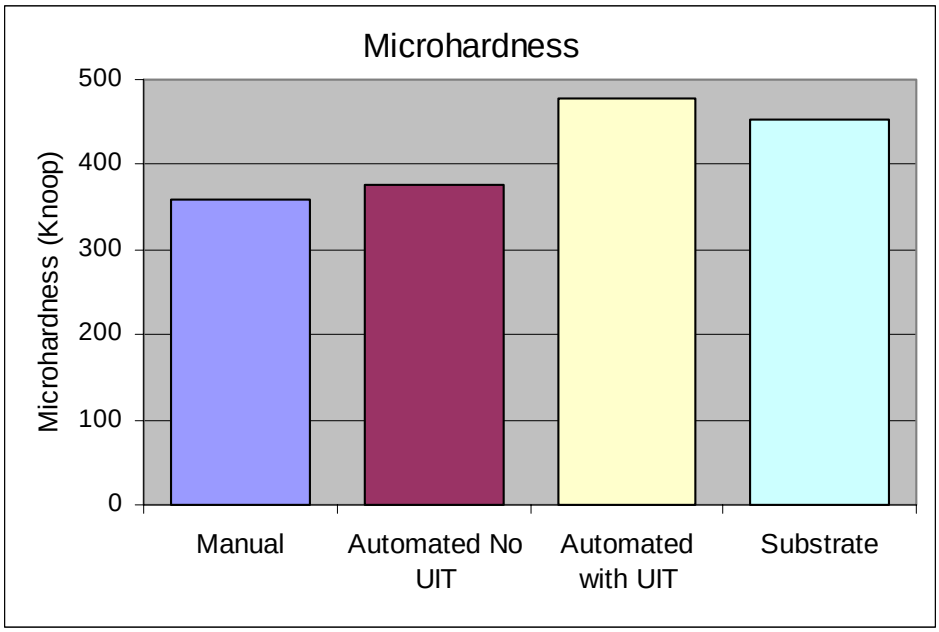

Figure 3-20 Hardness Versus Application Procedure

Table 3-11 Microhardness Measurements

Coupon #		Knoop Average	Knoop Standard Deviation	Rockwell C Average
UIT	T1A	482.3	6.0	46.3
	T1B	374.6	13.7	37.4
	T2A	575.4	15.4	52.0
	T2B	564.0	19.9	51.4
	T3A	488.7	11.0	46.7
	T3B	476.7	21.7	45.9
	T4A	474.5	27.9	45.7
	T4B	517.3	15.7	48.6
	T5A	482.9	22.7	46.3
	T5B	366.4	47.9	36.6
	T6A	476.1	27.2	45.8
	T6B	454.8	29.1	44.3
Abrasively Ground	T7	380.9	39.8	38.0
	T8	391.4	66.6	39.0
	T9	354.9	32.9	35.3
Manual	2 hr	335.6	11.8	33.1
	5 hr	382.1	20.2	38.1
	8 hr	361.3	19.5	36.0
Substrate		453.3	5.9	44.2

3.5.1.4. Deposition Rate Results

Automated ESD produced significantly higher deposition rates over the manual process (Figure 3-21 and Table 3-12). ATDR comparisons are not available but the PDR, based on thickness, increased a factor of 11 for automated applications with UIT compared to manual applications. Deposition rates based on weight gains were similar with an increase of approximately a factor of 9.

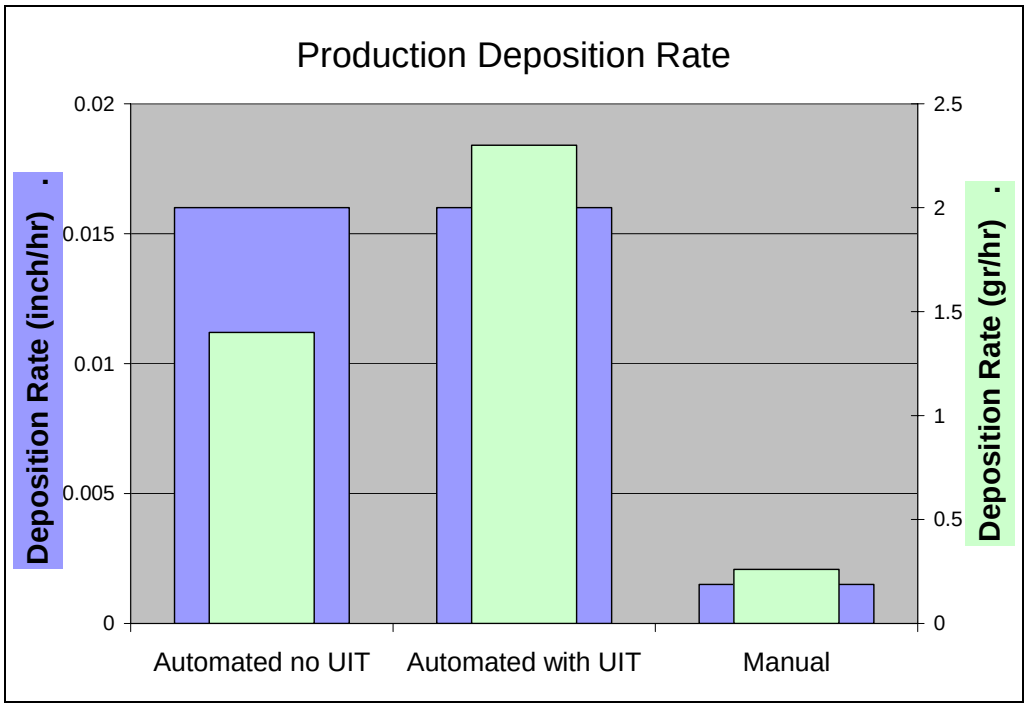

Figure 3-21 Production Deposition Rate Versus Application Procedure

Table 3-12 Deposition Rates

Surface Control Condition	Deposition Rate by Thickness (inches/hour)		Deposition Rate by Weight (grams/hours)	
	Arc	Production	Arc	Production
Manual 2 hr.	n/a	0.0020	n/a	0.24
Manual 5 hr.	n/a	0.0012	n/a	0.29
Manual 8 hr.	n/a	0.0013	n/a	0.25
Automated and UIT	0.024	0.016	3.4	2.3
Automated and Sanded	0.024	0.016	2.1	1.4

The ATDR for both the UIT and sanded coupons, prepared with automation, showed a fairly steady deposition rate. The UIT coupon started with a higher deposition rate, and then leveled off at a lower, consistent 0.50 to 0.60 g/min rate as shown in Figure 3-22. The sanded coupons began with a lower deposition rate and then increased to a steady 0.50 to 0.60 g/min rate.

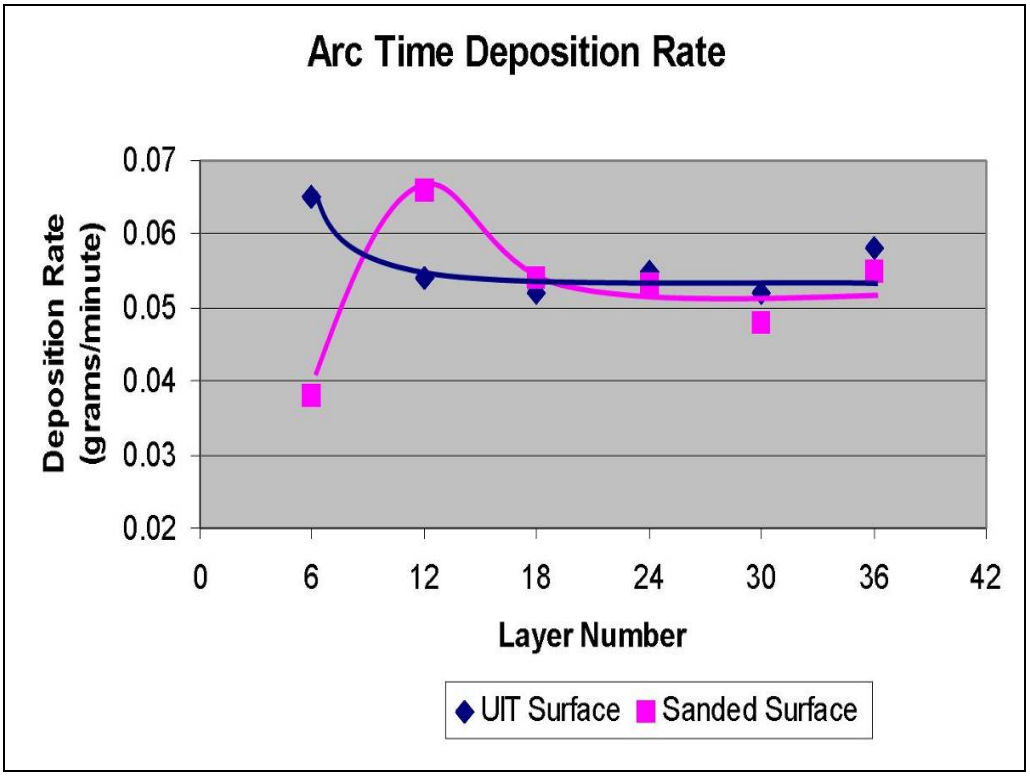

Figure 3-22 Change in Deposition Rate With Number of Layers

3.5.2.Phase Two

3.5.2.1. Porosity

The average level of porosity in the specimens was generally less than 1% as indicated in Table 3-13. There was no relationship between porosity percentage and deposition rate as shown in Figure 3-23.

Table 3-13 Average % Porosity of ESD Deposits Treated With UIT

Run Order	Sample #	Average	Std Dev
1	1C	1.1	1.0
2	11B	0.2	0.2
3	11C	0.3	0.2
4	12A	0.8	0.5
5	9C	0.4	0.3
6	7B	0.3	0.3
7	5B	0.1	0.1
8	1A	0.2	0.1
9	11D	0.6	0.5
10	8D	0.2	0.2
11	3A	0.2	0.2
12	5C	0.2	0.2
13	10C	1.4	1.9
14	3B	0.0	0.0
15	4B	0.1	0.1
16	4C	0.9	0.9
17	11A	0.5	0.4
18	2C	0.7	0.7

Run Order	Sample #	Average	Std Dev
19	5A	0.2	0.1
20	10D	0.2	0.2
21	5D	0.1	0.2
22	1B	0.2	0.2
23	4D	0.2	0.1
24	8C	0.6	0.4
Dup 24	9A	1.1	0.5
25	6A	0.1	0.1
26	3D	0.6	0.9
27	12B	0.3	0.3
28	10B	0.7	0.6
29	9B	2.0	1.4
30	2D	0.2	0.1
31	8A	0.3	0.1
32	4A	0.2	0.3
33	9D	0.9	0.6
34	3C	0.8	0.4
35	10A	0.5	0.7
36	7A	0.3	0.3

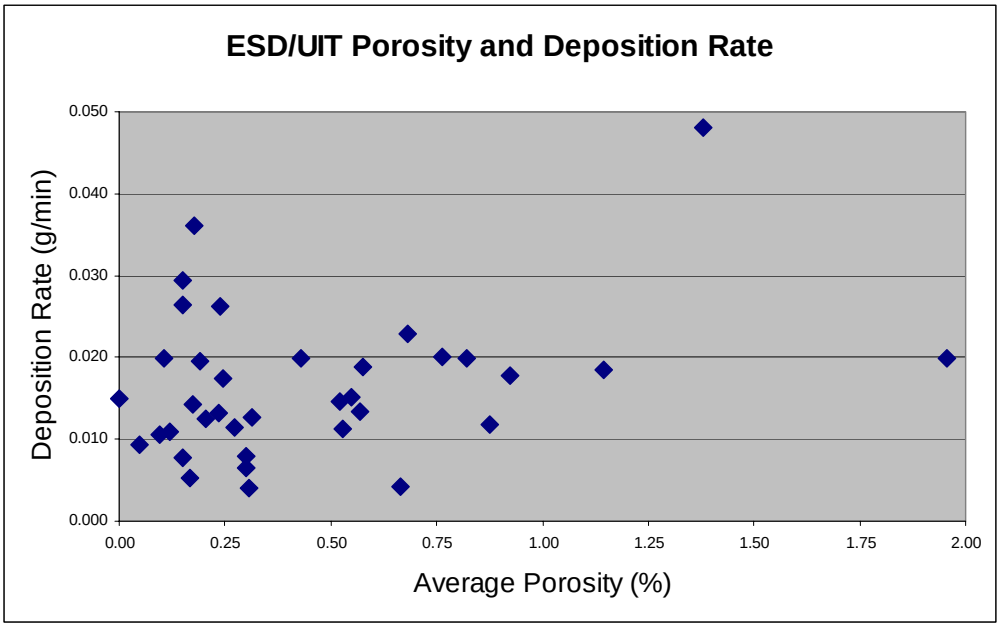

Figure 3-23 Deposition Rate and Percent Porosity

3.5.2.2. Microhardness

Average deposit hardness ranged from a high of 554 to a low of 389 Knoop as indicated in Table 3-14. Standard deviations were between 4% and 34% of the averages. In general the top one or two layers were softer than those below because the last layers were not subjected to UIT. The hardness from the fusion line to the top of the deposit of three representative specimens (high, mid and low average hardness) are shown in Figure 3-24. There was no direct relationship between deposition rate and hardness or UIT number and hardness as indicated in Figure 3-25 and Figure 3-26.

Table 3-14 Average Microhardness Values

Sample #	Average	Std Dev
1A	396.5	127.7
1B	507.4	69.5
1C	465.2	82.6
2C	458.6	42.8
2D	429.9	86.8
3A	441.9	74.9
3B	468.3	38.2
3C	425.8	70.7
3D	439.7	60.5
4A	439.9	53.9
4B	478.4	108.1
4C	448.3	151.2
4D	505.6	70.3
5A	522.1	94.7
5B	395.9	63.8
5C	537.3	57
5D	475.4	67.8
6A	461.3	98.8
7A	480.9	89.4

Sample #	Average	Std Dev
7B	389	76.9
8A	467.4	32.5
8C	443.9	32.3
8D	425.4	38.1
9A	419.3	50.9
9B	458.8	50.4
9C	455.4	20.4
9D	451.6	39
10A	475.3	45.1
10B	449.2	81.2
10C	470.3	63.5
10D	434.5	40.1
11A	554.6	84
11-B	503.4	118.1
11C	537.3	95.2
11D	499.7	46.3
12A	466.1	78.5
12B	439.7	60.5

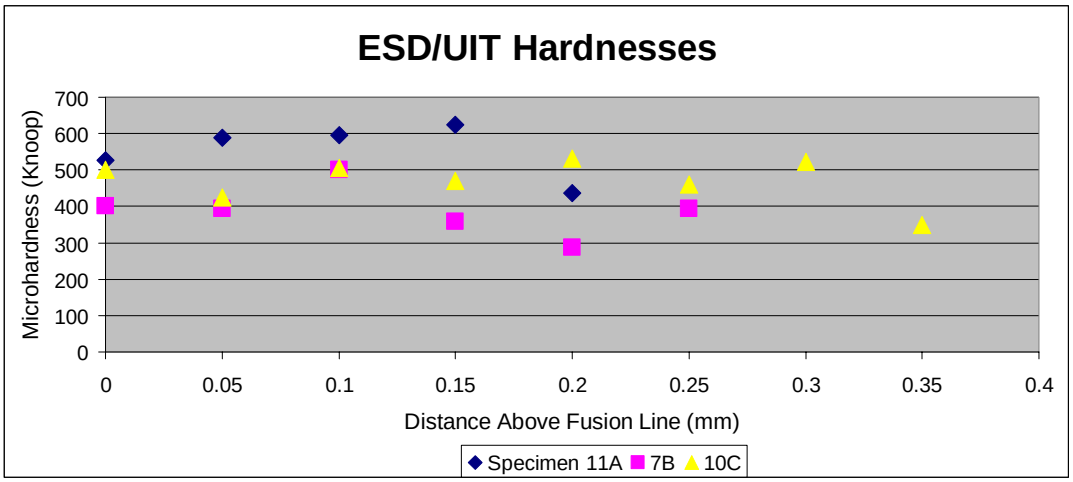

Figure 3-24 Microhardness from Fusion Line into ESD of Three Representative Samples (11A = Highest Average, 7B Lowest Average, and 10C Median Average Hardness)

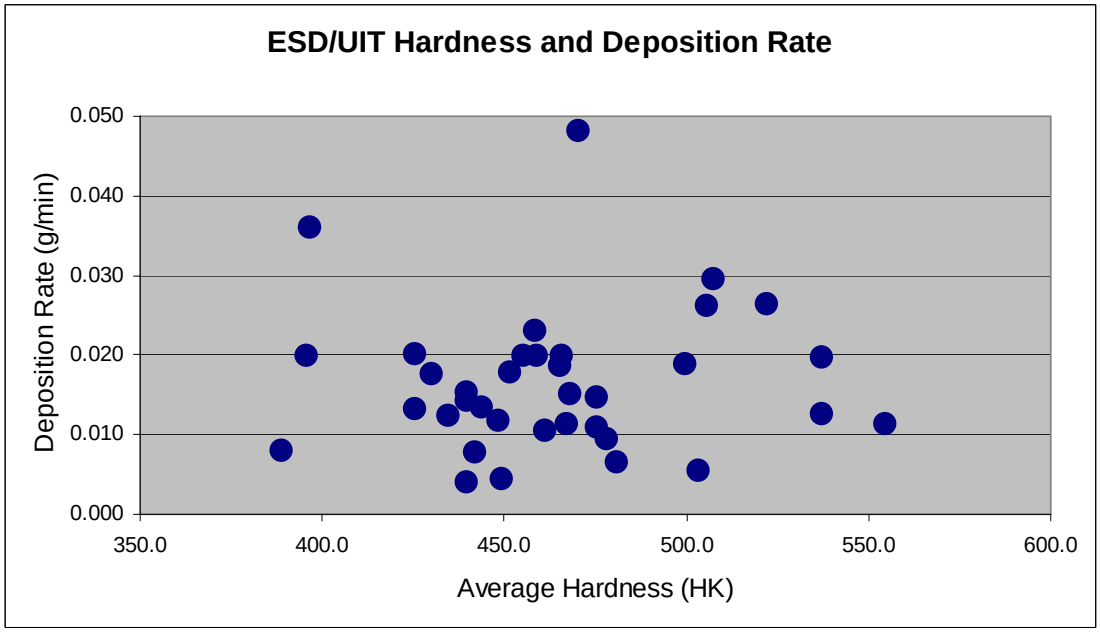

Figure 3-25 Average Hardness of UIT Treated ESD Deposits Versus Deposition Rate

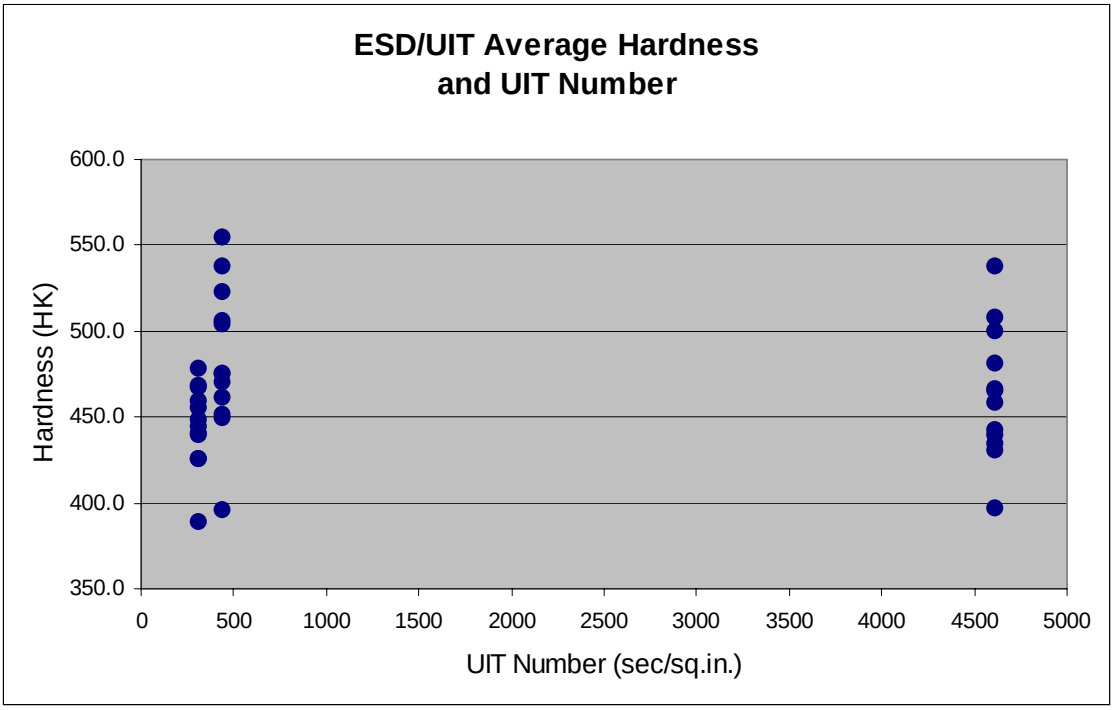

Figure 3-26 ESD Average Hardness Versus UIT Number

3.5.2.3. UIT Quantification

Several factors determine the amount of change UIT causes in a treated surface. Those factors are the UIT generator intensity setting, travel speed, pin diameter, pin geometry (rounded or flat), and the amount of overlap or times a particular area is treated. Intensity is a unitless number, 1 – 9, set on the UIT generator control panel. Higher travel speeds will decrease the amount of time a region is exposed to impact. Likewise larger and/or flat pins will distribute the ultrasonic energy over greater areas, decreasing energy density. Finally, if a pin is allowed to contact an area more than once, either intentionally or not, the repeated interaction will cause additional surface change (see Figure 3-27).

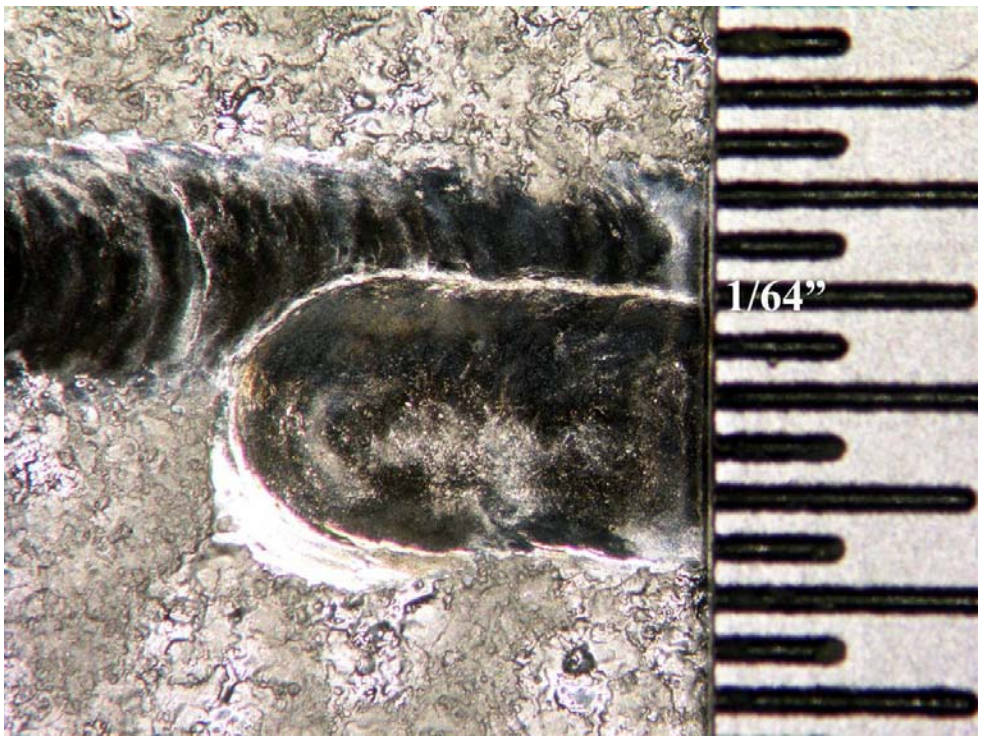

Figure 3-27 Example of 50% Overlap of UIT pass, 0.25 Inch Rounded Pin

The UIT number was calculated as indicated in Section 3.4.2.3.

The three levels in UIT intensity were 314, 442 and 4615 sec/sq.in. for UIT conditions 1 through 3 respectively (Table 3-15). The actual contact diameter for the 0.25 inch rounded tip pin was approximately 0.078 inches so overlap with the rounded pin is either 25% or 50% of 0.078 inches.

Table 3-15 UIT Number Calculations

Levels	Pin Geometry	Intensity	Travel Speed (inch/sec)	Overlap (%, inches)	Calculated UIT Number (sec/sq.in.)
1	Flat	9	0.11	No Overlap	314
2	Rounded	6	0.26	25% (0.2)	442
3	Rounded	9	0.05	50% (0.39)	4615

3.5.2.4. Surface Morphology

Some specimens were analyzed in terms of surface morphology. Specimens 9B, 9D and 11D were chosen to contrast the surfaces of three different UIT conditions. 11A was randomly selected for “before” and “after” UIT roughness using a single UIT condition. The experimental parameters of each specimen are detailed in Table 3-16.

Table 3-16 Experimental Parameters of Surface Roughness Quantified Specimens

	ESD Level	UIT Level	Gas Shielding	Number of ESD Layers per UIT
9B	3	1	Mixed	Every other ESD layer
9D	3	2	Mixed	Every other ESD layer
11D	3	3	Mixed	UIT every ESD layer
11A	2	2	Mixed	UIT every ESD layer

The data are presented in several forms. The first is the average of peak-to-valley distance for each layer (specimen 11A) before and after UIT in the specimen as shown in Figure 3-28. In general, neither the before UIT nor after UIT was consistently smoother or rougher.

A second way to consider the surface morphology data is by comparing the roughness of surfaces that were treated with different UIT levels. Specimens 9B, 9D and 11D were subjected to UIT levels 1, 2 and 3 respectively. The average roughness (peak-to-valley distance) is consistently around 100 microns for all three specimens as shown in Figure 3-29. No one UIT condition is consistently rougher or smoother than the others.

Regardless of what the roughness data indicates, surfaces subjected to UIT are visually significantly smoother than as deposited ESD. The lack of agreement between the two is probably the result of the roughness parameter (maximum peak-to-valley distance) used. Although the surfaces treated with UIT are smoother, it is possible that peak-to-valley distances are similar to the surface of as deposited ESD. Stated another way, although there are significantly fewer peaks on a UIT treated surface, the average height of the peaks are approximately equal to a non-UIT treated surface.

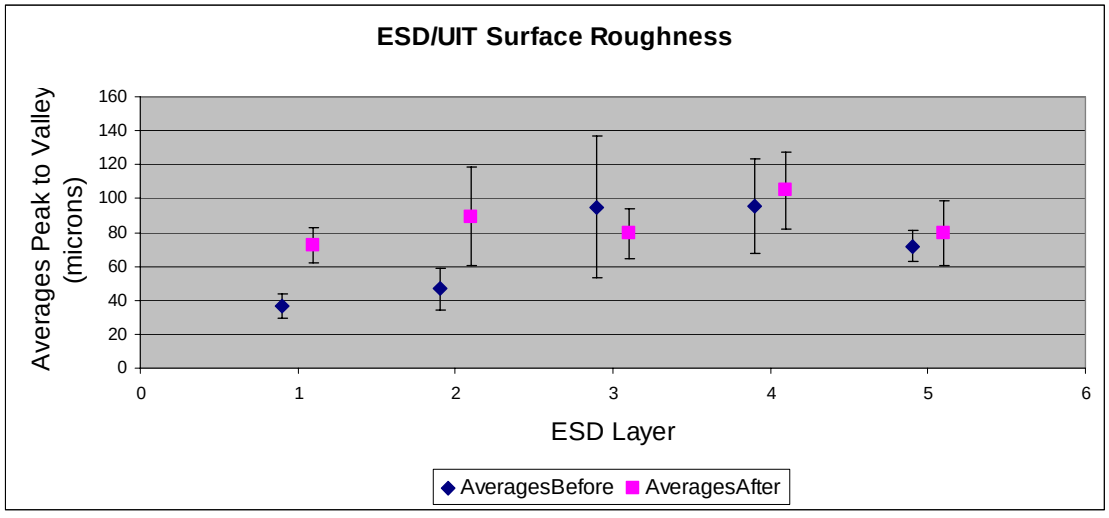

Figure 3-28 Average for Each Layer on 11A Before and After UIT (Error Bars Represent Plus and Minus One Standard Deviation)

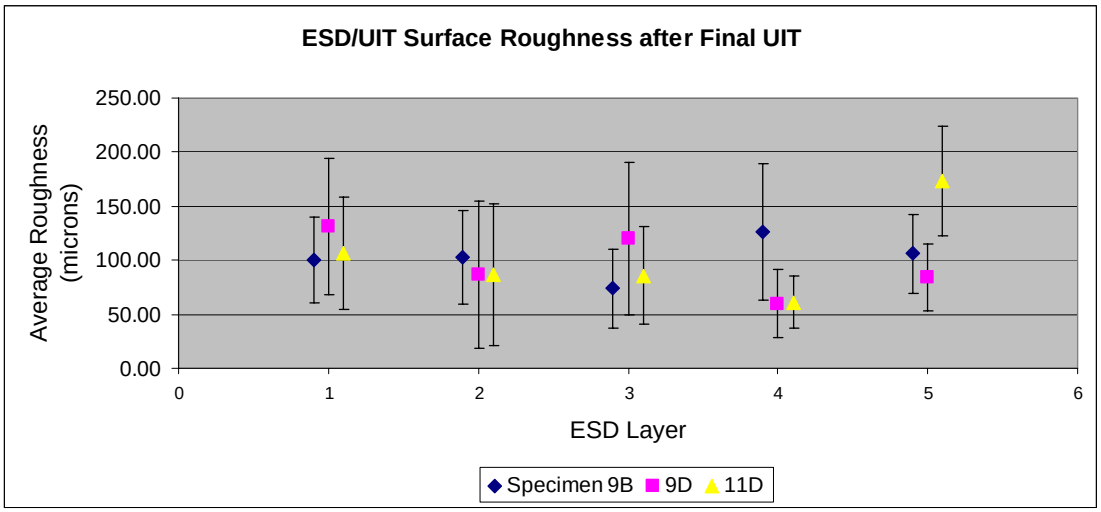

Figure 3-29 Surface Roughness Comparison of Three Different UIT Levels

3.5.2.5. DOE Analyses

In addition to designing the experimental matrix, the statistical software was used to analyze the data after testing. The data were evaluated in several ways including regressed functions, a test of correlation between outputs, effect of input on each output's mean value, interaction between experimental inputs and a prediction of optimized welding parameters based on maximizing deposition rate and minimizing discontinuities. Each type is discussed individually.

3.5.2.5.1. Regression Analysis

A regression analysis was conducted on the data. The results are summarized in Table 3-17. The linear regression output for deposition rate, hardness and porosity are available in the Appendix. The gas shielding types (argon or argon + hydrogen mixed) were represented as number (1 & 2 respectively) in the software.

Table 3-17 DOE Regression Analyses

Output	Constant	ESD Condition	UIT Condition	Shielding Gas	Number of Layers
Deposition Rate	0.116	0.000013	0.0	- 0.0045	- 0.00017
Hardness	457	0.0153	- 0.00006	5.8	- 9.6
Porosity	-0.44	0.000263	- 0.000012	0.257	0.21

A statistical test of how closely outputs are related to each other (or change simultaneously) is called Correlations. Two metrics were used, the Pearson Correlation and the P-Value. The Pearson range is from -1 to +1. Negative 1 indicates inverse relationships (one parameter increasing, the other decreasing), zero is no correlation and +1 is a direct relationship. The P-Value indicates a significant relationship if $P < 0.05$. Both of these metrics are listed in Table 3-18 correlating deposition rate, hardness and

porosity.

The largest Pearson term was 0.3 and the smallest P-Value was 0.076, indicating that neither metric found a significant relationship among the measured properties. This also means that it should be possible to control deposition rate, porosity and hardness independently.

Table 3-18 Correlations Among Outputs

		Hardness	Porosity
Porosity	Pearson	-0.040	
	P-Value	0.818	
Deposition Rate	Pearson	-.034	0.300
	P-Value	0.842	0.076

The effect of the four input parameters (ESD, UIT, gas, layers between UIT) on the outputs (deposition rate, porosity, hardness) can be characterized by a Mean Effect Plot which plots the mean of an output as a function of each input. Figure 3-30, Figure 3-31 and Figure 3-32 are the Mean Effect Plots for all three measured outputs. Deposition is strongly, positively affected by the ESD parameter (electrode speed), slightly positively by UIT conditions, slightly negatively by the welding gas type and not at all by the number of ESD layers between UIT treatments (Figure 3-30). Hardness is affected positively between the first and second ESD condition and not between the second and third. It is also affected by UIT parameters, both positively and negatively possibly indicating an optimum mid-UIT number. Gas type and number of layers between UIT treatments had less effect on hardness (Figure 3-31). Porosity is negatively influence by ESD, gas type and number of layers and partially positively by UIT conditions (Figure 3-32).

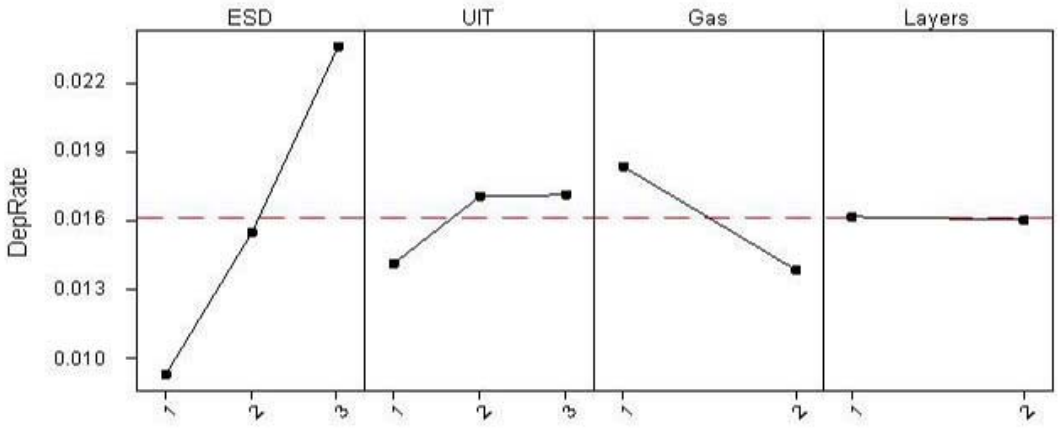

Figure 3-30 Effect of Input Parameters on Deposition Rate Mean

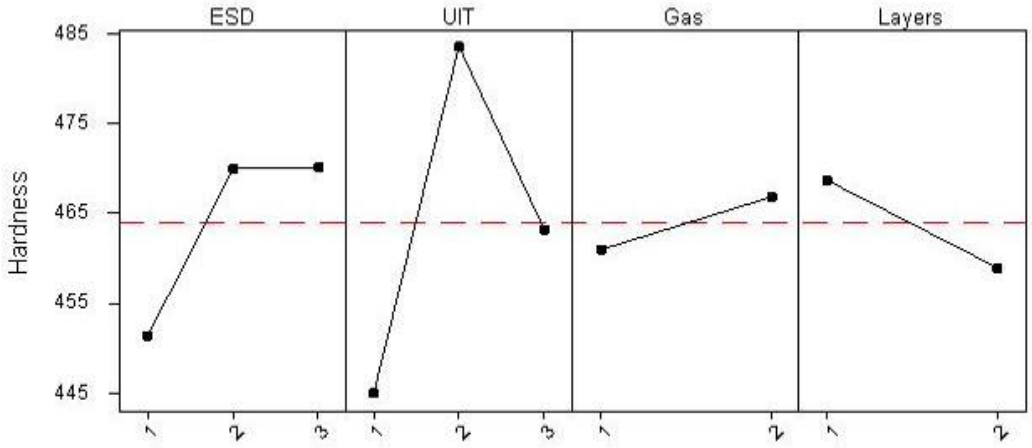

Figure 3-31 Effect of Input Parameters on Hardness Mean

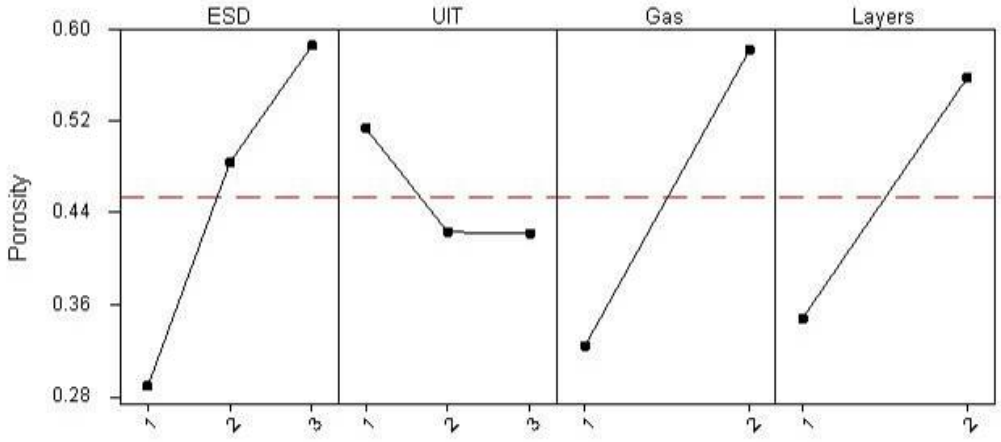

Figure 3-32 Effect of Input Parameters on Porosity Mean

Based on the relationships among the inputs and outputs, it is possible to statistically predict the best combination of inputs to achieve a desired optimized output. By specifying a desired output, the software calculates the necessary electrode speed, UIT intensity, number of ESD layers between UIT treatments and gas types to produce that output. Figure 3-33 illustrates the optimized inputs based on the request for maximized deposition rate, minimized porosity and an average hardness of 490 Knoop. The calculated optimum inputs are 700 rpm electrode speed, UIT condition 2, a gas mixture of approximately 2.5% hydrogen + argon and UIT every 1.5 ESD layers. The predicted outputs are a deposition rate of 0.016 g/minute, porosity of 0.46% and a hardness of 490 Knoop.

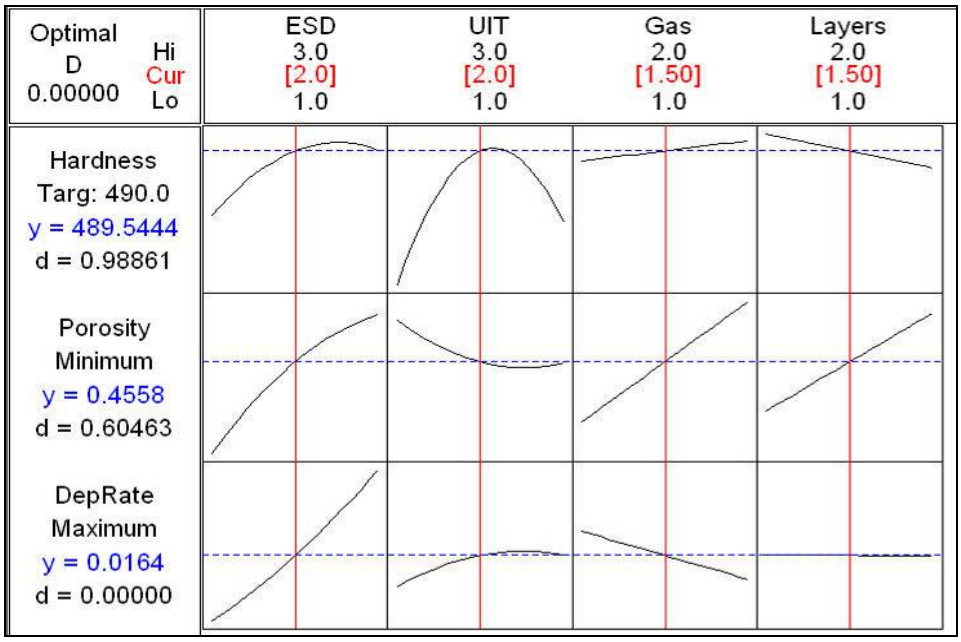

Figure 3-33 Statistical Analyses Optimization Plots

Interaction plots are graphical representations of how one input parameter affects the other input parameters for a given output. Interactions are indicated when the graphed lines depart from parallelism. Perpendicular lines mean strongest interaction. The statistical software produced three sets of interaction plots, one for each output (Figure 3-34, Figure 3-35 and Figure 3-36).

There was little interaction among the inputs for deposition rate. The strongest response occurred in the combination of highest ESD and UIT conditions (Figure 3-34). In the hardness set there were interactions between the number of ESD layers per UIT application and slowest electrode speed. Changing from argon to the mixed gas also interacted with the highest UIT parameter setting (Figure 3-35). For porosity there was a noticeable interaction between the two highest ESD and UIT conditions and a smaller but still notable interaction between shielding gas type and UIT and also between UIT and number of ESD layers between UIT treatments (Figure 3-36).

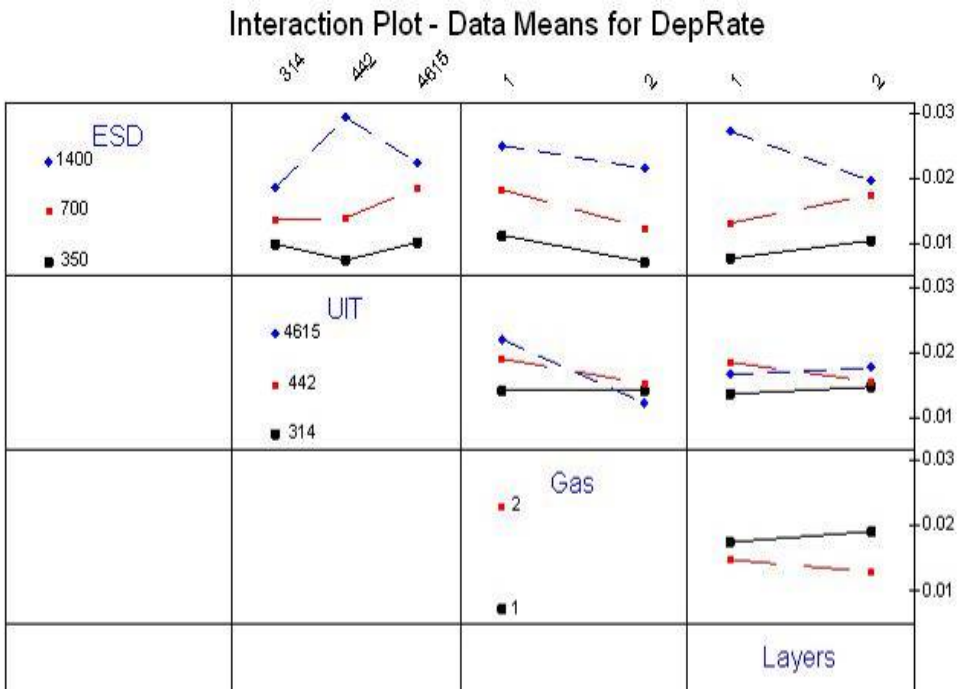

Figure 3-34 Statistical Interactions among Deposition Rate and Inputs

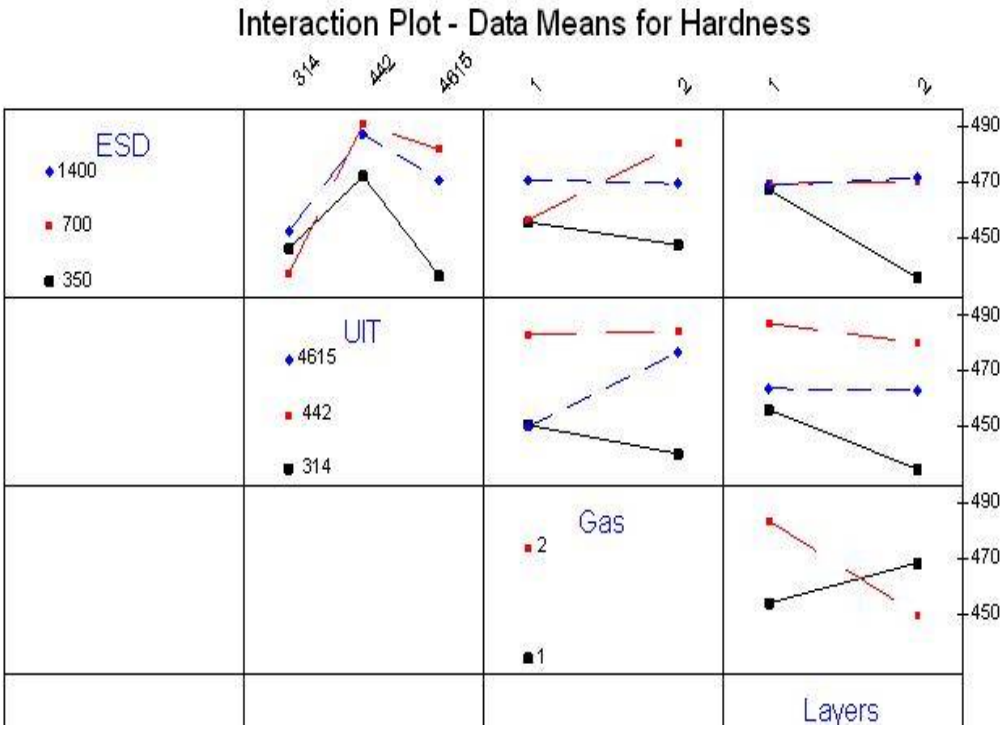

Figure 3-35 Statistical Interactions among Hardness and Inputs

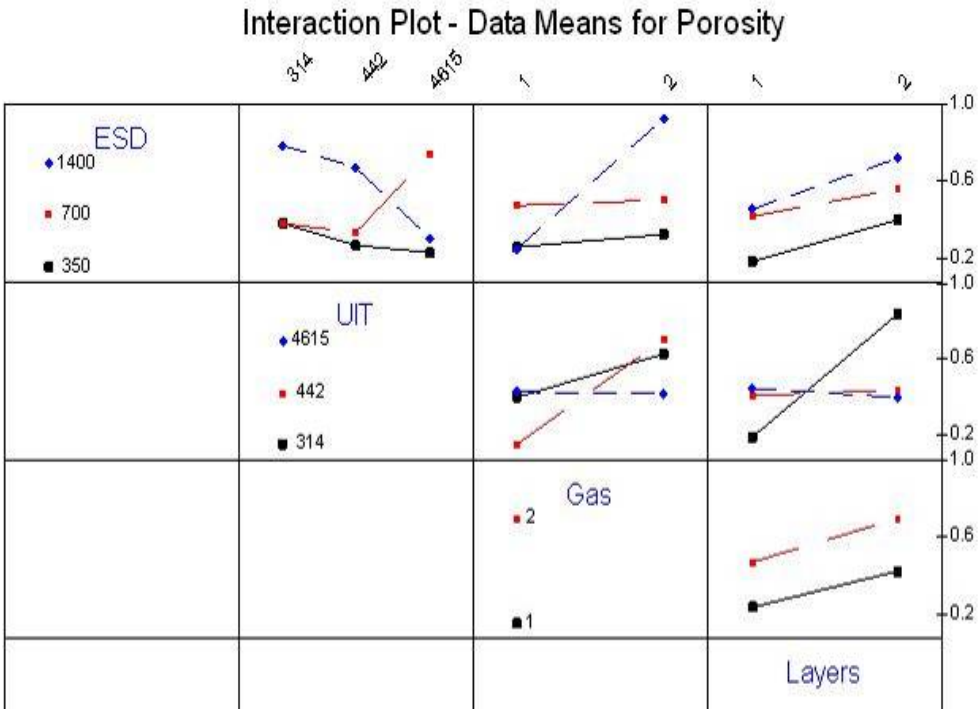

Figure 3-36 Statistical Interactions among Porosity and Inputs

3.5.2.6. Residual Stresses

Photos of the Residual Stress coupons with the chemically etched test spots are shown in Figure 3-37, Figure 3-38 and Figure 3-39.

Figure 3-37 Residual Stress Coupon (Baseline and As Deposited ESD)

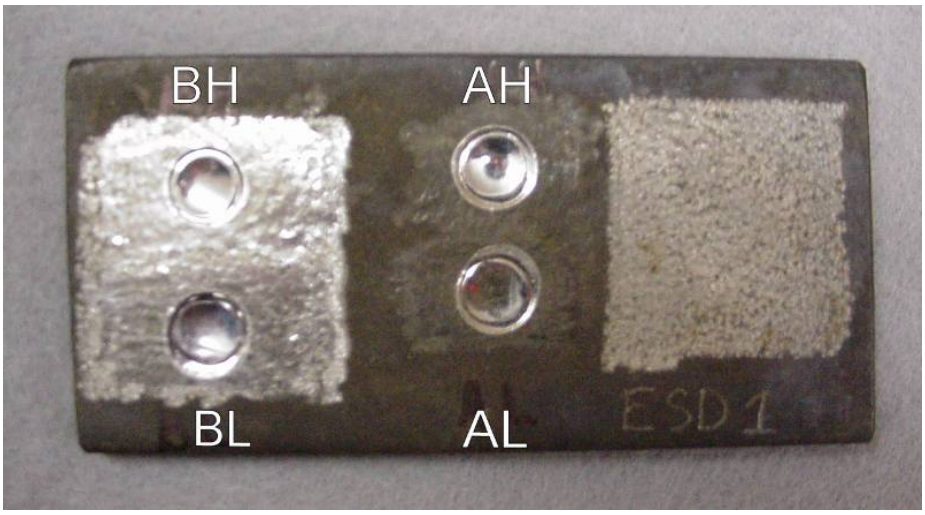

Figure 3-38 Residual Stress Coupon (Conditions AH, AL, BH and BL)

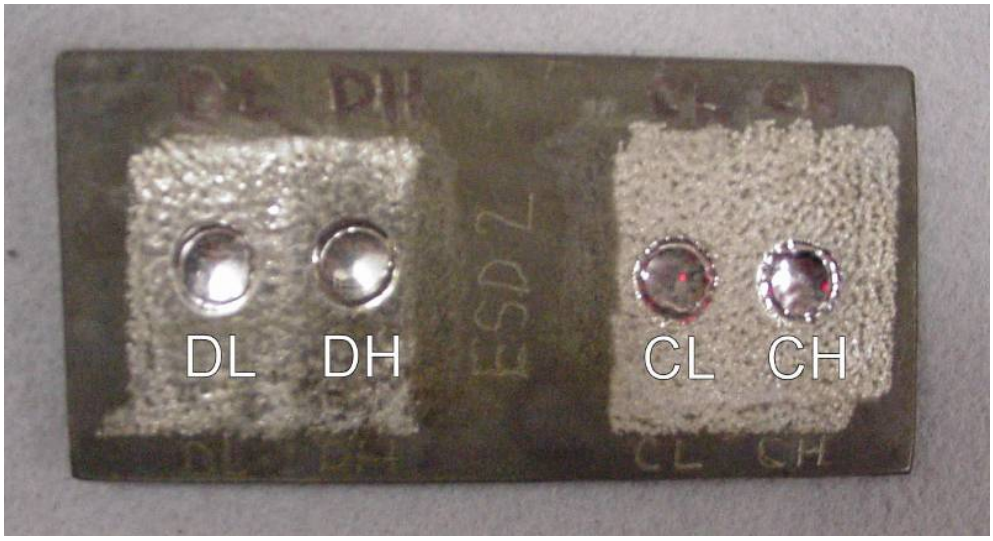

Figure 3-39 Residual Stress Coupon (Conditions CH, CL, DH and DL)

Residual stress results are listed in Table 3-19 as a function of the depth of reading. Figure 3-40, Figure 3-41 and Figure 3-42 compare the different conditions. Prior to any ESD or UIT the heat treated IN718 substrate was in compression to approximately 0.020" deep. The maximum stress was about - 60 ksi. ESD (no UIT) on the substrate was in tension, up to 100 ksi. Compressive stresses up to -150 ksi were developed in areas were UIT was employed. In all cases when ESD was the last treatment the surface was in tension. In all cases when UIT was the final step the surfaces and all areas underneath were in compression. Precision on the residual stress measurements varied between ±1 and ±4 ksi.

Table 3-19 ESD/UIT Conditions and Measured Residual Stress (ksi)

Depth (inches)	Base-line	ESD	AH	AL	BH	BL	CH	CL	DH	DL
0.0	-19	+67	-79	-83	-24	-54	+65	+55	-8	-45
0.005	-58	+93	-107	-118	-91	-116	-40	-63	-92	-115
0.010	-34	-47	-122	-137	-109	-127	-117	-101	-118	-123
0.015	-19	-31	-136	-138	-136	-149	-134	-119	-134	-141
0.020	-4	-11	-147	-138	-138	-143	-154	-113	-156	-136

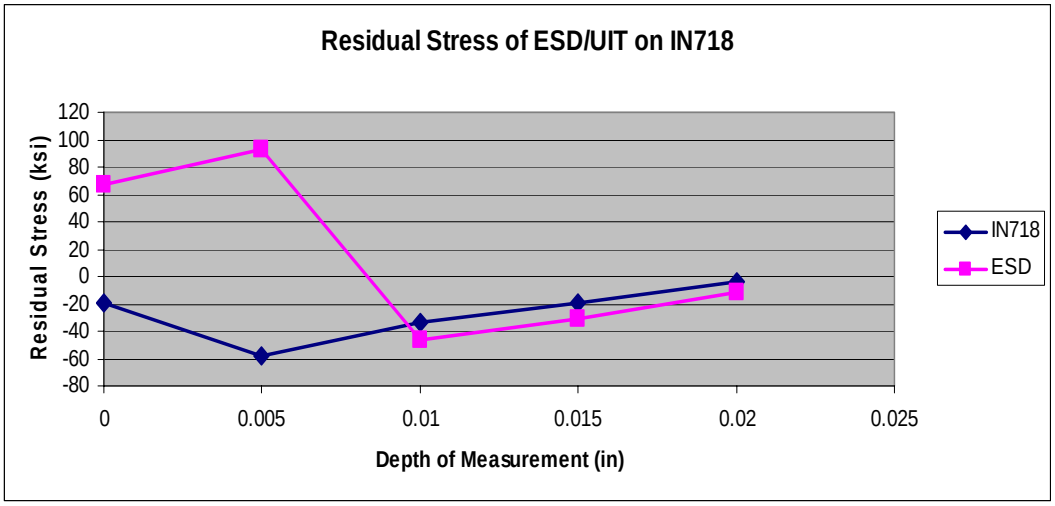

Figure 3-40 Residual Stress (ksi) of Baseline IN718 and IN718 As-Deposited with ESD

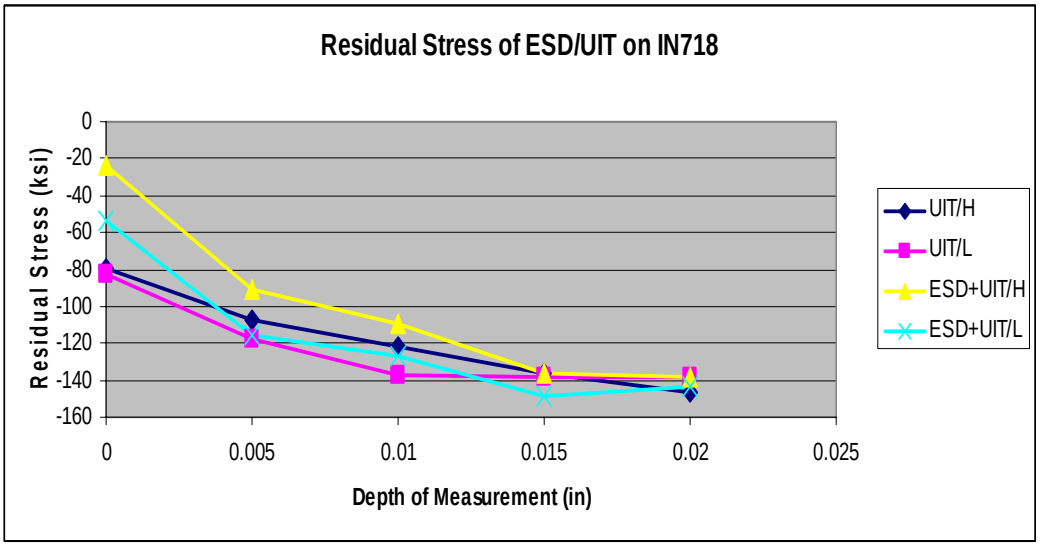

Figure 3-41 Residual Stress in IN718 with High and Low Intensity UIT and ESD Followed By High and Low Intensity UIT

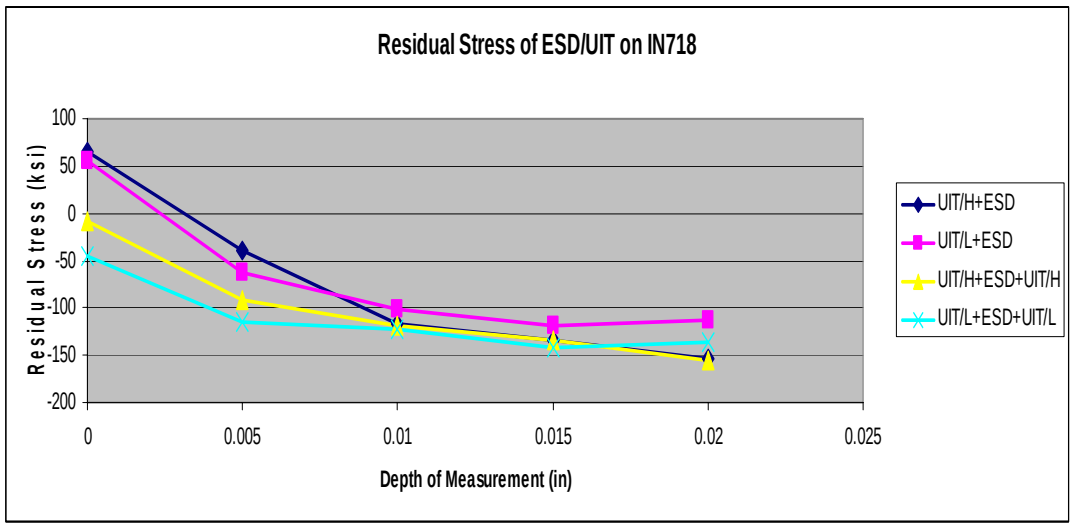

Figure 3-42 Residual Stress in IN718 with High and Low Intensity UIT Followed By ESD and High and Low UIT Followed By ESD and Followed Again By UIT Treatment

3.5.2.7. Deposition Rate

3.5.2.7.1. Deposition Rate Results

Deposition rates varied from 0.004 to 0.048 grams/minute as shown in Table 3-20. The amount of mass lost from the electrode compared to the amount of material actually deposited (% Efficiency) was between 40% and 93% with the majority of welding conditions producing at least 80%.

For this work, nearly all of the settings on the ESD power supply were held constant which resulted in the UIT Number and the electrode RPM being the two most important deposition rate controlling parameters. Multiplying the UIT number by the electrode rpm creates a single term that incorporates the two parameters. Table 3-21 lists the combined term for the different UIT and ESD experimental conditions. The deposition rate can then be plotted as a function of this combined term, grouped by either the electrode speed or UIT number. For a given UIT number, the deposition rate increased significantly for every increase in electrode rpm as shown in Figure 3-43. For example, in all three UIT number groups, as the electrode speed increases the deposition rate increases. However, when the electrode speed is held constant and the UIT number is varied, the deposition rate sometimes increased and sometimes decreased as shown in Figure 3-44.

When the shielding gas type is also incorporated into the ESD*UIT term (1 for argon, 2 for 95% argon + 5% hydrogen) the combined effect on deposition rate is shown in Figure 3-45. Except for one case, the deposition rate either remained the same or decreased when hydrogen was added to the shielding mix.

Table 3-20 Deposition Rates and Efficiencies

Run Order	Sample Number	ESD Level	UIT Level	# of UIT effected Layers	Gas Shielding	Electrode Material Loss (g)	Deposition Rate (g/min)	Percent Efficiency
8	1A	3	3	5	1	0.225	0.036	89.6
22	1B	3	3	2	1	0.231	0.029	87.2
1	1C	2	3	5	1	0.066	0.019	93.8
18	2C	2	3	2	1	0.175	0.023	87.6
11	3A	1	3	5	1	0.116	0.008	78.0
30	2D	1	3	2	1	0.113	0.017	89.2
14	3B	3	1	5	1	0.214	0.015	78.9
34	3C	3	1	2	1	0.124	0.020	89.7
32	4A	2	1	5	1	0.092	0.014	89.2
26	3D	2	1	2	1	0.173	0.015	82.5
15	4B	1	1	5	1	0.102	0.009	83.1
16	4C	1	1	2	1	0.116	0.012	84.5
19	5A	3	2	5	1	0.172	0.026	89.1
23	4D	3	2	2	1	0.188	0.026	88.2
7	5B	2	2	5	1	0.136	0.020	88.7
12	5C	2	2	2	1	0.122	0.020	89.6
21	5D	1	2	5	1	0.076	0.011	88.5
25	6A	1	2	2	1	0.088	0.011	86.5
5	9C	3	1	5	2	0.228	0.020	82.3
29	9B	3	1	2	2	0.221	0.020	82.9
10	8D	2	1	5	2	0.190	0.013	78.8
24	8C	2	1	2	2	0.185	0.013	79.6
31	8A	1	1	5	2	0.157	0.011	79.6
6	7B	1	1	2	2	0.200	0.008	67.9
13	10C	3	2	5	2	0.314	0.048	89.1
33	9D	3	2	2	2	0.200	0.018	82.7
17	11A	2	2	5	2	0.306	0.011	66.5
35	10A	2	2	2	2	0.177	0.015	81.6
2	11B	1	2	5	2	0.191	0.005	60.0
28	10B	1	2	2	2	0.111	0.004	67.5
3	11C	2	3	5	2	0.251	0.013	73.0
9	11D	3	3	5	2	0.256	0.019	79.8
27	12B	1	3	5	2	0.328	0.004	39.8
4	12A	2	3	2	2	0.200	0.020	84.2
20	10D	1	3	2	2	0.200	0.012	76.9
36	7A	3	3	2	2	0.077	0.006	81.8

Table 3-21 Combined (UIT Number) (Electrode RPM) Factor

		UIT Number (sec/sq.in.)		
		314	**442**	**4615**
Electrode Speed (RPM)	350	109,900	154,700	1,615,250
	700	219,800	309,400	3,239,500
	1400	439,600	618,800	6,461,000

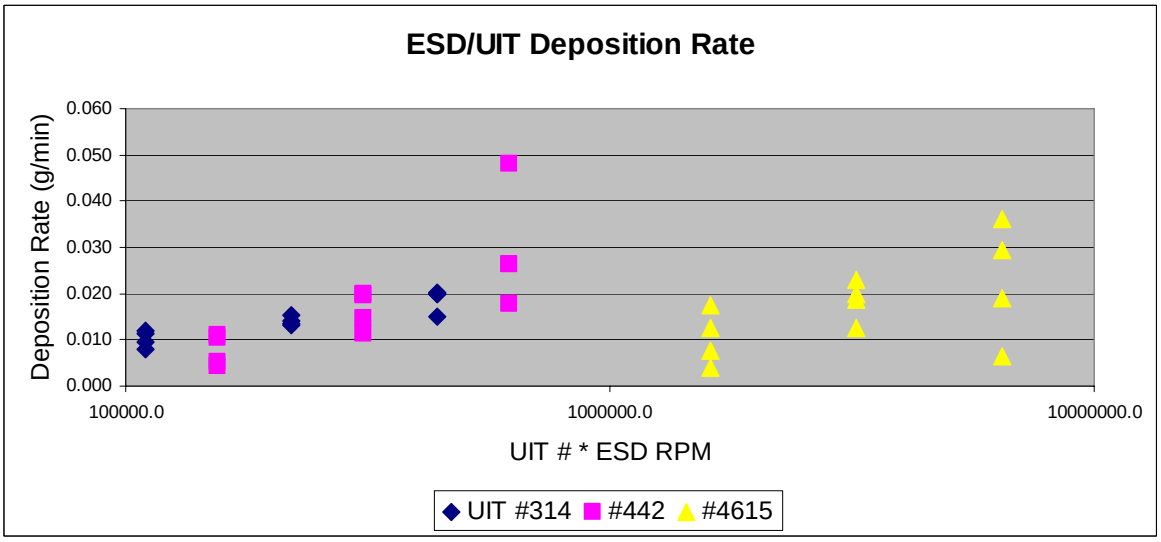

Figure 3-44 Deposition Rate as a Function of the Product of UIT # and Electrode Speed grouped by UIT Number

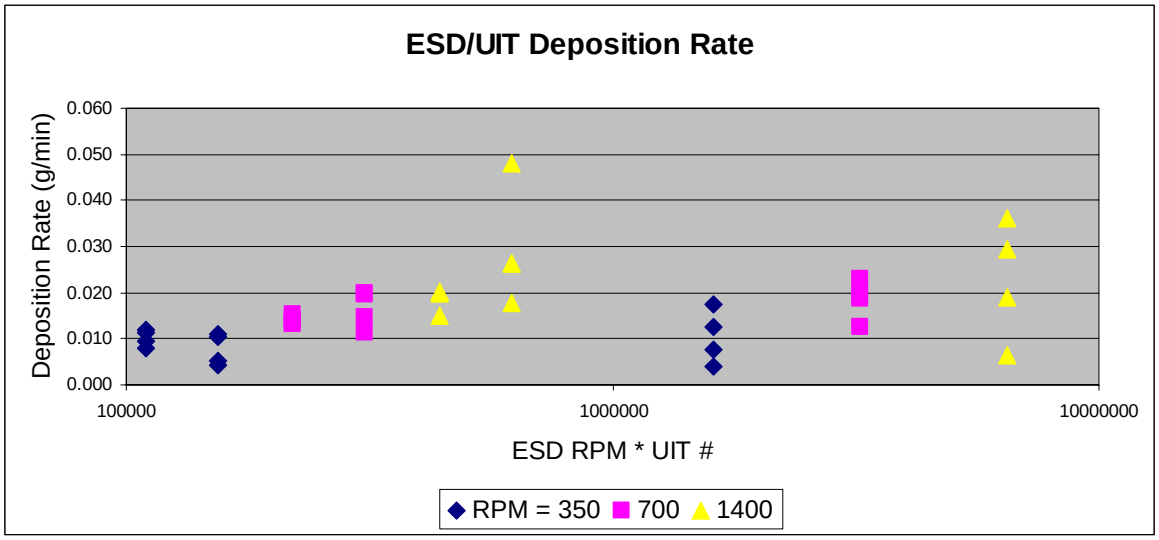

Figure 3-43 Deposition Rate as a Function of the Product of UIT # and Electrode Speed Grouped by Electrode Speed

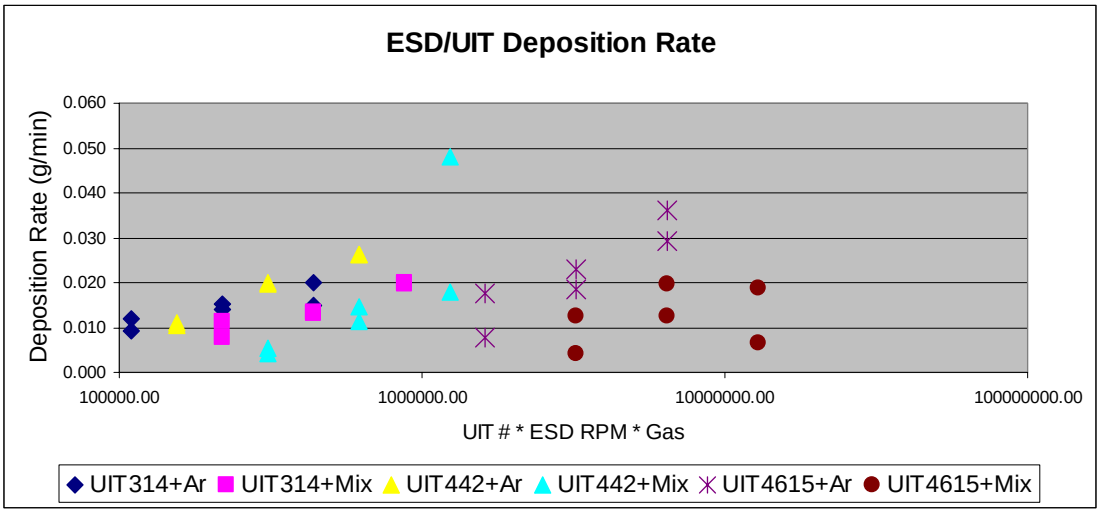

Figure 3-45 Deposition Rate as a Function of the Product of Electrode Speed, UIT # and Shielding Gas Type Grouped By UIT #

3.5.3. Improvement with Each Phase

Optimizing ESD welding parameters and the addition of UIT to the process has resulted in significant improvement in the ESD process. Each successive phase of this effort has resulted in increased deposition rates and decreased discontinuities. The change in deposition rates and discontinuities for each phase of this project are shown in Figure 3-46.

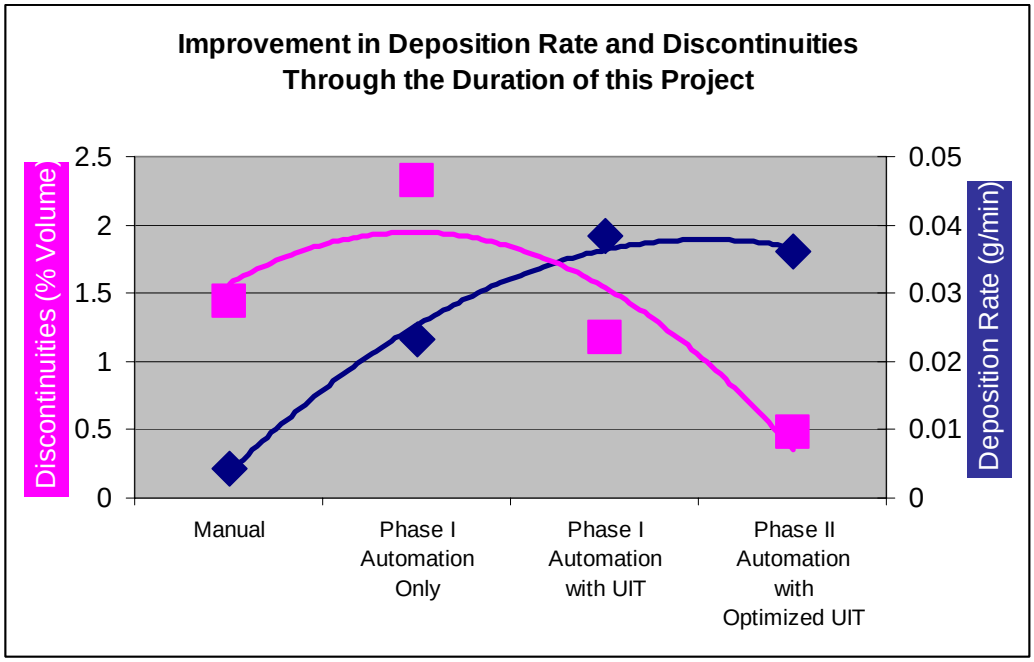

Figure 3-46 Deposition Rates by Project Phase

At the conclusion of this work two additional attempts were made to increase the deposition rate based on the project results and operator experience. The welding conditions for those two additional attempts were a pulse rate of 800 Hz, current of 8 A, capacitance of 30 µF, voltage of 200 V, electrode rotation of 1400 rpm, UIT power supply setting of 9, Y-direction traverse speed 14% of maximum on the controller dial (0.11 in/min).

The resulting deposition rates of the two conditions were approximately 0.052 and 0.055 g/min as shown in Figure 3-47. The deposition doubled in phase two, averaging approximately 0.02 g/min with a maximum of 0.035 g/min. compared to less than 0.01 g/min average in the first phase. The two maximized deposition rates were more than five times the average of the first phase and almost 60% higher than the best results from the DOE matrix. Initially deposition increases were achieved at the expense of porosity, an increase in one resulting in a decrease in the other. This effort has produced better deposition rates with reduced discontinuity levels. Porosity has decreased from an average of approximately 1.5% to typically below 0.5%.

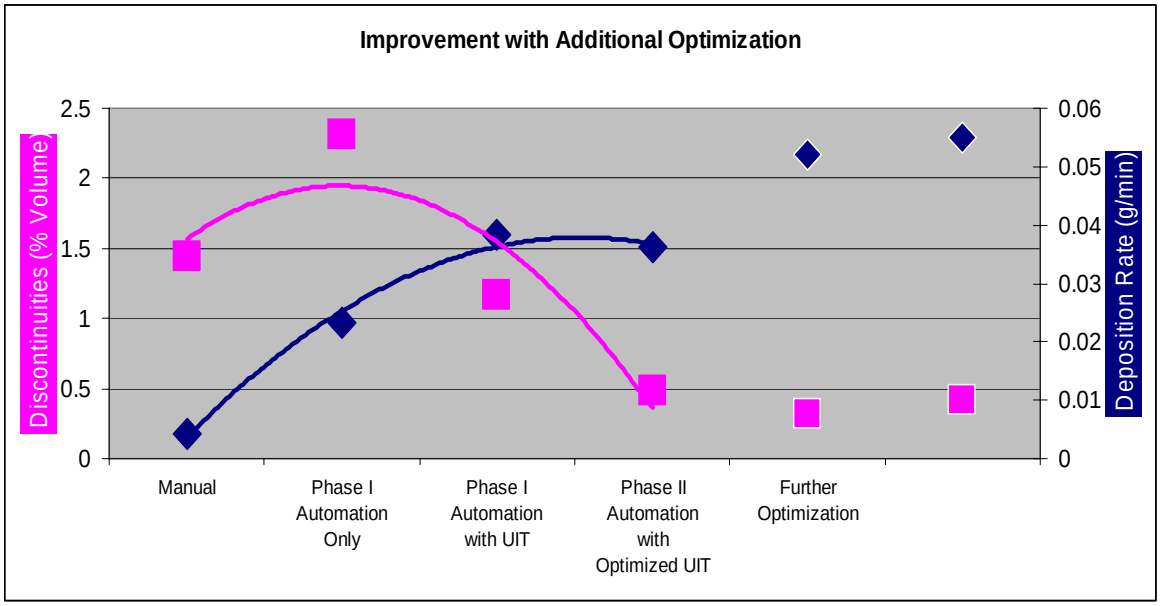

Figure 3-47 Further Improvement with Additional Optimization

3.6. Conclusions

- The ESD deposit, when applied with robotic automation and treated with UIT, shows an improvement in PDR over ESD applied manually without UIT by approximately a factor of 13.
- The ESD deposit, when applied with robotic automation and treated with UIT, shows a decrease in discontinuities over ESD applied manually without UIT of approximately a factor of 4.5.

- The microhardness of the ESD deposit, when applied with robotic automation and treated with UIT, was 1.5 times higher than the ESD applied manually without UIT.
- This work demonstrated a vast improvement in quality (discontinuities) and deposition rates of an ESD deposit on IN718 through automation and UIT.

This page intentionally left blank.

4. Application of ESD for Repair of Gas Turbine Engine Components

4.1. Introduction

4.1.1.Background

The objective of this project was to qualify ESD as technically feasible and economically viable for the repair of gas turbine engine components. As discussed in Section 1.2, a complete Demonstration Plan titled "Electrospark Deposition for Localized Repair of Gas Turbine Engine Components" [1] was developed in accordance with ESTCP requirements for the validation of the ESD process. Incorporated into the Demonstration Plan was a Joint Test Protocol (JTP) that covered the materials testing of the ESD process related to GTE components. The JTP was produced through meetings and electronic communication involving all of the stakeholders and delineates all of the materials testing required to qualify ESD for a production-scale process. The stakeholders included DOD GTE repair facilities and GTE OEMs.

Prior to the execution of the JTP, the ESD process was optimized and the information gathered in the optimization process was used in preparing the mechanical test specimens for the JTP. Optimization also included the selection of materials (substrates, electrodes and non-ESD coatings), metallurgical evaluation and some mechanical testing. The results of optimizing the ESD process are presented in Section 4.2.

Using the optimum ESD parameters and techniques, mechanical test specimens were prepared and additional material data was generated. This data was crucial in determining the ESD repair procedures for selected and future GTE components. The results of the mechanical testing are presented in Section 4.3.

Using the optimum ESD parameters and techniques, mechanical test specimens were prepared and additional material data was generated in accordance with the JTP. This data was crucial in determining the ESD repair procedures for potential GTE components. The results of the mechanical testing are presented in Section 4.3.

In addition to materials testing, demonstration of the ESD process for repair of selected GTE components was part of this effort and the results of those demonstrations are presented in Section 4.4.

4.1.2. Materials Selection

Substrate materials for evaluation were selected based on an assessment of the types of alloys principally used for fabrication of GTE components in DOD engines. These included Inconel 718 (IN718), Ti-6Al-4V and 410 stainless steel (410SS). Because of its primary importance to OC-ALC, IN718 was used for the materials testing. For self-repair of components, ESD electrodes of the same material were fabricated and coatings applied to each of these substrate materials. In addition, IN718 specimens were prepared with EHC coatings for the purpose of demonstrating repair of damage in EHC. For this application, the ESD electrode material was Inconel 625 (IN625). The materials

evaluated are shown in Table 4-1. The heat treat conditions for the substrate materials

Table 4-1 Materials Selected for Evaluation

Substrate	ESD Electrode	Non-ESD Coating
IN718	IN718	None
Ti-6Al-4V	Ti-6Al-4V	None
410SS	410SS	None
IN718	IN 625	Electrolytic hard chrome

Table 4-2 Heat Treat Condition of Substrate Alloys

Alloy	Heat treat
IN718	Age @ 1325°F for 8 hr, F/C to 1150 and age @ 1150°F for 18 hr total time per AMS 2774
Ti-6Al-4V	as received
410SS	Preheat @ 1400°F for 1 hr, Austenitize @ 1800°F for 30 min, Temper @400°F for 2 hr per AMS 2759/5

are shown in Table 4-2.

4.1.3.Preparation of Test Defects

Since the objective of this work was to demonstrate that ESD could be used to repair localized damage such as wear scars and corrosion pits on GTE components, in order to perform materials tests that would demonstrate this capability it was necessary to develop and define "standardized" defects in test coupons. Table 4-3 describes the defect geometries that were developed. Each defect was designated with a specific type number. The purpose of selecting these geometries was to assess reparability and reproducibility in typical repair situations.

Table 4-3 Defect Geometries

Groove type	Dimensions	Applications
Type 1	0.25" diameter, 0.020" deep	Point repair
Type 1a	0.10" diameter, 0.006" deep	Point repair of non-ESD coating, not penetrating substrate
Type 1b	0.15" diameter, 0.014" deep	For tensile and fatigue tests
Type 2	0.375" wide, 0.020" deep, axial groove	For Hamilton Sundstrand wear test

Type 1, 1a and 1b defects. Type 1 defects are "point" defects made by ball milling or ball grinding a surface divot with dimensions as shown in Figure 4-1. Type 1a defects are designed to be used for evaluating repair of a coating such as EHC as opposed to a bulk material and are illustrated in Figure 4-2. For this type of defect, the coating to be repaired is thicker than the defect depth (~ 0.015"). Flat coupons (1" x 1" x 0.125") were

used for these specimens and one "defect" was made in each specimen. The defect was filled with ESD material and was used as-deposited or ground flat, as specified in the JTP. Type 1b defects, illustrated in Figure 4-3, are for tensile and fatigue specimens. Because of the geometry of these test specimens, a smaller diameter defect was required to prevent the defect from being wider than the gage length of the test specimens. A typical coupon with a Type 1 defect is shown in Figure 4-4.

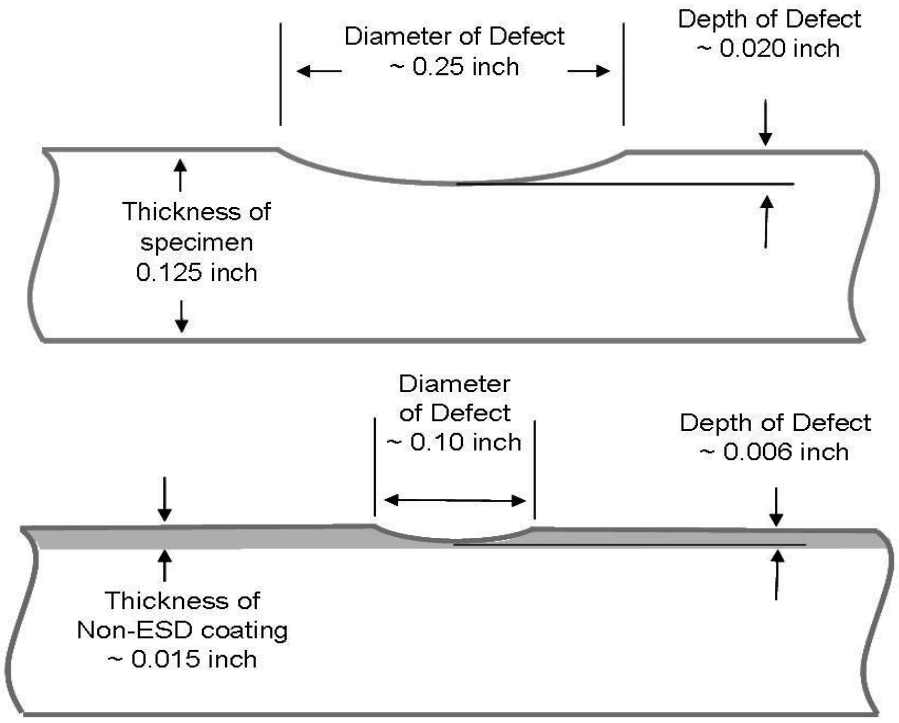

Figure 4-2 Illustration of Type 1a Defect

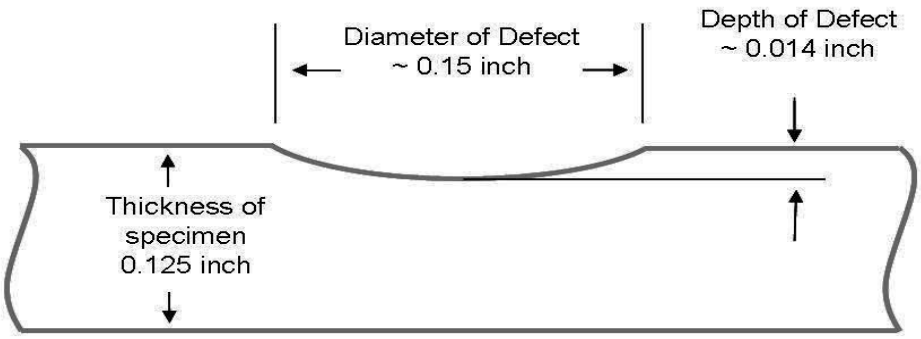

Figure 4-3 Illustration of Type 1b Defect

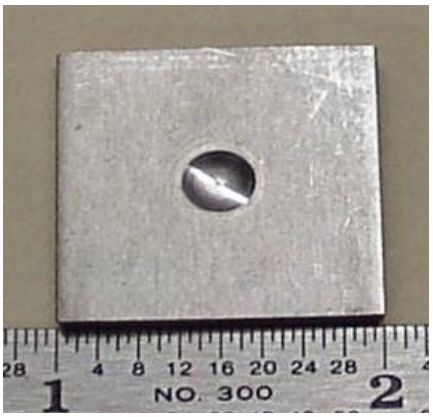

Figure 4-4 Type 1 Defect in Coupon

Type 2 defects. Type 2 defects were axial groove defects used on wear test plates. The wear tests performed for these studies utilized test equipment designed and constructed by Hamilton Sundstrand, with the wear testing performed by United Technologies Research Center. The description of the wear test apparatus is provided in Section 4.3. The Type 2 defects were made by ball milling or ball grinding a surface groove with dimensions as shown in Figure 4-5. An illustration of a Type 2 defect in a test plate made using a 5/8" ball end mill is shown in Figure 4-6. The defect was filled with ESD material and the specimen machined or ground to a uniform flat surface. (There were actually four defects in each test specimen, as described in Section 4.3)

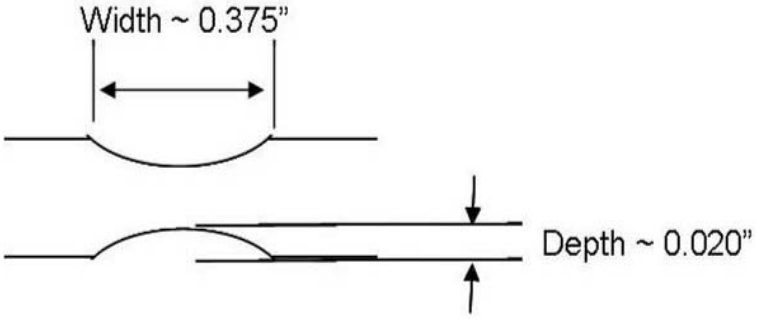

Figure 4-5 Illustration of Type 2 Defect

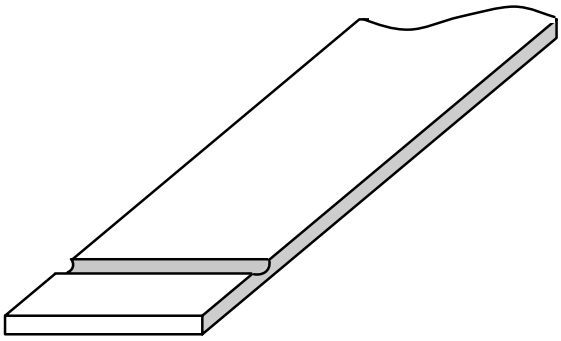

Figure 4-6 Illustration of Type 2 Defect in Test Plate

4.1.4. Welding Procedure Specification

For each deposition, the deposition conditions and quality control (QC) measurements were recorded, together with any additional data required to reproduce a particular repair. Sufficient data was recorded to ensure that the repair conditions could be reproduced elsewhere. A typical deposition record is shown in Figure 4-7.

Welding Procedure Specification (WPS) For Electro-Spark Deposition (ESD)

Company: HCAT/PEWG Prepared By: Jim Reynolds (EWI)
Welding Procedure Specification No.: Date: 01/05/04
Revision No.: Date:

Configuration/Application Details
Notes:
Divot is produced using a ball mill with a 0.5-in radius.

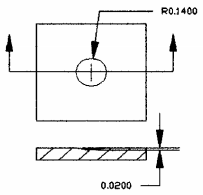

Base Metal
Specification Type and/or Grade: IN718 Fully Heat Treated
Chemical Analysis and Mechanical Properties:
Part Description: Optimization Sample
Notes:

Filer Metal/ Electrode
Specification Type and/or Grade: AMS5832, IN718
Manufacturer: e Heat: Size: Per DOE
Manufacturing Method: Wire Preparation: 45 Deg. Blunt Point

Electrode Motion
☒ Rotation
Electrode RPM: Per DOE Direction: Clockwise

☐ Oscillation-Rotation
Step-Rate: Swing: RI:
Rotation: Interval:

Shielding Gas:
Gas Composition: 100%Ar
Flow Rate: 50CFH
Method: External

Preheat
Minimum Preheat Temperature: N/A
Maximum Interpass Temperature: N/A
Preheat Maintenance Temperature: N/A

Position
Position of Joint/Surface: Flat
Progression: Up ☐ Down ☐

Post Weld Heat Treatment
Temperature: Refer to attached heat treat schedule
Time: Refer to attached heat treat schedule

Electrical Characteristics
Power Supply Manufacturer/Model: ASAP/Model PS 98 MKII
Capacitance: Per DOE Frequency: Per DOE Current: Floating Voltage: Per DOE
Voltage Control (Reference Only): 5.6 Current: AC ☐ DC ☒ Polarity: DCRP
Notes:

Technique
Technique: Weave
Pre-Cleaning (Brushing, Grinding, etc): Acetone Wipe
Interpass Cleaning (Brushing, Grinding, etc): Wire brush and grind as needed to minimize lumping
Notes: Stick out = 0.75

Authorized By: **Date:**

Figure 4-7 Typical ESD Process Sheet

4.1.5.Post ESD treatments

Although some previous studies have shown that heat treatment following ESD deposition can affect the properties of the coatings, for these studies post-deposition heat treatments were not conducted because the intent was to minimize the number of process steps required to provide an adequate repair to a component. Ultrasonic impact treatment

(UIT) as described in Section 3, which is basically used in conjunction with ESD deposition, was utilized on some test specimens for inducing and/or relieving stresses and for improving the density of the coatings. Post-ESD surface finishing such as grinding or polishing was normally conducted on specimens in order to bring the surface finish of the coating to that of the surrounding, non-defected material.

4.1.6. Test Standards

The JTP used standard tests as much as possible, with non-standard tests being used where standard tests were considered to be non-existent or inadequate. The ASTM tests listed in Table 4-4 were used in the execution of the JTP. For additional information, the reader is referred to the Performance Review Institute's website (http://www.pri.sae.org/ipt/viewbest.htm).

Table 4-4 Test Standards Used in Execution of JTP

Test	Description
ASTM B117	Standard methods of Salt spray (fog) corrosion testing
ASTM B578	Standard methods for microhardness of electroplated coatings
ASTM C633	Standard methods of an Adhesion/Bond strength test
ASTM E3	Standard methods of preparation of metallographic specimens
ASTM E340	Standard methods of macro-etching metallographic specimens
ASTM E384	Standard methods of microhardness – applied loads less than 1 kgf – for both interior and surface – Knoop and Vickers
ASTM E466	Standard methods of low cycle fatigue (LCF) testing
ASTM E8	Standard methods of room temperature tensile testing

4.2. ESD Optimization

4.2.1. Introduction

The main thrust of the JTP was to evaluate the material properties and performance of ESD deposits relevant to GTE applications. In order to insure that ESD parameters were used that provided the highest quality coatings, it was necessary to consider the optimization, control and characterization of the ESD being deposited. A design of experiment (DOE) routine was selected as the appropriate method for evaluating optimization of the ESD process. The optimized parameters were then used for coating deposition on the mechanical test specimens.

A DOE is a statistical methodology for analyzing and later predicting relationships

between two or more factors. DOEs are constructed with two fundamental concepts: conducting the DOE and evaluating the DOE. The steps vital to proper execution and evaluation of a DOE are as follows:

1. Define goals and establish objectives to select proper responses to measure
2. Determine influential factors
3. Define factors limits
4. Define test matrix
5. Establish test matrix
6. Execute test matrix
7. Collect data for each response in each trial
8. Analyze data collected to build optimization equations for each response
9. Determine optimal ESD parameters
10. Validate results by testing developed parameters

The DOE can optimize both technical performance and economic viability (deposition rate, etc.). It is believed that by using the DOE methodology the interaction that occurs between factors can be resolved and the process optimized with a minimal amount of experimental work.

4.2.2.DOE Inputs

Initially, the DOE was conducted by Edison Welding Institute (EWI) on IN718 material only. The key variables were determined to be pulse frequency, voltage, capacitance, electrode speed and electrode size. Once these parameters are selected, the current, as displayed by the ESD equipment, is a dependant variable. Current limitations were established based on the capabilities of the available ESD equipment. Figure 4-8 displays the limitation of the current as a function of voltage and pulse frequency for each capacitance setting. The equipment operates best under 8 amps. Any point above the curves displayed in Figure 4-8 would result in a current that exceeds this limit. Therefore, combinations of voltage and pulse rate frequency at a selected capacitance were always limited to the region below the curves in Figure 4-8.

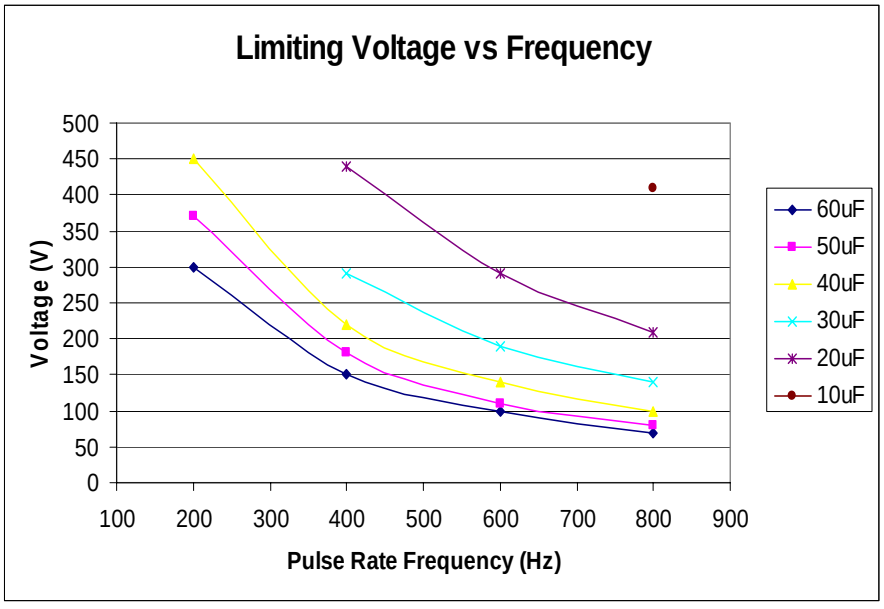

Figure 4-8 Limiting Voltage vs. Frequency

Several types of DOE approaches were evaluated and the Box Behnken method [10] was selected, due to its increased statistical stability and its ability to interpret the interactions between factors. The initial test matrix in this work, conducted on IN718, evaluated five factors at three levels. An outline of the trials is provided in Table 4-5

Table 4-5 IN718 DOE Test Matrix

Run Order	Pulse Rate	Voltage	Capacitance	Electrode Speed	Electrode Size
	Hz	**Volts**	**μF**	**rpm**	inch
1	300	80	40	1200	0.09375
2	500	80	40	1200	0.09375
3	300	130	40	1200	0.09375
4	500	130	40	1200	0.09375
5	400	105	30	800	0.09375
6	400	105	50	800	0.09375
7	400	105	30	1600	0.09375
8	400	105	50	1600	0.09375
9	400	80	40	1200	0.0625
10	400	130	40	1200	0.0625
11	400	80	40	1200	0.125
12	400	130	40	1200	0.125
13	300	105	30	1200	0.09375
14	500	105	30	1200	0.09375
15	300	105	50	1200	0.09375
16	500	105	50	1200	0.09375
17	400	105	40	800	0.0625
18	400	105	40	1600	0.0625
19	400	105	40	800	0.125
20	400	105	40	1600	0.125
21	400	80	30	1200	0.09375
22	400	130	30	1200	0.09375
23	400	80	50	1200	0.09375
24	400	130	50	1200	0.09375
25	300	105	40	800	0.09375
26	500	105	40	800	0.09375
27	300	105	40	1600	0.09375
28	500	105	40	1600	0.09375
29	400	105	30	1200	0.0625
30	400	105	50	1200	0.0625
31	400	105	30	1200	0.125
32	400	105	50	1200	0.125
33	300	105	40	1200	0.0625
34	500	105	40	1200	0.0625
35	300	105	40	1200	0.125
36	500	105	40	1200	0.125
37	400	80	40	800	0.09375
38	400	130	40	800	0.09375
39	400	80	40	1600	0.09375
40	400	130	40	1600	0.09375
41	400	105	40	1200	0.09375
42	400	105	40	1200	0.09375
43	400	105	40	1200	0.09375
44	400	105	40	1200	0.09375
45	400	105	40	1200	0.09375
46	400	105	40	1200	0.09375

The DOE coupons were prepared at both EWI and ASAP. This allowed for comparison of the effect of applying ESD at different sites. It was assumed that there would be no effect.

The DOE was executed on flat coupons, containing Type 1 defects as shown in Figure 4-4. Each defect was filled, based on the settings described for each trial. If the defect did not fill after four hours, the process was stopped. All ESD was performed at room temperature with argon cover gas. IN718 parameters used (DOE inputs) are summarized in Table 4-6 and Table 4-7.

Table 4-6 IN718 DOE Inputs - Multiple Levels

Multiple Levels	
Parameter	**Range**
Pulse Rate	300 – 500 Hz, increments of 100
Voltage	80 -130 V, increments of 25
Capacitance	30 – 50 μF, increments of 10
Electrode Revolution speed	800 – 1600 rpm, increments of 400
Electrode Size	0.125 - 0.09375 inch (1/8, 1/16, 3/32)

Table 4-7 IN718 DOE Study - Fixed Levels

Parameter	Fixed Value
Shielding Gas	Argon
Cleaning Frequency	As needed
ESD Surface reshaping (i.e. filing)	As needed
Operating Environment	Room temperature

4.2.3. DOE Outputs

The DOE was evaluated using measured outputs. The recorded outputs were deposition rate, microhardness and deposit discontinuities. Other outputs that were noted included current, surface finish, microstructure, and the results of non-destructive evaluation (NDE).

The outputs were recorded in a spreadsheet and/or on forms designed by Edison Welding Institute. One, the Welding Procedure Specification (WPS) (Figure 4-7 in Section 4.1), was used to record inputs which would not vary, such as the shielding gas composition and flow rate. The other, the ESD Trailer Data Sheet shown in Figure 4-9, used to record varied inputs, such as capacitance and voltage, as well as measured outputs such as the initial and final weights of the coupons (Figure 4-9).

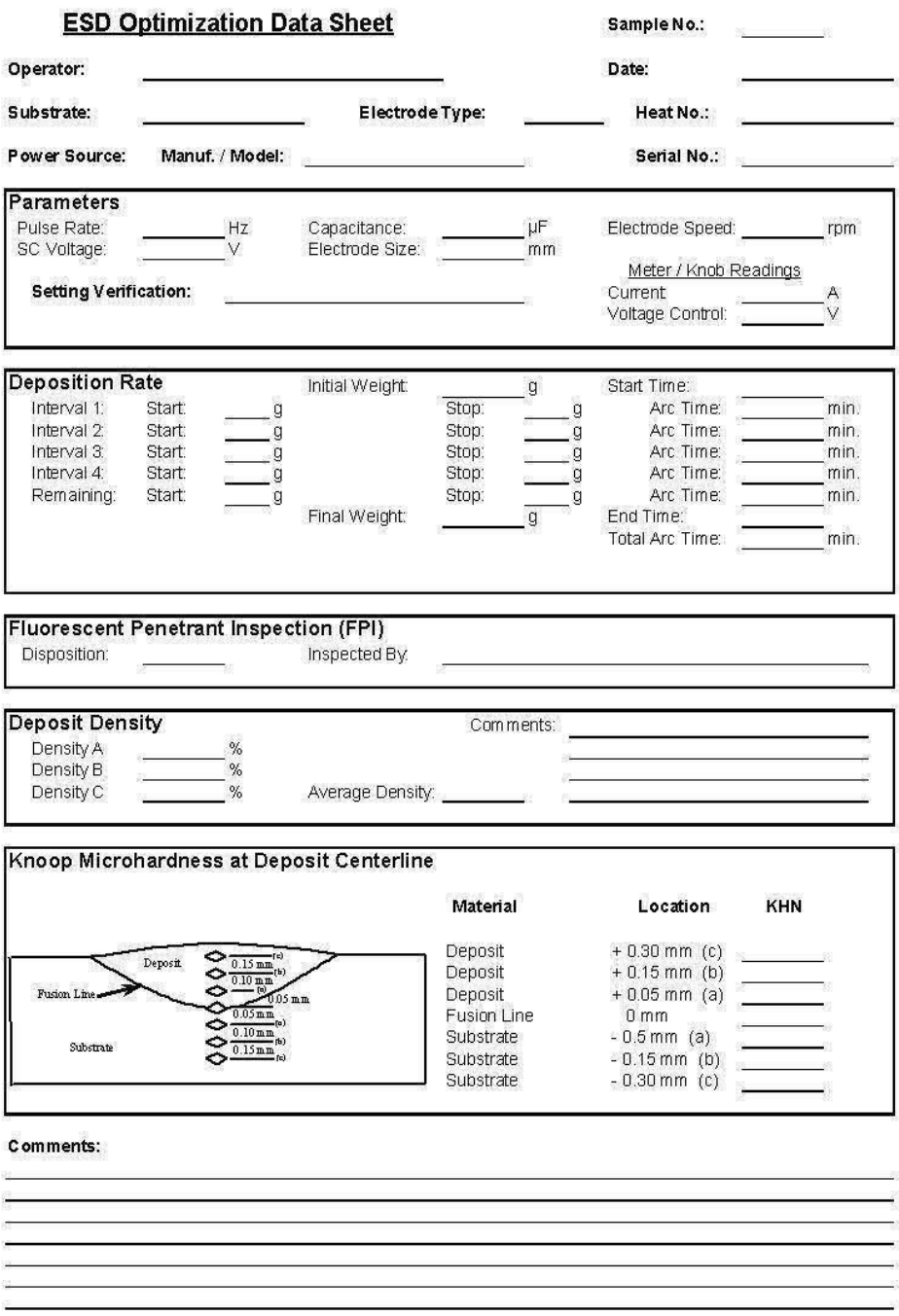

Figure 4-9 The ESD Trailer Data Sheet

These outputs were analyzed by generating statistical models that represent the response each output has to the selected factors and the compounding that occurs as each factor has an effect on other factors. Next, regression analysis was conducted that defines an optimization algorithm that most accurately depicts the measured outputs. The optimization algorithm was then confirmed via validation trials. The outcome of the validation trials was compared to the prediction produced by the optimization algorithm.

The correlation between the actual measured outputs and the predicted outputs was used to establish statistical certainty.

Following is a description of each of the outputs and how they were obtained.

4.2.3.1. Deposition Rate

Deposition rate may be the most important output parameter, as it is critical to the cost benefit analysis (CBA) of an ESD repair on GTE components. However, deposition rate alone should not be the basis for selecting ESD as a viable repair. The entire component repair time (including fixturing, masking, post heat treat, post machining, etc.) should be included when comparing the ESD process to other processes. Deposition rate is a measurement of the amount of material deposited (as recorded by weight gain of the coupon) and time required to perform the repair. Two measurements were recorded; material transfer rate and actual component repair rate. The former was recorded as the actual rate at which material is deposited while the equipment is running. The latter included the time spent on tip reshaping, surface filing, and other necessary jobs.

Each coupon was weighed prior to and after ESD and recorded. The change in weight divided by the recorded time provided the deposition rate. A stopwatch was used to record the actual time that the ESD equipment was operating (sparking). This was the material transfer deposition rate (also referred to as ATDR or "weld deposition rate"). In addition, the operator recorded the total time spent on ESD application, including time to reshape the electrode tip and resurface the deposited material if necessary. This was the repair deposition rate (referred to as PDR or "total weld time deposition rate"). It did not include operator breaks or non-production activities (such as weighing the coupon).

4.2.3.2. Microhardness

The objective of obtaining microhardness was two-fold; one, to determine the characteristics of the heat-affected zone (HAZ), and two, to establish a relationship between microhardness and wear characteristics of the ESD deposit. The microhardness of an ESD repair is critical as it may be important to attain microhardness (and presumably wear characteristics) similar to the parent material. If the microhardness is not similar, the wear characteristics of the part and/or mating part may be affected. While an increase in microhardness of the part repaired via ESD may be desirable, optimization was based on matching the parent material microhardness. In general, microhardness of ESD-repaired area should be within ±20% of the base material.

Coupons prepared in cross-section were used for the microhardness analysis. ASTM B578, a standard method for microhardness of electroplated coatings, was used to measure microhardness at several locations across the substrate, through the interface between the substrate and the ESD repair (constituting the HAZ), and the ESD repaired area itself. Knoop measurements were taken with a 500 g load and a 15 second dwell time. Seven measurements was taken; three in the parent material, one in the interface (HAZ) and three in the ESD material. The measurements were taken 0.15 mm apart, with the resulting indentations horizontal, as shown in Figure 4-10. The average of the three in the parent material and the three in the ESD deposit were used as outputs for the DOE, as well as the single measurement taken at the interface.

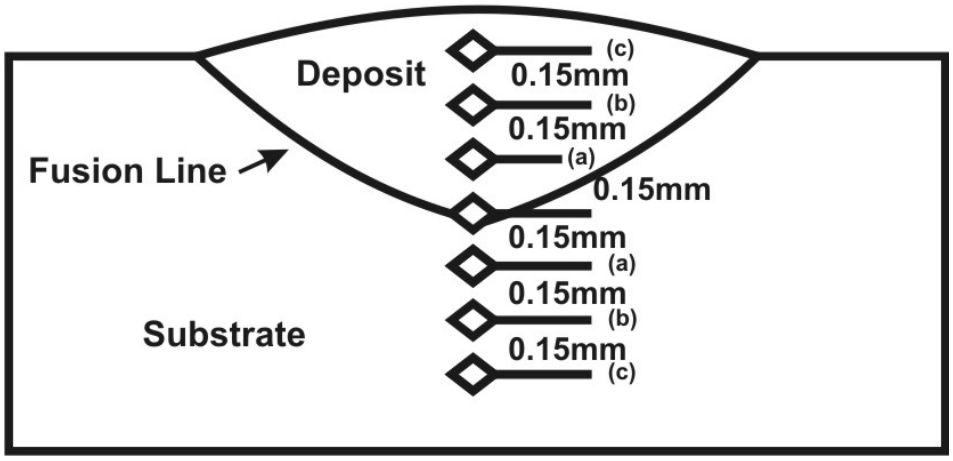

Figure 4-10 Location of Microhardness Measurements

4.2.3.3. Discontinuities

Discontinuities include porosity, inclusions, oxides and other irregularities seen in the microstructure of an ESD deposit. Discontinuities (porosity, inclusions, cracks, etc.) may be a critical factor in optimizing the ESD process. Quantifying and describing discontinuities were performed, as well as capturing an image of the coupon.

A standard method of preparation of metallographic specimens (ASTM E3, accepted practices used for thermal spray, plasma spray and electroplate) was used. The ESD filled area was cross-sectioned through the repair. The coupon was mounted (cross-section face exposed), ground and polished. Optical images were taken at 50 and 500 X. The unetched coupons were subjected to grey scale image analysis and the discontinuities were quantified as a percent of the total area. The coupons were then etched with an appropriate etchant to sufficiently display grain structure.

4.2.3.4. Current

Current, as displayed by the ESD equipment, is a variable that is dependant on the capacitance, voltage and pulse rate. Current was not controlled; it was only recorded.

4.2.3.5. Surface Finish

The final surface of the coupon, after machining, was measured to determine if there is a difference in surface finish in the ESD repair vs. the parent material. After ESD, some of the coupons were machined to an Ra surface finish of 8 to 16 microinches. The surface finish of the machined surface was recorded for a subset of 5 to 10 IN718 coupons. The surface roughness was measured with a profilometer across the parent material and the ESD. Standard methods of measuring the surface finish of thermal spray coatings were used.

4.2.3.6. Microstructure

Microstructure includes items such as grain size, inclusions, and mixed phases. The images used for quantification of the discontinuities were reviewed for anomalies and outstanding artifacts. The evaluation was to determine if the microstructure of ESD-deposits was similar to the base material.

4.2.3.7. Non-Destructive Evaluation (NDE)

Non-destructive evaluation (NDE) was performed to detect any defects in the ESD deposit. The objective of this task was to evaluate whether or not fluorescent penetrant inspection (FPI) is a viable method of determining the quality of the ESD deposit. This information was not an input to the DOE.

Standard FPI methods of NDE were performed by ASAP on the ESD area of each of the 46 DOE coupons prepared by ASAP after a final surface finishing process was performed.

The presence of FPI indications was recorded and compared to the micrographs and discontinuities data to evaluate whether or not this is a viable NDE method for ESD. The results were presented in a PowerPoint presentation, available on request or in the Appendix.

4.2.4. Validation

After the completion of the DOE, trend lines indicating the optimum ESD parameters were created. These trend lines presented the optimum ESD parameters, based on the highest deposition rate. The results of the DOE were then validated.

Parameters to be used to validate the DOE results were selected by EWI from the trends generated by the DOE (Table 4-8). The chosen parameters constituted a higher energy input than the energy input of any of the 46 DOE coupons, as depicted in Figure 4-11.

Table 4-8 Parameters Selected for Validation

Validation Coupon Number	Pulse Rate (Hz)	Voltage (V)	Capacitance (µF)	Electrode Size (mm)	Electrode Speed (rpm)	Curre (A)
V1	500	130	50	2.4	1200	
V2	400	150	60	2.4	1200	
V3	600	100	60	2.4	1200	
V4	400	180	50	2.4	1200	
V5	600	115	50	2.4	1200	

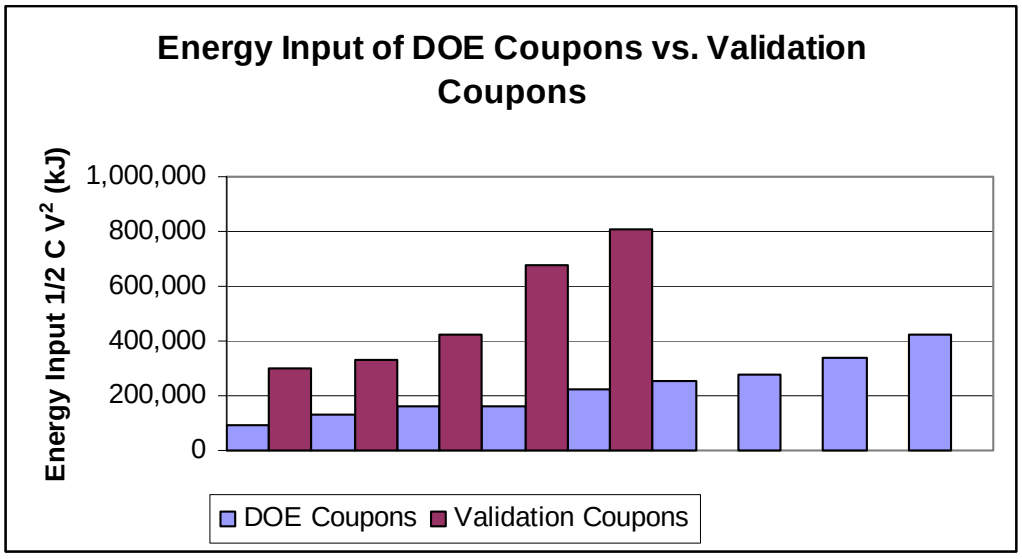

Figure 4-11 Energy Input of DOE Coupons vs. Validation Coupons

EWI and ASAP each prepared 5 validation coupons, using the five different parameter sets, resulting in ten validation coupons. The validation coupons were analyzed by PSU. The ten coupons were sectioned through the center of the ESD deposits and then were mounted and polished with the same procedure as the two sets of 46 optimization coupons. Discontinuities were measured with grey scale image analysis. Six fields were analyzed for each coupon. Microhardness testing was conducted in accordance with prior test procedures. A minimum of 5 and a maximum of 9 hardness readings were taken for each ESD condition average. The results were sent to EWI for validation against the DOE predicted outputs.

Two parameter sets were then chosen as the parameters to be used on the mechanical test specimens. Prior to preparing the test specimens, these two parameter sets were also validated. ASAP prepared five of each of the two parameter sets, resulting in the preparation of ten coupons.

4.2.5. DOE Repeated

The DOE analysis was conducted to optimize the deposition rate of an ESD repair. Initially, the ESD equipment parameters were to be optimized to also provide the most advantageous hardness of the ESD deposit, as well as the best quality, based on discontinuities. As the DOE evolved, it became apparent that the equipment parameters had little effect on hardness or discontinuities. Deposition rate seemed to be the most influenced outcome from varying the ESD equipment parameters. Consequently, hardness and discontinuities were not optimized nor were they correlated to the deposition rate. Therefore, PSU replicated the DOE analysis, with some variations on the previous DOE analysis. Deposition rate was again evaluated, as were hardness and discontinuities. The results dictated the optimum ESD equipment parameters to achieve the "best" ESD deposit take into account all three properties.

PSU replicated the DOE analysis (based on the same data provided to EWI) using the Minitab™ statistical analysis software. EWI used the Box-Behnken DOE technique. Minitab includes the Box-Behnken technique in its suite of statistical techniques. The Box-Behnken technique allows for three Input levels for between 3 and 23 factors.

The data were subjected to a series of regression and plotting routines. The result was a series of regressed mathematical equations describing each particular ESD output as a function of the five specific inputs. Those equations were used to produce three types of plots: 1) a comparison of the influence of two different inputs on selected example outputs, 2) 3D contours of selected outputs as a function of two inputs, and 3) interaction plots which give some indication of the relationship among various inputs and outputs. Also extracted from the data were measures of the strength of each input on a particular output's function (P Factors). This metric provides an indication of the influence of each input has on the regressed output's equation.

4.2.6. Optimization Results

4.2.6.1. Results of ESD applied at two different sites

Six comparison coupons were prepared; three each were made at ASAP and three at EWI. The objective was to verify that different operators, using the same welding equipment and parameters, would produce essentially identical deposits. Both ASAP and EWI video recorded captured their procedures with a short movie. These movies are available upon request.

The deposition rate was calculated for both "total weld time" (which includes stopping to file the electrode or resurface the ESD) and "arc time" (which only records the quantity of ESD deposited during the arcing process). Table 4-9 shows the deposition rate data.

Table 4-9 ASAP and EWI Deposition Rate Data for Comparison Coupons

Coupon	Total Weld Time (min)	Arc Time (min)	Δ weight (g)		Deposition Rate (g/min)	
			final - initial	(sum of all ESD)	Total Weld Time	Arc Time
A EWI - W	13	12	0.091	0.0915	0.00700	0.00763
B EWI - Z	35	10	0.081	0.1020	0.00231	0.01020
C EWI - Y	18	14	0.098	0.0982	0.00544	0.00701
A ASAP - U	64	24	0.0740	0.0549	0.0012	0.0023
B ASAP X	59	16	0.0698	0.0489	0.0012	0.0031
C ASAP - T	55	22	0.0810	0.0810	0.0015	0.0037

PSU evaluated the six coupons relative to similarities and differences between EWI and ASAP. Evaluation was conducted on discontinuities, microhardness and general visual appearance. It was found that the deposits were identical within the precision of the measured parameters. It was not possible to differentiate between the amount of discontinuities of the two sets of coupons (inter-lab comparison). It was also not possible to differentiate among the three samples from each set (intra-lab comparison). Micrographs of the coupons were taken at 50 and 500x. Table 4-10 shows the microhardness and discontinuities data. Figure 4-12 and Figure 4-13 show the microhardness and discontinuities, respectively, presented in graphs.

Table 4-10 ASAP and EWI Hardness and Discontinuities Data for Comparison Coupons

Coupon	Microhardness Average (Knoop)	Microhardness Standard Deviation	Discontinuities Average (%)	Discontinuities Std. Deviation
A EWI - W	374.37	15.09	1.32	0.36
B EWI - Z	375.28	5.48	1.62	2.10
C EWI - Y	361.90	19.85	0.95	0.35
A ASAP - U	297.71	48.25	1.66	0.74
B ASAP X	358.14	14.42	1.19	0.61
C ASAP - T	336.44	19.16	1.23	0.39

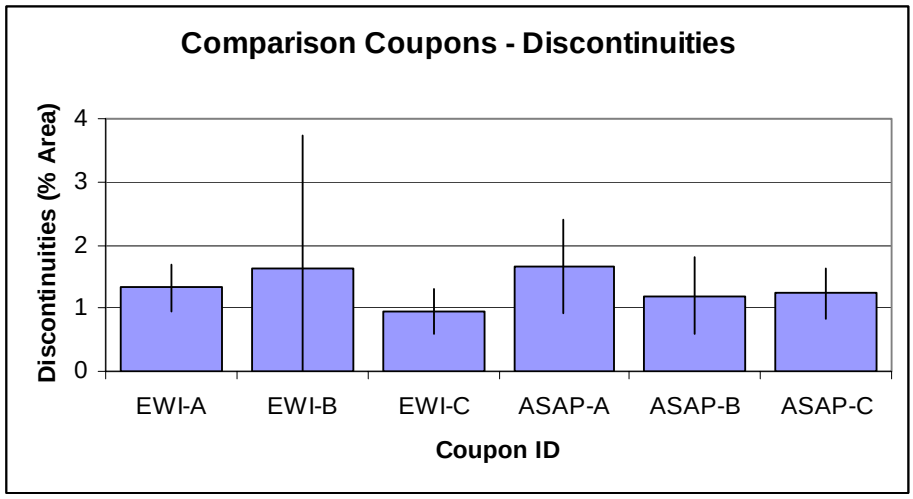

Figure 4-12 ASAP/EWI Percent Discontinuities for Comparison Coupons. Error Bars are ± One Standard Deviation

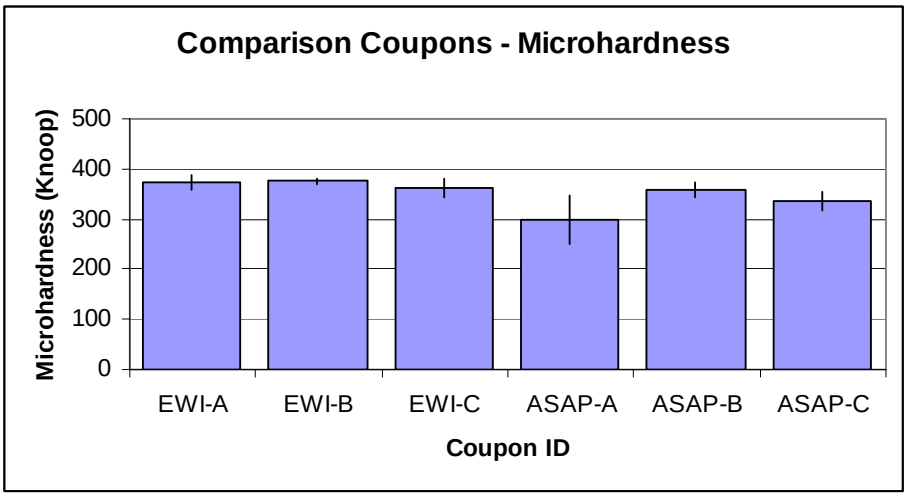

Figure 4-13 ASAP/EWI Microhardness for Comparison Coupons. Error Bars are ± One Standard Deviation

4.2.6.2. Results of Deposition Rate Evaluation

The deposition rate was calculated for both "total weld time" (PDR) and "arc time" (ATDR). The data recorded as ATDR for the EWI coupons contains only the deposited amount of ESD during the first interval (until the process was stopped to resurface the ESD). The data recorded for the ASAP coupons uses the sum of all deposited material for all intervals. Only "total weld time" deposition rate were used as a DOE input. Deposition rate data for ASAP's and EWI's coupons are shown in Figure 4-14.

There was noteworthy variation in the deposition rate data taken for all the DOE coupons. This would indicate that, since a variety of ESD parameters were employed, altering these parameters has a considerable effect on the ESD deposition rate.

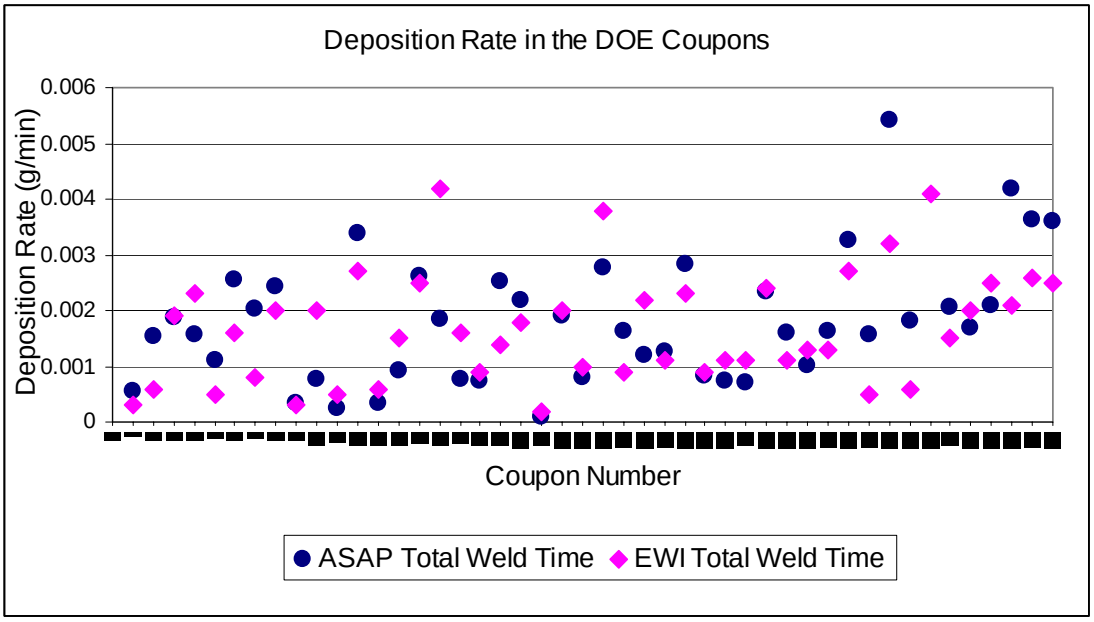

Figure 4-14 Deposition Rates for DOE Coupons

4.2.6.3. Results of Microhardness Evaluation

The results of microhardness evaluation, in Knoop, are shown in Figure 4-15 through Figure 4-18. Both the set of coupons prepared by ASAP and those prepared by EWI exhibited an average microhardness in the ESD of approximately 350 Knoop and an average microhardness in the substrate of approximately 450 Knoop. The difference (22%) is slightly greater than the desired ESD microhardness, targeted for within ±20% of the base material. However, as ESD is a rapid solidification process, and IN718 relies on the formation of precipitates for the hardening mechanism, these results are to be expected.

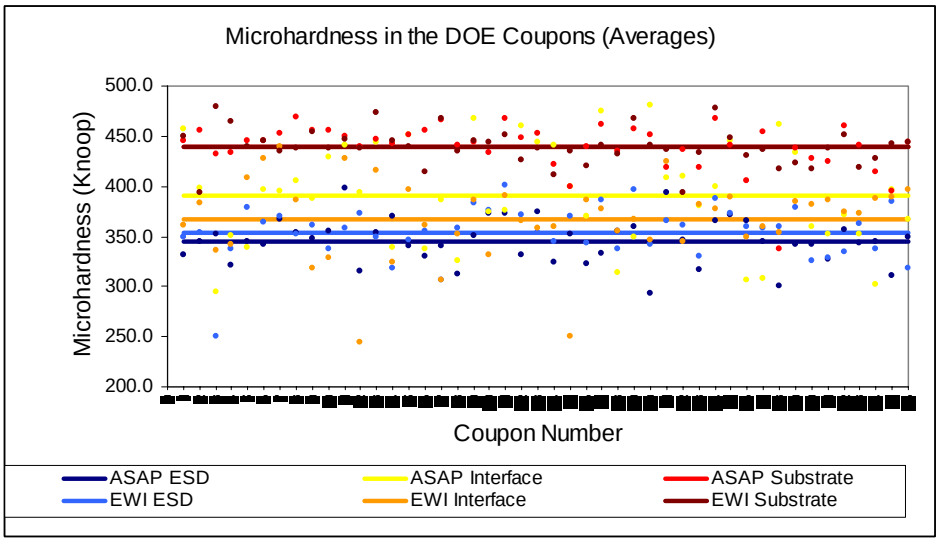

Figure 4-15 Microhardness in the DOE Coupons (Averages)

There was very little difference in the microhardness measurements taken in the ESD deposit (Figure 4-16). This would indicate that, although a variety of ESD parameters were employed, they had little effect on the microhardness of ESD. There was a greater variation in the microhardness measurements taken at the ESD interface (Figure 4-17) and virtually no difference in the microhardness taken in the substrate material (Figure 4-18).

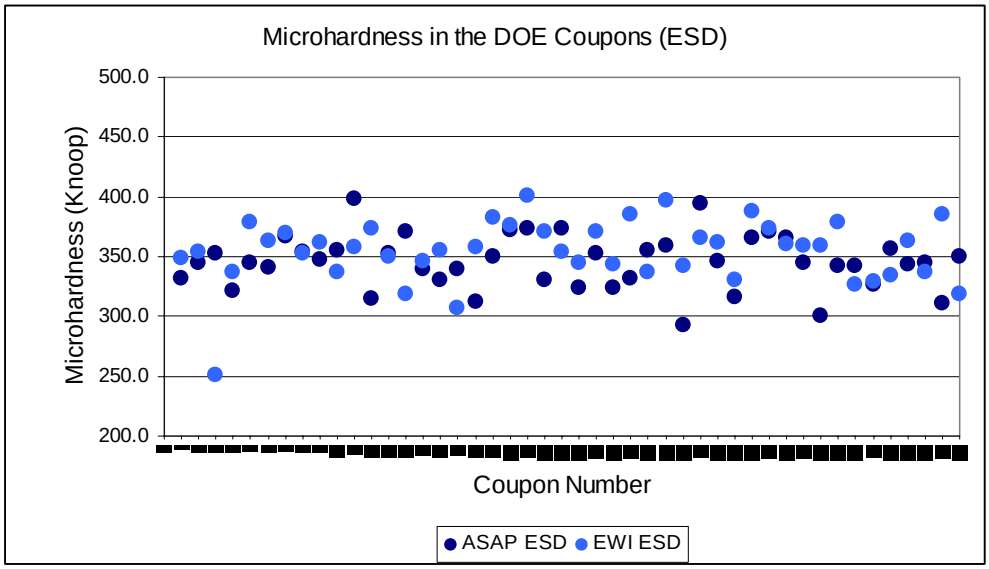

Figure 4-16 Microhardness in the DOE Coupons (ESD deposit)

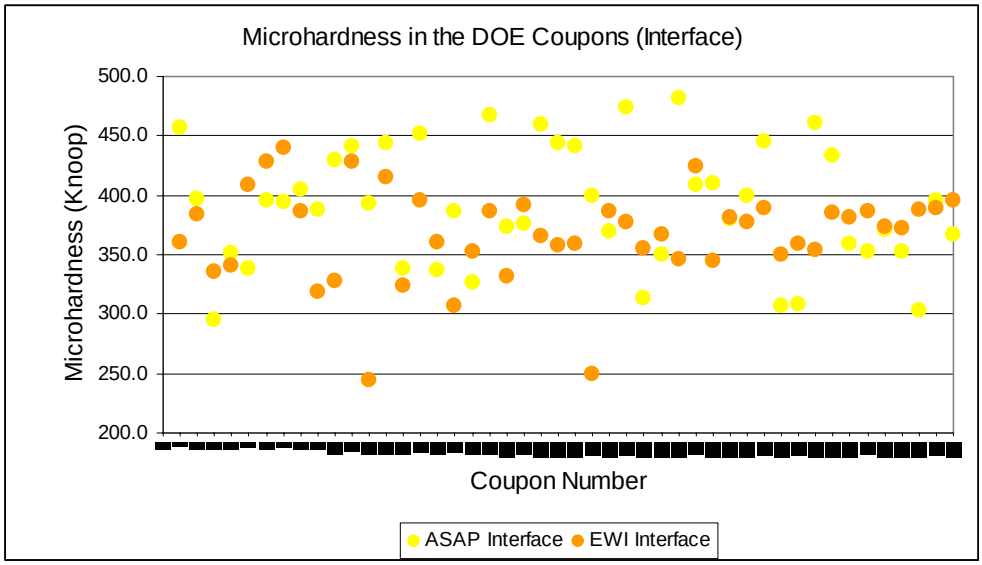

Figure 4-17 Microhardness in the DOE Coupons (Interface)

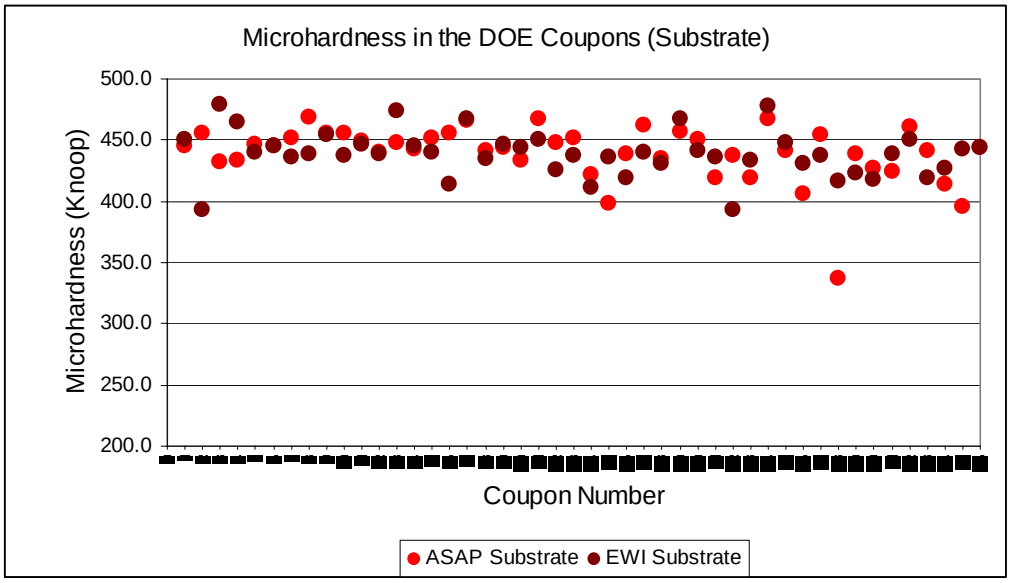

Figure 4-18 Microhardness in the DOE Coupons (Substrate)

4.2.6.4. Results of Discontinuities Evaluation

The results of the grey scale image analysis of discontinuities, in percent of area and averaged, are shown in Figure 4-19. Although a few coupons exhibited discontinuities in the 3% to 4% range, most coupons exhibited discontinuities under 2% which is considered satisfactory for most applications.

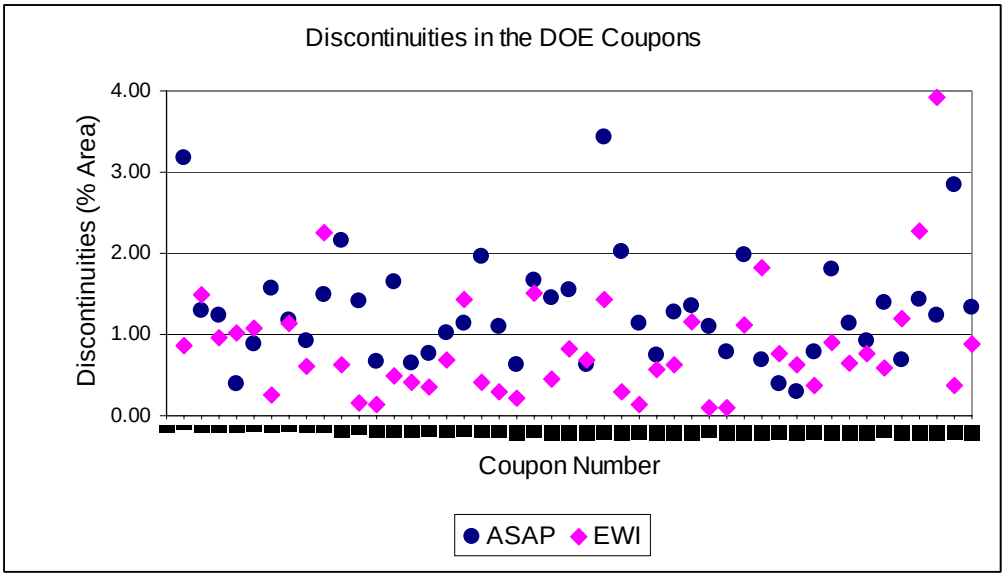

Figure 4-19 Discontinuities in the DOE Coupons

4.2.6.5. Results of Surface Finish Evaluation

The coupons were selected in random so they include divots that were completely filled and visually fully dense, and ones that had visible discontinuities. The readings were taken perpendicular to the surface grinding marks. The profilometer was calibrated prior to testing on a roughness standard. Those coupons that were completely filled had surface finish measurements that closely matched the parent material, as seen in Table 4-11. Some coupons (#11, #13 and #17) were not completely filled. Therefore, this measurement was not of a finished surface, but rather a measurement of the as-deposited ESD surface. One example (#17) is shown in Figure 4-20. This coupon has been prepared for FPI and the lack of a complete deposit is evident.

Table 4-11 Surface Finish of Coupons

Coupon number	ESD surface roughness	Parent surface roughness
	(Microinches)	
7	8	2
9	17	2
11	105	2
13	64	3
14	14	2
17	77	2
19	3	2
24	4	2
28	2	3
35	2	2
38	5	2
40	3	2

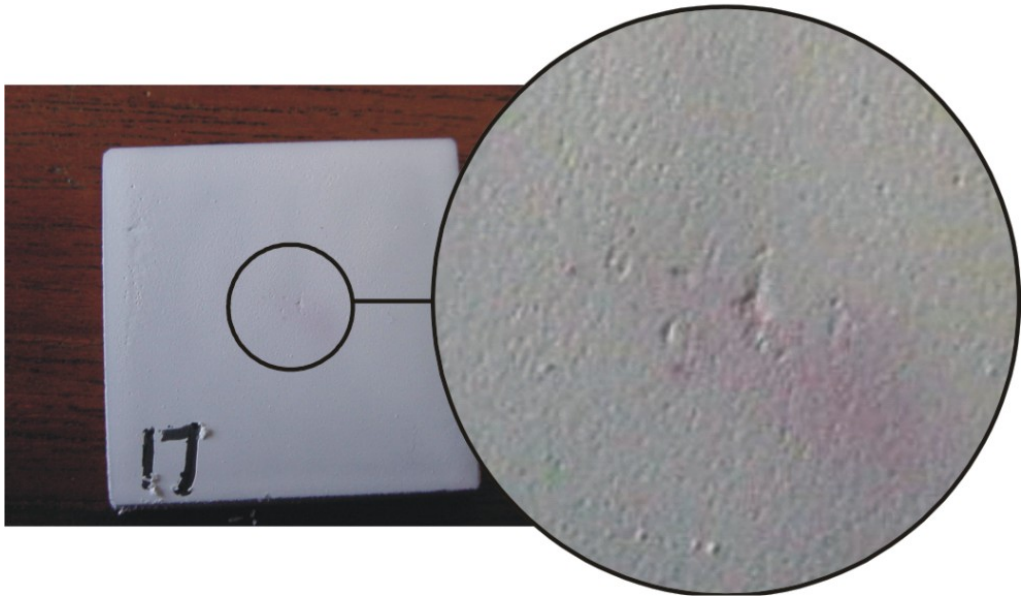

Figure 4-20 Surface of Coupon #17 with FP

4.2.6.6. Results of Non-Destructive Evaluation (NDE)

All of the 46 DOE coupons prepared by ASAP were surface finished and subjected to FPI. Each coupon was photographed, visually inspected and "rated" as one of the following:

- Good = no discontinuities observed and the coupon looked clean
- Medium = small discontinuities observed in the ESD coating or as small pink spots
- Poor = many pink spots observed throughout ESD area

The discontinuities data, in percent area, was also "rated" as on of the following:

- 0.00% to 1.00% = Good
- 1.01% to 1.50% = Medium
- 1.51% to 3.50% = Poor

This information was intended to answer the following questions:

- Is there a correlation between the micrograph and the discontinuities data?
- Is there a correlation between the micrograph and the FPI image?
- Based on the presence or lack of the correlations above, what is the overall assessment of FPI as an NDE method for evaluating the quality of ESD?

Figure 4-21 through Figure 4-24 show a selection of slides depicting all the images, data and assessments.

Coupon Number:	36
Discontinuities (%Area):	0.29
Qualitative Assessment of the ESD, based on Discontinuities Data*:	Good
FPI Comments: "Good" (Im agrees)	
Qualitative Assessment of the ESD, based on FPI**:	Good
Qualitative Assessment of the ESD, based on Micrograph:	Good
Correlation Between Micrograph and Discontinuities Data:	Yes
Correlation Between Micrograph and FPI Image:	Yes
Overall Assessment of FPI as an NDE Method:	Good

* 0.00 to 1.00 =Good 1.01 to 1.50 = Medium 1.51 to 3.50 = Poor

**Good = no porosity is observed and the coupon looked clean
Medium = little porosity is observed around the ESD or as spots of pink
Poor = lots of pink is observed all over the ESD area

Figure 4-21 Coupon #36. FPI Indicates Good Quality. Discontinuities Data and Micrograph Confirm This to be the Case.

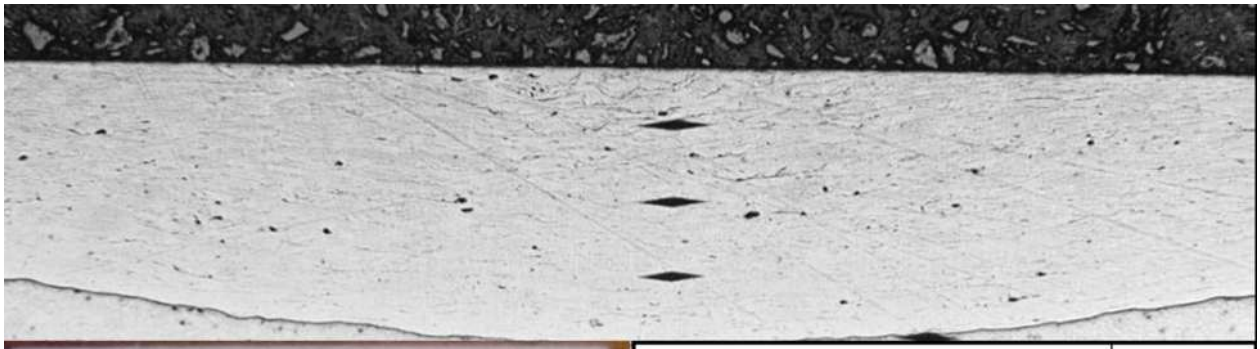

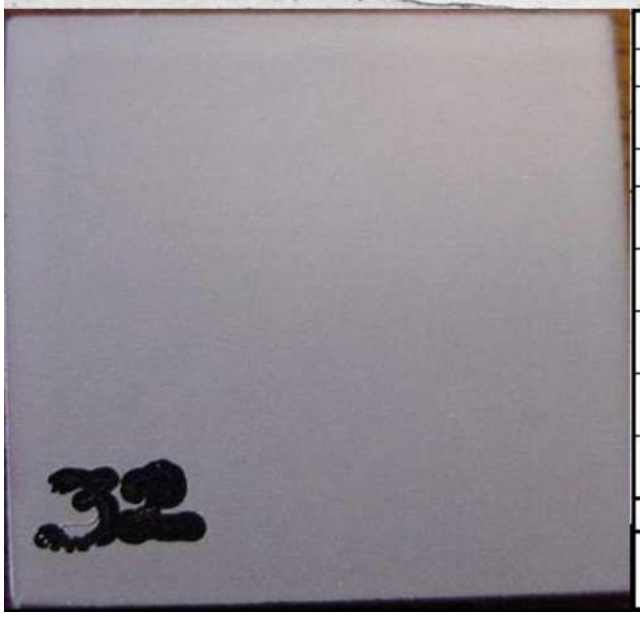

Coupon Number:	32
Discontinuities (%Area):	0.79
Qualitative Assessment of the ESD, based on Discontinuities Data*:	Good
FPI Comments: "Good" (Im agrees)	
Qualitative Assessment of the ESD, based on FPI**:	Good
Qualitative Assessment of the ESD, based on Micrograph:	Good
Correlation Between Micrograph and Discontinuities Data:	Yes
Correlation Between Micrograph and FPI Image:	Yes
Overall Assessment of FPI as an NDE Method:	Good

* 0.00 to 1.00 =Good 1.01 to 1.50 = Medium 1.51 to 3.50 = Poor

**Good = no porosity is observed and the coupon looked clean
Medium = little porosity is observed around the ESD or as spots of pink
Poor = lots of pink is observed all over the ESD area

Figure 4-22 Coupon #32. FPI Indicates Good Quality. Discontinuities Data and Micrograph Confirm This to Be the Case.

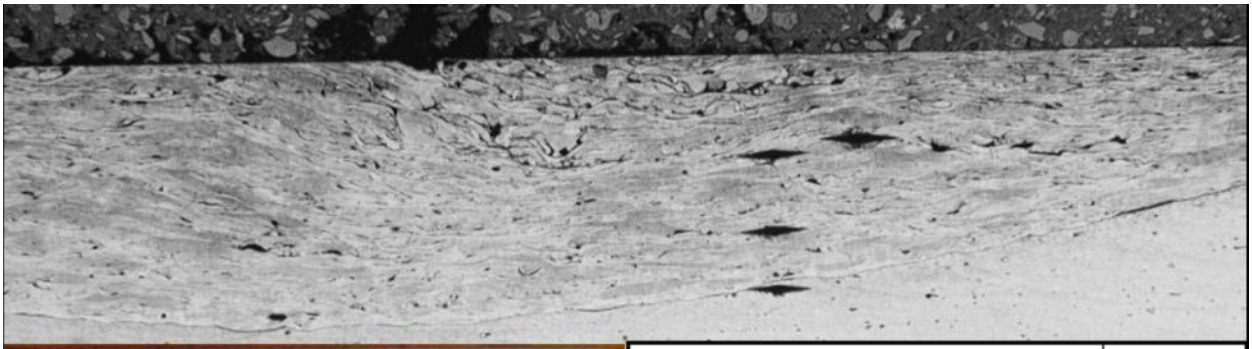

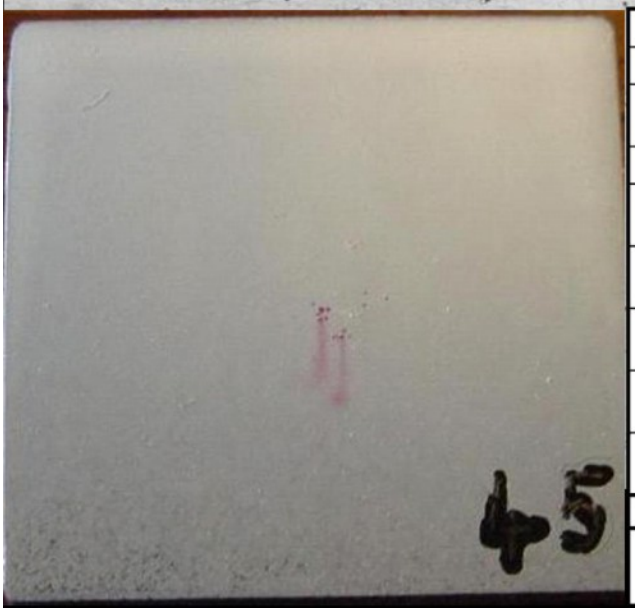

Coupon Number:	45
Discontinuities (%Area):	2.83
Qualitative Assessment of the ESD, based on Discontinuities Data*:	Poor
FPI Comments: "linear pink"	
Qualitative Assessment of the ESD, based on FPI**:	Poor
Qualitative Assessment of the ESD, based on Micrograph:	Poor
Correlation Between Micrograph and Discontinuities Data:	Yes
Correlation Between Micrograph and FPI Image:	Yes
Overall Assessment of FPI as an NDE Method:	Good

* 0.00 to 1.00 =Good 1.01 to 1.50 = Medium 1.51 to 3.50 = Poor

**Good = no porosity is observed and the coupon looked clean
Medium = little porosity is observed around the ESD or as spots of pink
Poor = lots of pink is observed all over the ESD area

Figure 4-23 Coupon #45. FPI indicates poor quality. Discontinuities data and micrograph confirm this to be the case.

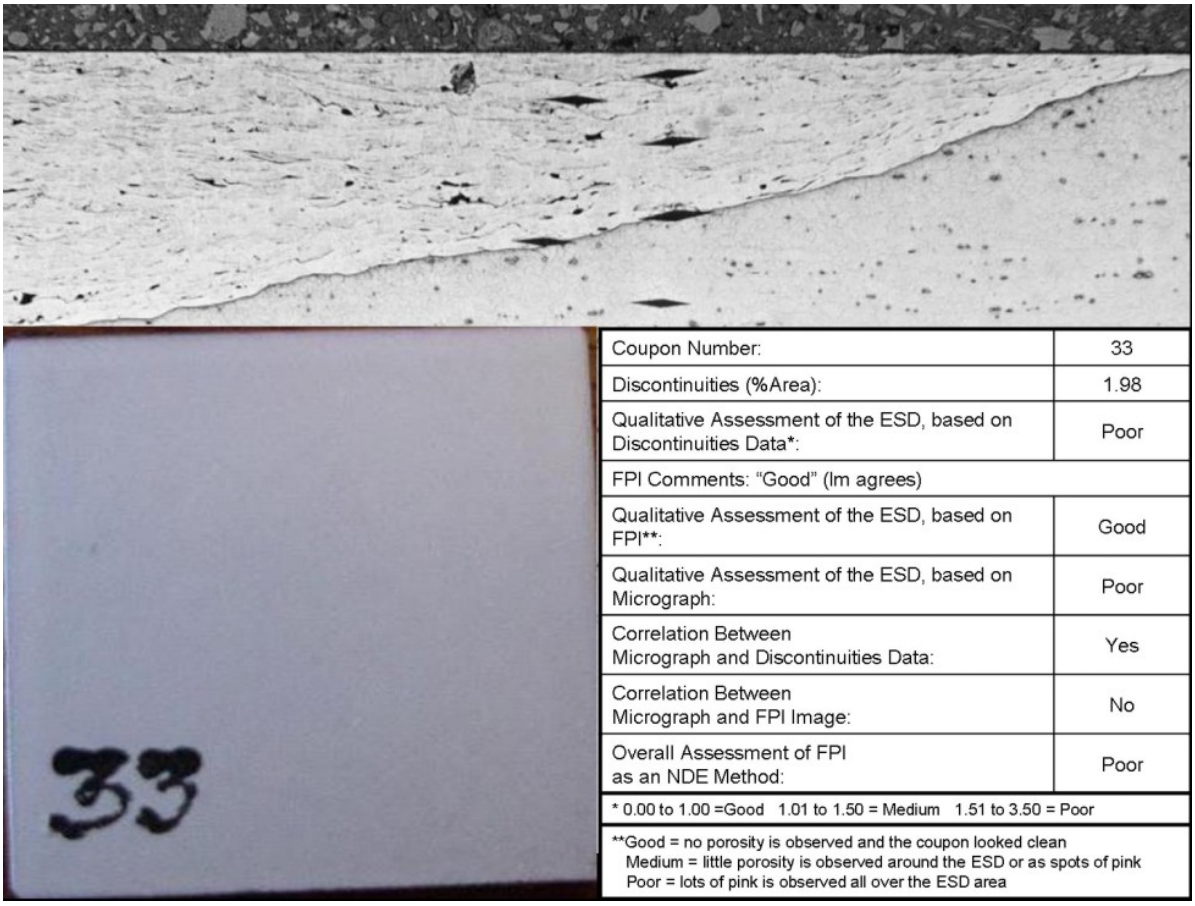

Coupon Number:	33
Discontinuities (%Area):	1.98
Qualitative Assessment of the ESD, based on Discontinuities Data*:	Poor
FPI Comments: "Good" (Im agrees)	
Qualitative Assessment of the ESD, based on FPI**:	Good
Qualitative Assessment of the ESD, based on Micrograph:	Poor
Correlation Between Micrograph and Discontinuities Data:	Yes
Correlation Between Micrograph and FPI Image:	No
Overall Assessment of FPI as an NDE Method:	Poor

* 0.00 to 1.00 =Good 1.01 to 1.50 = Medium 1.51 to 3.50 = Poor

**Good = no porosity is observed and the coupon looked clean
Medium = little porosity is observed around the ESD or as spots of pink
Poor = lots of pink is observed all over the ESD area

Figure 4-24 Coupon #33. FPI Indicates Good Quality. However, Discontinuities Data and Micrograph Report Poor Quality.

In most cases, FPI gave an accurate assessment of the quality of the ESD. However, in approximately 10% of the coupons, the FPI indications did not represent the quality of the ESD. The FPI method for NDE is a surface quality method. Examination of the micrographs and quantification of discontinuities was conducted on the entire depth of the deposit.

4.2.6.7. Validation Results

Ten validation coupons, prepared by EWI and ASAP using five different parameter sets, were analyzed by PSU. The results were sent to EWI for validation against the DOE predicted outputs. EWI determined the predicted deposition rate, based on the DOE results. They then compared the predicted deposition rates to the actual deposition rates. The results are shown in Figure 4-25.

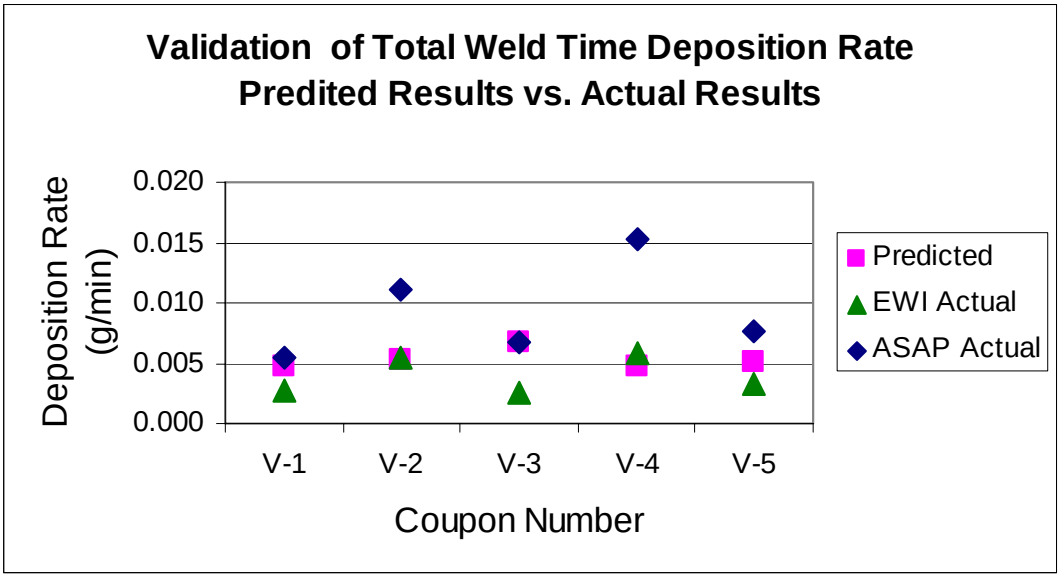

Figure 4-25 Predicted vs. Actual Deposition Rate

In addition, the microhardness and discontinuities data for the validation coupons were compared to the data obtained for the optimization coupons.

Two parameter sets were then selected as the parameters to be used on the mechanical test specimens. Prior to preparing the test specimens, these two parameter sets were also validated. ASAP prepared five of each of the two parameter sets, resulting in the preparation of ten coupons. One set replicated the optimization coupon #32; the other replicated the validation coupon, V4. The validation coupons were then compared to the original coupons prepared under identical parameters, as well as compared to the average of all the optimization coupons. Figure 4-26 shows the discontinuities data points for the first two coupons, prepared in the Optimization Phase or in the Validation Phase, the five coupons prepared for final validation, and compares these data to all of the coupons prepared in the Optimization Phase. Figure 4-27 shows the microhardness data points for the first two coupons, prepared in the Optimization Phase or in the Validation Phase, the average of the five coupons prepared for final validation, and compares these data to the averages of the coupons prepared in the Optimization Phase.

The discontinuities in the parameter set #32 remained at the same level as the optimization coupons prepared under identical parameter. The discontinuities in the parameter set V4 were greater than seen in the validation coupons prepared under identical parameters but within the range of all of the optimization coupons.

The microhardness measurements for the validation coupons prepared under parameter set #32 were very similar (in the ESD deposit, at the interface and in the substrate) to the optimization coupons prepared using identical parameters. Microhardness in the substrate for #32 validation coupons was lower than the average for the optimization coupons. The microhardness measurements for the validation coupons prepared under parameter set V4 were also very similar (in the ESD deposit, at the interface and in the

substrate) to the validation coupons prepared under identical parameters. Microhardness in all of the V4 validation coupons was lower than the average for the optimization coupons.

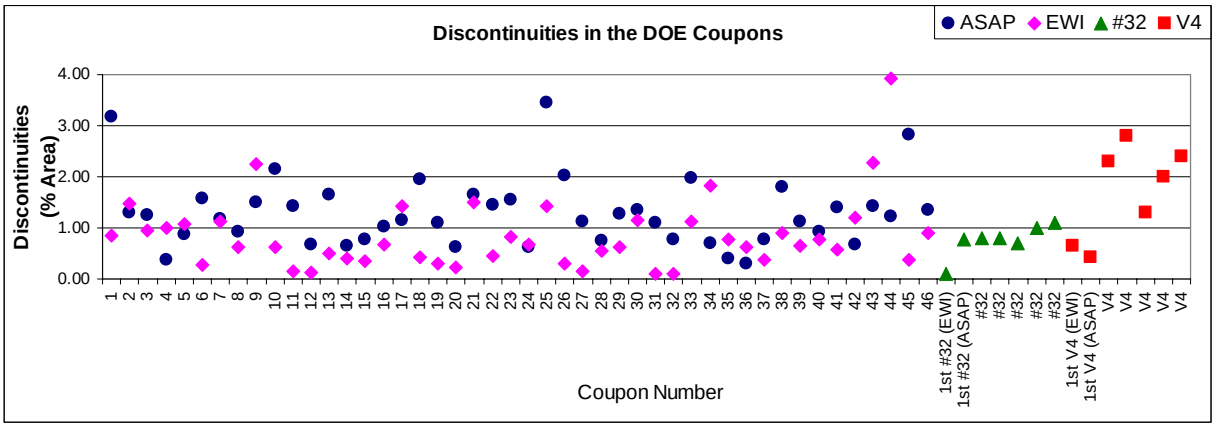

Figure 4-26 Validating Discontinuities Data for Selected Parameters

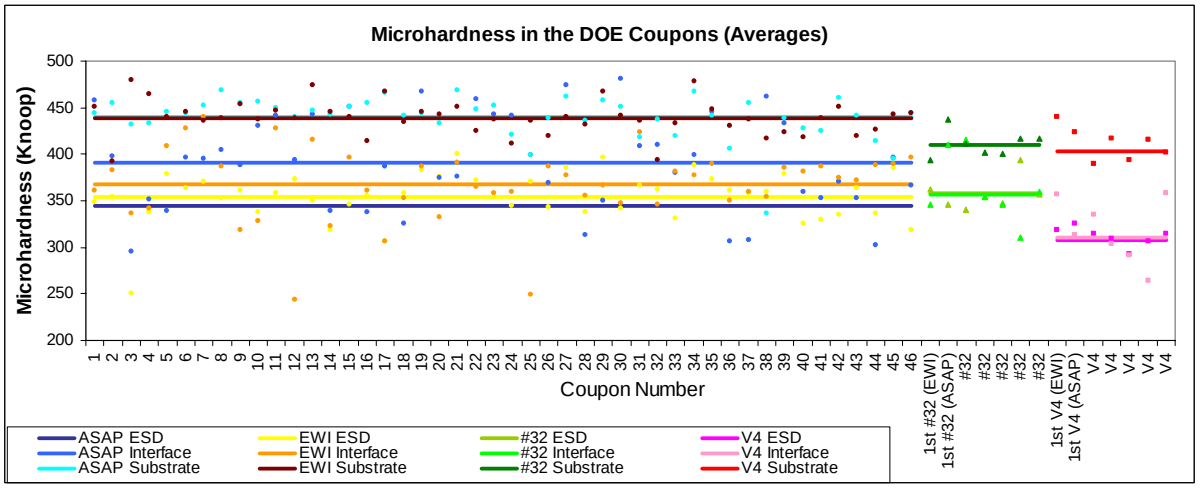

Figure 4-27 Validating Microhardness Data for Selected Parameters

4.2.6.8. Results of Statistical Analysis

The result of the statistical analysis performed by PSU was the formulation of equations, which can be used to predict deposition rate, microhardness and discontinuities. PSU reported the following equations:

Arc Time Deposition Rate = - 0.0173 + 0.000012(Pulse Rate) + 0.000107(Voltage) + 0.000182(Capacitance) + 0.000001(Electrode Speed) - 0.0257(Electrode Size).

Production Deposition Rate = 0.00992 + 0.000002(Pulse Rate) + 0.000059(Voltage) + 0.000051(Capacitance) + 0.000001(Electrode Speed) + 0.0143(Electrode Size).

Microhardness = 389 + 0.0068(Pulse Rate) - 0.539(Voltage) - 1.08(Capacitance) + 0.0122(Electrode Speed) + 418(Electrode Size).

Discontinuities = - 5.86 - 0.00417(Pulse Rate) - 0.00810(Voltage) - 0.0078(Capacitance) - 0.000648(Electrode Speed) - 10.5(Electrode Size).

A statistical re-analysis was conducted by PSU on the optimization data, using the Minitab™ statistical program at PSU. Four regressed mathematical expressions were calculated describing each output as a function of the five inputs. A new test matrix was developed in the software using the original inputs and compared to the EWI DOE. Using the statistical functions, numerous plots were produced. Additional statistical data generated include input significance values and some welding parameter optimization combinations. Interaction plots for all four outputs were calculated for each input combination.

The regressed functions developed in the statistical modeling can be used to examine the various outputs as a function of specific inputs. For example, ATDR (grams/min) is plotted as a function of capacitance and electrode diameter in Figure 4-28), microhardness as a function of capacitance and voltage is plotted in Figure 4-29, and % discontinuities (porosity) is plotted as a function of capacitance and electrode rotation in Figure 4-30.

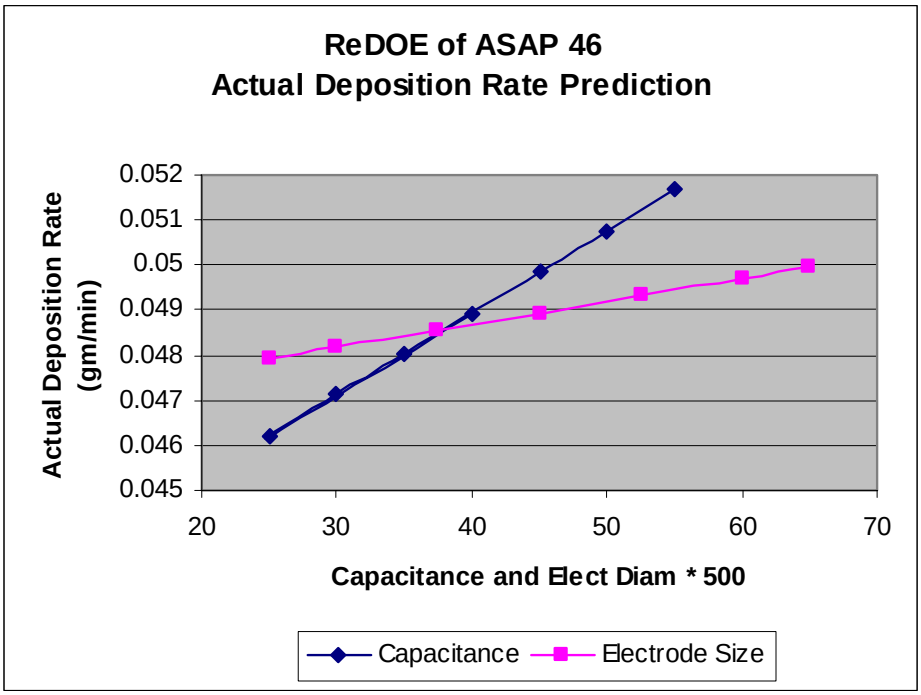

Figure 4-28 Plot of Arc Time Deposition Rate as a Function of Capacitance and Electrode Size Using the Regressed Equations From the Statistical Analyses.

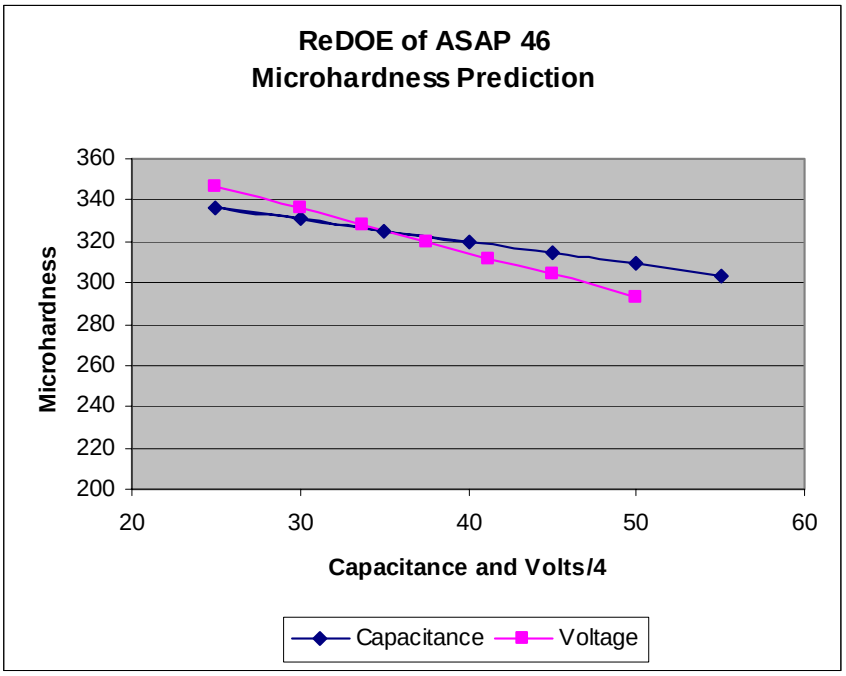

Figure 4-29 Plot of Microhardness as a Function of Capacitance and Voltage Using the Regressed Equations From the Statistical Analyses.

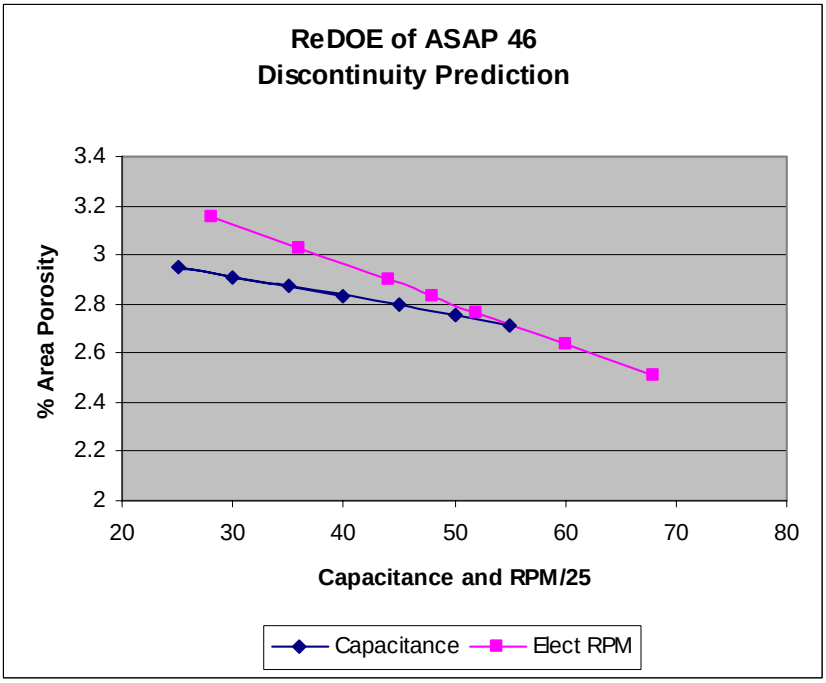

Figure 4-30 Plot of % Discontinuity as a Function of Capacitance and Electrode Speed Using the Regressed Equations From the Statistical Analyses.

The statistical software can be used to plot the results of regressed functions in a variety of forms including 3D surface plots. Several of these 3D plots were produced based on past experience of significant input/output relationships.

Table 4-12 lists the possible combinations of two-input grouping for every output. Since there are four outputs and ten possible two-input groupings there are 40 possible combinations of two-input analyses. Only a few examples are presented here. Figure 4-31 presents ATDR as a function of capacitance and pulse rate, Figure 4-32 presents % discontinuities (porosity) as a function of voltage and capacitance, and Figure 4-33 presents microhardness as a function of capacitance and pulse rate.

Table 4-12 Potential 3D Plot Combinations of ESD Inputs for Each Output

	Voltage	**Capacitance**	**Pulse Rate**	**Electrode Speed**	**Electrode Size**
Voltage	X	Duplicate	Duplicate	Duplicate	Duplicate
Capacitance	Available	X	Duplicate	Duplicate	Duplicate
Pulse Rate	Available	Available	X	Duplicate	Duplicate
Electrode Speed	Available	Available	Available	X	Duplicate
Electrode Size	Available	Available	Available	Available	X

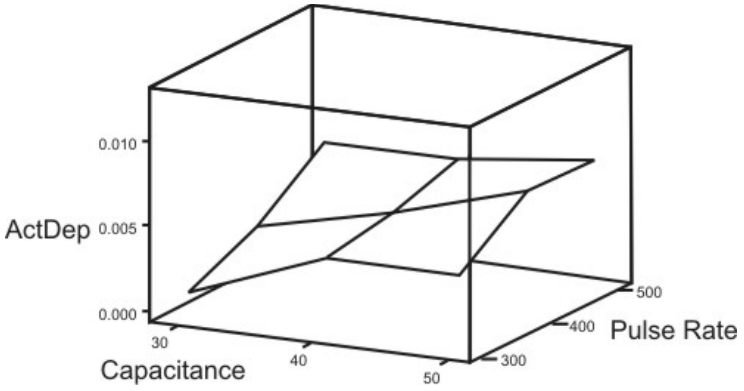

Figure 4-31 Regressed 3D plot of Actual Deposition Rate as a Function of Capacitance and Pulse Rate.

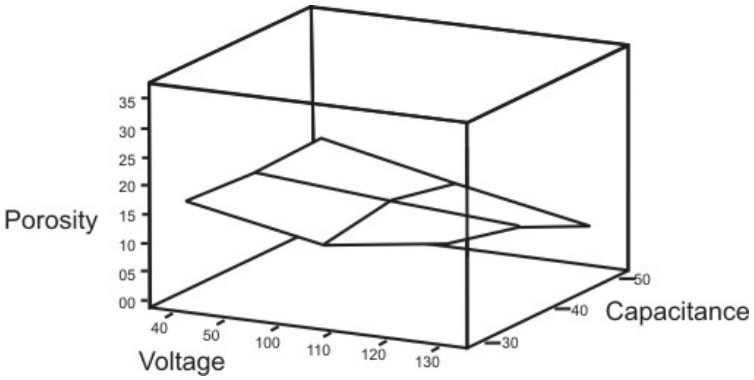

Figure 4-32 Regressed 3D plot of Discontinuities as a Function of Voltage and Capacitance.

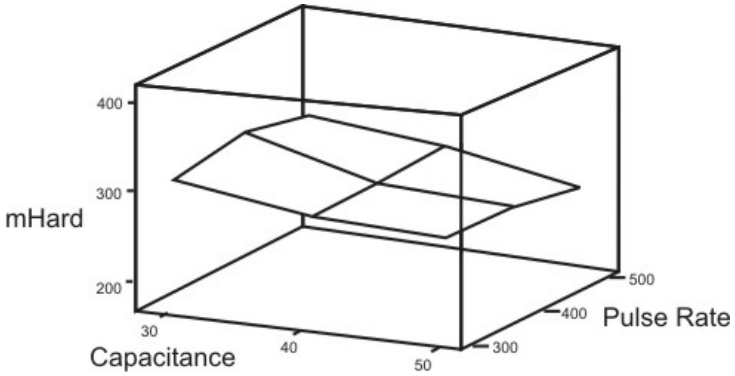

Figure 4-33 Regressed 3D plot of Microhardness as a Function of Capacitance and Pulse Rate.

One result of the statistical analyses is an indication of the relative influence of each input on the regressed functions. For example, voltage may have a stronger influence than electrode diameter on deposition rate. One of these strength descriptors is the P Factor. Generally P factor values less than 0.05 indicate a strong influence of that input on the regression function. The P Factor is somewhat analogous to a standard deviation – it is a measure of whether that factor has a strong cause/effect relationship in the regressed function. Table 4-13 lists the P factors for each Output Regression function for both the 46 ASAP and 46 EWI samples. Significant P factors are highlighted.

Table 4-13 Input P Factors from Statistical Analyses

Output		Inputs				
		Voltage	Capacitance	Pulse Rate	Electrode Speed	Electrode Diameter
Actual Deposition Rate	ASAP	0.0	0.0	0.019	0.482	0.062
	EWI	0.0	0.0	0.0	0.118	0.747
Production Deposition Rate	ASAP	0.002	0.26	0.708	0.196	0.263
	EWI	0.0	0.0	0.002	0.446	0.068
Microhardness	ASAP	0.005	0.021	0.88	0.284	0.002
	EWI	0.021	0.081	0.740	0.407	0.98
Discontinuities	ASAP	0.172	0.597	0.007	0.083	0.015
	EWI	0.348	0.675	0.777	0.566	0.011

Note: $P < 0.05$ is considered significant.

The statistical program has the option of calculating optimal input levels based on desired outputs. The programmer lists the desired outputs (maximize, minimize or a specific target) and ranges (high, low and specific target). Calculations are then conducted that predict specific inputs that will produce those outputs.

The program was not able to optimize all four inputs simultaneously. When asked to perform that calculation it terminated the action. The actual program response was "No optimal solution found" (Table 4-14).

Table 4-14 Minitab™ Four-Output Optimization response.

Response Optimization: All Four Outputs						
Parameters	Goal	Lower	Target	Upper	Weight	Import
Microhardness	Maximum	350.00	400.00	400.00	1	1
Discontinuities	Minimum	1.00	1.00	2.00	1	1
Prod Dep Rate	Maximum	0.05	0.07	0.07	1	2
Arc Time Dep Rate	Maximum	0.06	0.10	0.10	1	1
* NOTE * No optimal solution found.						

When optimized inputs were requested on two or three outputs the program *did* produce input suggestions. For example, when optimized inputs based on only discontinuities and hardness were requested, the program provided an output. The program was also able to calculate optimized inputs based on three of the four outputs (Table 4-15)

Table 4-15 Minitab™ Three Output Optimization response.

Response Optimization: Microhardness, Discontinuities, Actual Deposition Rate

Parameters	Goal	Lower	Target	Upper	Weight	Import
Microhardness	Target	300.00	380.00	400.00	1	1
Discontinuities	Minimum	2.00	2.00	6.00	1	1
Arc Time Dep Rate	Target	0.01	0.02	0.02	1	1

Local Solution
Pulse Rate = 500.00
Voltage = 130.00
Capacitance = 50.00
Electrode Speed = 1600.00
Electrode Size = 0.06
Predicted Responses
Microhardness = 355.158, desirability = 0.68948
Discontinuities = 0.014, desirability = 1.00000
Arc Time Dep Rate = 0.006, desirability = 0.06129
Composite Desirability = 0.34831

Local Solution
Pulse Rate = 500.00
Voltage = 130.00
Capacitance = 50.00
Electrode Speed = 1600.00
Electrode Size = 0.13
Predicted Responses
Microhardness = 370.598, desirability = 0.88248
Discontinuities = -0.317, desirability = 1.00000
Arc Time Dep Rate = 0.007, desirability = 0.20550
Composite Desirability = 0.56603

Global Solution
Pulse Rate = 500.00
Voltage = 130.00
Capacitance = 50.00
Electrode Speed = 1600.00
Electrode Size = 0.13
Predicted Responses
Microhardness = 370.598, desirability = 0.88248
Discontinuities = -0.317, desirability = 1.00000
Arc Time Dep Rate = 0.007, desirability = 0.20550

Composite Desirability = 0.56603

4.2.6.9. Parameters Selected for Test Specimens

Selecting the parameters to be used in the mechanical test specimens was the objective of optimizing ESD. The parameters that were selected performed well in an ESD "repair" of a Type 1 defect. That is, they were optimized for filling a divot that is surrounded by parent material. These parameters may not be as effective if attempting to use ESD to coat a surface or perform a repair on an edge or in a non-line-of-sight application. Another critical factor in applying the selected ESD parameters to a repair is the relative thermal mass of the object. For example, the selected ESD parameters may not be appropriate for a repair in a section of a component that is very thin, or for a component with a much greater mass-to-defect ration.

Another consideration when selecting "optimized parameters" is the heat affected zone that is created. Although ESD is a micro-arc process and a very minimal HAZ in detected, with depths on the order of micrometers, the depth of the HAZ is a function of the energy into the part during the ESD process. So, while an increase in energy may result in an increase in deposition rate of material, it may also adversely affect the component by creating an unacceptable HAZ. This project evaluated the depth of the HAZ by taking microhardness measurements at the interface and by metallurgical evaluation of the micrographs. The effect of the HAZ was not optimized in this project.

The parameters for the mechanical test specimens were selected by the project team. Reviewing the data and micrographs, the parameters selected were V4 (from the validation coupons) and #32 (from the optimization coupons) as indicated in Table 4-16.

Parameter set #32 was chosen because it had a medium deposition rate and excellent quality (based on discontinuities and images). Parameter set V4 was chosen because of its high deposition rate and good quality, although microhardness was lower than for most other parameter sets.

Table 4-16 Parameters Selected for Mechanical Test Specimens

Coupon Number	Pulse Rate (Hz)	Voltage (V)	Capacitance (μF)	Electrode Size (mm)	Electrode Speed (rpm)	Current (A)
V4	400	180	50	2.4	1200	7
#32	400	105	50	3.2	1200	4

4.3. Results of Materials Testing

4.3.1.Introduction

In order to evaluate the mechanical properties of an ESD deposit, and the effect ESD may have on the components, multiple mechanical tests were performed. The function performance of ESD was tested using ASTM standard tests, including fatigue (ASTM E466), tensile (ASTM (E8), wear (ASTM G99 and Hamilton Sundstrand), corrosion (ASTM B-117) and adhesion bond (ASTM C 633) strength tests. Residual stress analysis was also performed.

4.3.2.Fatigue

4.3.2.1. Test Rationale

The purpose of fatigue testing was to evaluate the effect of ESD on the fatigue properties of the underlying material. Since there are several different types of fatigue tests, it was essential to define the one that best represents the conditions that a gas turbine engine component would encounter in service. For most ESD testing to-date, axial fatigue testing (ASTM E466) has provided the most useful data for evaluation. The need for low-cycle-fatigue (LCF) testing in GTE applications is driven by design consideration for the number of engine take-off/landing cycles. Therefore, only LCF testing was conducted. Because of the types of stresses encountered by most gas turbine engine components, the fatigue test specimens in this project were only subjected to tensile stresses.

4.3.2.2. Specimen Fabrication

The specimens were fabricated with flat plate geometry and a constant gage width. The defect was a small divot in the center of the gage length, to allow the evaluation of the affect an ESD deposit has on the fatigue life of the substrate, the ESD fill and the interface between the two.

Test specimens, shown in Figure 4-35, were used to provide full S-N curves in order to determine both fatigue life and fatigue initiation locations. Some specimens had a Type 1b defect (described in Section 4.1) at the center of the gage section which was filled via ESD and machined back to specification. Others had a defect without an ESD fill. Still others had no defect, but an ESD overlay (bead-on-plate). Baseline data was established on specimens with and without a defect and without ESD as shown in Figure 4-36.

Specimen production method:

- Grind to shape, 0.002” oversize on the thickness.
- Machine defect as required by the fatigue test matrix, using the defect dimensions defined in Figure 4-3
- Deposit the ESD, filling the defect above the surface of the specimen.
- Apply UIT to some of the repaired specimens, per the test matrix.
- Low-stress grind to specified gauge thickness, with a surface finish of 32μ in or better.

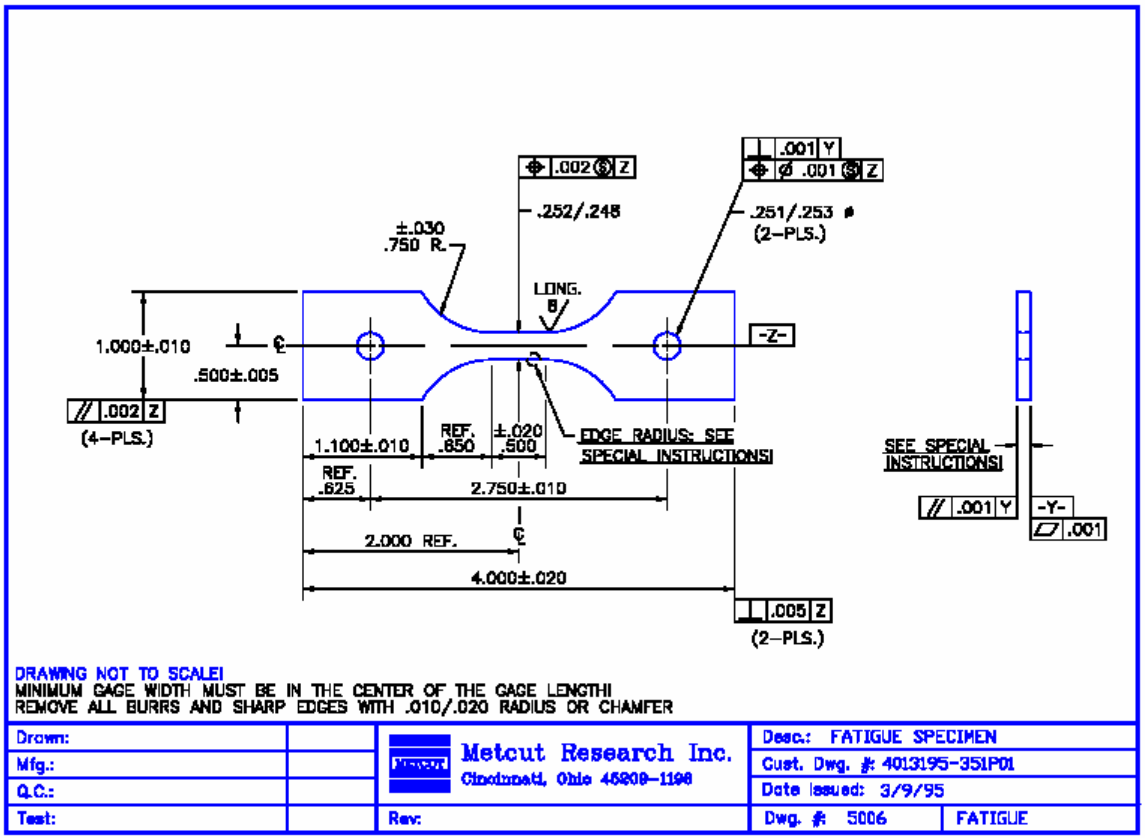

Figure 4-34 Fatigue Specimen Specifications

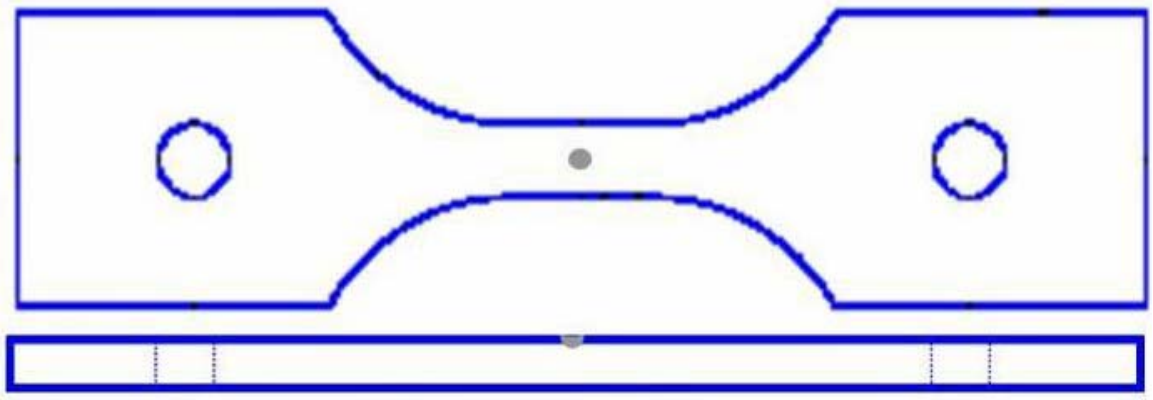

Figure 4-35 Fatigue Specimen with Defect (Defect not to Scale)

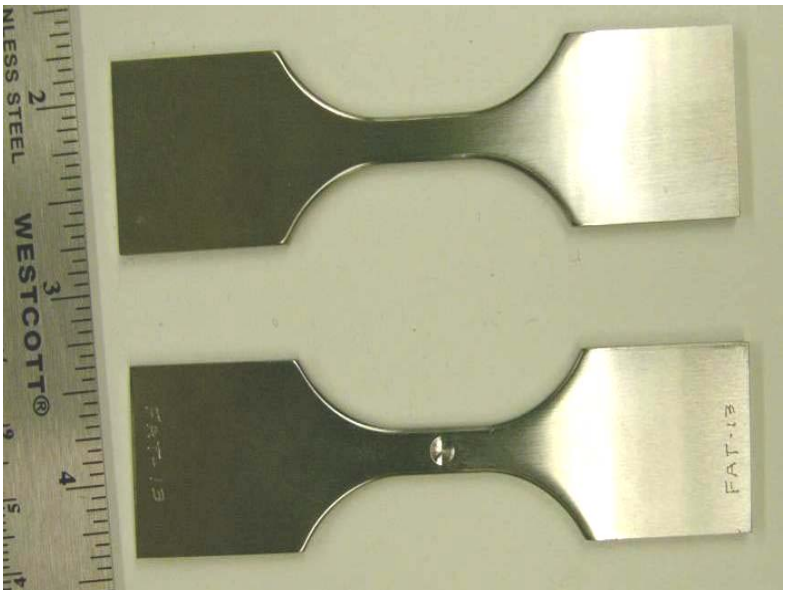

Figure 4-36 IN718 Baseline Fatigue Specimens

4.3.2.3. ESD Deposit Methodology

Two sets of ESD parameters were used to apply the ESD to the test specimens as discussed in Section 4.2. Parameter set #32 was chosen because it had a medium deposition rate and excellent quality. Parameter set V4 was chosen because of its high deposition rate and good quality. However, V4 used high ESD equipment energy settings. It was anticipated that LCF testing of these parameters should indicate if fatigue is affected when a higher energy setting (and consequently higher deposition rate) is employed. 58 specimens were prepared per the test matrix in Table 4-17.

Table 4-17 Fatigue Test Matrix for IN718 on IN718.

Substrate Material	Defect type	ESD Material	Qty	Comments
IN718	none	none	10	baseline
IN718	Type 1b	none	10	No ESD - baseline
IN718	Type 1b	IN718	10	Defect filled with Parameter set #32
IN718	Type 1b	IN718	10	Defect filled with Parameter set V4
IN718	Type 1b	IN718	10	Defect filled with Parameter set #32 and UIT applied
IN718	none	IN718	8	ESD overlay of Parameter set #32, no defect
		Total	58	

4.3.2.4. Test Methodology

The fatigue test was a load-controlled constant amplitude axial fatigue LCF test in accordance with ASTM E466. Determination of the applied stress was based on the load and original cross-sectional area of the specimen in the gage area. It assumed the specimen was rectangular and ignored features of the actual test specimens such as the rounded corners and the defects machined into some of the specimens. Stress levels were selected for each specimen group in a manner best suited to generating a complete curve of number of cycles-to-failure at given maximum stress levels (S-N curve). Testing was conducted in laboratory air at room temperature. Failure analysis of the specimens was also performed.

Figure 4-37 Instron 8500 with Mechanical Grips used for Fatigue Testing

Fatigue testing was carried out using two Instron Mechanical Test Frames, a larger Instron 8800 (Model No. 8800D1335, Serial No. 1089) and a smaller Instron 8500 (Model No. 109 20, Serial No. 1626) (Figure 4-37).

Fatigue testing consisted of repeated load application in tension-tension (the applied load never reached zero or compression) with a load ratio of 0.05 (minimum load/maximum load). The number of load cycles was counted until the specimens broke. The cycles and location of fracture were recorded. The data was plotted on a semi-log plot of maximum applied stress (load/specimen cross sectional area) vs. cycles to failure. This format is a standard S-N (stress-number of cycles) fatigue curve. The reinforcement (excess material above the bar surface) in the Bead-on-Plate was measured and recorded but not included in the stress calculations.

4.3.2.5. Acceptance criteria

Because ESD repair generally has tensile residual stresses, some fatigue debit is anticipated. Amount of allowable debit depends on application but generally should be no worse than encountered with hard chrome plating (per ASTM E466).

4.3.2.6. Test Results

The total cycles to failure at different maximum stress levels of all the test specimens are listed in Table 4-18. The equations determined from a regression analysis that provide a best-fit to the data points for each configuration (calculated without including run-out data points) are presented in Table 4-19. Individual test results are in Figure 4-38 through Figure 4-44.

Table 4-18 Fatigue Results

Specimen	ESD Condition	Max Stress (psi)	Cycles to Failure	Failure Location	Comments
FAT-1	V4	160000	12,666	Opposite ESD	
FAT-2	V4	140000	20,289	Through ESD	
FAT-3	V4	120000	31,063	Through ESD	
FAT-4	V4	100000	58,167	Through ESD	
FAT-5	V4	80000	126,140	Through ESD	
FAT-6	V4	60000	351,723	Through ESD	
FAT-7	32	160000	30,841	Top, Rear	
FAT-8	32	140000	50,697	Top, Rear	
FAT-9	32	120000	45,241	Through ESD	
FAT-10	32	100000	87,443	Through ESD	
FAT-11	32	120000	65,287	Through ESD	Surface not smooth
FAT-12	32	80000	1,780,301	Through ESD	Run-Out
FAT-13	Divot	90000	138,501	Front, Right Corner near	
FAT-14	Divot	120000	64,504	Divot	
FAT-15	Divot	140000	34,814	Divot	
FAT-16	Divot	160000	17,870	Divot	
FAT-17	Divot	100000	110,500	Divot	Estimate, counter did not stop
FAT-18	Divot	80000	198,497	Divot	
FAT-19	Divot	130000	44,548	Divot	
FAT-20	Divot	110000	80,380	Divot	
FAT-21	Divot	60000	4,771,958	Divot	Run-Out
FAT-22	Divot	100000	n/a	Divot	Estimate, counter did not stop
FAT-23	V4	100000	88,414	Through ESD	
FAT-24	V4	120000	48,570	Through ESD	
FAT-25	V4	140000	17,585	Through ESD	
FAT-26	V4	80000	260,297	Through ESD	
FAT-27	32	130000	45,059	Through ESD	
FAT-28	32	90000	70,172	Through ESD	
FAT-29	32	110000	135,387	Top, Rear	
FAT-30	32	90000	346,623	Bottom, Front	
FAT-31	32	120000	111,003	Bottom, Front	
FAT-32	UIT	100000	285,866	Through ESD	
FAT-33	UIT	120000	73,337	Top, Rear	
FAT-34	UIT	140000	50,962	Top, Rear	
FAT-35	UIT	160000	31,053	Bottom, Front	
FAT-36	UIT	80000	2,767,740	Bottom, Front	
FAT-37	UIT	180000	15,233	Bottom, Front	
FAT-38	UIT	120000	98,674	Top, Rear	
FAT-39	Bead-on-plate	160000	27,138	Middle, Right, Below Repair	Deposit thickness: 0.1275
FAT-40	Bead-on-plate	140000	42,189	Middle, Right, Above Repair	Deposit thickness: 0.124
FAT-41	Bead-on-plate	120000	65,040	Middle, Right, Below Repair	Deposit thickness: 0.1265
FAT-42	Bead-on-plate	100000	100,988	Middle, Right, Below Repair	Deposit thickness: 0.1255
FAT-43	Bead-on-plate	80000	196,756	Middle, Front, Right, Below	Deposit thickness: 0.129
FAT-44	Bead-on-plate	60000	522,552	Middle, Right, Above Repair	Deposit thickness: 0.128
FAT-45	Bead-on-plate	170000	17,673	Middle, Right, Below Repair	Deposit thickness: 0.132
FAT-46	Bead-on-plate	110000	62,405	Middle, Right, Above Repair	Deposit thickness: 0.129
FAT-47	Baseline	141029	47,409	Bottom, Rear	
FAT-48	Baseline	120000	106,727	Bottom, Rear	
FAT-49	Baseline	100000	130,484	Bottom, Rear	
FAT-50	Baseline	160000	39,528	Top, Rear, Left	
FAT-51	Baseline	180000	16,749	Top, Rear, Center	
FAT-52	Baseline	80000	2,410,148	None	Run-Out
FAT-53	Baseline	160000	50,934	Bottom, Rear	
FAT-54	Baseline	130000	90,052	Bottom, Front, Right	
FAT-55	Baseline	110000	174,012	Top, Rear	
FAT-56	Baseline	90000	403,780	Top, Rear	
FAT-57	Bead-on-plate	70000	315,085	Middle, Right, Above Repair	Deposit thickness: 0.128
FAT-58	Bead-on-plate	50000	1,108,393	Middle, Right, Below Repair	Deposit thickness: 0.131 Run-

Table 4-19 Equations for Fatigue Life for Different Specimen Configurations

Specimen Configuration	Fatigue Life Function	R2
Baseline	y = -31032Ln(x) + 482847	0.9118
Baseline with Defect	y = -33886Ln(x) + 493108	0.9975
Bead-on-Plate	y = -33953Ln(x) + 498163	0.9649
#32	y = -23237Ln(x) + 379226	0.5385
V4	y = -27202Ln(x) + 408190	0.9494
#32 and UIT	y = -28474Ln(x) + 450261	0.9475

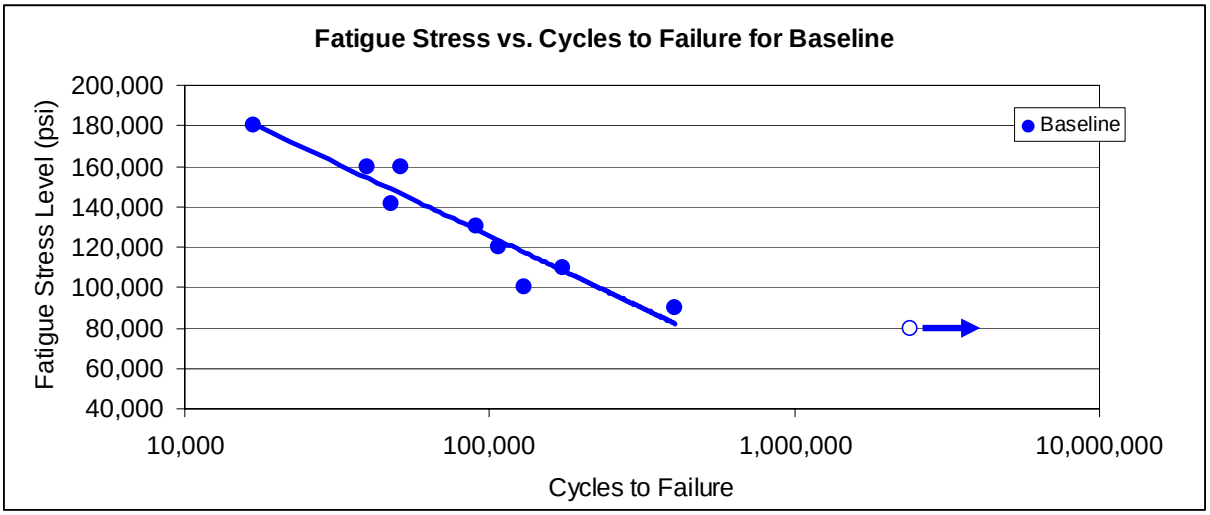

Figure 4-38 Cycles-to-failure at different maximum stress levels (S-N) for baseline

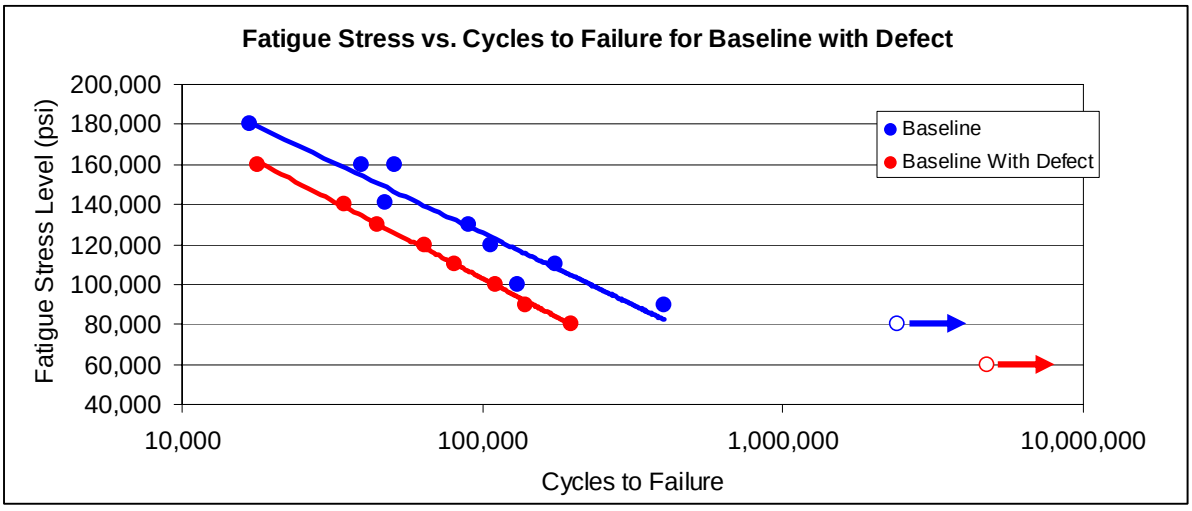

Figure 4-39 S-N of Baseline with Defect.

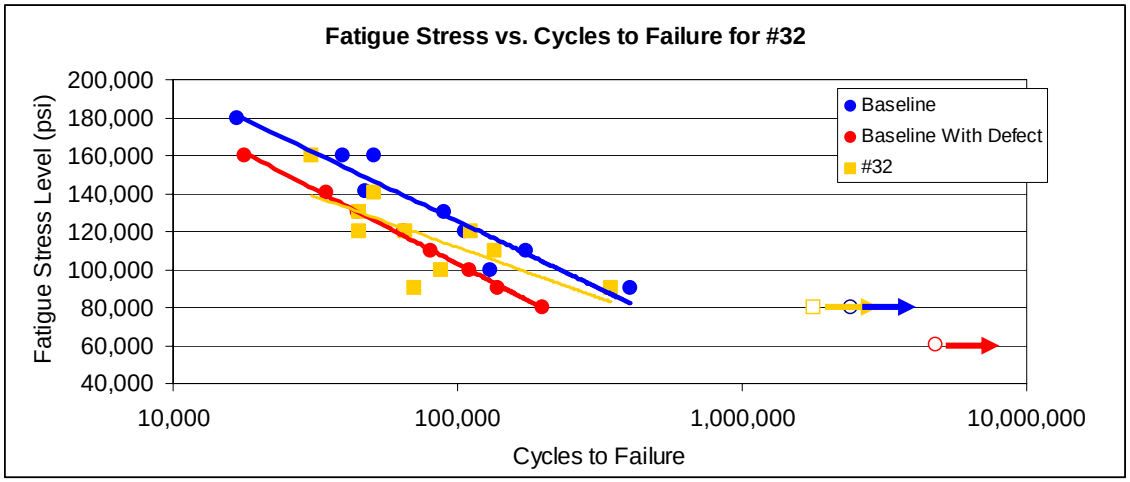

Figure 4-40 S-N of ESD #32.

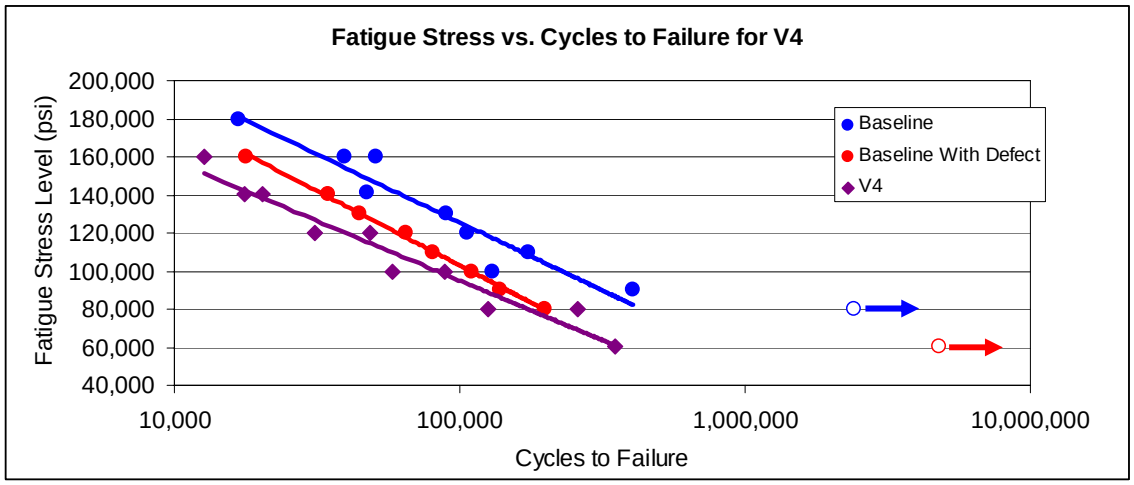

Figure 4-41 S-N of ESD V4.

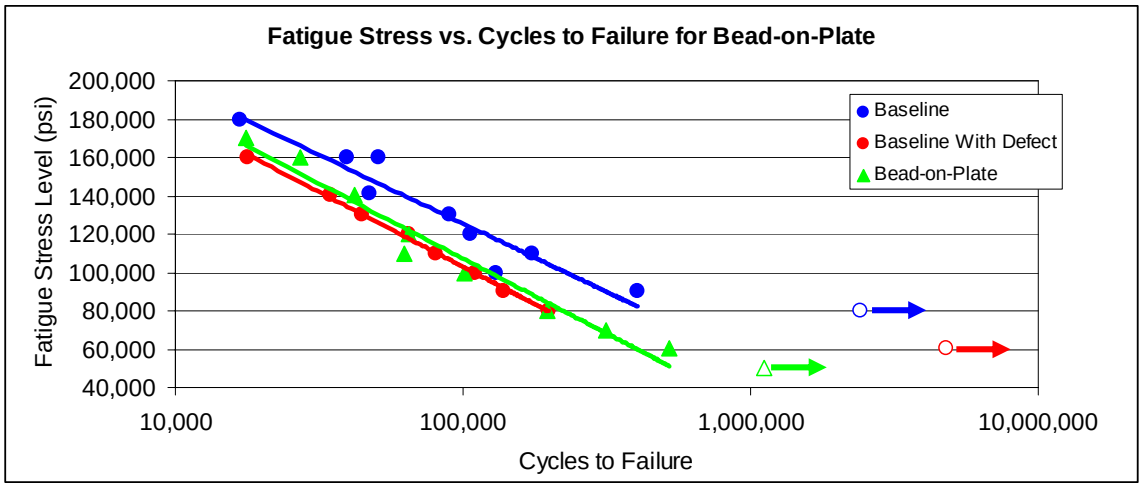

Figure 4-42 S-N of Bead-on-Plate with #32

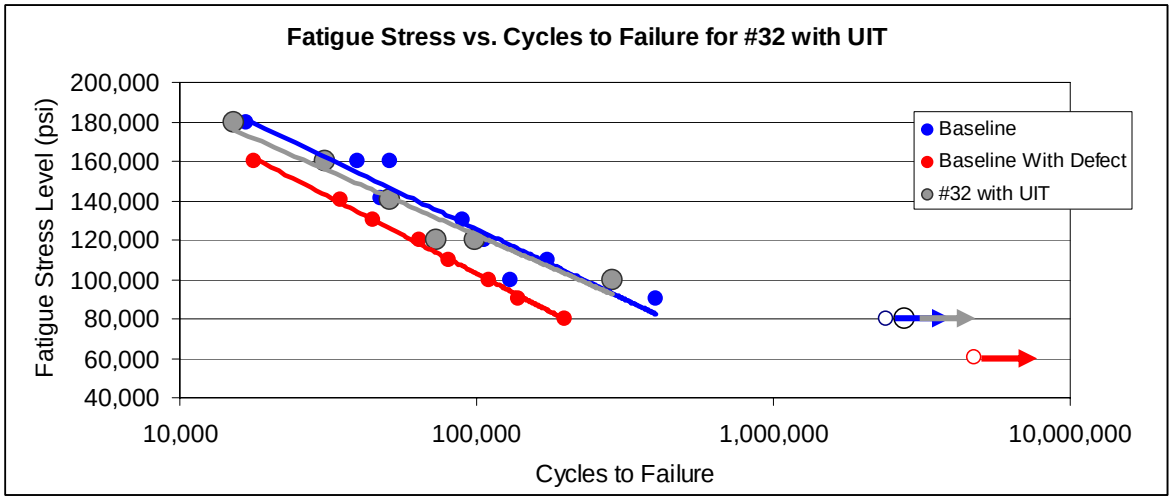

Figure 4-43 S-N of ESD #32 with UIT.

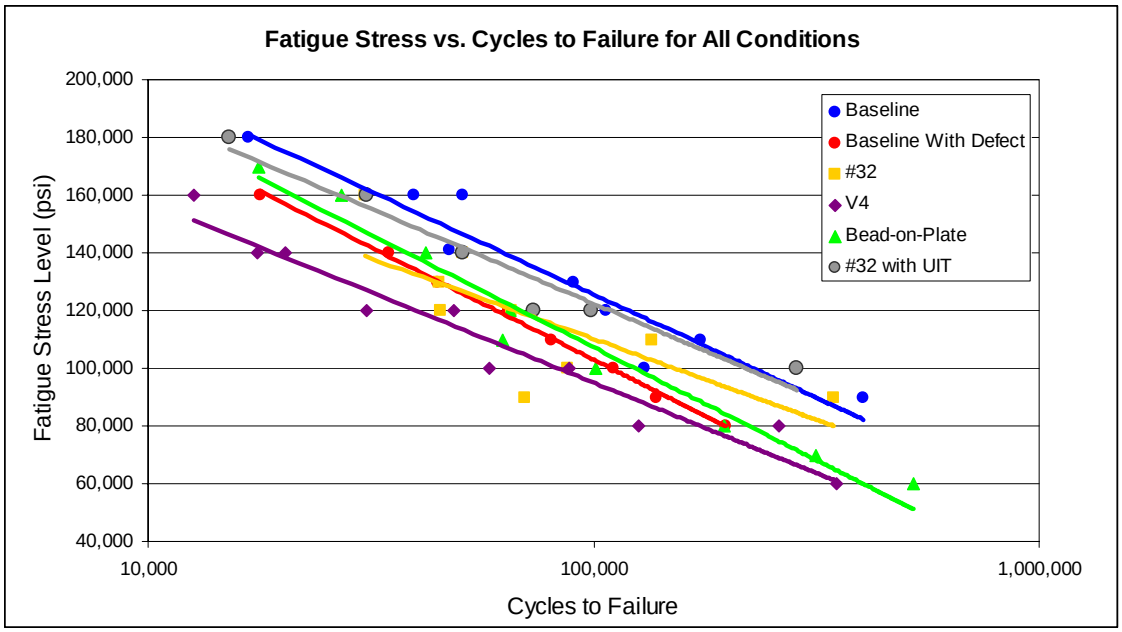

Figure 4-44 S-N of All Conditions.

In order to quantify the fatigue debit information, cycles-to-failure values at four stress levels were extracted from the S-N plots. These approximate values were tabulated in Table 4-20 and Table 4-21. It is especially interesting to note the fatigue debits as a percentage of baseline fatigue life data (Figure 4-45). The UIT treated ESD #32 repairs approach to within 1% fatigue debit at 100 ksi stress level, and to within 12% fatigue debit at 160 ksi. This is a favorable result, and should provide good incentive to investigate the fatigue behavior of ESD repairs in other important GTE alloys, and to further study the UIT technique on ESD processes.

Table 4-20 Approximate Cycles to Failure (Percentage Fatigue Debit from Baseline)

Stress Level (kpsi)	Baseline	Baseline with Defect	#32	V4	#32 with UIT	Bead-on-plate
100	123K	102K (7%)	115K (7%)	82K (33%)	122K (1%)	108K (12%)
120	105K	63K (40%)	72K (31%)	40K (62%)	102K (3%)	75K (29%)
140	66K	33K (50%)	30K (55%)	19K (71%)	57K (14%)	19K (71%)
160	32K	18K (44%)	13K (59%)	<10K (<70%)	28K (12%)	19K (41%)

Table 4-21 Approximate Cycles to Failure (Percent of Baseline)

Stress Level (kpsi)	Baseline	Baseline with defect	#32	V4	#32 with UIT	Bead-on-Plate
100	123	83%	93%	67%	99%	88%
120	105	60%	69%	38%	97%	71%
140	66	50%	45%	29%	86%	29%
160	32	56%	41%	31%	88%	59%

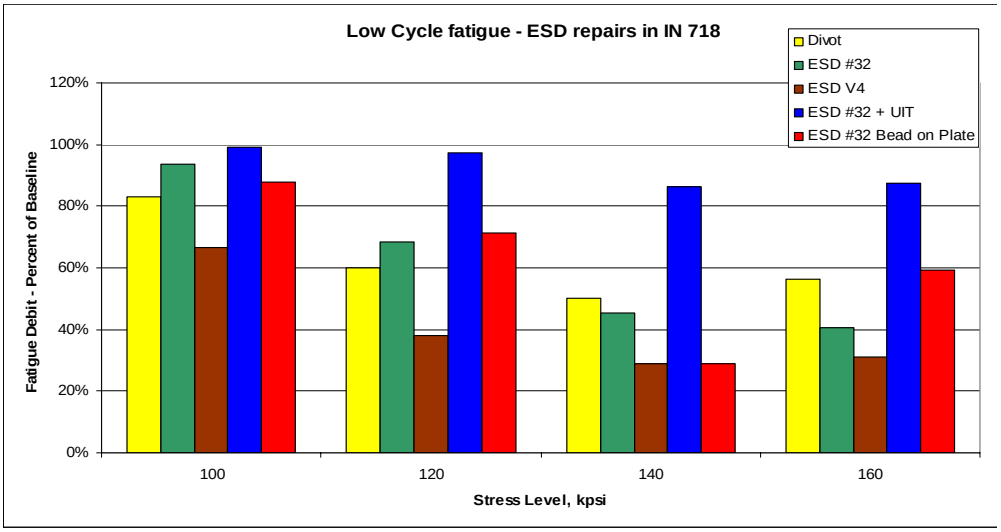

Figure 4-45 Fatigue as a Percent of Baseline

4.3.2.7. Failure Analysis

The baseline (no defect, no ESD) fatigue specimens fractured in a variety of locations with no apparent pattern. Most failed outside of the gage section. All but one of the baseline-with-defect specimens broke through the divot, and one broke outside of the divot. All specimens with defects repaired with ESD parameter set #32 failed in the ESD deposit. One specimen, FAT-11, had some area of as-deposited ESD below the ground surface (incomplete fill of the defect), but still had a fatigue life higher than a similar

specimen with no visible defective deposit. All specimens with repaired divots treated with V4 parameters failed through the ESD deposit. Most repaired specimens with UIT failed in areas outside of the ESD deposit; one of the eight failed through the deposit. Bead-on-plate specimens all failed at the edge of the ESD deposit rather than through the deposit as was seen in the divot repairs. Typical fracture locations for the baseline and baseline-with-defect specimens are shown in Figure 4-46.

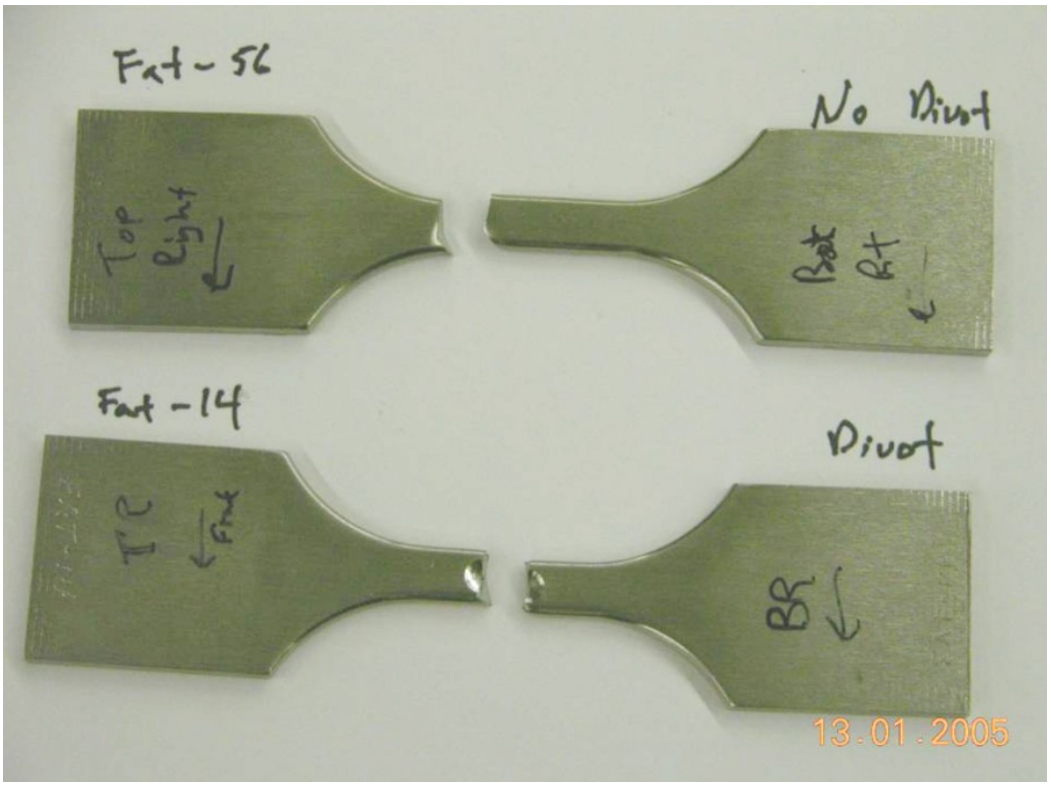

Figure 4-46 Typical fracture locations in baseline and divoted fatigue specimens.

4.3.2.8. Conclusion

As expected, all combinations of ESD repairs, with and without post-ESD treatments, produced a fatigue debit over baseline fatigue life. For ESD repaired divots, the high energy parameter set (V4) produced a greater fatigue debit than did the moderate energy level ESD repairs (#32). A most important finding was that the UIT post-ESD treatments increased the fatigue life over ESD-only repairs, to near that of baseline life.

Most of the ESD repairs failed through the ESD deposit, however, those that were post-ESD treated with UIT failed outside of the ESD deposit area. This means that it could be possible to use UIT with ESD to restore the fatigue life of damaged components. More work on optimizing this effect on a variety of materials is warranted.

Bead-on-plate ESD deposits using the #32 parameters showed greater fatigue debit than the divot repairs using the same parameters. An important observation is that the failures occurred on the edge of the ESD deposit.

It is also readily evident that the higher energy ESD treatment, parameter set #V4, caused a significantly higher fatigue debit in IN-718 than the lower energy parameter set, #32. This is proof that ESD applied with a higher energy input (and a higher deposition rate) negatively affects the fatigue life of the component.

Another comparison that can be easily seen is ESD repair in a divot versus ESD repair as "bead-on-plate" on a surface. In the lower stress levels, 100-120 ksi, the fatigue debits are about the same, but at higher stress levels, the "Bead-on-Plate repairs provide less fatigue debit than the divot repairs.

4.3.3. Tensile Testing

4.3.3.1. Test rationale

The purpose of tensile testing was to evaluate the effect of ESD on the tensile properties of the underlying material (yield strength, ultimate (tensile) strength, elongation, and area reduction).

4.3.3.2. Specimen Fabrication

The specimens were fabricated with flat plate geometry and a constant gage width, identical to those used in fatigue testing. The defect was a small divot in the center of the gage length, to allow the evaluation of the effect an ESD deposit has on the tensile properties of the substrate, the ESD fill and the interface between the two (Figure 4-35).

Test specimens, shown in Figure 4-1 and Figure 4-4, were used to provide stress-strain curves in order to determine both tensile properties and failure initiation locations. Some specimens had a Type 1b defect at the center of the gage section which was filled via ESD and machined back to specification. Others had a defect without an ESD fill. Still others had no defect, but an ESD overlay (bead-on-plate). Baseline data was established on specimens with and without a defect and without ESD (Figure 4-36).

Specimen production method:

- Grind to shape, 0.002" oversize on the thickness.
- Machine defect as required by the tensile test matrix, using the defect dimensions defined in Figure Figure 4-3
- Deposit the ESD, filling the defect above the surface of the specimen.
- Apply UIT to some of the repaired specimens, per the test matrix.
- Low-stress grind to specified gauge thickness, with a surface finish of 32μ in or better.

4.3.3.3. ESD Deposit Methodology

Parameter sets #32 and V4 as discussed in Section 4.2 were used to apply the ESD to the test specimens. It was anticipated that tensile testing of these parameters should indicate if the strength of the component is affected when a higher energy setting (and consequently higher deposition rate) is employed. 24 specimens were prepared per the test matrix in Table 4-22.

Table 4-22 Tensile Test Matrix for IN718 on IN718

Substrate Material	Defect type	ESD Material	Qty	Comments
IN718	none	none	6	baseline
IN718	Type 1b	none	6	No ESD - baseline
IN718	Type 1b	IN718	3	Defect filled with Parameter set #32
IN718	Type 1b	IN718	3	Defect filled with Parameter set V4
IN718	Type 1b	IN718	3	Defect filled with Parameter set #32 and UIT applied
IN718	none	IN718	3	ESD overlay of Parameter set #**32**, no defect
		Total	24	

4.3.3.4. Test Methodology

The tensile test was conducted in accordance with ASTM E8, a standard method of tension testing of metallic materials to determine the yield strength, yield point, ultimate (tensile) strength, elongation, and area reduction of a specimen. Testing was conducted in laboratory air at room temperature. Standard stress-strain curves were generated for the resulting test data. Failure analysis of the specimens was performed.

The tensile specimens were mounted in the load frame grips and pulled at a constant rate to failure. The strain rate was 0.1 inch/minute. Before testing, the width and thickness of each specimen was measured in the gauge section with a dial caliper. These measurements were then used to calculate the cross sectional area of each specimen. That area was used to calculate the yield stress (load/area). This analysis assumes that the test specimen is rectangular, and ignores features of the real test specimens (e.g., rounded corners and the divots cut into the divoted samples). Ultimate tensile stress was calculated by dividing the highest load attained by the cross sectional area of the failed specimen.

4.3.3.5. Acceptance criteria

Tensile, yield strength and ductility of ESD-repaired area should be no lower than that of base material (per ASTM E8).

4.3.3.6. Test Results

Individual specimen data, including yield strength (0.2%), ultimate tensile strength, reduction in area, and elongation, are shown in Table 4-24. Averages of the six specimen configurations are shown in Table 4-23, as well as graphically in Figure 4-47 through Figure 4-50. The average yield strength of all configurations was between 170 and 173 ksi, and the average ultimate tensile strength between 196 and 198 ksi.

Table 4-24 Individual Specimen Tensile Data

Specimen Number	Specimen Configuration	.2% Yield Strength (ksi)	Ultimate Tensile Strength (ksi)	% Reduction in Area	% Elongation in 0.5 Inch
1	Baseline	174.4	198.8	39.3	30.27
2	Baseline	173.8	198.9	36.0	27.71
3	Baseline	172.9	196.7	39.3	28.15
4	Baseline	173.7	197.7	38.8	28.03
5	Baseline	172.9	199.3	37.9	30.50
6	Baseline	172.6	199.0	36.5	29.69
7	Bead-on-Plate	173.6	196.6	34.4	23.34
8	Bead-on-Plate	171.1	197.4	36.0	27.36
9	Bead-on-Plate	170.0	198.4	39.8	27.91
16	Baseline with Defect	169.6	197.0	32.3	17.54
17	Baseline with Defect	169.7	198.1	29.4	18.22
18	Baseline with Defect	170.3	198.8	29.8	18.13
19	Baseline with Defect	168.4	197.6	27.9	16.92
20	Baseline with Defect	169.4	199.0	28.6	17.58
21	Baseline with Defect	171.6	197.8	29.0	16.24
22	#32	173.0	197.7	30.5	22.12
23	#32	170.7	196.2	27.5	20.40
24	#32	171.0	196.5	23.9	19.07
25	#32 with UIT	168.9	196.0	22.7	18.19
26	#32 with UIT	170.1	197.1	28.4	21.10
27	#32 with UIT	170.4	195.5	29.0	19.18
28	V4	173.5	193.6	23.8	17.19
29	V4	172.7	198.1	26.8	18.16
30	V4	170.8	195.3	28.2	20.24

Table 4-23 Tensile Data Summary

Specimen Configuration	Average Yield Strength (ksi)	Average Tensile Strength (ksi)	Average Reduction in Area (%)	Average Elongation (%)
Baseline	173.4	198.4	38.0	29.06
Baseline with Defect	169.8	198.1	29.5	17.44
#32	171.6	196.8	27.3	20.53
V4	172.3	195.7	26.3	18.53
Bead-on-Plate	171.6	197.5	36.7	26.20
#32 with UIT	169.8	196.2	26.7	19.49

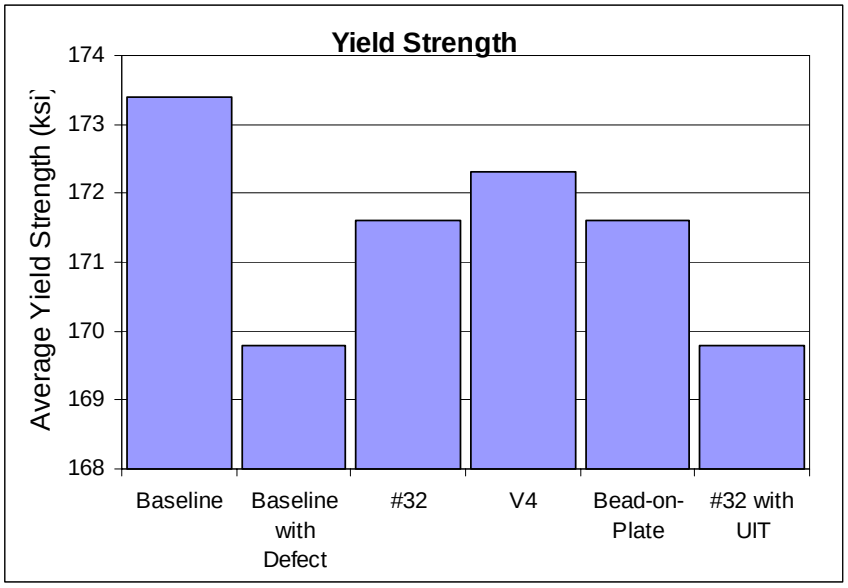

Figure 4-47 Average Yield Strength of IN718 Tensile Specimens

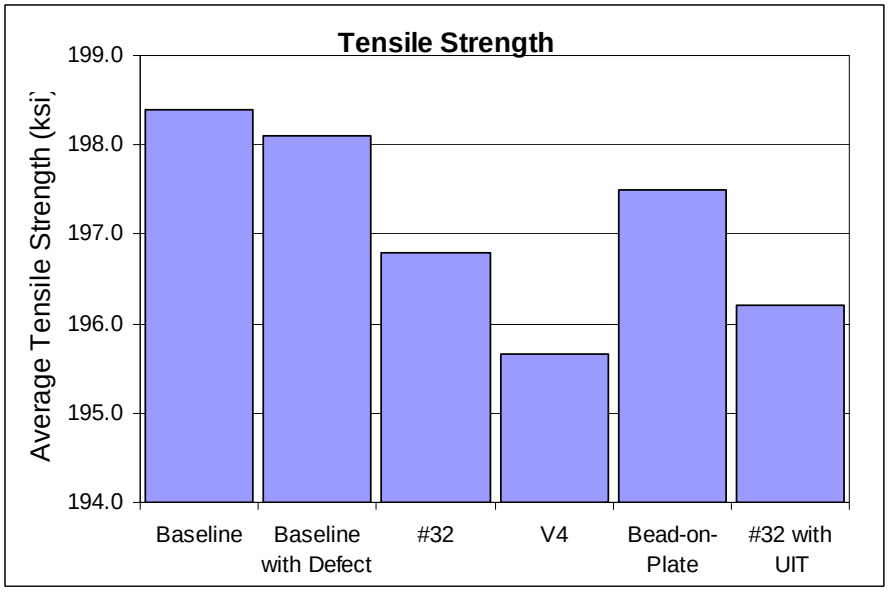

Figure 4-48 Average Tensile Strength of IN718 Tensile Specimens

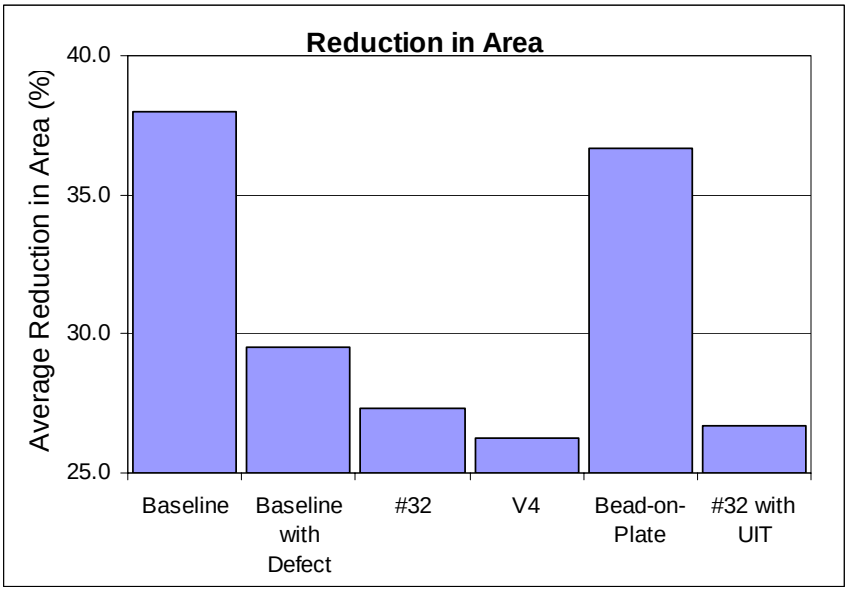

Figure 4-49 Average Reduction in Area of IN718 Tensile Specimens

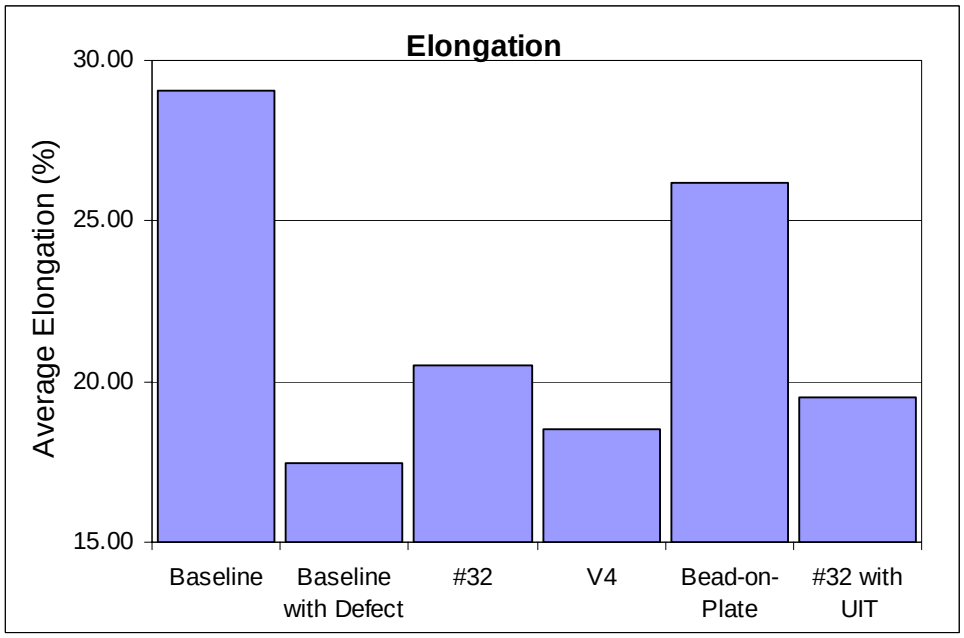

Figure 4-50 Average Elongation of IN718 Tensile Specimens

The Stress-Strain curves are shown in Figure 4-51 through Figure 4-57.

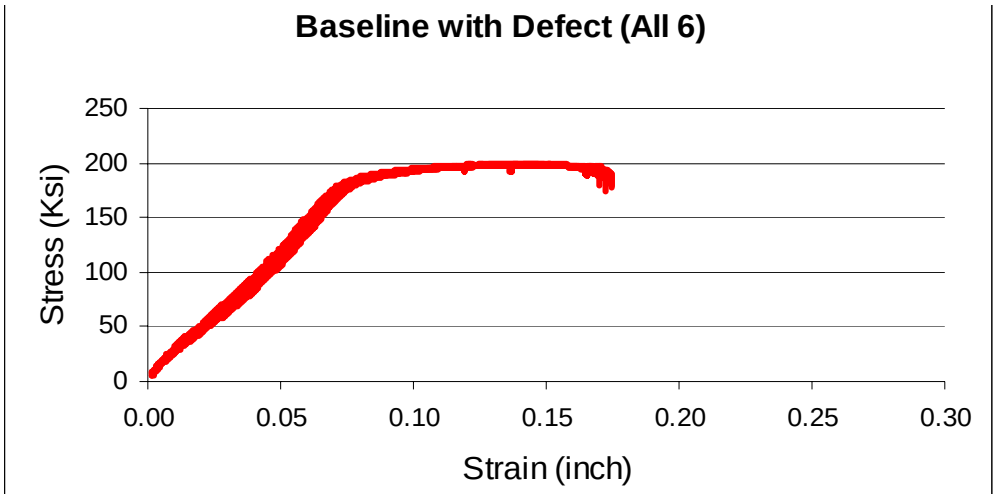

Figure 4-51 Stress-Strain Curve for Baseline with Defect Tensile Specimens

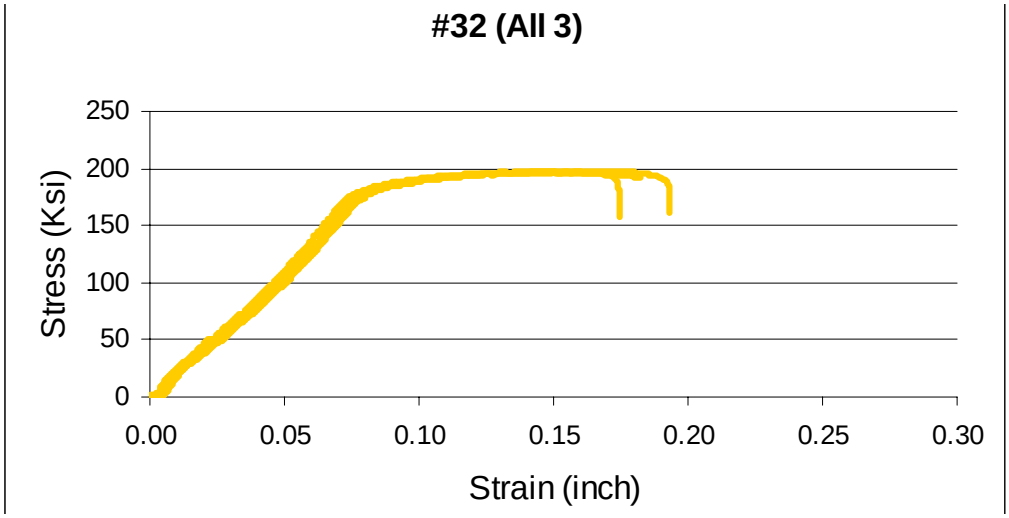

Figure 4-52 Stress-Strain Curve for #32 Tensile Specimens

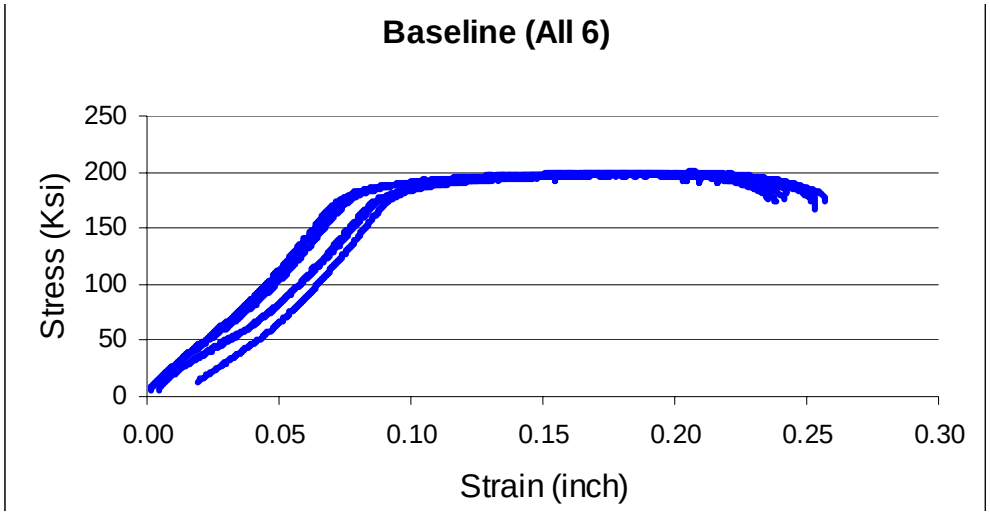

Figure 4-53 Stress-Strain Curve for Baseline Tensile Specimens

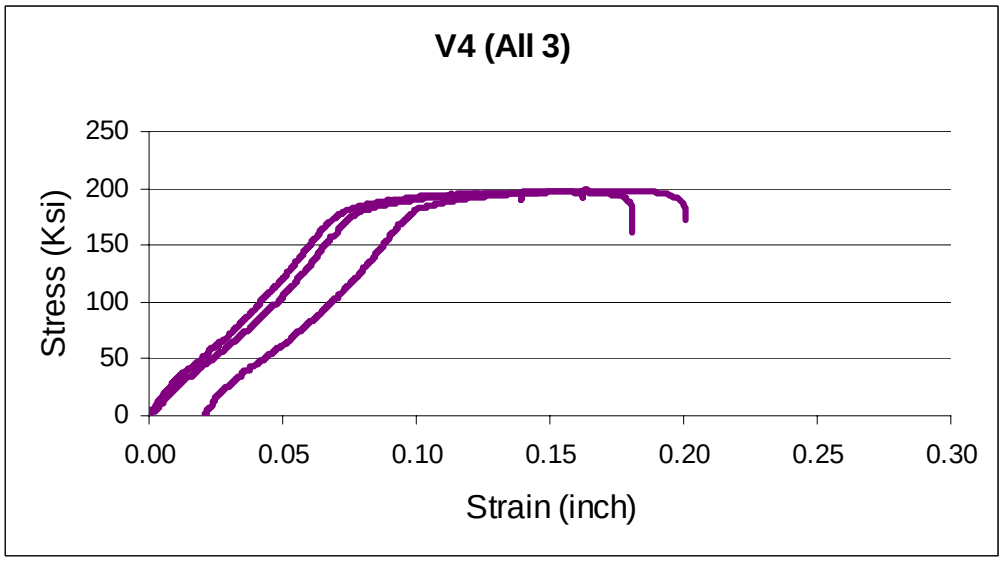

Figure 4-54 Stress-Strain Curve for V4 Tensile Specimens

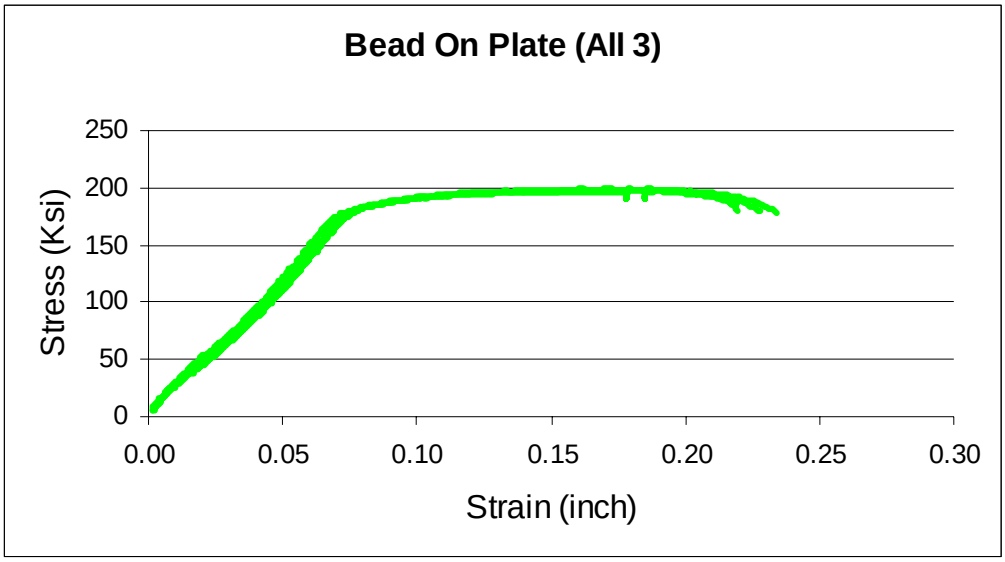

Figure 4-55 Stress-Strain Curve for Bead-on-Plate Tensile Specimens

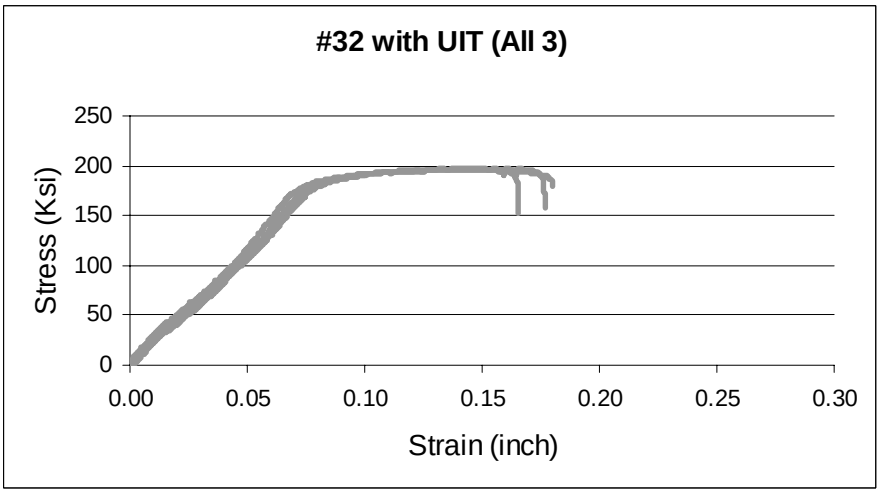

Figure 4-56 Stress-Strain Curve for #32 with UIT Tensile Specimens

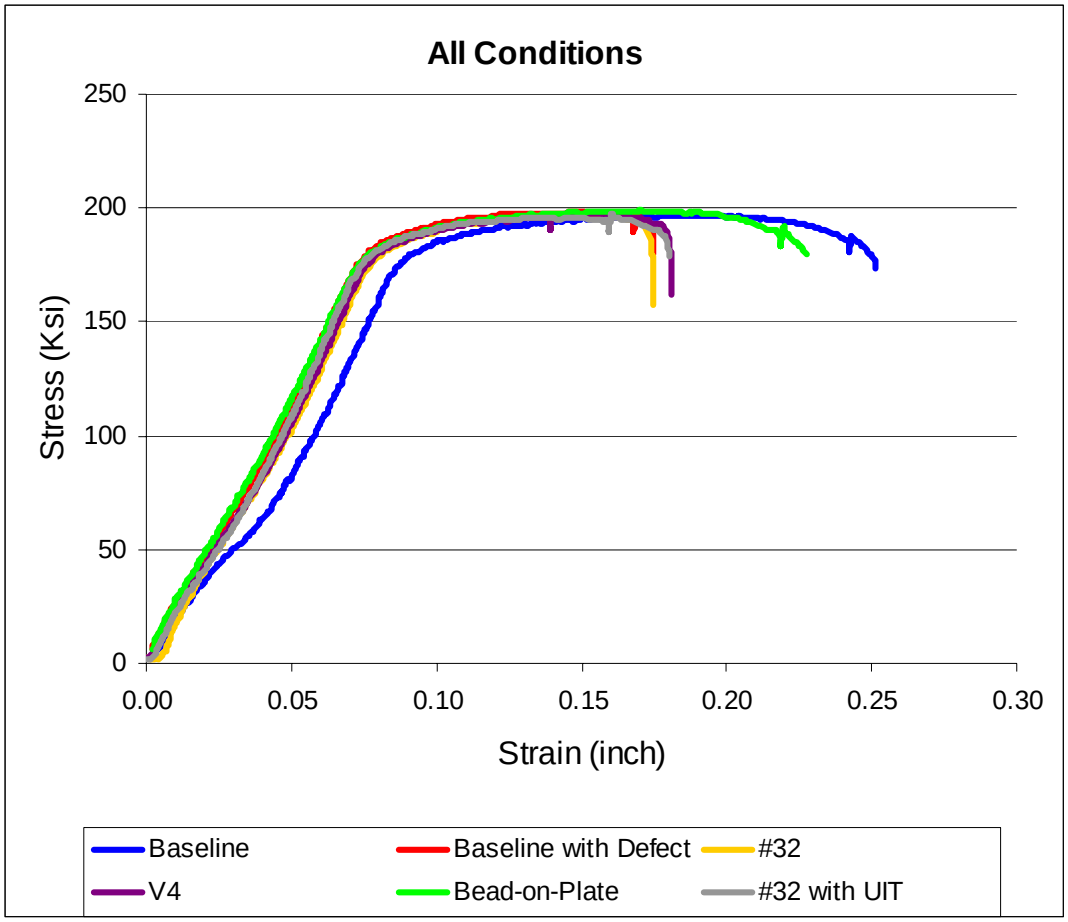

Figure 4-57 Stress-Strain Curve for all Conditions

4.3.3.7. Failure Analysis

All fractures occurred through the center of the gauge section and the ESD material except for the Bead-on-Plate configuration, which tended to break at the edge of the ESD repair rather than at the center. Examples of typical fracture locations for the six specimen configurations are shown in Figure 4-58 through Figure 4-63.

Figure 4-58 Typical Fracture of Baseline Tensile Bar.

Figure 4-59 Typical Fracture of Baseline with Defect Tensile Bar.

Figure 4-60 Typical Fracture of #32 Tensile Bar.

Figure 4-61 Typical Fracture of V4 Tensile Bar

Figure 4-62 Typical Fracture of Bead-on-Plate Tensile Bar.

Figure 4-63 Typical Fracture of #32 with UIT Tensile Bar.

4.3.3.8. Conclusion

The tensile strength behavior (yield strength and ultimate tensile strength) of all six specimen configurations was essentially identical. No strength debit was noted for ESD repairs. Ductility (reduction in area and elongation) was approximately 25% higher for the ESD bead-on-plate condition compared to the divot repair condition.

The higher energy ESD treatment, parameter set #V4, resulted in virtually no difference than the lower energy parameter set, #32. This is proof that ESD applied with the higher energy input (and higher deposition rate) does not affect the tensile strength of the component.

4.3.4. Wear (Pin-on-Disk)

4.3.4.1. Test rationale

The purpose of this wear test was for optimizing the ESD process. This test did not specifically simulate wear conditions, but provided a fairly simple method of evaluating wear and determining a correlation to hardness.

4.3.4.2. Specimen Fabrication

The specified disk was a 1.9”-diameter, 0.125”-thick flat disk of the substrate alloy. Two

0.125”-thick disks were used in the pin-on-disk test apparatus, by applying one as a “backer” for the other. The “pin” used in this test was a standard 52100 steel ball bearing.

Specimen production method:

- Grind to shape, 0.002” oversize on the thickness.
- Machine defect as required by the wear test matrix, using the defect dimensions defined in Figure 4-1.
- Deposit the ESD, filling the defect above the surface of the specimen.
- Apply UIT to some of the repaired specimens, per the test matrix.
- Surface grind flush with the parent material, with a surface finish of 32μ in or better. Note: The surface grinding was done in a linear pattern across the disk surface.

The disk had three defects, as indicated in Figure 4-64. The pin wore across both the ESD and the parent material. All specimens were fabricated from flat plate. One test specimen, after ESD was applied but before surface finishing, is shown in Figure 4-65.

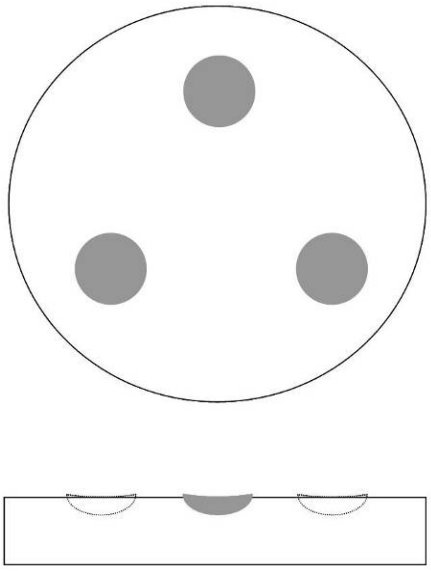

Figure 4-64 Wear Specimen with Defects

Figure 4-65 Pin-on-Disk Wear Test Specimen (Before Surface-finishing)

4.3.4.3. ESD Deposit Methodology

Parameter sets #32 and V4 as discussed in Section 4.2 were used to apply the ESD to the test specimens. It was anticipated that pin-on-disk wear testing of ESD coatings deposited using these parameters would indicate whether or not there is a relationship between hardness and wear characteristics. Five specimens were prepared per the test matrix in Table 4-25. Each specimen had three defects, all filled under identical conditions.

Table 4-25 Wear Test Matrix for IN718.

Substrate Material	Defect type	ESD Material	Qty	Comments
IN718	Type 1	IN718	2	Defect filled with Parameter set #32
IN718	Type 1	IN718	2	Defect filled with Parameter set V4
IN718	Type 1	IN718	1	Defect filled with Parameter set #32 and UIT applied
		Total	5	

4.3.4.4. Test Methodology

This test was conducted in accordance with modified ASTM G 99, a standard method for wear testing with a pin-on-disk apparatus. The elements of this test, shown schematically in Figure 4-66, are a "pin" sliding on the flat face of a disk rotating in a vertical plane, with provisions for controlling load, and speed, and for measuring friction. Friction force is measured by restraining the pin motion with a force transducer. Wear is measured by profilometry to determine the geometry of the wear scar after the test. A photograph of the apparatus is shown in Figure 4-67.

The ASTM G-99 pin-on-disk wear test protocol results in a measurement of wear rate expressed as mass loss per unit sliding distance. Because of the sample morphology, a solid surface with three ESD repair areas on the wear track, wear loss measurements could be compromised if there were measurable differences in hardness and wear resistance of the base metal (disk) and the ESD material. To avoid problems with this, wear rate was not determined. Rather, the groove depth and friction coefficient were measured. All other aspects of the test followed the standard.

The ends of the pins were machined to a hemispherical shape. They had an average hardness of 680 Knoop or 58 Rc. Hardness testing was conducted on 6 separate pins. A new pin was used for each wear test.

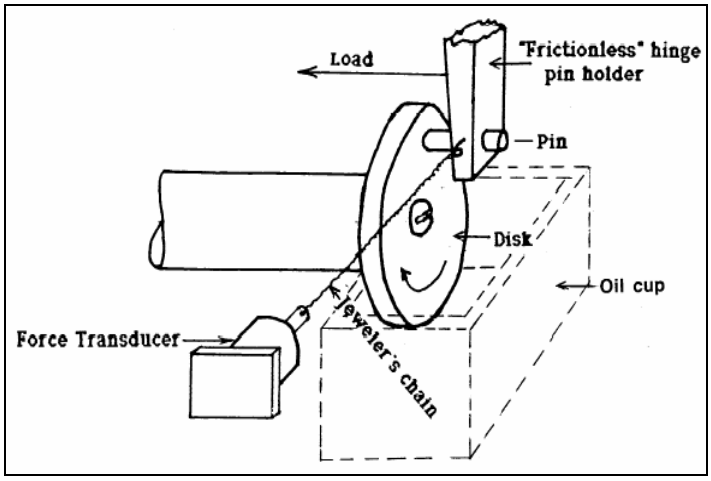

Figure 4-66 Pin-on-Disk Wear Testing Apparatus. Source:
http://www.luboron.com/pdf/PinDiskTestDescrip.pdf

Figure 4-67 Implant Sciences Corp. ISC – 200 Pin-on-Disk Tribometer

One disk was installed with unfilled divots exposed. The steel pin was inserted into the pin vise and the load arm was positioned to locate the pin in the divot center. (Figure 4-68) The arm was then fixed at this diameter and the test disk was flipped over with the ground surface up. Disk rotation was started and weights were added to the load arm until the resultant lateral forces (dragging load) were approximately mid-range on the sensing load cell. The final applied vertical load was 200 grams. When the load arm lengths are taken into consideration the vertical load on the pin was 138 grams. Figure 4-69 shows the pin sliding against the rotating disk.

The rotational speed was adjusted to provide the most uniform sliding action, avoiding any resonant vibrations. The speed was kept slow enough so that any variations in lateral force would be registered by the lateral load cell. A speed of 26 rpm was selected to fulfill these requirements.

Figure 4-68 Adjusting the Pin Track Diameter to Match the Center of the ESD

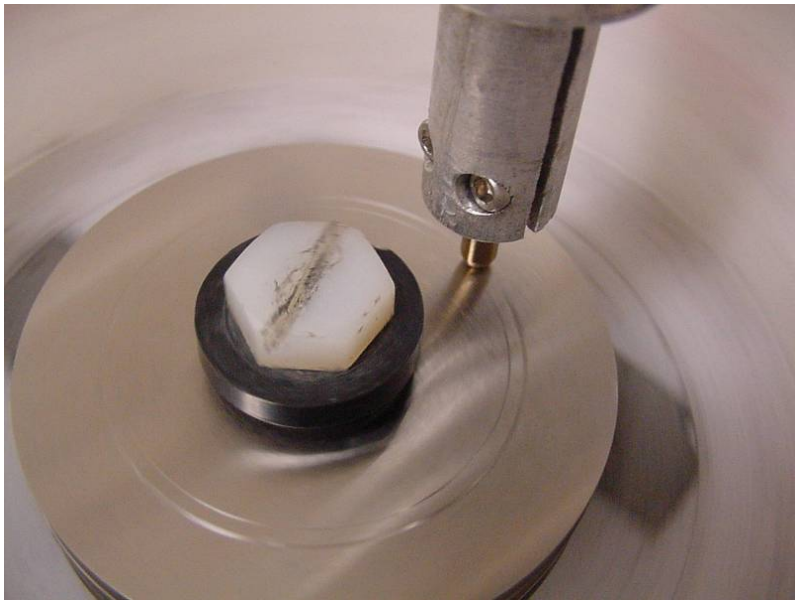

Figure 4-69 Running Pin/Disk Set-up Tests

Steady state frictional force was reached in approximately 50 revolutions so each test was run for 100 revolutions. The tests were run without lubricant. Prior to each test the specimens (disks and pins) were cleaned with mild detergent and dried with forced, heated air. Pins and disks were weighed to the nearest 0.1 gram. For the final test the pin was weighed to ±0.0001 grams before and after the test.

To generate a deeper groove and extended friction data, a longer test was run on one specimen. The total number of revolutions was 2000 which produced a sliding distance of 651 feet (198 m). The test was run at a higher speed with the same load to maximize groove generation. Friction loads were also recorded. There was no significant bulk temperature increase for this or the shorter tests.

The wear grooves in the disks were measured with a surface profilometer. Because the disks had been surface ground, creating a relatively uniform reference surface, the profilometer was set to measure maximum groove depth. Six measurements were taken on each disk, one in each ESD area and three on the base metal between the ESD.

4.3.4.5. Acceptance criteria

Since this test was conducted only for "optimization", there is no acceptance criterion.

4.3.4.6. Test Results

Lateral friction loads average 35 grams ($\mu = 0.25$) on as-finished (ground) surfaces at the start of the tests. The friction steadily increased for approximately 50 revolutions at which point it reached a steady-state level, approximately 120 grams ($\mu = 0.87$) (Table 4-26). The pin/disk machine was unable to differentiate between the base metal and ESD. There was an audible difference when the pin was sliding either parallel to or perpendicular to the surface grind pattern. In the extended test, friction started at 120 grams sliding resistance ($\mu = 0.87$) because a wear groove had been generated in the shorter test conducted on the same sample. The friction did not vary significantly for the duration of that 2000 revolution test.

Table 4-26 Pin-on-Disk Friction Summary

Specimen Number	ESD Parameter set	Normal Load (grams)	Lateral Load (grams)		Approximate Friction Coefficient μ	
			Start	End	Start	End
2 - 1	V4	138	35	135	0.25	0.98
2 - 2	V4	138	30	125	0.22	0.91
2 - 3	#32	138	40	110	0.29	0.8
2 - 4	#32	138	35	120	0.25	0.87
2 - 6	#32 with UIT	138	30	120	0.22	0.87
2 - 3 (long test)	#32	138	120	120	0.87	0.87

The maximum groove depth formed in the disk surface averaged 112 μin in the base metal and 124 μin in the ESD (Table 4-27). The extended test produced maximum groove depths of 194 and 218 μin for the base metal and ESD, respectively.

Table 4-27 Pin-on-Disk Groove Depth

Specimen	ESD Parameter set	Maximum Groove Depth (μ- inch, average of three readings)	
		Base Metal	ESD
2 - 1	V4	114	134
2 - 2	V4	92	153
2 - 4	#32	128	123
2 - 5 (No ESD)		120	NA
2 - 3 (Long Test)	#32	218	194
2 - 6 (UIT)	#32	108	85

The maximum weight loss for both pins and disks was 0.3 grams with some components not losing or gaining weight. Because neither component consistently gained or lost weight, no conclusions could be made on the relative performance of the ESD and base metal.

The wear surfaces consisted of irregularly deep grooves with mounds of disturbed metal that had been re-deposited in the groove as shown in Figure 4-70. The only difference between the groove in base metal and ESD was occasionally an ESD void was exposed as shown in Figure 4-71. Other than that there was no visible difference up to magnifications of approximately 50x. Some of the metal removed from the groove adhered to the pin tip (Figure 4-72). It was not possible to distinguish the deposits on the resurfaced UIT specimen. It was also not possible to find areas where the wear groove was significantly deeper or shallower

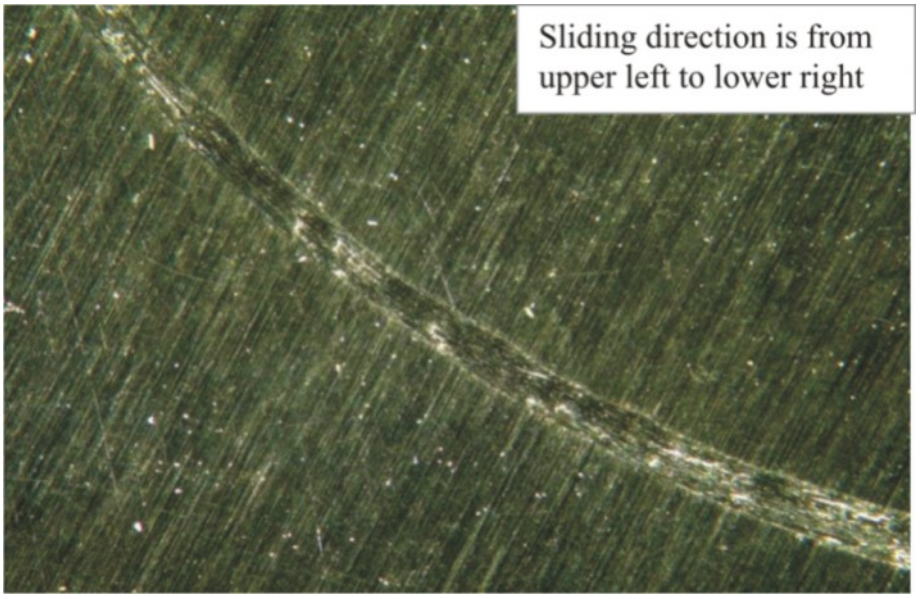

Figure 4-70 Wear Groove in Disk Base Metal.

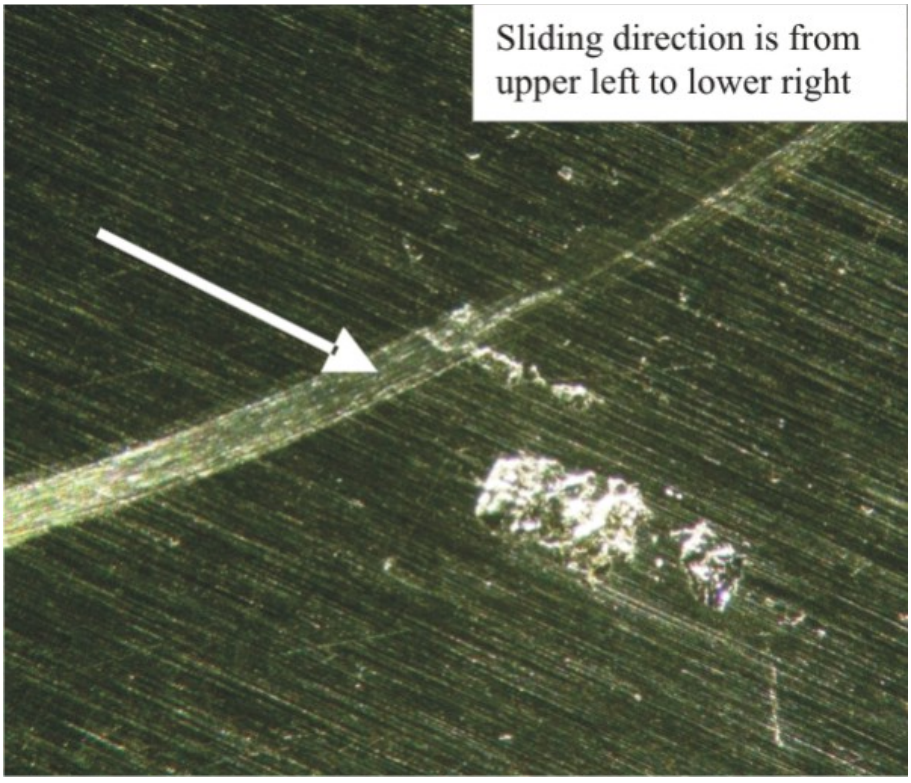

Figure 4-71 Wear Groove Encountering ESD Void

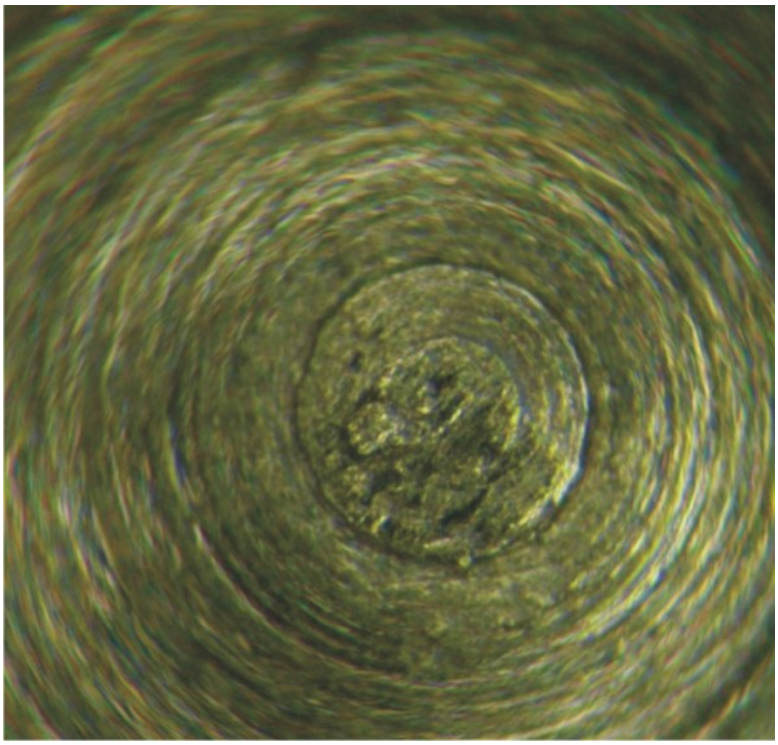

Figure 4-72 Accumulated Disk Material on Pin

4.3.4.7. Conclusions

One of the objectives of this test was to determine whether or not there is a relationship between microhardness and wear characteristics. The results would indicate that for the ESD parameter set V4, the deposit is less wear-resistant than the parent material. This coincides with the microhardness data, which shows microhardness of the parent material to be approximately 411 Knoop, and the microhardness of the parameter set V4 to be 311 Knoop. Microhardness and wear resistance both decreased compared to the parent material.

For the ESD parameter set #32, the results would indicate that the deposit is more wear-resistant than the parent material. However, the microhardness data of this parameter set was approximately 357 Knoop, a decrease from the parent material. Therefore, a conclusive relationship between microhardness and wear resistance cannot be drawn.

It is interesting to note that the increased hardness in #32 over V4 did demonstrate better wear characteristics of #32 over V4. Based on the groove depth in the ESD as a percentage of the groove depth in the parent material, #32 with UIT seemed to demonstrate the best wear resistance.

The pin/disk machine did not register a noticeable difference in friction between ESD and base metal. This is probably because the actual friction differences were too small to be measured or too short in duration to be sensed by the load cell. They were all within the experimental error of the test method, as noted by the standard deviation of the tests.

It was possible to hear a difference in the sound of the pin on the disk when the sliding changed from parallel to perpendicular to the surface grinding direction. It was not possible, however, to produce different measurable and repeatable friction coefficients on the two grinding orientations.

There was a significant vibration of the pin when it crossed an ESD area only if there was a discontinuity in the surface of the ESD. The pin would momentarily catch on the discontinuity and then break free, similar to a slip/stick motion. This did not happen when there were no visible surface discontinuities in the ESD.

The wear mechanism appears to be abrasion followed by adhesion (a.k.a. galling). Initially the contacting surfaces are clean, hard steel and softer IN718. Abrasion of the IN718 by the steel occurs until enough IN718 has accumulated on the pin. At this point the contact zone is probably predominantly IN718 on IN718. This type of contact is an ideal condition for adhesive wear. The factors that will promote adhesion include fresh clean surfaces, little to no hardness differences between components, identical materials on either side of the contact zone and susceptible microstructure.

The wear groove depth was somewhat greater in the ESD material than in the base metal for the samples prepared with ESD parameters set V4. However, the reverse was found for those samples prepared with the #32 parameter set. These samples showed slightly shallower depths in the ESD material than in the base metal. This is not a significant difference, being within the experimental error of the test, and therefore the ESD wear behavior of the material was similar to that of the base metal.

The sample that was UIT processed showed a slightly shallower groove depth in the ESD than in the base metal. But that is probably still not a significant difference, owing to the experimental error (standard deviation) of 15 to 20 percent for these tests.

4.3.5. Wear Testing (Sliding and Fretting)

4.3.5.1. Test Rationale

The purpose of these tests was to quantify the wear rate between virgin IN718 (baseline) and ESD repaired IN718 under both long (sliding) and short (fretting or dither) stroke conditions. In the JTP, a wear test apparatus and procedure designed by Hamilton Sundstrand was selected.

The fretting wear test was selected to simulate the dithering or vibration movement between two mating components that are typical in gas turbine engines. It was believed that there were no standard ASTM wear tests that would accurately reflect conditions of use for GTE components, so the Hamilton Sundstrand test (hereinafter referred to as the H-S test) was selected.

The H-S wear testing was performed on IN718 specimens only. The mating material was IN718, as that is the material of the mating component for the 10-12 stator segment discussed in Section 4.2.2. The design of these tests was driven by actual GTE component operating conditions.

4.3.5.2. Specimen Fabrication

All specimens were fabricated from flat plate.

Specimen production method:

- Manufacture the test specimens as shown in Figure 4-73 through Figure 4-76, but rough-finish both 2" x 0.25" faces with a total thickness of approximately 0.256" (0.003" per side over size).
- Machine defect as required by the wear test matrix, using the defect dimensions defined in Figure 4-5 and Figure 4-6. Machine defects completely across the width of the specimen face on both sides of the panel wear specimen. The location of the grooves must match the location of the counter face specimens. Since it is possible that the stresses involved in machining and repairing the test defects will cause the panel to bend, it is expected that this location for the test defect and its placement on both sides will balance out the stresses and prevent bending. Furthermore, should bending occur it will have minimal impact on the test.
- Deposit the ESD, filling the defect above the surface of the specimen.
- Low stress grind both sides to remove 0.003" and provide the required surface finish.

Figure 4-77 is a photograph of the wear specimens.

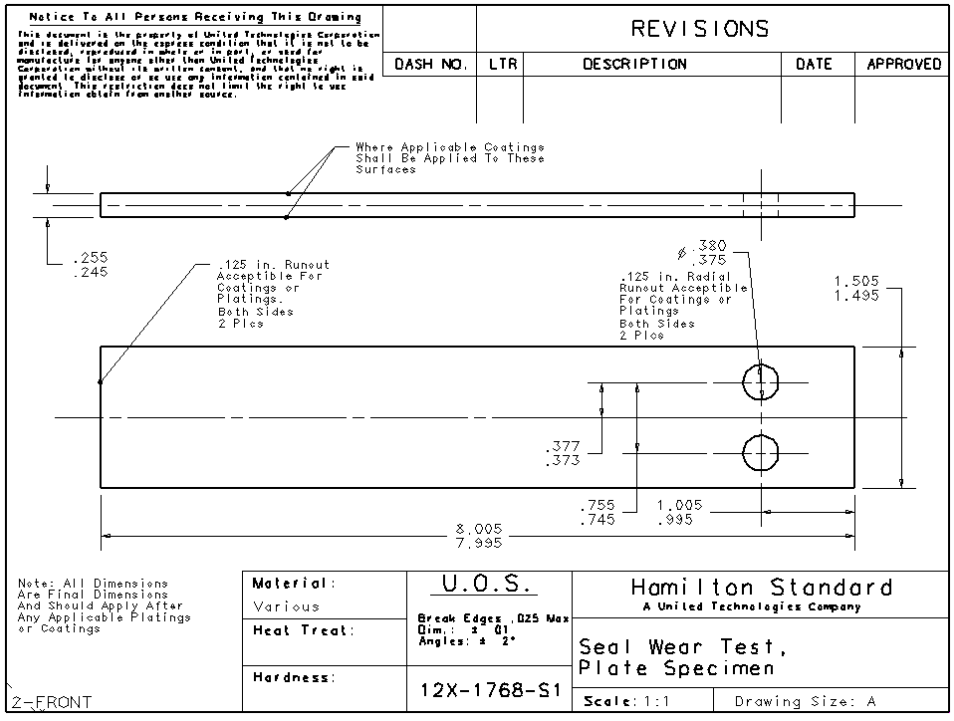

Figure 4-73 Hamilton Sundstrand Wear Specimen – Before Defects

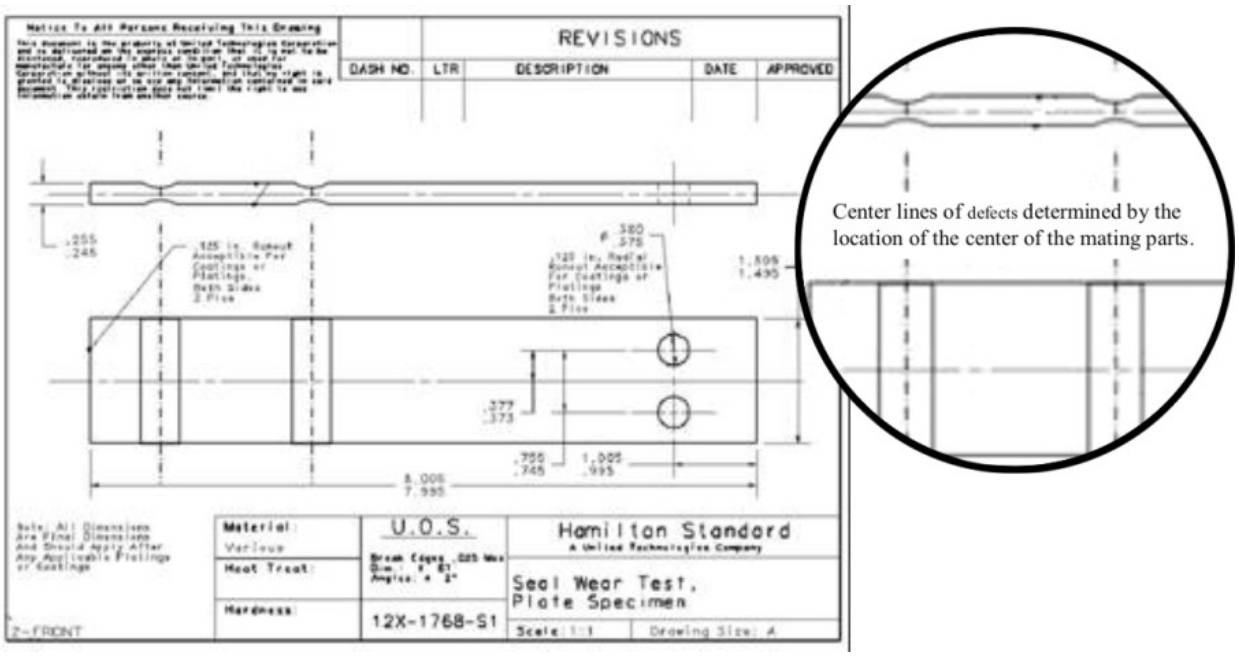

Figure 4-74 Hamilton Sundstrand Wear Specimen – With Defects

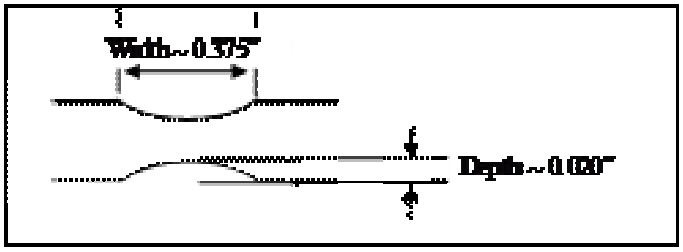

Figure 4-75 Defect Specifications for HS Test Specimens

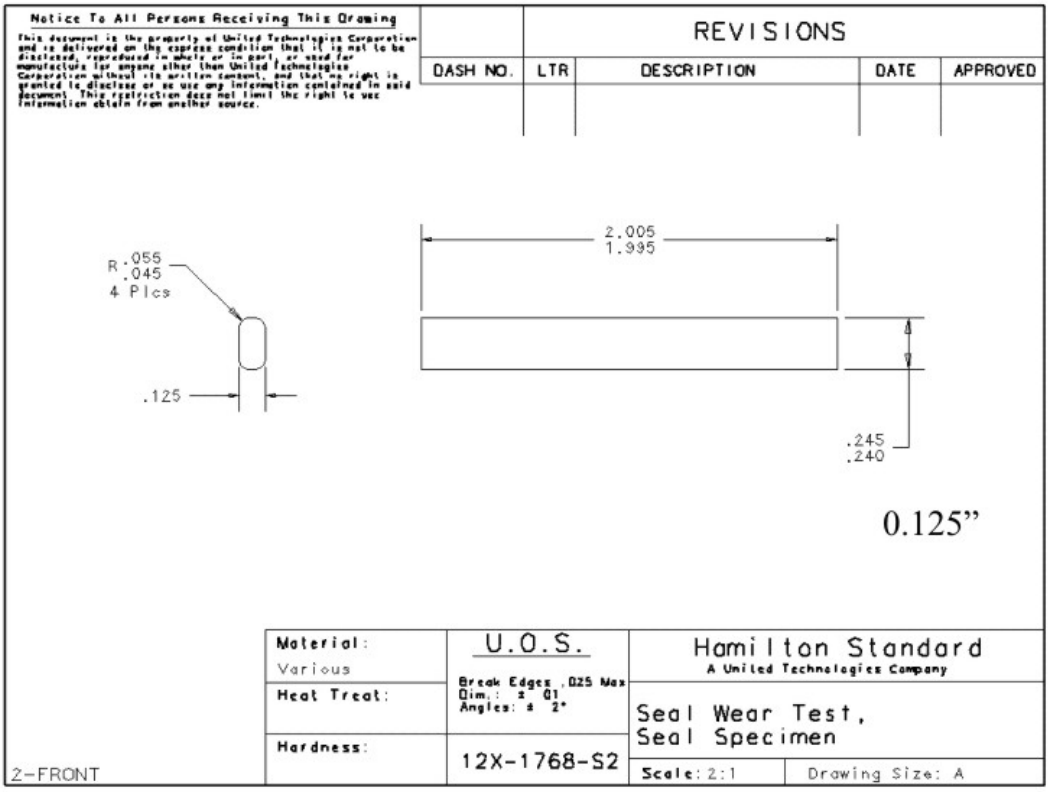

Figure 4-76 Hamilton Sundstrand Mating (Counterface) Wear Specimen

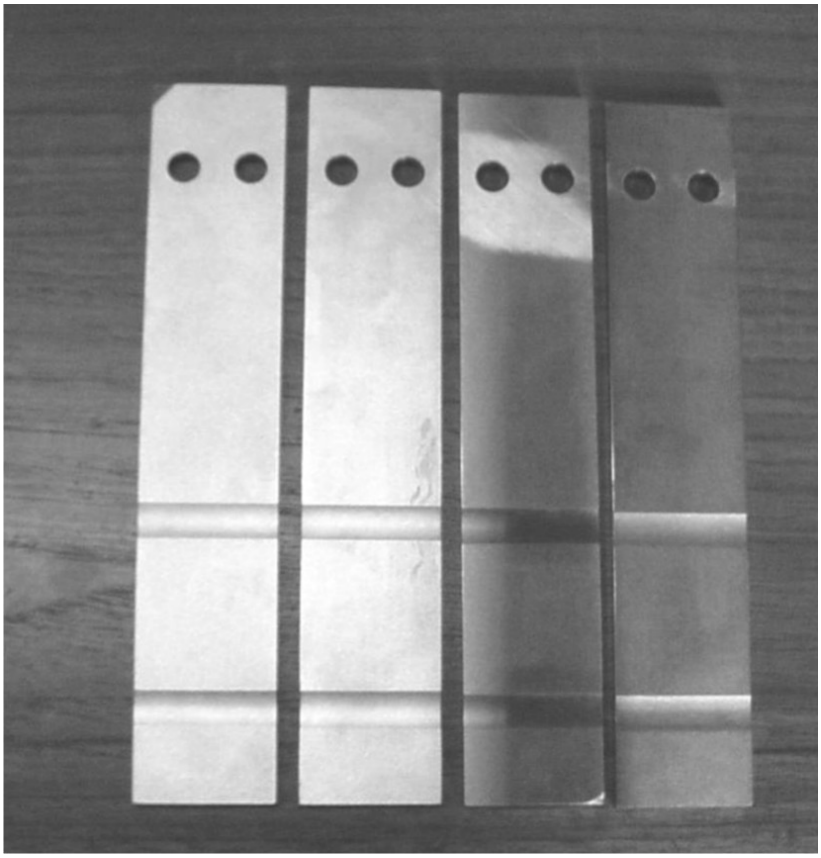

Figure 4-77 Hamilton Sundstrand Wear Test Specimens

4.3.5.3. ESD Deposit Methodology

Parameter sets #32 and V4 as discussed in Section 4.2 were used to apply the ESD to the test specimens. It was anticipated that H-S wear testing of ESD coatings deposited using these parameters would indicate whether or not there is a relationship between hardness and wear characteristics. Ten IN718 specimens were prepared and tested per the test matrix in Table 4-28 and Table 4-29.

Table 4-28 H-S Wear Test Matrix for IN718 on IN718.

Substrate Material	Specimen Number	Defect type	ESD Material	Qty	ESD Parameters	Stroke Length
IN718	S1 and S12	none	none	2	Baseline	Short stroke (fretting)
IN718	S2 and S13	none	none	2	Baseline	Long stroke (sliding)
IN718	N5	Type 2	IN718	1	#32	Short stroke (fretting)
IN718	N3	Type 2	IN718	1	#32	Long stroke (sliding)
IN718	N2	Type 2	IN718	1	V4	Short stroke (fretting)
IN718	N6	Type 2	IN718	1	V4	Long stroke (sliding)
IN718	N1	Type 2	IN718	1	#32 with UIT	Short stroke (fretting)
IN718	N4	Type 2	IN718	1	#32 with UIT	Long stroke (sliding)
			Total	5		

Table 4-29 Test Parameters for Wear Test on IN718 Panels With and Without ESD Repair

Wear Test Matrix for ESD Applied IN718						
Test #	**Panel**	**Frequency (Hz)**	**Cycle**	**Displacement (inch)**	**Clamping Load (lbf)**	**ESD Repaired?**
1	S-1	15	1,000,000	0.01 to -0.01	150	No
2	S-2	1.5	100,000	0.1 to -0.1	150	No
3	S-12	15	1,000,000	0.01 to -0.01	150	No
4	S-13	1.5	100,000	0.1 to -0.1	150	No
5	N-1	15	1,000,000	0.01 to -0.01	150	Yes
6	N-4	1.5	100,000	0.1 to -0.1	150	Yes
7	N-2	15	1,000,000	0.01 to -0.01	150	Yes
8	N-3	1.5	100,000	0.1 to -0.1	150	Yes
9	N-5	15	1,000,000	0.01 to -0.01	150	Yes
10	N-6	1.5	100,000	0.1 to -0.1	150	Yes

4.3.5.4. Test Methodology

The wear testing was performed by United Technologies Research Center (UTRC). Four test specimens were held in a fixture that uses a screw driven lever arrangement to apply a fixed load to the four test specimens, to hold them against a counter face. Relative motion between specimens and counter face was provided by a standard tensile test frame. The fixture was installed in a standard tensile test frame (see Figure 4-78 through Figure 4-80). The fixture design allowed four repaired areas to be tested simultaneously with each test panel. Loads were chosen to obtain visible wear on the specimens. Wear tests were performed in unlubricated conditions.

The tests were conducted using a 20,000 lb servo-hydraulic MTS load frame. A special fixture was used to keep the panels and counterface specimens in place throughout the test.

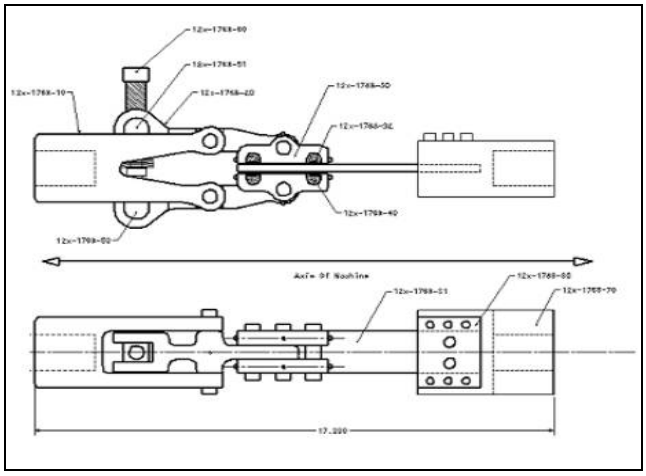

Figure 4-78 Wear Test Specimen Assembly.

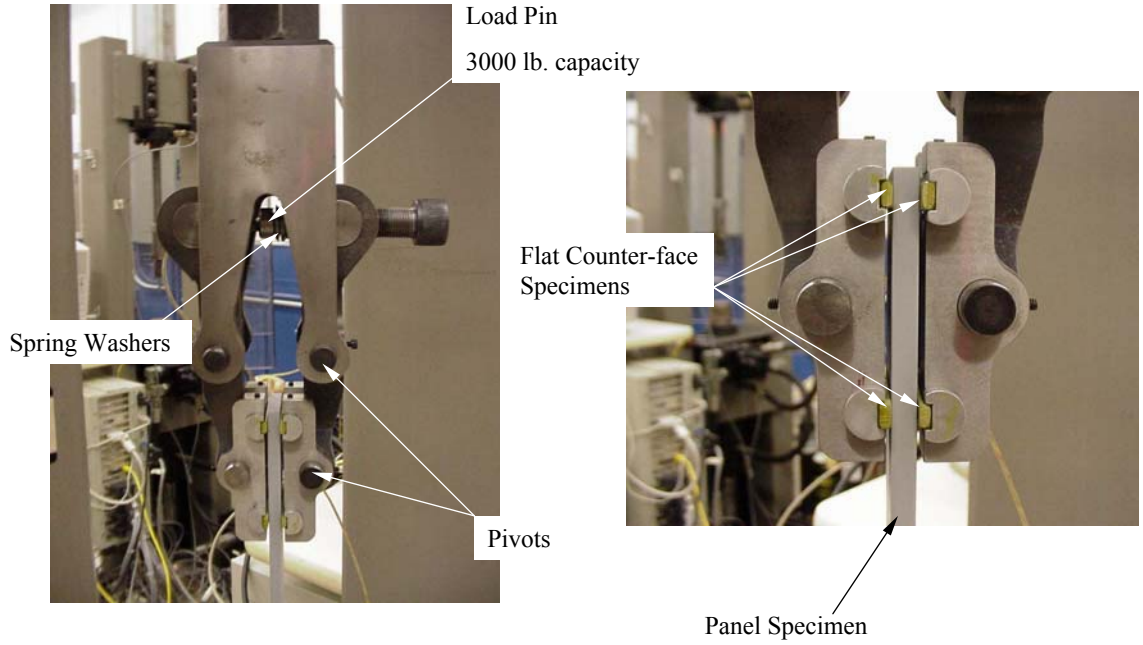

Figure 4-79 Wear Test Assembly With Test Specimens.

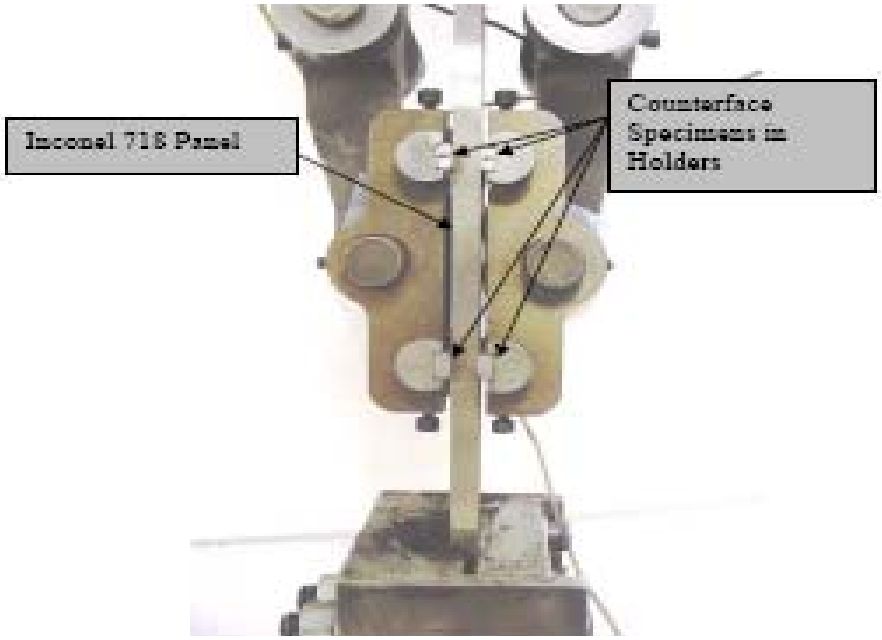

Figure 4-80 Photograph of the Test Setup with Panel and Counterface Specimens

Each test consisted of four counterface specimens per panel, with a total of ten panels and forty counterface specimens. Six of the Inconel panels had undergone ESD repair and four of the panels were virgin IN718 panels. Photographs, dimensional measurements, and weight measurements were recorded for each test. The dimensions of the IN718 panel's were 8.00" x 1.50" x 0.25" and dimensions for the counterface specimens were 2.000" x 0.250" x 0.125".

The counterface specimens and panels were photograph before testing, and the counterface specimens and panels were each weighed using the same scale for all specimens to the nearest 0.1 mg. Once the pre-test weight measurements were completed for the specimens, one of the flat surfaces on all of the counterface specimens was grit blasted with 250 micron alumina grit to enable bonding between the counterface specimen and holders. The roughened faces of the counterface specimens were bonded to the holders using M-Bond 200 strain gage adhesive, and the counterface specimens in the holder were weighed before testing. Once all the weight measurements and photographs were completed, the panels and four counterface specimens in holders were loaded into the test fixture in the test frame. The panels were secured in the test fixture by six ¼-20 bolts and two ½-20 bolts. Four counterface specimens in the holders were slid into the four recesses in the top wear fixture. The set-screws used to fasten the holders in place were left loose, while the counterface specimens were adjusted to ensure parallelism between the panels and counterface specimens. The load bolt was tightened down till the strain gage indicated a clamping force of 100 lbf and the set screws on the counterface specimen holders were tightened. With all test specimens in place in the fixture and load frame, the load bolt was tightened down with a clamping force of 150 lbf for the test. An MTS 458 controller was programmed to run the test in the load frame in displacement control at the appropriate frequencies. In addition, the maximum cycle count was set in the controller so as to stop the test once the maximum cycle count was achieved. The linear variable displacement transducer located in the actuator of the load frame was used to monitor the displacement of the panel, and maintain the displacement range for all tests. The load cell on the test frame was used to monitor the axial load on the panels, while a strain gage was used to establish and monitor the clamping load between the counterface specimens and the panels. The ESD repaired region was located 1” from the top of the panel, and there was a 2” separation between the repaired grooves. This was the location where the counterface specimens were in contact with the ESD repaired panels throughout the wear test.

Once the test was in progress, LabView data acquisition software was used to monitor the displacement, axial and clamping loads, frequency, and cycle count of the test.

4.3.5.5. Acceptance criteria

Sliding and abrasive wear rates of ESD-repaired area should be equal or less than those for base material

4.3.5.6. Test Results

Images of the wear section on two specimens (one Baseline and one with an ESD repair), before and after testing, are shown in Figure 4-81 through Figure 4-86.

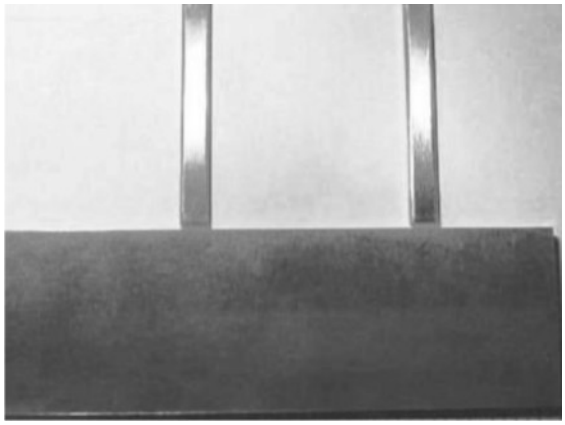

Figure 4-81 Test 1, Panel S-1 and Ends of Counterfaces Pre-test

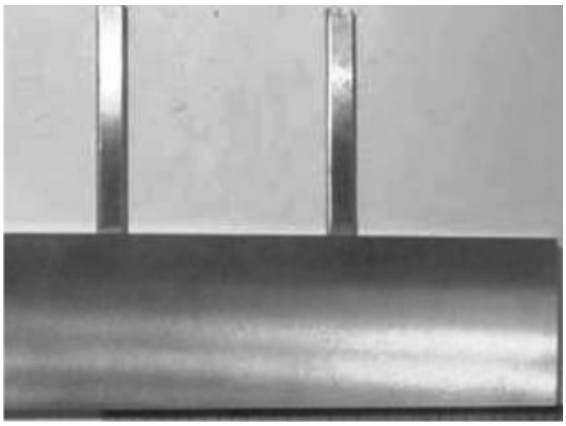

Figure 4-82 Test 10, Panel N-6 and Ends of Counterfaces Pre-test

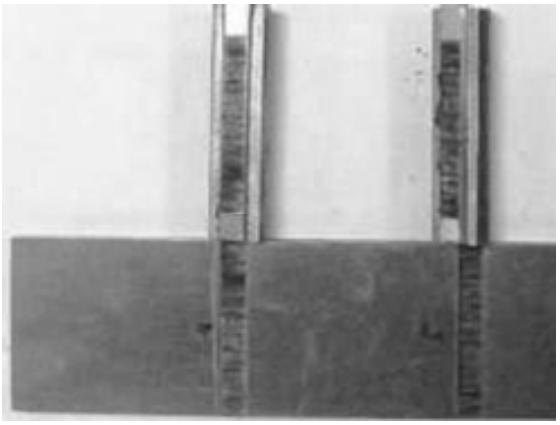

Figure 4-83 Post-test of Panel S-1 with Counterface Specimen 4 & 5

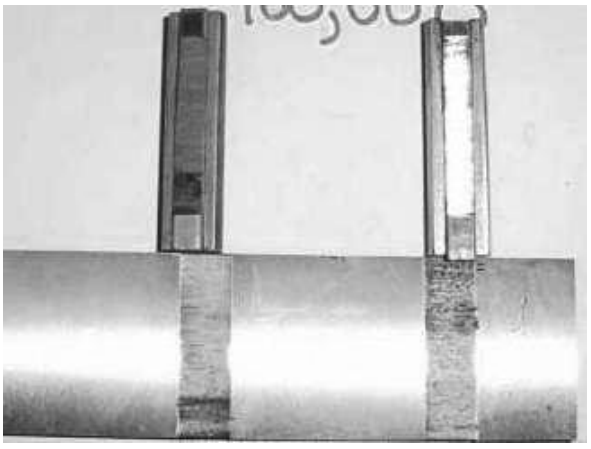

Figure 4-84 Post-test of Panel N-6 with Counterface Specimen 718-13 & 718-14

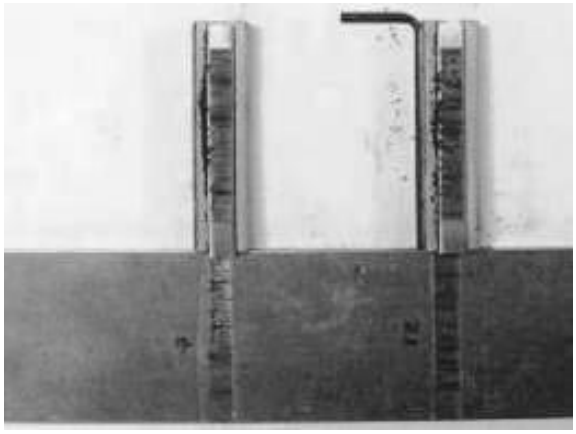

Figure 4-85 Post-test of Panel S-1 with Counterface Specimen 7& 12

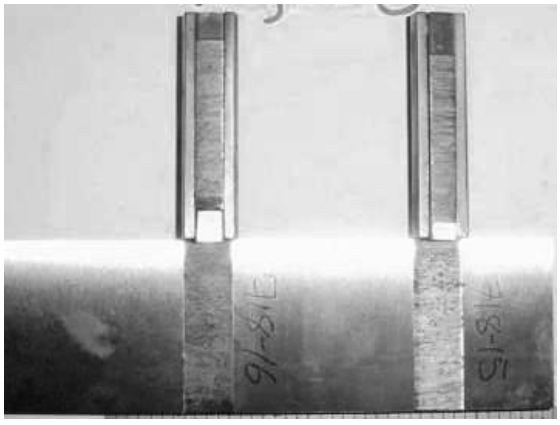

Figure 4-86 Figure 4.x: Post-test of Panel N-6 with Counterface Specimen 718-15 & 718-16

The weight measurements for all the specimens, before and after testing, are given in Table 4-30.

Table 4-30 Weight Measurements Before and After HS Wear Test

Specimen Set #	ESD Parameters	Cycle Type	Panel #	Panel Weight (g)		Counterface Specimen #	Specimens Weight (mg)		Specimen + Holder Weight (mg)	
				Before	After		Before	After	Before	After
1	Baseline, No ESD	± 0.010 @ 15 Hz, 1,000,000 cycles	S-1	366.47	366.17	4	7802	7723	44148	44064
						5	7774	7684	44162	44062
						7	7589	7507	43827	43738
						12	7710	7631	43759	43687
2	Baseline, No ESD	± 0.10 @ 1.5 Hz, 100,000 cycles	S-2	366.24	364.98	16	7660	6925	44118	43380
						17	7689	6959	44084	43351
						23	7613	6788	43831	43004
						24	7657	6822	43832	42983
3	Baseline, No ESD	± 0.010 @ 15 Hz, 1,000,000 cycles	S-12	390.21	389.78	1	7783	7670	43947	43852
						2	7594	7479	43802	43691
						3	7658	7660	44114	44011
						6	7748	7626	44043	43912
4	Baseline, No ESD	± 0.10 @ 1.5 Hz, 100,000 cycles	S-13	392.56	391.23	8	7743	6960	43837	43036
						9	7666	6609	43997	43044
						10	7803	7044	43841	43079
						11	7800	6894	43999	43088
5	#32 with UIT	± 0.010 @ 15 Hz, 1,000,000 cycles	N-1	384.88	384.57	13	7530	7420	43791	43791
						14	7502	7377	43747	43747
						15	7476	7359	43844	43844
						18	7573	7441	43981	43891
6	#32 with UIT	± 0.10 @ 1.5 Hz, 100,000 cycles	N-4	391.39	390.52	19	6864	5848	43247	42231
						20	6881	5939	42901	41962
						21	6871	5892	42933	41922
						22	6856	5858	42893	41930
7	V4	± 0.010 @ 15 Hz, 1,000,000 cycles	N-2	381.74	381.44	718-1	7688	7623	43988	43922
						718-2	7566	7456	43960	43853
						718-3	7729	7627	44219	44110
						718-4	7691	7576	43929	43823
8	#32	± 0.10 @ 1.5 Hz, 100,000 cycles	N-3	358.31	357.44	718-5	6873	6027	43075	42231
						718-6	6742	5885	43175	42355
						718-7	6875	6062	43172	42364
						718-8	6789	5933	42966	42094
9	#32	± 0.010 @ 15 Hz, 1,000,000 cycles	N-5	374.24	373.93	718-9	7778	7680	44002	43909
						718-10	7737	7614	43920	43828
						718-11	7746	7646	44002	43909
						718-12	7709	7582	44073	43966
10	V4	± 0.10 @ 1.5 Hz, 100,000 cycles	N-6	373.05	372.13	718-13	7714	7083	43816	43195
						718-14	7645	6895	44027	43282
						718-15	7761	7112	43817	43170
						718-16	7670	6827	43712	42868

Figure 4-87 illustrates (both in data and graphically) the difference between the pre-test weight measurements and the post-test weight measurements of the test panels, with respect to stroke length.

Specimen	Weight Loss (g)
S-1 (dither)	0.300
S-12 (dither)	0.430
N-1 (dither)	0.312
N-2 (dither)	0.306
N-5 (dither)	0.310
S-2 (long stroke)	1.259
S-13 (long stroke)	1.330
N-3 (long stroke)	0.874
N-4 (long stroke)	0.861
N-6 (long stroke)	0.917

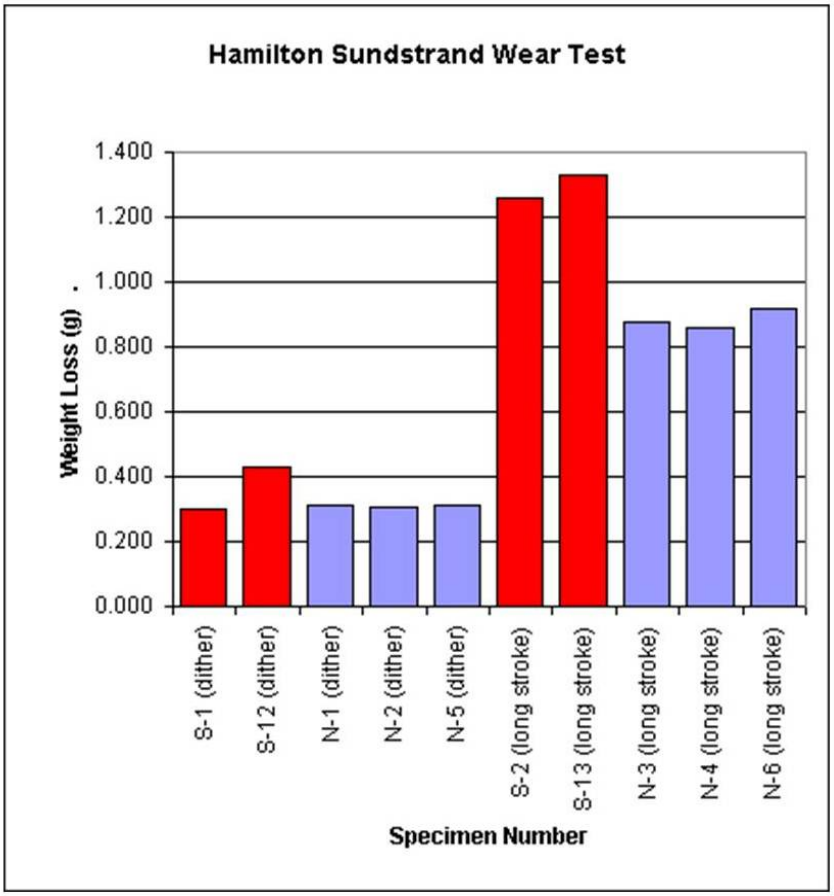

Figure 4-87 Summary of IN718 Panel's Weight Differential Between Pre-test and Post- test Weight Measurements

The data is presented graphically in Figure 4-88 based on the ESD parameters used in the preparation of each test specimen.

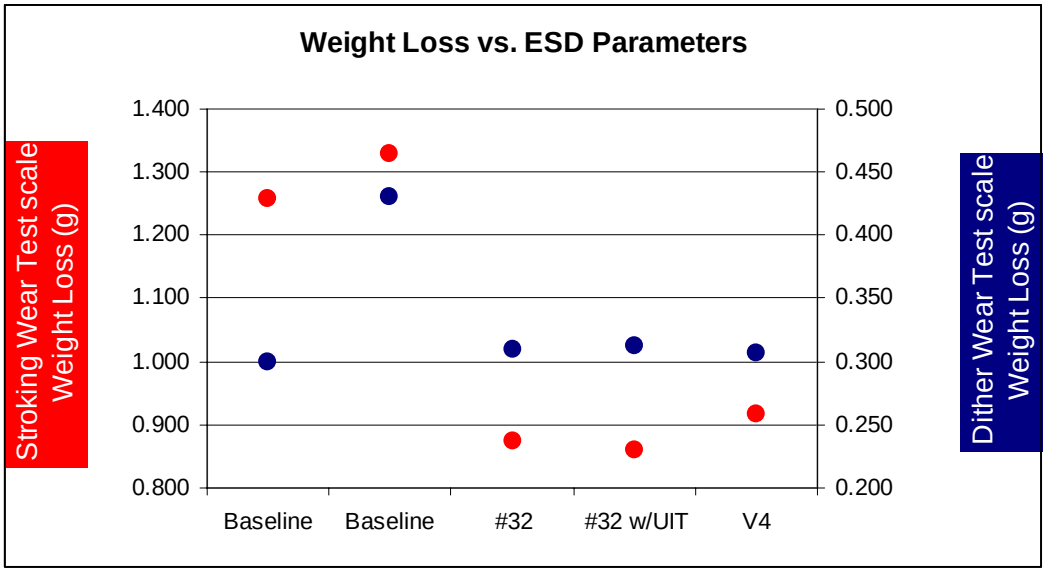

Figure 4-88 Weight Loss of Wear Specimens vs. ESD Parameters

The wear coefficients for the panels and counterface specimens were calculated using a modified Archard's equation:

$$K = \frac{Wear\_volume}{DxL}$$

where K, D and L represents the wear coefficient, total distance traveled, and the applied normal load respectively. The results compiled in Table 4-31 show the wear coefficient of the panels, and the average wear coefficient for all four counterface specimens related to each panel. In addition, the wear coefficients for the dithering and stroking wear conditions are shown graphically in Figure 4-89 and Figure 4-90.

Table 4-31 Summary of the Wear Coefficients for the Panels and Counterface Specimens in the Wear Test

Panels	Wear Coefficient	Counterfaces	Wear Coefficient
S-1	1.856E-10	Counterfaces for S-1	2.042E-10
S-2	7.789E-10	Counterfaces for S-2	1.933E-09
S-12	2.660E-10	Counterfaces for S-12	2.772E-10
S-13	8.228E-10	Counterfaces for S-13	2.112E-09
N-1	1.930E-10	Counterfaces for N-1	2.994E-10
N-4	5.327E-10	Counterfaces for N-4	2.434E-09
N-2	1.893E-10	Counterfaces for N-2	2.425E-10
N-3	5.407E-10	Counterfaces for N-3	2.086E-09
N-5	1.918E-10	Counterfaces for N-5	2.772E-10
N-6	5.673E-10	Counterfaces for N-6	1.777E-09

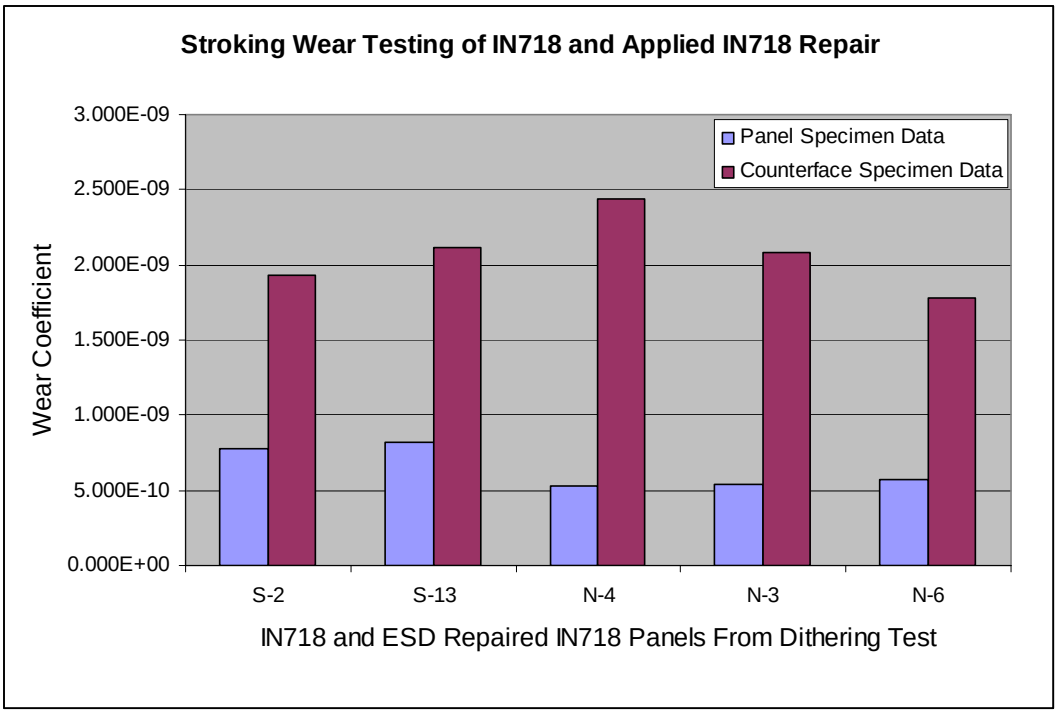

Figure 4-89 Wear Coefficient of IN718 and ESD Under Stroking Wear Conditions

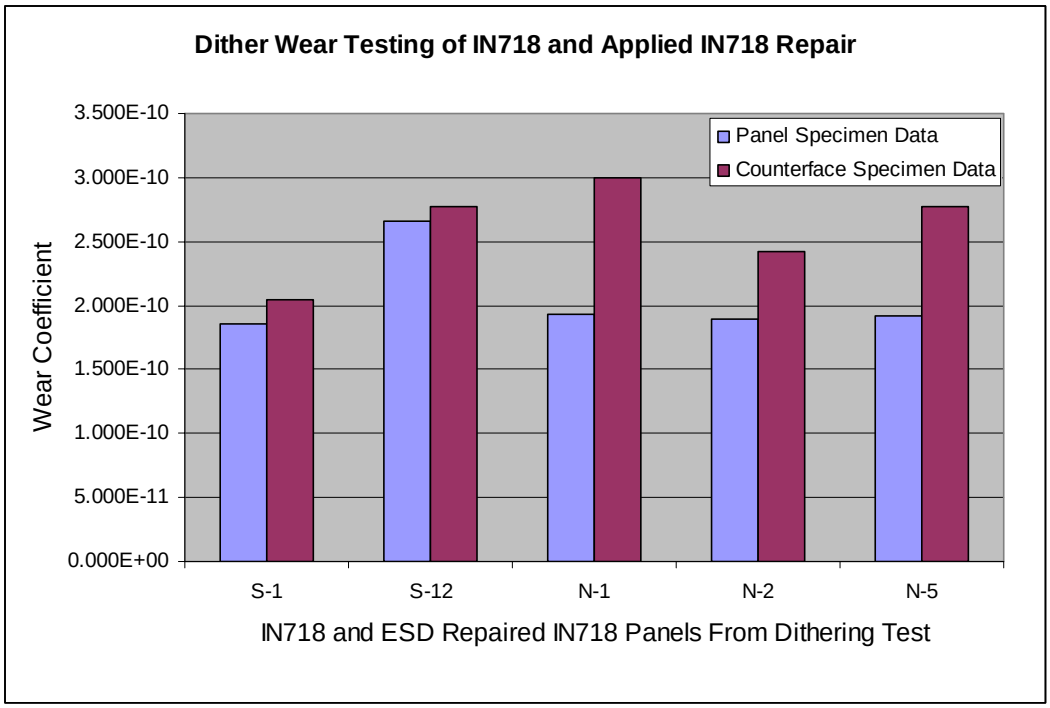

Figure 4-90 Wear Coefficient of IN718 and ESD Under Dither Wear Conditions

4.3.5.7. Conclusions

Based on the results in Table 4-30, the specimens that were run at dither stroke (±0.01 in), show a lower level of material loss than the tests that were run at long stroke (±0.1 in) in all the panels. In addition, the panels that were ESD repaired showed less material loss than the virgin panels, specifically for the panels tested in sliding wear conditions.

For the panels that were ESD repaired, the wear coefficients were lower than the wear coefficients of the virgin panels. In the case of dithering wear, the wear rates for the ESD-repaired and virgin panels were approximately the same.

There was little difference in the wear characteristics of the ESD deposit with respect to the various parameters used to prepare the test specimens. For example, in the dither test, the ESD performed identically for #32, #32 with UIT and V4 parameter sets. In the sliding wear test, #32 exhibited slightly better wear resistance than V4, which mimics the results seen in the pin-on-disk wear test.

4.3.6.Corrosion

4.3.6.1. Test rationale

Corrosion testing was conducted to determine if ESD deposition causes the materials to be more sensitive to corrosion. Because it is a commonly used test, the ASTM B117 salt-fog corrosion test was selected.

4.3.6.2. Specimen Fabrication

Flat coupons (1" x 1" x 0.125") was used for these specimens as shown in Figure 4-91. These are the same coupons that were used for optimization and metallurgical evaluation.

Specimen production method:

- Grind to shape, 0.002" oversize on the thickness.
- Machine defect as required by the fatigue test matrix, using the defect dimensions defined in Figure 4-1
- Deposit the ESD, filling the defect above the surface of the specimen.
- Apply UIT to some of the repaired specimens, per the test matrix.
- Grind the surface, flush with the parent material.
- Dip-coat the edges of the specimen with an inert epoxy to prevent galvanic corrosion or corrosion of the uncoated ends. The epoxy coating must completely seal the bare metal and cover the edges by 1/8"-1/4". The back of the specimen were protected by the same dip coating.

Figure 4-91 Corrosion Specimen

4.3.6.3. ESD Deposit Methodology

Parameter sets #32 and V4 as discussed in Section 4.2 were used to apply the ESD to the test specimens. It was anticipated that corrosion testing of ESD coatings deposited using these parameters would indicate if the corrosion resistant properties of ESD are affected

when a higher energy setting (and consequently higher deposition rate) is employed. 12 specimens were prepared per the test matrix in Table 4-32. The ESD parameters associated with each test specimen are defined in Table 4-33.

Table 4-32 Corrosion Test Matrix for IN718 on IN718.

Substrate Material	Defect type	ESD Material	Qty	Comments
IN718	Type 1	IN718	3	Defect filled with Parameter set #32
IN718	Type 1	IN718	3	Defect filled with Parameter set V4
IN718	Type 1	IN718	3	Defect filled with Parameter set #32 and UIT applied
IN718	none	IN718	3	ESD overlay of Parameter set #32, no defect
		Total	12	

Table 4-33 IN718 Corrosion Coupon Numbers and Parameters

Coupon #	Parameters	Surface Finish	Corrosion Test
11	V4	Yes	ASTM B 117
12	V4	Yes	ASTM B 117
13	V4	Yes	ASTM B 117
14	#32	Yes	ASTM B 117
15	#32	Yes	ASTM B 117
16	#32	Yes	ASTM B 117
17	#32 + UIT	Yes	ASTM B 117
18	#32 + UIT	Yes	ASTM B 117
19	#32 + UIT	Yes	ASTM B 117
20	#32 bead-on-plate	No	ASTM G 48
21	#32 bead-on-plate	No	ASTM G 48
22	#32 bead-on-plate	No	ASTM G 48
23	#32 bead-on-plate	No	ASTM B 117
24	#32 bead-on-plate	No	ASTM B 117
25	#32 bead-on-plate	No	ASTM B 117

4.3.6.4. Test Methodology

An ASTM standard corrosion test, the B117-9 salt fog test, was used to determine if there was any difference in the corrosion behavior of base metal IN-718, ESD deposited IN-718, or the fusion zone interface between the base metal and the ESD deposit. The ASTM-B-117-9 tests were done by Cascade Technical Sciences, Inc., Hillsboro, Oregon, with standardized, certified and calibrated equipment.

The test specimens were exposed to 168 hours of 5% salt fog at 35°C temperature, with readings and measurements recorded every 24 hours. The specimens were placed in the preconditioned salt fog chamber and photos were taken.

Prior to the decision to go with the salt-fog test, Portland State University performed ASTM G-48, Pitting and Crevice Corrosion Resistance of Stainless Steels and Related

Alloys by Use of Ferric Chloride Solution, Method C. The specimens were remnants of those prepared for metallurgical evaluation. PSU performed ASTM G-48 on three of these coupons. Although this test was not specified in the JTP, the results are included in the report.

4.3.6.5. Acceptance criteria

In salt-fog or atmospheric corrosion tests, time until observing corrosion product for ESD-repaired area should be less than or equal to time for base material. (Per ASTM B117).

4.3.6.6. Test Results

Corrosion coupons #11–19 following 168 hours of salt fog exposure are shown in Figure 4-92. No corrosion was observed either inside or outside the ESD-repaired areas. It was not possible to visually determine where the ESD-repaired area was, so the coupons were etched following standard etching procedures for IN718 to visually show the location of the ESD-repaired areas and these specimens are shown in Figure 4-93.

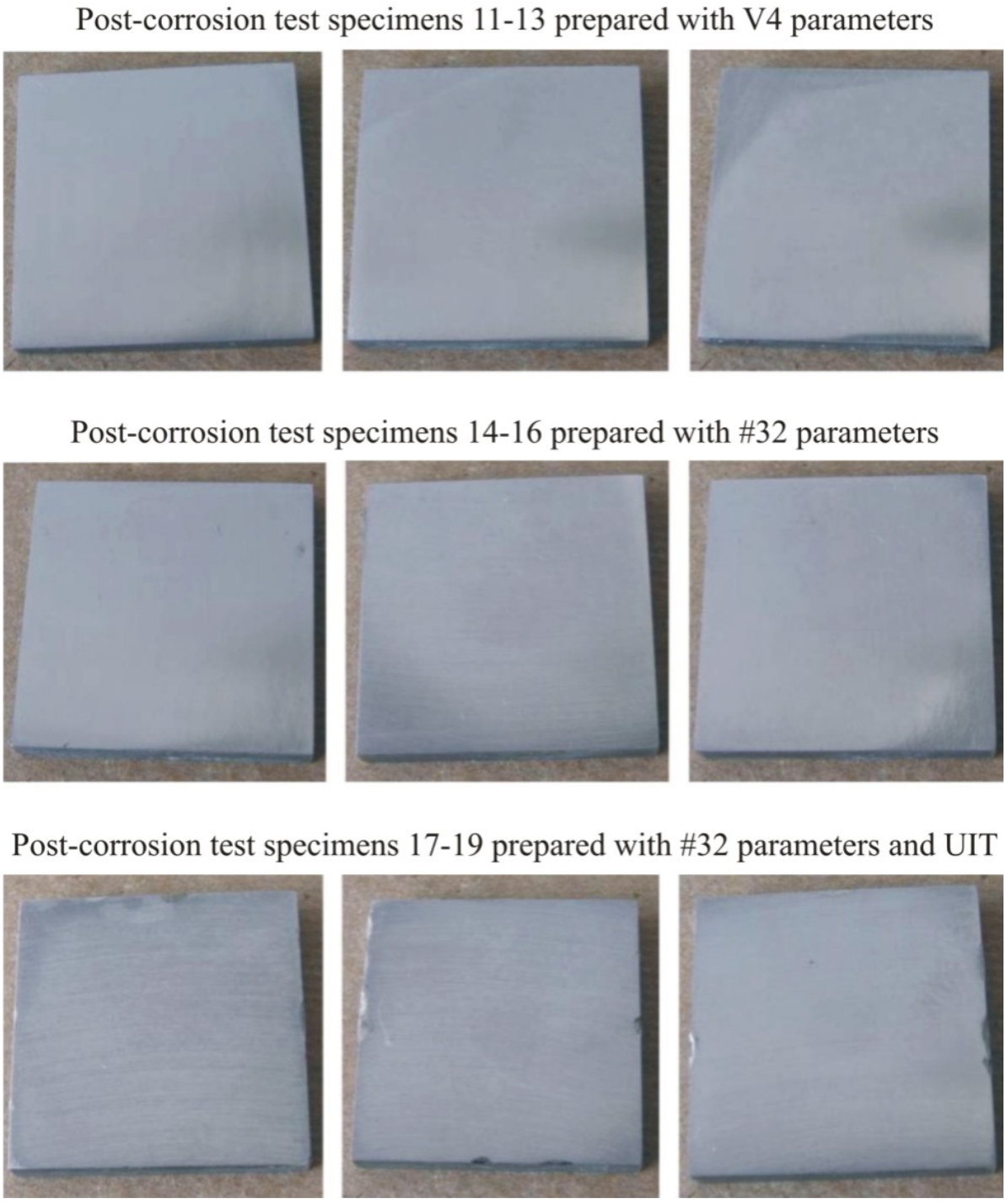

Figure 4-92 Corrosion Specimens 11-19 Following 168 Hours Salt Fog Exposure

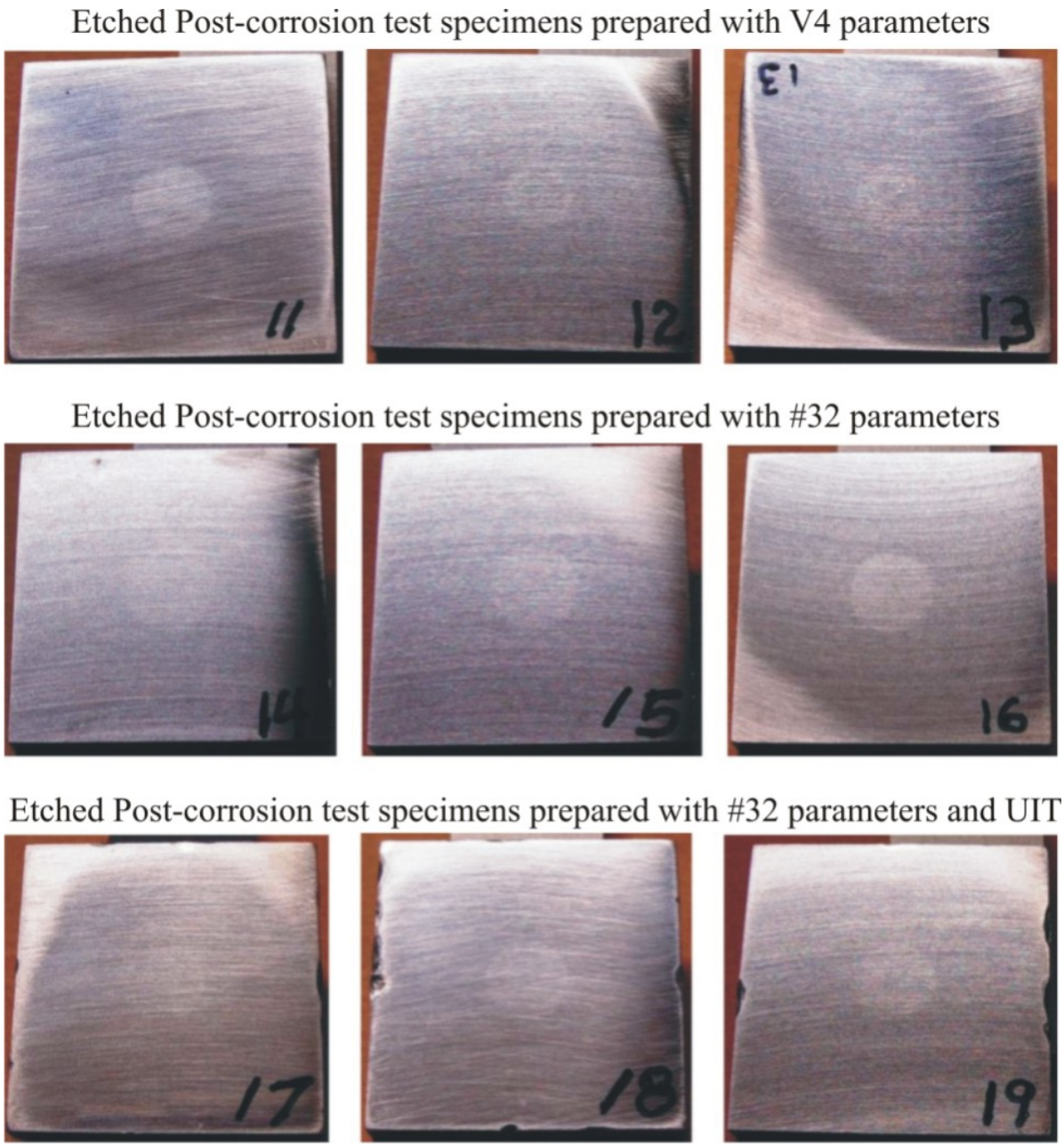

Figure 4-93 Etched Corrosion Specimens 11-19 Following Salt Fog Testing

The three specimens (#20, 21, and 22) that were subjected to the ASTM G-48 (Method C) test are shown in Figure 4-94.

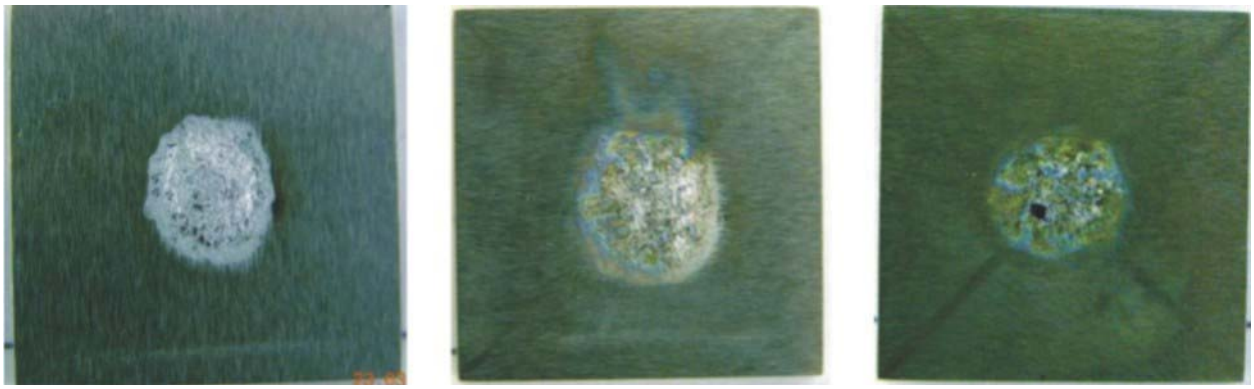

Figure 4-94 Corrosion Specimens 20-22 (left to right) following ASTM G48 Corrosion Testing

4.3.6.7. Conclusions

None of the ESD repaired IN-718 coupons showed visible corrosion from the 168 hour salt fog exposure. The ESD deposit, the substrate, and the fusion zone between the ESD deposit and the substrate were all clear of corrosion products. Some red rust was noted on the edges and backsides of those coupons that received UIT. This is believed to be from fine steel particles that detached from the steel UIT impact probe and anvil under the coupons, and is not associated with the ESD process.

The three specimens that were subjected to the ASTM G-48 (Method C) test showed no corrosion pitting on coupon #20, but an etching or cleaning effect was seen on the deposit. However, coupons #21 and 22 showed minor pitting corrosion on the ESD deposit, but not on the base metal. This test, which is more chemically aggressive than the salt fog test, points out the fact that the ESD deposits are more susceptible to corrosion than the base metal in this type of environment.

4.3.7. Residual Stress Analysis

4.3.7.1. Test rationale

Residual stress analysis was conducted on a minimal quantity of specimens to obtain an indication of stresses introduced by the ESD process.

4.3.7.2. Specimen Fabrication

Almen N strips were used for the residual stress tests. Almen N strips are pieces of steel approximately 3” long by 0.75” wide and 0.0625” thick.

4.3.7.3. ESD Deposit Methodology

Only enough specimens were tested to obtain an indication of the presence of residual stresses due to the ESD process.

4.3.7.4. Test Methodology

The Almen Residual Stress test was invented by J.O. Almen of General Motors Corporation in 1942. The test was originally developed to measure the type (tensile or

compressive) and magnitude of residual stresses imparted to metal in sand blasting or shot peening operations. Almen strips are subjected to a surface treatment on one side only, and the resulting curvature is measured. A convex curvature indicates a resulting compressive stress within the strip, and a concave curvature indicates a state of tensile stress. The amount of curvature, or vertical deflection, is an indication of the magnitude of the residual stresses. The net effect on Almen strips with ESD is quite similar to other surface treatments. Therefore the Almen method was used in an attempt to analyze the residual stress formed by ESD.

Six Almen strips were treated with an overlay of IN-718 by ESD. Three were treated with ESD parameter set #32 and three with ESD parameter set #V4.

4.3.7.5. Acceptance criteria

Since the objective of this test was only to determine whether or not ESD imparts residual stresses, there were no acceptance criteria.

4.3.7.6. Test Results

Almen strips treated with #32 parameters are shown in Figure 4-95, with the treated sides facing out of the page. These strips were curved inward (concave), indicating tensile stresses were produced by the ESD process. Almen strips treated with #V4 parameters are shown in Figure 4-96, and also show tensile stresses. The magnitude of the stresses, indicated by the amount of curvature, was measured with a Mitutoyo digital height gauge, as shown in Figure 4-97. Deflection data are shown in Table 4-34 and Figure 4-98 for ESD treated Almen strips (no UIT).

Figure 4-95 ESD #32 on Almen strips

Figure 4-96 ESD V4 on Almen strips

Figure 4-97 Digital Height Gauge for Deflection Measurements

Table 4-34 Deflection from ESD Deposit

#32				V4		
Total Deflection	**Almen strip and coating thickness**	**Net Deflection**		**Total Deflection**	**Almen strip and coating thickness**	**Net Deflection**
0.0535	0.0310	0.0225		0.0575	0.0315	0.0260
0.0515	0.0310	0.0205		0.0560	0.0315	0.0245
0.0570	0.0320	0.0250		0.0600	0.0315	0.0285
	Average	0.0227			**Average**	0.0263

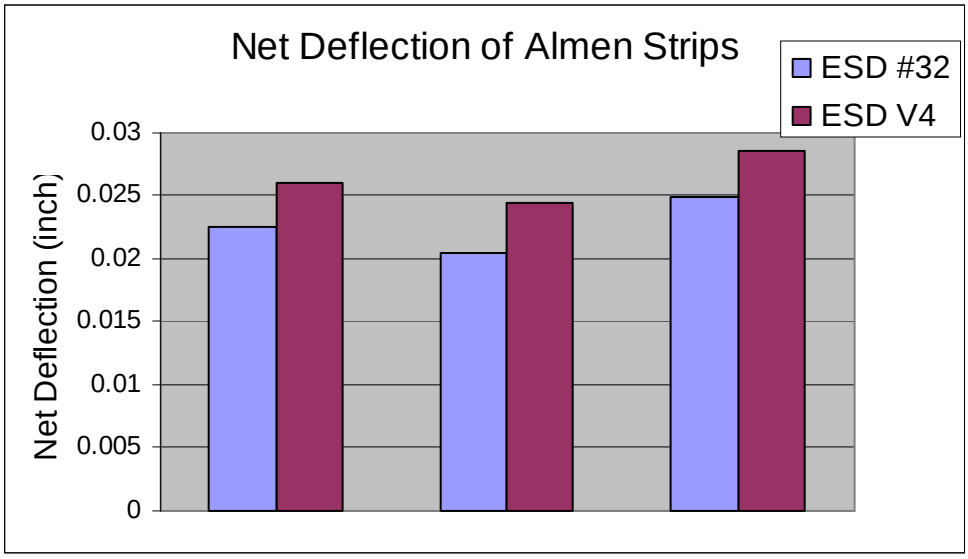

Figure 4-98 Net Deflection from ESD Treatment

4.3.7.7. Conclusions

The results of this test indicate that ESD does impart tensile residual stresses. It is clear that higher ESD energy produces a higher level of tensile residual stresses.

4.3.8.Bond strength

4.3.8.1. Test rationale

An adhesion bond test was conducted to demonstrate that the adhesive bond of an ESD deposit is as good as or better than thermal spray processes.

4.3.8.2. Specimen Fabrication

Cylindrical specimens, as configured in Figure 4-99 was used for this test. The cylinders were 1" in diameter and 4 inches long.

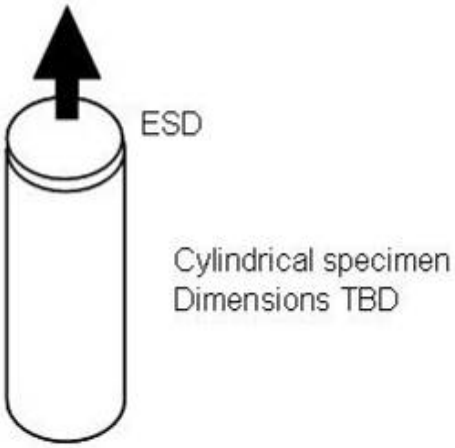

Figure 4-99 Adhesion/Bond Strength Specimen

4.3.8.3. ESD Deposit Methodology

ESD was applied to one end of a cylinder. No ESD was applied to the mating cylinder. Five cylinders were prepared with ESD, all under ESD parameter set #32. The applied ESD was approximately 0.005" thick. The diameter of the cylinder was 1", therefore the area of the ESD, used for calculating lb/sq.in., was 0.785 in^2.

4.3.8.4. Test Methodology

The bond strength was tested in accordance with

ASTM C 633. Per ASTM C 633, ESD is applied to the end of a cylinder. That surface is then adhesively attached to another cylinder and pulled in a tensile test. After failure the surfaces were examined to determine if the failure occurred between the ESD and base metal or between the adhesive and ESD. One pair did not receive ESD and this pair was used to test the adhesive. This test was conducted by Flame Spray, Inc., located in San Diego, CA.

4.3.8.5. Acceptance criteria

The bond strength of ESD-repaired area should exceed that of adhesive used (per ASTM C633).

4.3.8.6. Test Results

All paired specimens failed in the adhesive, as seen in Table 4-35 Adhesion Bond Test Results. Images of each individual specimen pair are shown in Figure 4-100.

Table 4-35 Adhesion Bond Test Results

Specimen Number	Load (lbs)	Lb/sq"	Failure Code
Adhesion	8206	10453	C
1	7453	9494	C
2	8061	10268	C
3	8822	11238	C
4	7017	8938	C
5	8490	10815	C
Failure Codes: (A) Coating (B) Coating-Substrate Surface (C) Adhesive Bond (D) Bond Coating and Surface Coat			

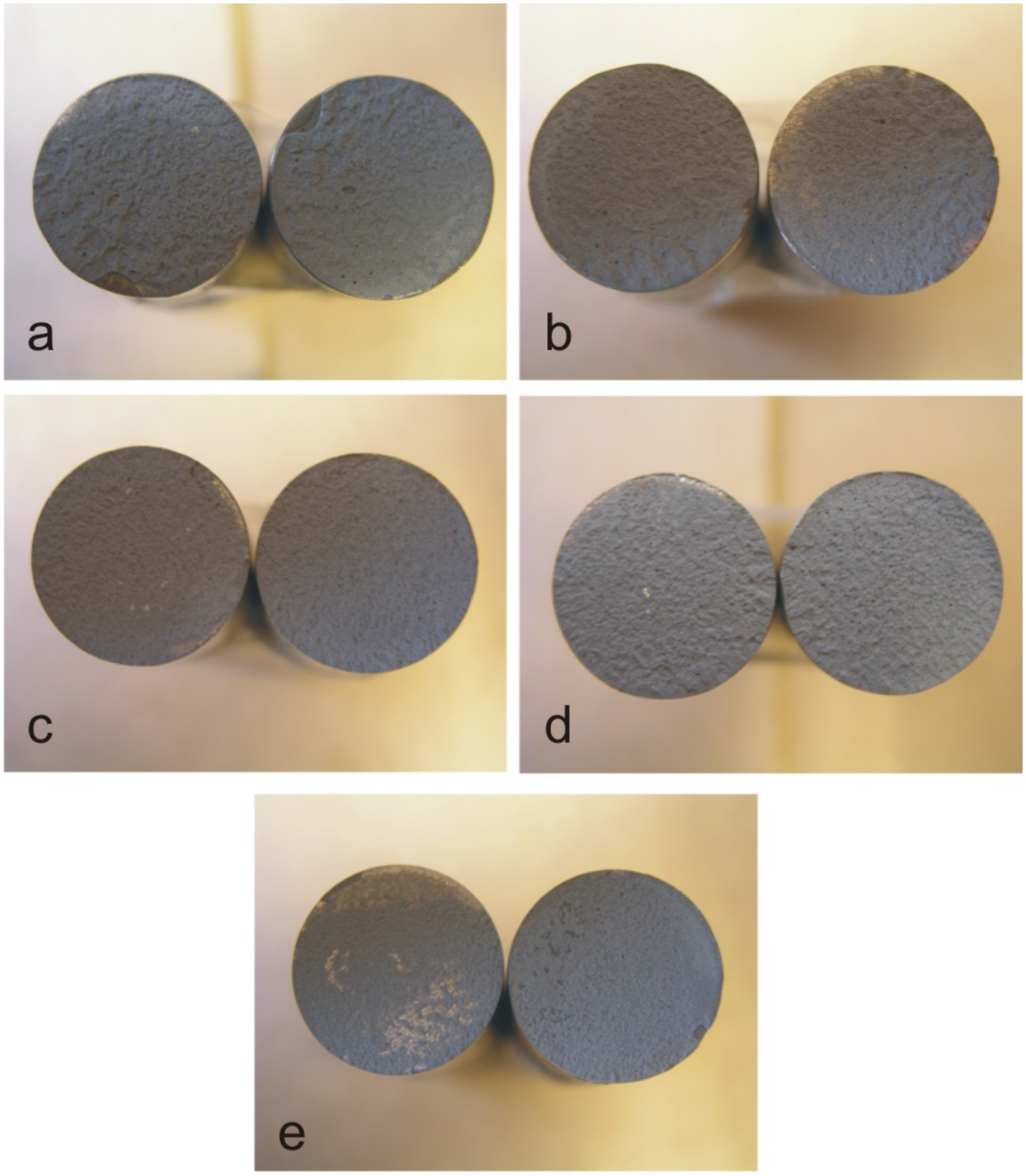

Figure 4-100 Adhesion Bond Test Specimens, Post-Test

4.3.8.7. Conclusions

All adhesion bond test specimens failed in the adhesive. Therefore, it can be concluded that the adhesive bond strength of the ESD to the substrate is greater than that of the adhesive used.

4.3.9. Material Testing Conclusions

All ESD repairs produced a fatigue debit over baseline fatigue life. For ESD repaired divots, the high energy parameter set (V4) produced a greater fatigue debit than did the moderate energy level ESD repairs (#32). This is proof that ESD applied with a higher energy input (and higher deposition rate) negatively affect the fatigue life of the component. The UIT post-ESD treatments increased the fatigue life over ESD-only repairs, to near that of baseline life. In the lower stress levels, the fatigue debits are about the same, but at higher stress levels, the bead-on-plate repairs provide less fatigue debit than the divot repairs.

The tensile strength of all specimens was essentially identical. No strength debit was noted for ESD repairs. Ductility was approximately 25% higher for the ESD bead-on-plate condition compared to the divot repair condition. The higher energy ESD treatment, parameter set #V4, resulted in virtually no difference in IN-718 than the lower energy parameter set, #32. This is proof that ESD applied with a higher energy input (and higher deposition rate) does not affect the tensile strength of the component.

The pin-on-disk wear test results indicate that for the ESD parameter set V4, the deposit is less wear-resistant than the parent material. This coincides with the microhardness data. Microhardness and wear resistance both decreased compared to the parent material. For the ESD parameter set #32, the results indicate that the deposit is more wear-resistant than the parent material. However, the microhardness data of this parameter set was less than the parent material. Therefore, a conclusive relationship between microhardness and wear resistance cannot be drawn. Based on the groove depth in the ESD as a percentage of the groove depth in the parent material, #32 with UIT seemed to demonstrate the best wear resistance.

The H-S wear test results indicated that there was little difference in the wear characteristics of the ESD deposit. The ESD performed identically for all parameter sets. In the sliding wear test, #32 exhibited slightly better wear resistance than V4, which mimics the results seen in the pin-on-disk wear test. All panels that were ESD repaired showed less material loss than the virgin panels and the wear coefficients were lower than virgin panels. All specimens that were run at dither stroke show a lower level of material loss than the tests that were run at long stroke.

None of the ESD repaired IN-718 coupons showed visible corrosion from the 168 hour salt fog exposure. Two coupons that were subjected to the ASTM G-48 test showed minor pitting corrosion on the ESD deposit, but not on the base metal. This test, which is more chemically aggressive than the salt fog test, points out the fact that the ESD deposits are more susceptible to corrosion than the base metal in this type of environment.

The results of the residual stress analysis indicated that ESD imparts tensile residual stresses and higher ESD energy produces a higher level of tensile residual stresses.

All adhesion bond test specimens failed in the adhesive, demonstrating that the adhesive bond strength of the ESD to the substrate is greater than the adhesive.

4.4. Components

4.4.1. Introduction

The objectives of this portion of the project were to demonstrate ESD repairs to damage on actual GTE components, to document the repair procedures, and to transition ESD repairs for use on gas turbine engine and other types of components. Oklahoma City Air Logistics Center (OC-ALC) was the demonstration site identified specifically for GTE components.

A screening matrix was developed to look at what parts may be possible candidates for ESD repair. A preliminary Candidate Part Selection Criteria document was designed to record all information on candidate components. Requirements were that the candidate component should be:

- A GTE part
- Non-flight critical
- Fabricated from one of the materials studied
- One for which no current repair exists for the damage or the existing repair process meets one or more of the following:
    - A process that is not environmentally friendly
    - A process with unsatisfactory results
    - A process that is not conducive to an in-situ environment

With input from OC-ALC, as well as Pratt & Whitney and GEAE, multiple components were considered. The material tests discussed in Section 4.3 were selected based on the repair needs of the candidate components.

At the end of the project, new repair procedures were documented for OC-ALC. Local process specifications were written for operation and maintenance of the ESD process. Repair specifications were developed to ensure acceptable quality and a reproducible process.

4.4.2. Candidate Components

Multiple candidate parts were suggested and considered for this project. These parts are described in Table 4-36. The majority of the components were not selected for demonstration because the base material had not been investigated with ESD or there was insufficient information on the requirements for the repair. Titanium alloys are especially difficult to repair with ESD and additional qualification work is required to develop the optimum parameters.

Table 4-36 Candidate Components

Image of Part	Part Number	OEM	Description	Material
			Titanium Rings	AMS 4972 (Ti-8Al-1V-1Mo)
	1864M71P01	GE	F110 HPTR Aft Shaft	AMS 5662 (IN718)
	4017949	P&W	F100 Gearbox Spur Gearshaft	AMS 6265 (E9310)
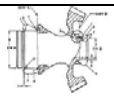	4025444	P&W	F100 Gearbox Drive Bevel Gearshaft	AMS 6260 (E9310)
	4033778	P&W	F100 Turbine Shaft Coupling	AMS 1202, AMS 4928 (Ti-6Al-4V)
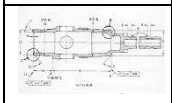	4038802	P&W	F100 Gearbox Deaerator Impeller Shaft	Ti-6Al-4V
	4057828		Augmenter Diversion Nozzle Segment	AMS 6265 (E9310)
	4060955		Convergent Seal Liners	AMS 5544 (Waspaloy)
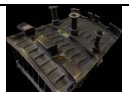	4077880	P&W	F100 Stator Segment 10-12 Stage	IN 718
	6032T27P08	GE	T700 Blisk, Stage 2	IN 718?
	712141	P&W	TF33 #5 Bearing Housing Lugs	AMS 5613 (410 SS)
	9103M58G12	GE	TF39 Compressor Rear Shaft	IN 718
No Photo Available	950M12G02	GE	F110 Primary Seal	AMS 5800 (Rene 41)
	9673M66G12		Vane Actuation Lever	17-4 PH

The components selected for the demonstration were:

#5 Bearing Housing:

The #5 bearing housing, part number 71214, is from the TF33 engine. This component is fabricated from 410 stainless steel and requires dimensional restoration (loss of material due to wear). The current repair process is such that if the damage is less than 0.005" deep, then it is blended away; if the damage is greater than 0.005" deep, no repair process is available and the part is scrapped. These components are no longer manufactured and, without a repair process, the availability of these components is declining. An ESD repair using a 410 stainless steel electrode would replace the worn material, resulting in a component that has been restored to its original dimensions and with the same wear performance as the initially manufactured component.

10-12 Stator Segment:

The 10-12 stage stator segment, part number 4077880, is from the F100 engine. This component is fabricated from Inconel 718 and requires dimensional restoration of deep wear scars that occur on the hook. The damaged area is non-line-of-sight. Therefore, many traditional repair processes cannot be used. The current repair process is to cut off the damaged hook and weld a new one in its place, followed by a heat treatment. Because this component is only allowed three heat treat cycles, in many cases the repair process cannot be performed. An ESD repair using an Inconel 718 electrode would dimensionally restore the worn areas without the need for post-process heat treatment, resulting in a component with the same wear performance as the initially manufactured component.

TF39 Compressor Rear Shaft:

The compressor rear shaft, part number 9103M58G12, is from the TF39 engine. This component is fabricated from Inconel 718 and is chrome plated. There are two types of problems that occur with this part. One is scratches in the hard chrome plate on the journal and the second is incomplete or damaged chrome plating on the "step" (the area perpendicular to the axis of the shaft, where the outer diameter of the shaft is increased or reduced). The current repair for the chrome plating is to completely strip the coating and re-plate with hard chrome. An ESD repair of the scratch using a Stellite electrode would eliminate the need to strip and re-chrome the entire journal area. An ESD repair of the step using a Stellite electrode will eliminate the chrome plating process altogether in these areas.

4.4.3.#5 Bearing Housing

4.4.3.1. The Need for a Repair

The #5 bearing housing is shown in Figure 4-101. This component is subject to different types of damage in service, of which all are potential candidates for development of an ESD repair. As can be seen in the figure, one of the lugs is missing. This was due to a failure that was potentially the result of an undercut weld in a process used to hardface the lugs. This project did not address that issue; however, discussions with OC-ALC indicate that ESD may be used in that application in the future. This project addressed

the repair and dimensional restoration of the wear scars that occur on the front face of the housing (loss of material due to wear), as seen in Figure 4-102.

Figure 4-101 #5 Bearing Housing

Figure 4-102 Damaged Area to Receive ESD Repair

4.4.3.2. Acceptance Criteria

The acceptance criteria, provided by OC-ALC, for an acceptable ESD repair for this part was

- Acceptable metallography
- Hardness same as parent material
- Good surface finish

4.4.3.3. ESD Process Development and Repair Procedure

An ESD repair procedure was developed. It consisted of the following steps:

- Identify the defective areas
- Excavate the damage to produce a smooth surface for repair
- Fill the excavated area
- Surface finish back to original dimensions
- Evaluate (via FPI) the repair

The photographs shown in Figure 4-103 through Figure 4-106 demonstrate these steps.

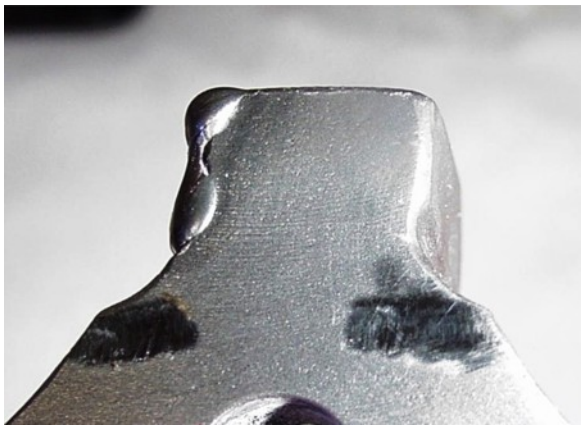

Figure 4-103 Excavate Damages Area

Figure 4-104 Repair Excavated Area

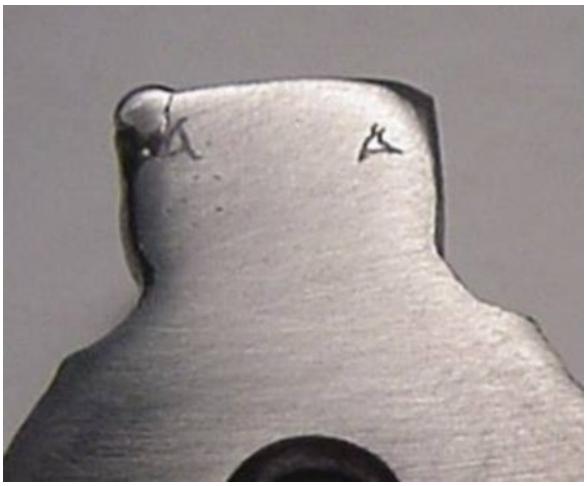

Figure 4-105 Surface Finish Repair Area

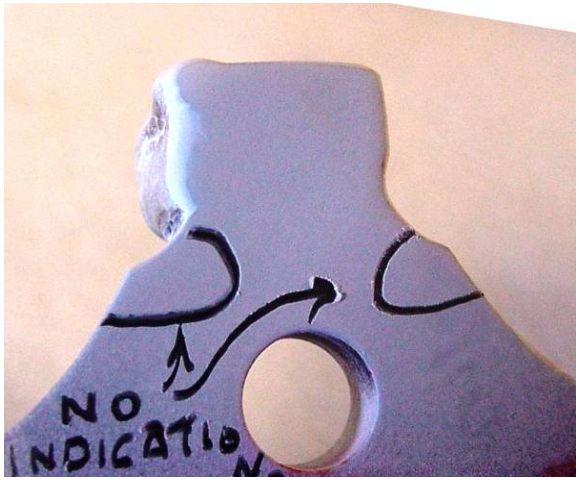

Figure 4-106 Perform FPI on Repair

In the process development, a metallurgical evaluation of the repaired area was performed. The objective of the extensive metallurgical evaluation was to determine if the acceptance criteria was met. The evaluation was performed on five lugs cut from a bearing housing and eight 410SS test coupons. Each coupon had two filled grooves, one was ground and one was as-deposited.

The density of the deposit was evaluated and used to determine the quality of the deposit. Density measurements were conducted using an image analysis program that quantified the areas of porosity based on gray levels in a cross sectional image. The results showed an average porosity of 1.7%. Figure 4-107 and Figure 4-108 present the micrographs, taken at 50x and 200x respectively. OC-ALC reported that this was acceptable metallography.

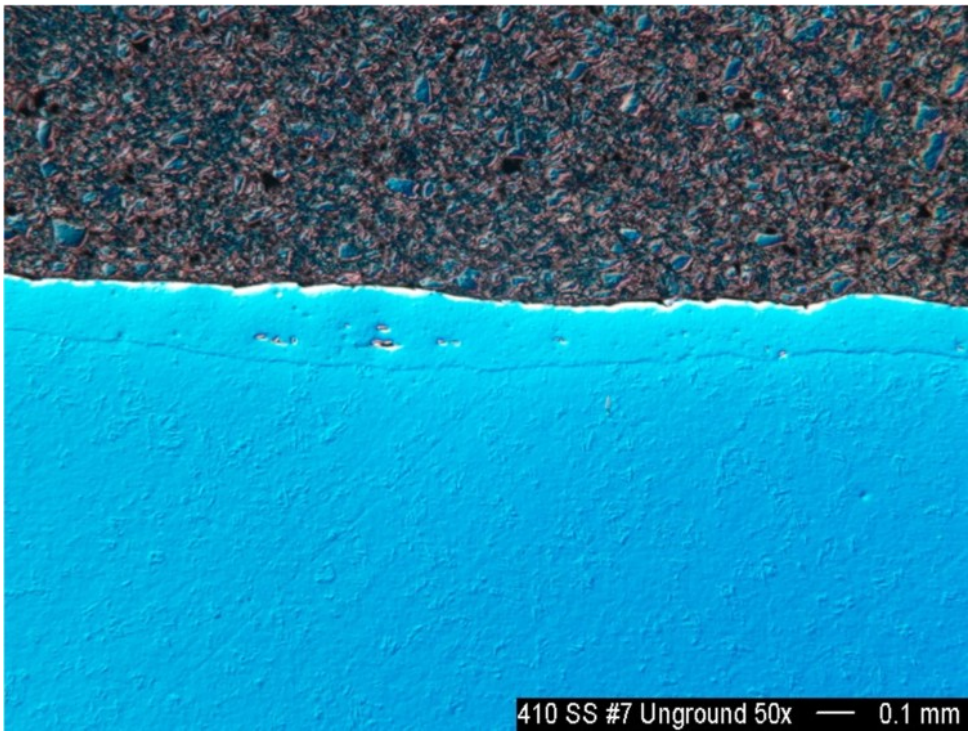

Figure 4-107 Typical Microstructure of the ESD Deposit (50x)

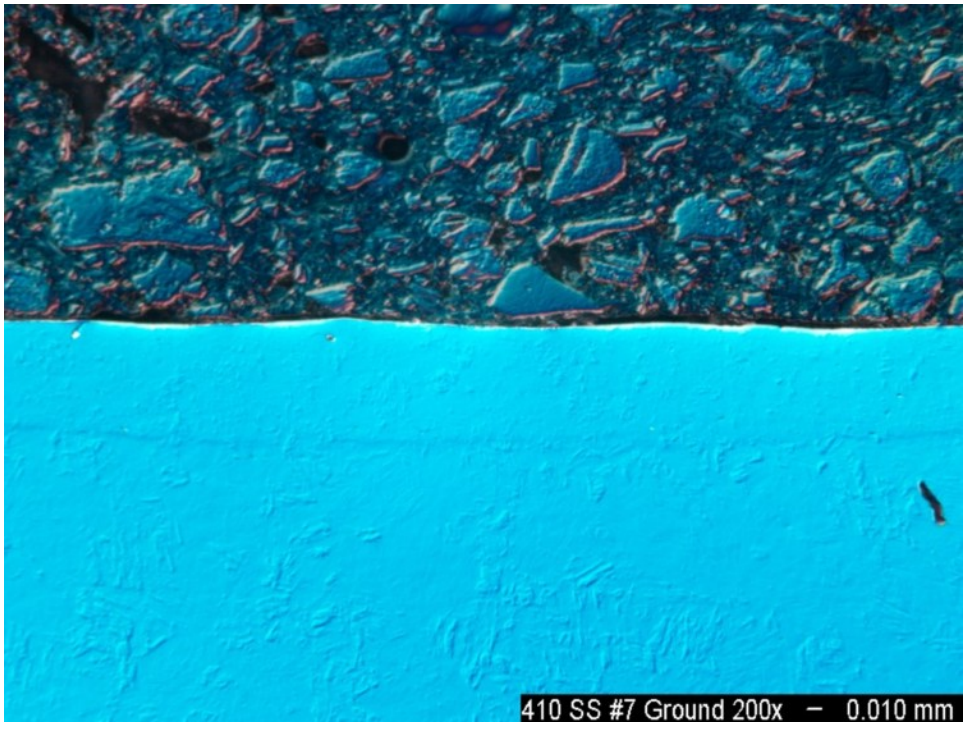

Figure 4-108 Typical Microstructure of the ESD Deposit (200x)

The microhardness of the deposit was evaluated for deposits which were "as-deposited", "after heat-treating" and "after heat-treating and shot peening". The reason for evaluating the ESD deposit after performing the post-ESD processes (heat-treat and shot peen) was because this component, due to the other repair processes it may need (such as the macro weld process on the lug face), may be subjected to these post ESD processes. If so, the effect the other processes may have on the ESD deposit had to be determined.

Heat treating was performed in a controlled atmosphere belt furnace to avoid altering the surface carbon composition. The specimens were austentized at 1875^{o} F, held for approximately 45 minutes, quenched in dissociated ammonia to approximately 150^{o} F, and tempered for two hours at 350^{o} F. This is a standard heat treatment for 410 stainless steel.

The specimens were shot peened to an Almen A6 condition using a witness strip to measure the final condition. This followed standard procedures used for this component.

Microhardness readings were taken with the indentation parallel to the substrate. Five readings were taken on all specimens. The results are shown in Table 4-37 and Figure 4-109. The average microhardness of the as-deposited ESD was 606 Knoop; and of the parent material, 567 Knoop. OC-ALC reported that this met the criterion of "hardness same as parent". In addition, after heat treating, the average microhardness of the ESD deposit was 633 Knoop, which was slightly greater than the parent material. After shot peening, the average microhardness of the ESD deposit was 702 Knoop, again greater than the parent material. OC-ALC reported that the increased hardness was acceptable and actually desirable. The increase in hardness would result in prolonged wear life, yet was minimal enough as to not transfer the wear to the mating component.

Table 4-37 Microhardness Data

Conditions	Microhardness (Knoop)
Parent Material	567
As Received	703
As Received	588
As Received	526
Average	606
Heat Treat	630
Heat Treat	638
Heat Treat	631
Average	633
Heat Treat and Shot Peen	719
Heat Treat and Shot Peen	685
Average	702

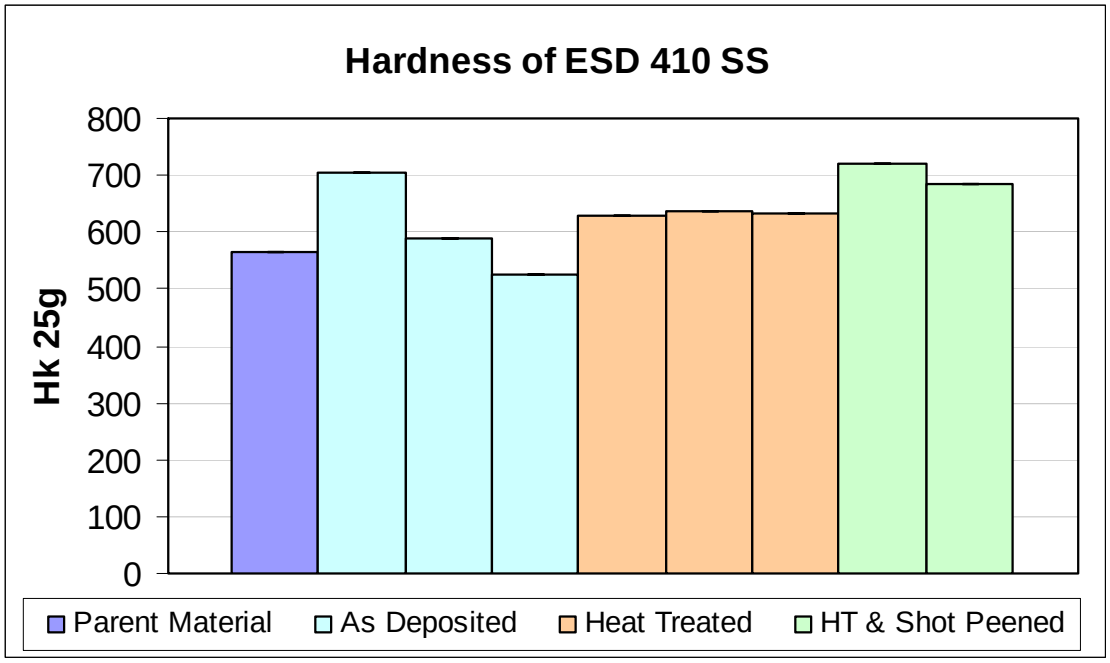

Figure 4-109 Graph of Microhardness Data

The repaired area was surface finished and restored to the original dimensions. The results showed a surface finish similar to the original component. OC-ALC reported that this finish met the criterion of "good surface finish".

4.4.3.4. Implementation

Welding Specification Documents were created to facilitate in the implementation of the repair process. One document provides sufficient information on the ESD process in general, to allow an operator to perform the ESD process. Two other documents provide the information necessary for an operator to make the specific repair on this specific component. A hands-on demonstration of the repair was provided to OC-ALC engineers in 2004. The Welding Specification documents were delivered to OC-ALC at the same time. The Technical Order (TO) for repair of this components at OC-ALC has been modified to include the ESD repair. Actual implementation of the repair in production has not yet taken place.

4.4.4.10-12 Stator Segment

4.4.4.1. The Need for a Repair

The 10-12 stage stator segment is shown in Figure 4-110. The problem is deep wear scars that occur on the underside of the "hook" as shown in Figure 4-111. There are three hooks per stator segment and all three exhibit the same wear patterns.

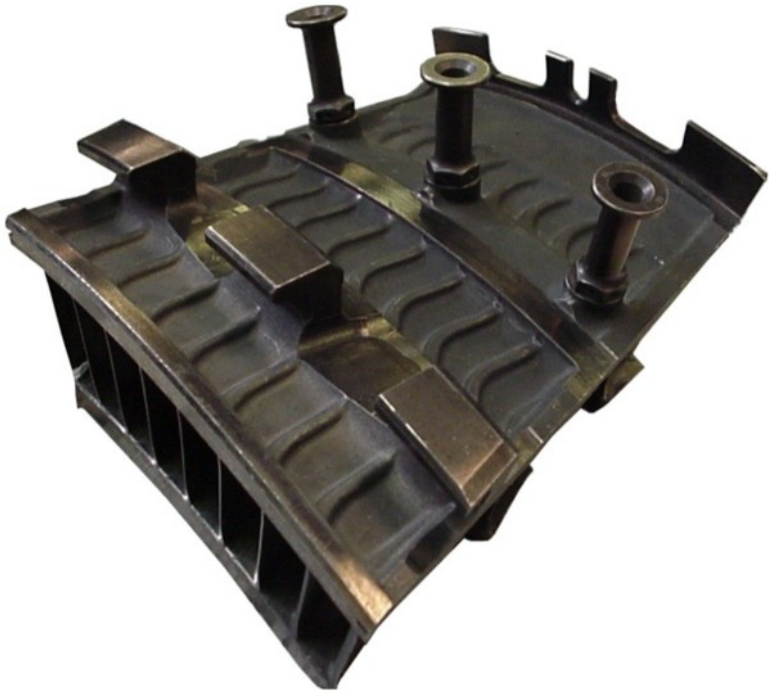

Figure 4-110 10-12 Stator Segment

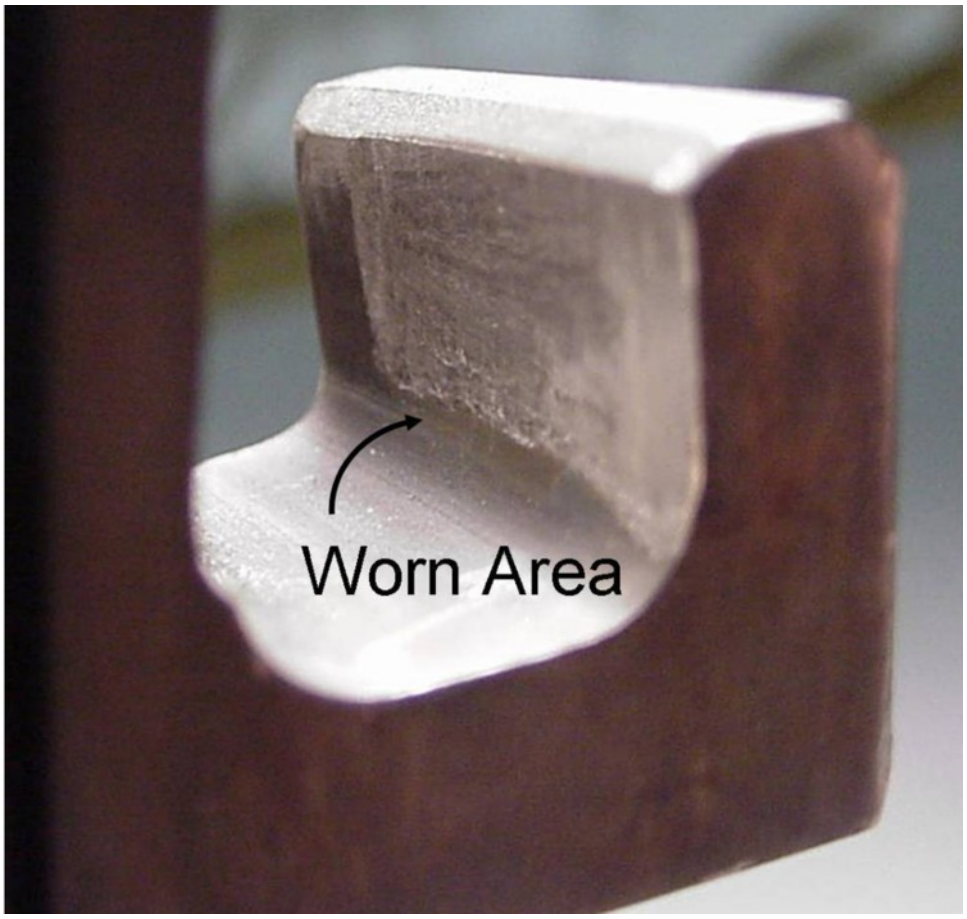

Figure 4-111 Damaged Area Suited for an ESD Repair

4.4.4.2. Acceptance Criteria

The acceptance criteria, provided by OC-ALC, for an acceptable ESD repair for this part was

- Hardness same as parent material
- Wear resistant to “chattering”

4.4.4.3. ESD Process Development and Repair Procedure

An ESD repair procedure was developed. It consisted of the following steps:

- Identify the defective areas
- Excavate the damage to produce a smooth surface for repair
- Fill the excavated area
- Surface finish back to original dimensions

This area was difficult to access and deemed a non-line-of-sight application. However, using unique ESD techniques and a custom applicator head, the area was excavated and repaired. The repaired area is seen in Figure 4-112.

Figure 4-112 Repaired Area on 10-12 Stator Segment

A metallurgical evaluation was performed on the repaired area. The hook was cut, cross-sectioned through the repaired area, and prepared for metallography. Images were taken at 50x. Based on visual examination it appeared that the ESD deposit had little porosity. Quantitative density and microhardness measurements on this repair were not conducted. Surface finishing of the repaired area was also not conducted.

4.4.4.4. Implementation

A Welding Specification has not been written for this repair. However, the process is well documented and ready for a hands-on demonstration to OC-ALC.

4.4.5.TF39 Shaft

4.4.5.1. The Need for a Repair

The compressor rear shaft is shown in Figure 4-113. There are a number of reasons why this component is either rejected during the repair process or removed from service, including:

- Area did not chrome plate completely.
- Dents on the surface.
- Unsuccessful plating (chrome not adhering).
- Diameters undersized, with no rework procedure available.
- Air erosion on flange surface.

The major issues are dents or scratches in the hard chrome plate on the journal and incomplete or damaged chrome plating on the "step". Figure 4-114 reveals a severely worn chrome surface on the journal but does not show a particular dent or scratch. A close-up of the "step" area on the journal is shown in Figure 4-115. Another issue detected on this component was hot air erosion damage in the underside of the flange at the base of the component (Figure 4-116). All of these types of damage are candidates for ESD repair.

Figure 4-113 TF39 Shaft

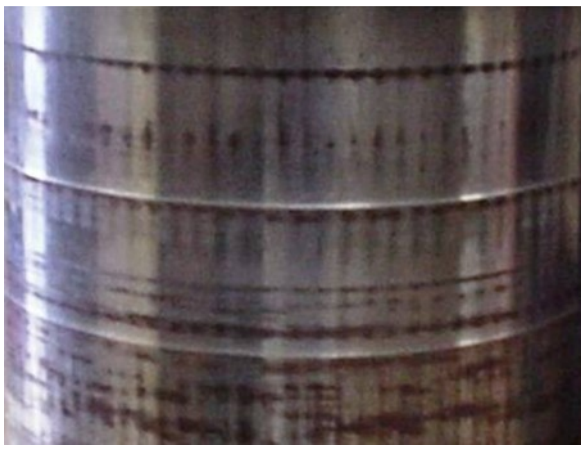

Figure 4-114 Worn Chrome Surface on Journal of TF39 Shaft

Figure 4-115 Undersized "Step" Area on Journal of TF39 Shaft

Figure 4-116 Hot Air Erosion on flange of TF39 Shaft

4.4.5.2. Acceptance Criteria

Acceptance criteria for a successful repair were not provided by OC-ALC. In fact, as the project continued, this component was deemed inappropriate for an ESD repair, as it is a rotating, flight critical part. However, it was reasoned that if a repair process could be developed for repairing the dents and scratches on the chrome plate on this component, that repair process could easily be transitioned to non-flight critical components that require chrome repair.

4.4.5.3. ESD Process Development and Repair Procedure

Minimal process development was conducted on repairing the hot air erosion damage. The width of the damage was approximately 0.03" and approximately 0.014" deep (Figure 4-117). The repair (Figure 4-118) was performed with no pre-ESD surface preparation (no excavation of the defect prior to repairing it). The ability to affect this repair with no surface preparation is somewhat revolutionary. The metallography of the repaired area (Figure 4-119) showed a complete fill, good interface and good density of the deposit.

Figure 4-117 Hot Air Erosion Defect

Figure 4-118 ESD Repair of Defect (Before Surface Finishing)

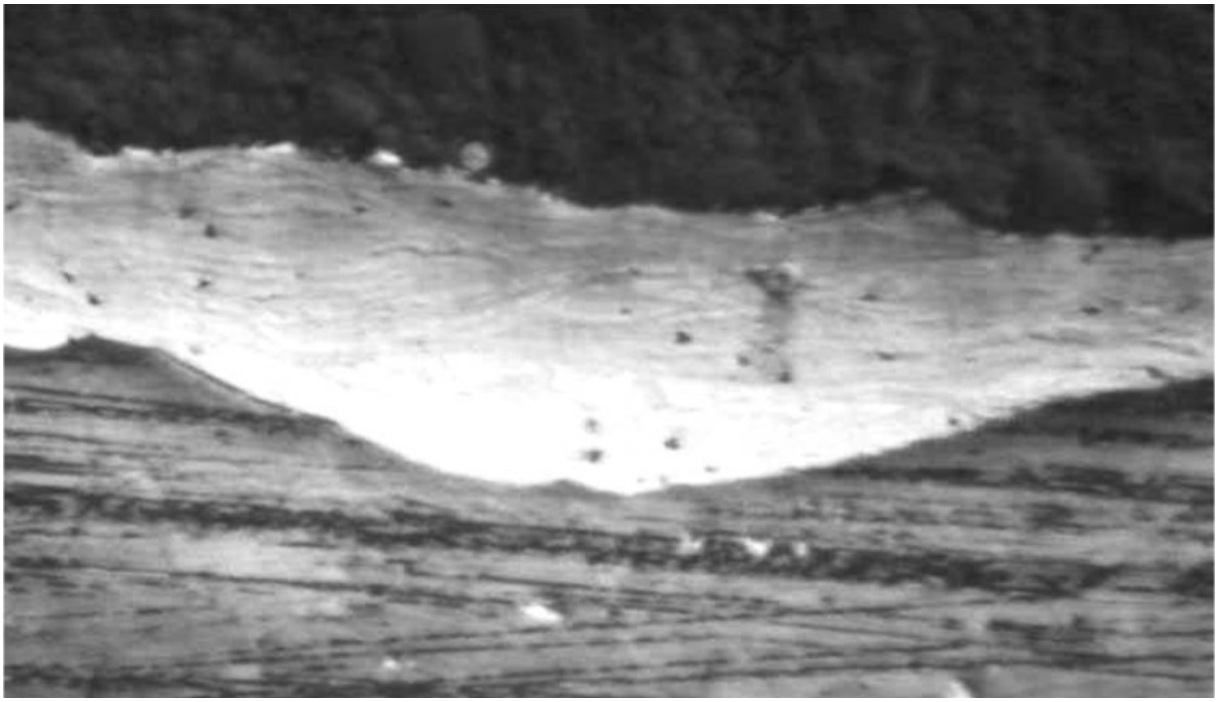

Figure 4-119 Metallography of Repaired Hot Air Erosion

To complete the repair process and deliver a demonstration requires that a non-flight critical component, with similar damage, be found.

4.4.6. Conclusion

Of the three components selected for this project, the ESD repair process for the #5 Bearing Housing has matured the most. A Welding Specification has been provided to OC-ALC and the repair process entered into the TO. The ESD repair process for the 10-12 Stator Segment was also completely developed although a final metallurgical

evaluation of the repair is to be performed. Although a Welding Specification document has not been formally written for this component, the process is well documented and ready for a hands-on demonstration to OC-ALC engineers. The ESD repair of the TF39 Shaft was the least successful. To complete the repair process and deliver a demonstration requires that a non-flight critical component, with similar damage, be found.

A large number of components were considered as candidate components to receive an ESD repair. Many were not accepted into this project, often because they were fabricated of materials that were not studied in this project. The material and mechanical properties of materials, applied via ESD, continues to be evaluated for other super alloy materials. As this data becomes available, an increasing number of components can be considered for an ESD repair.

This page intentionally left blank.

5. Application of ESD for Repair of Army Main Battle Tank Components

5.1. Introduction

This section describes the development of an ESD repair for components from an Army main battle tank. The components chosen for the demonstration were the M1A1 cannon cradle and the M1A1 helical (sun) gear shaft, with their selection based principally on the potential for significant cost savings utilizing ESD. Previous to the implementation of ESD technology, each part had been inspected, removed from service and put into storage because of corrosion pits and wear. New parts had to be acquired for installation into M1A1 tanks in order to place them back into service. The rejection rate became an important issue, since there was a shortage of available replacement parts, so the ability to repair these components using ESD affected not only total ownership cost but readiness of the combat system.

5.2. Repair of M1A1 Cannon Cradle

A cannon cradle on an actual M1A1 tank is shown in Figure 5-1, while Figure 5-2 shows a cradle that has been removed from a tank. This component is fabricated from 4130 steel.

Figure 5-1 M1A1 Main Battle Tank Cannon Cradle (indicated by arrow).

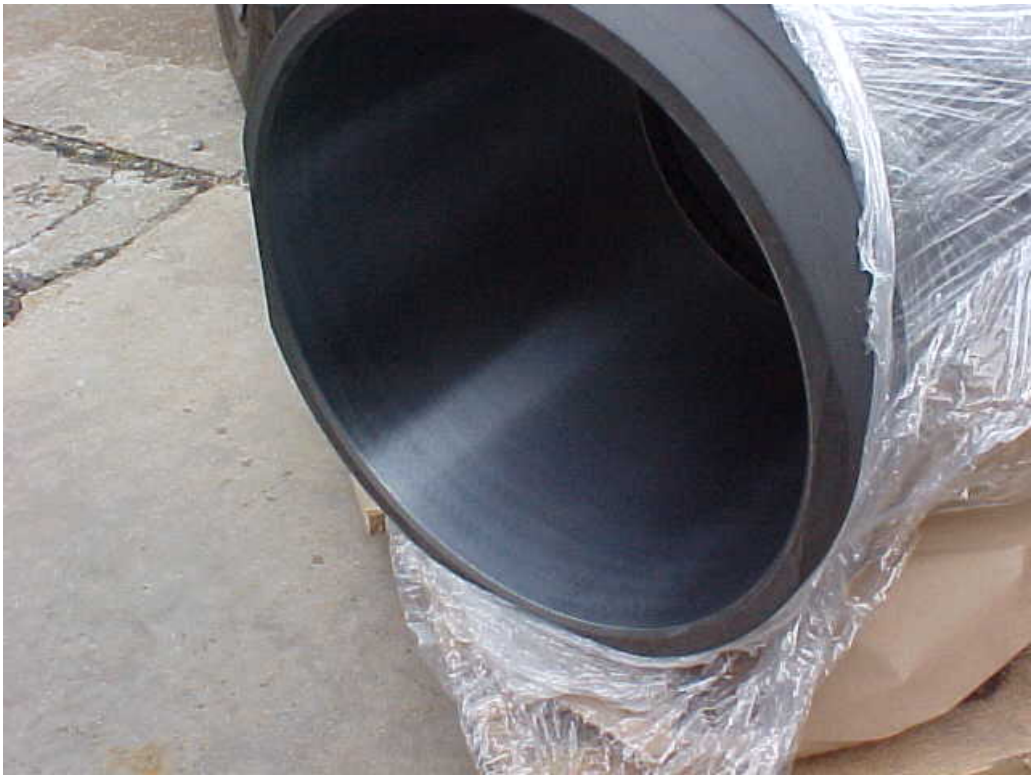

Figure 5-2 Cannon Cradle Disassembled from Tank.

Optimal parameters and repair procedures for the M1A1 cannon cradle were developed at ANAD and subsequently refined and proved out at ARL. Table 5-1 indicates the two sets of deposition parameters that were used for optimization of the ESD process on the cannon cradles with Inconel 718 as the deposited material. Condition 2 parameters were determined to provide the best coatings.

The repair qualification of the components was based upon the ability of the coating to adhere adequately to the substrate in order to withstand a finish grinding procedure. ARL conducted tests where mechanical pits were machined into AISI 4130 steel blocks, representative of the base material, and subsequently filled utilizing the ESD repair procedure developed for the component. Additional samples that were chrome plated were also repaired by ESD and compared to the initial test group to determine the feasibility of performing an ESD repair on chrome plated parts. A subsequent grinding operation was performed, after the pits were completely filled, to simulate subsequent manufacturing to bring the part back to the final dimension and surface finish requirement. Metallographic examination and hardness testing was performed on the samples and compared to the substrate.

Metallography was utilized to examine test specimens that had been processed, to ensure that the deposit did not contain significant voids, porosity or cavities. This would give an indication that the adhesion to the substrate material was adequate. Specimens were sectioned and mounted in phenolic powder. The mounted specimens were subsequently rough polished using silicon carbide paper ranging in grit size from 240 to 2400. Final polishing was accomplished with 1 μm diamond followed by 0.05 μm alumina. For the most part, the interface between the substrate and the ESD deposit shown in Figure 5-3 was determined to be acceptable; however, areas of surface porosity were sometimes encountered with the chrome plated samples as shown in Figures 5-4 and 5-5. ASAP, Inc. describes this phenomenon as the "halo-effect" which consists of small defects where ESD meets the hard chrome. ASAP indicated that improvements are seen in reducing or eliminating this effect specifically when the ESD equipment parameters were maintained at low energy while applying ESD at the interface. Figure 5-6 shows a polished cross section displaying the porosity associated with the "halo-effect", while Figure 5-7 shows no anomalies for a different ESD deposit on chrome plate.

Table 5-1 ESD Parameter Optimization for M1A1 Cannon Cradle

	Condition 1	Condition 2
Base Material	4130 Steel	4130 Steel
Non-ESD Coating	Chrome Plating	Chrome Plating
Electrode Alloy	Inconel 718	Inconel 718
Electrode Diameter (inch)	0.125	0.125
Pulse Rate (Hz)	580	400
Capacitance (μF)	20	30
Voltage (V)	100	150
Step Rate (Hz)	270	340
Swing	3	3
Rotate Increment	3	3
Direction	CW	CW
Interval	6	6
Shielding Gas	Argon	Argon
Shielding Gas Flow Rate (CFH)	35	35

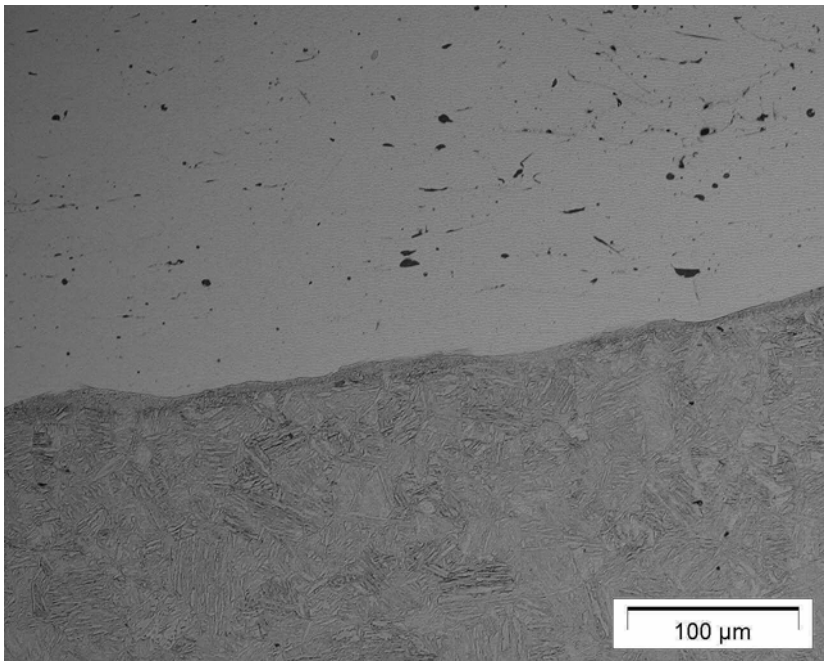

Figure 5-3 Photomicrograph Showing Interface Between Deposit and Substrate; Substrate was AISI 9310 Steel Etched with 2% Nital

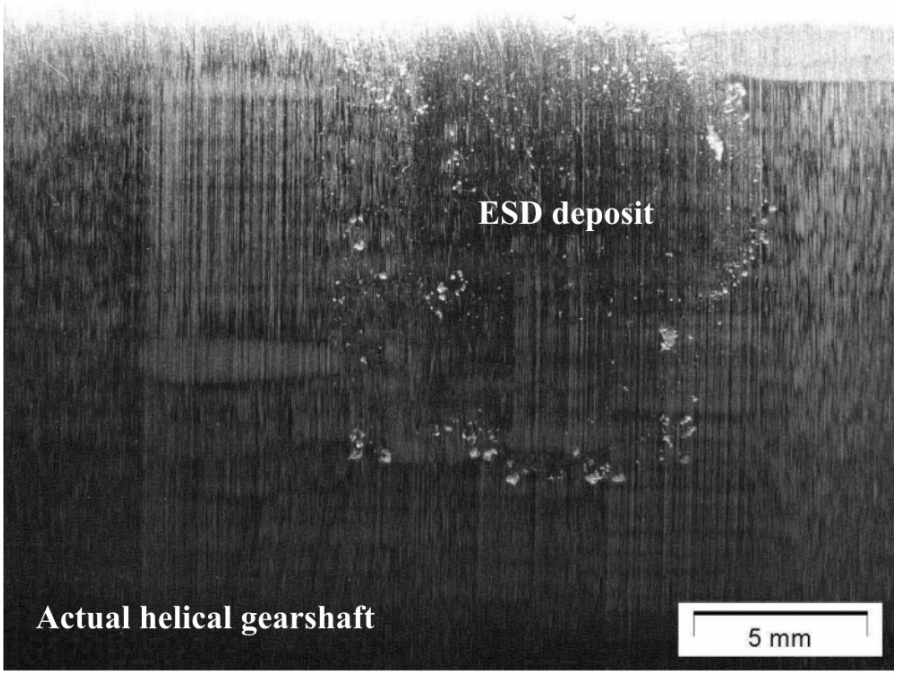

Figure 5-4 Porosity Around the ESD Deposit ("halo-effect") of a Chrome Plated Sample.

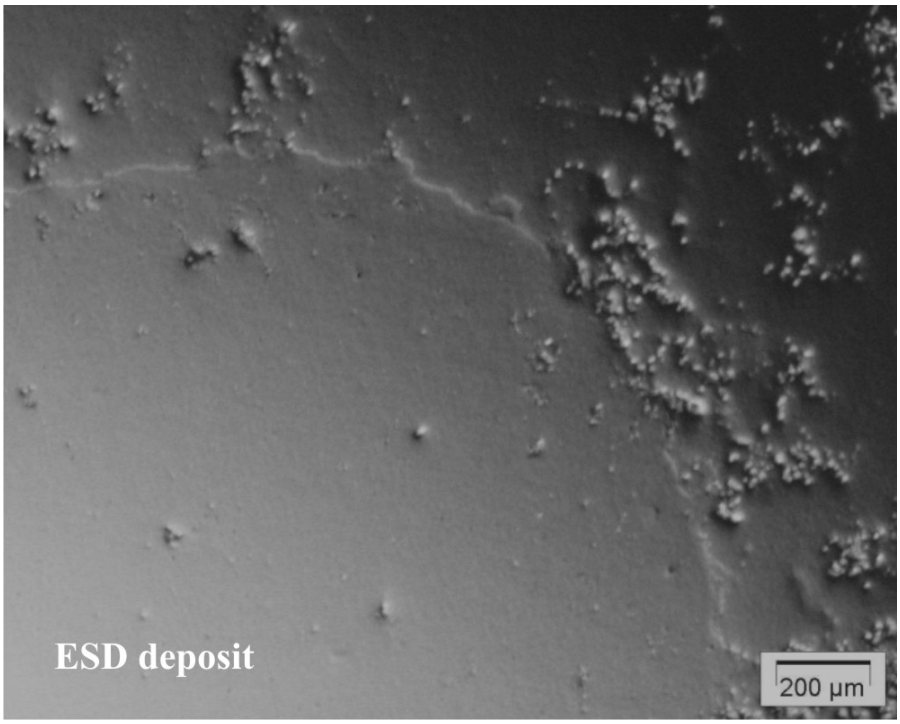

Figure 5-5 Magnified View of Figure 5-4 Utilizing the Differential Interference Contrast (DIC) Mode for Optical Viewing

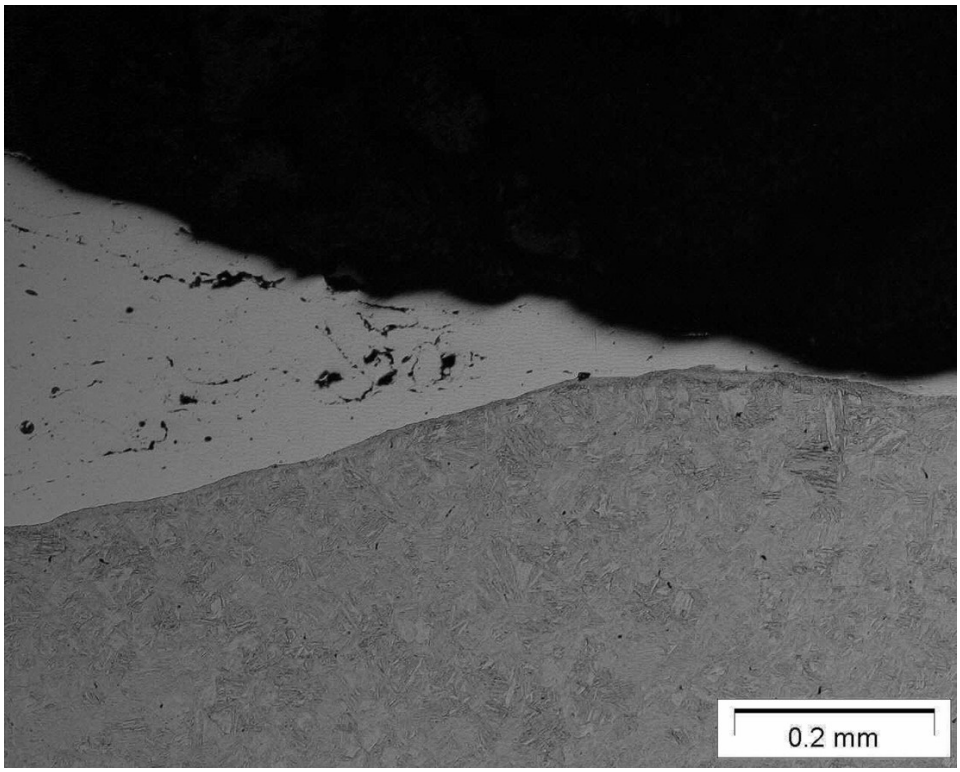

Figure 5-6 Polished and Etched Cross-Section Showing Porosity Associated with the "Halo-Effect" in a Chrome-plated 9310 Steel Sample

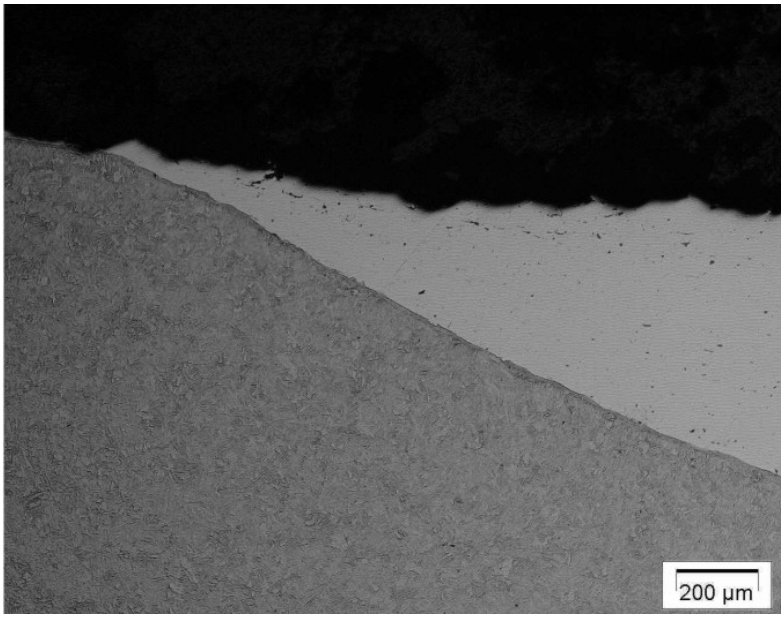

Figure 5-7 Polished Sample Cross-Section of an ESD-Filled Chrome-Plated Defect Showing No Anomalies

Knoop microhardness measurements (with a load of 500 g) were made to assess the hardness of the ESD deposits compared to the 4130 substrate material. The hardness of the deposit and the base metal were essentially the same. In addition, the hardness of the base metal was not altered as a result of the ESD process. Figure 5-8 shows a graph of the hardness data, and Figure 5-9 includes a micrograph of the hardness indents through the deposit into the base metal.

Table 5-2 Knoop Microhardness Measurements in Various Locations for ESD-deposited Inconel 718 on 4130 Steel

Reading	*Knoop*	*Approx. HRC*	*Reading*	*Knoop*	*Approx. HRC*
1	331.0	32.6	13	313.6	30.3
2	326.1	32.0	14	372.4	37.2
3	361.4	36.1	15	390.9	38.9
4	390.9	38.9	16	377.3	37.7
5	361.9	36.1	17	381.8	38.1
6	365.0	36.5	18	395.0	39.3
7	390.3	38.9	19	397.9	39.6
8	364.5	36.4	20	395.0	39.3
9	405.2	40.2	21	396.8	39.5
10	405.8	40.3	22	392.6	39.1
11	390.3	38.9	23	401.5	39.9
12	391.5	39.0	24	397.9	39.6

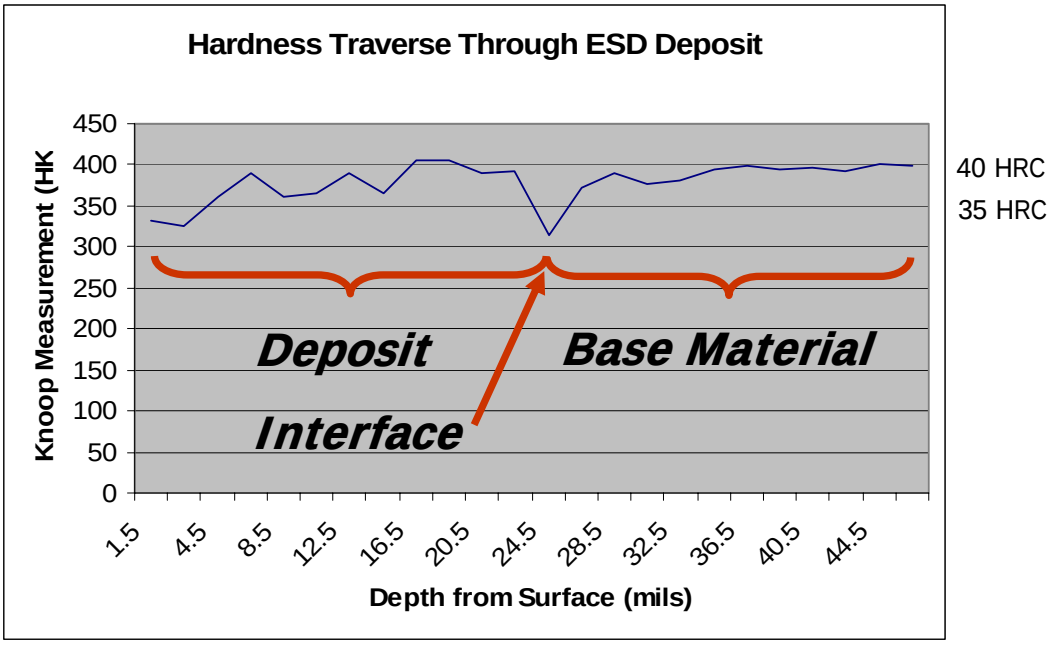

Figure 5-8 Plot of Hardness Through ESD Deposit into the Base Metal, Showing Similar Hardness Values

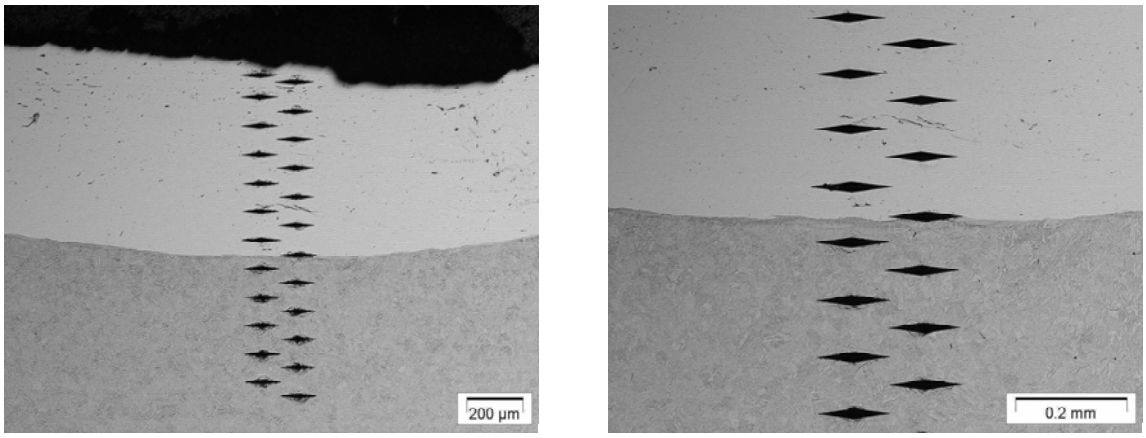

Figure 5-9 Micrographs of Knoop Microhardness Indents Through the ESD Deposit into the Base Metal

The methods of inspection employed for the repair of the cannon cradle reflect the concerns of serviceability (visual inspection), dimensional conformance and surface finish. Stereoscopic inspection was performed utilizing a 10x lens to examine the repaired surface for evidence of blistering, peeling and/or cracking, which is not allowed and would be a cause for rejection.

The reclamation procedure for the cannon cradle was approved by ANAD Engineering and has been performed since 25 June 2003. Figure 5-10 shows the application of an ESD coating to a cannon cradle at ANAD. The total amount of time required for this repair, including surface preparation prior to deposition and finishing subsequent to deposition, has averaged nine hours. A formal Reclamation Procedure PMD 03-39 has been developed for repair of this component and that is provided in Appendix A.

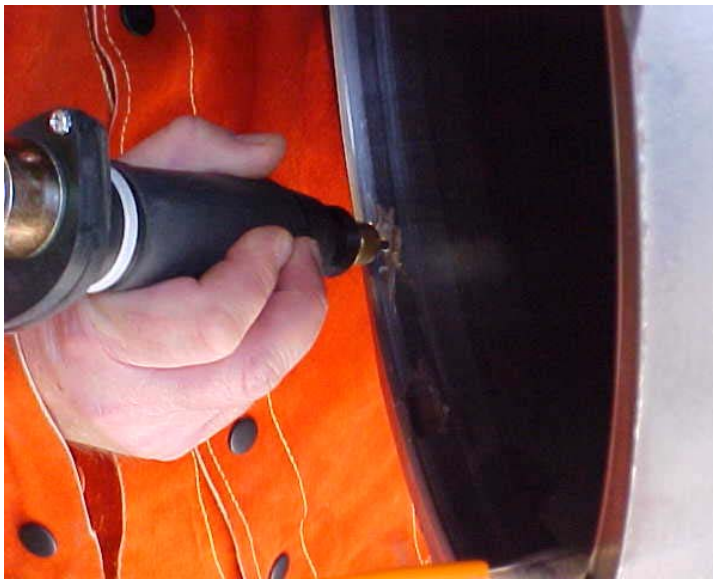

Figure 5-10 Photo Showing ESD Torch Applying Deposit on the ID of a Cannon Cradle Using a Rotating Electrode

Since the approval of the ESD repair for the M1A1 cannon cradle by the Tank Automotive Command (TACOM) there have been 15 parts identified for reclamation. This equates to a potential cost savings of approximately $360,000 to be realized by ANAD, based upon the rejection rates during the fourth quarter FY03 and the first half of FY04. A total of 189 parts were inspected and 15 were identified for reclamation. To date 9 of these parts have been successfully repaired by ESD technology.

A cursory cost analysis was performed to determine the cost savings to date by the implementation of ESD for the nine M1A1 cannon cradles that have been repaired, as well as the anticipated cost savings for all 15 parts that have been identified for repair. The cost to purchase a new component is $24,636. The reclamation costs have been determined to be $698.50, based on a labor rate of $76.50/manhour for 9 hours and a material cost of $10.00.

Using these factors, the cost savings for repairing nine components was calculated as follows:

The Cost to Purchase (9) New Parts is: $24,636.00 x 9 = $221,724.00

The Cost to Repair (9) Pitted Parts: $698.50 x 9 = $6,286.50

The Total Cost Savings *equals* the Cost to Purchase (9) New Parts *minus* the Cost to Repair (9) Pitted Parts or $221,724.00 - $6,286.50 = $215,437.50

The cost savings for repairing (15) parts was calculated as follows:

The Cost to Purchase (15) New Parts is: $24,636.00 x 15 = $369,540

The Cost to Repair (15) Pitted Parts: $698.50 x 15 = $10,477.50

The Total Cost Savings *equals* the Cost to Purchase (15) New Parts *minus* the Cost to Repair (15) Pitted Parts or $369,540 - $10,477.50 = $359,062.50

5.3. Repair of M1A1 Helical Gear Shaft

The helical gear shaft is shown in a cut-away section of an AGT-1500 gas turbine engine in Figure 5-11while Figure 5-12 shows a schematic of the gear and its relation to other engine components. Figure 5-13 shows an actual gear shaft that was shipped from ANAD to ARL for this project.

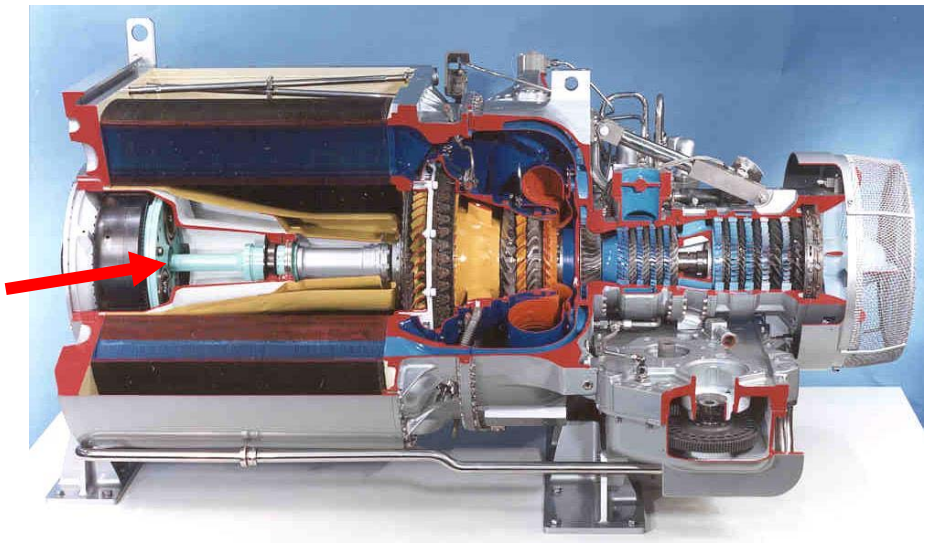

Figure 5-11 M1A1 Main Battle Tank AGT1500 Engine. Arrow Indicates Location of the Helical Gear Shaft Within the

This component is fabricated from 9310 steel and hard chrome plating is applied for wear resistance. However, after several years of service wear scars or large corrosion pits (up to 1/8" x 3/8" and 0.060" deep) are formed as indicated in Figure 5-14. Systems were taken out of service based on surface anomalies discovered during inspection and insufficient replacement parts were available. There was no approved repair procedure for these components and conventional weld repair technologies had been eliminated at ANAD to repair these large defects.Approximately 8% of the components overhauled at ANAD in 2003 were determined to be defective, removed from the systems and put in storage.

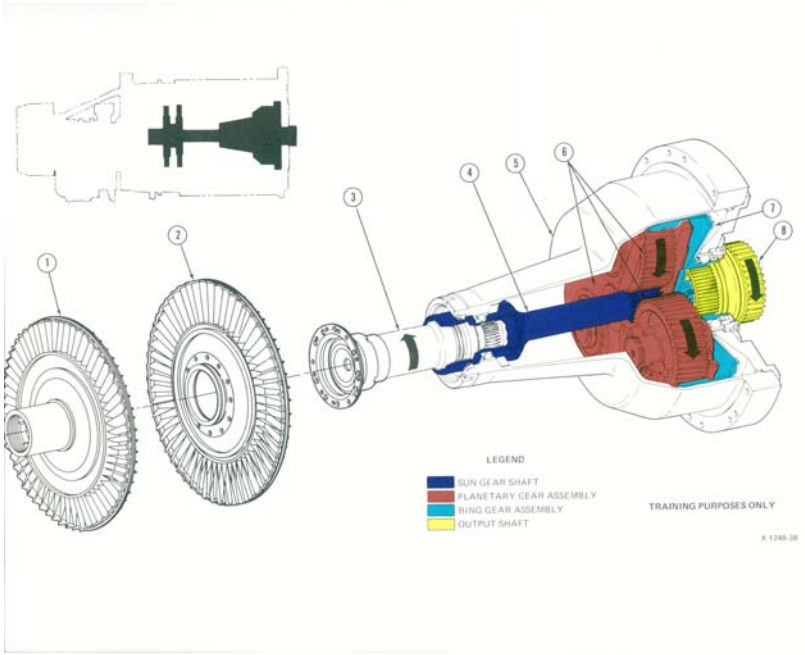

Figure 5-12 Schematic of the Helical Gear Shaft and its Relation to Other Engine Components

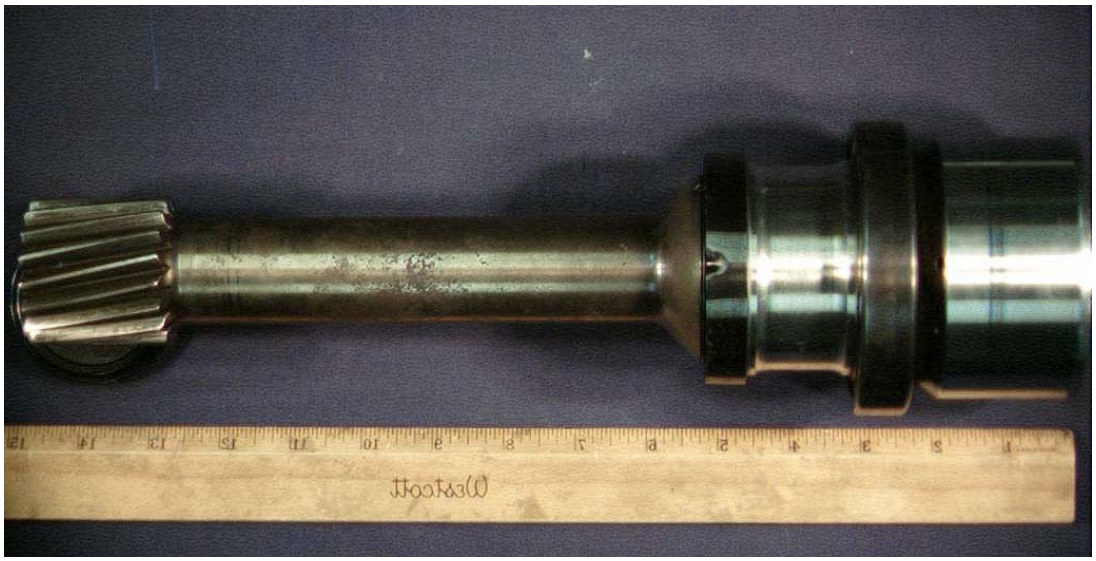

Figure 5-13 Photograph of an M1A1 helical gearshaft

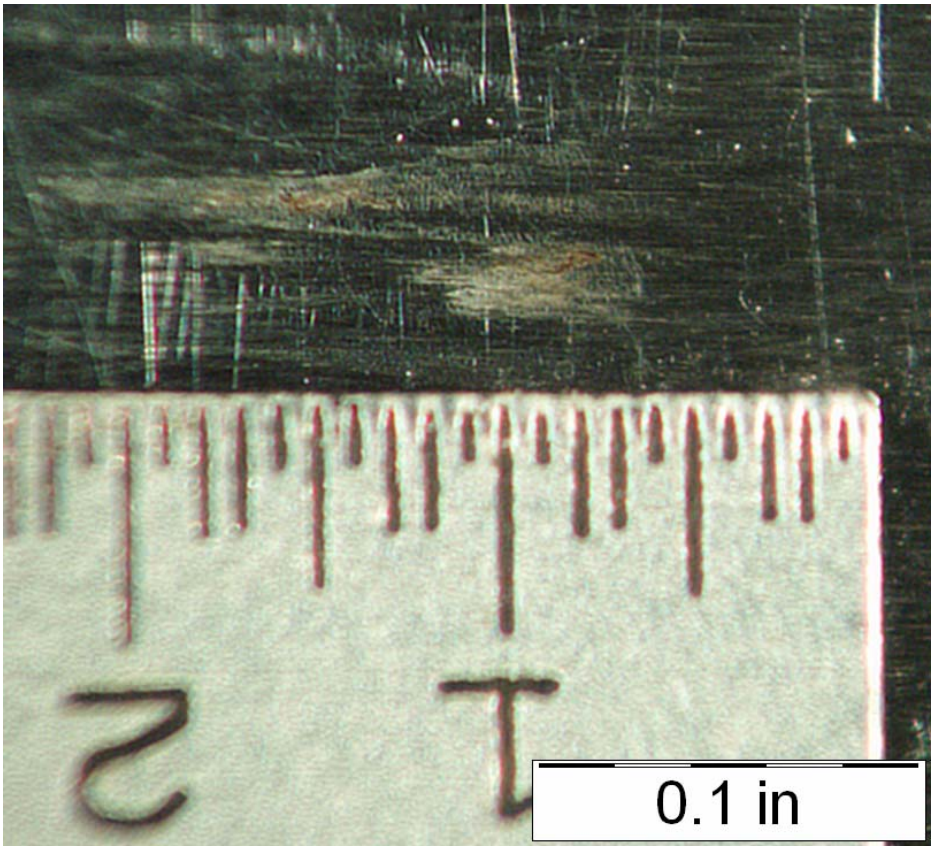

Figure 5-14 Example of Corrosion Pits Formed on a Helical Gear Shaft in Service

The ESD repair procedure for this component was developed at and proved out at ARL. Numerous ESD trials were conducted in order to determine the optimal set of process parameters that would result in a dense, adherent deposit. These trials were performed on coupons representing the material of the gear shaft (chrome-plated AISI 9310 steel). Defects were machined into test samples (Figure 5-15), and subsequently filled using ESD. Table 5-3 summarizes the iterative process utilized for each of the six defects, while Figure 5-16 shows a representative scanning electron micrograph of a section of each defect. Condition 4 was considered to exhibit the optimal coating characteristics and is highlighted in Table 5-3.

Table 5-3 ESD Parameter Optimization for M1A1 Helical Gear Shaft

	Condition 1	Condition 2	Condition 3	Condition 4	Condition 5	Condition 6
Base Material	9310 Steel	9310 Steel	9310 Steel	9310 Steel	9310 Steel	9310 Steel
Non-ESD Coating	Chrome Plating	Chrome Plating	Chrome Plating	Chrome Plating	Chrome Plating	Chrome Plating
Electrode Alloy	Inconel 718	Inconel 718	Inconel 625	Inconel 718	Inconel 718	Inconel 718
Electrode Diameter (inch)	0.125	0.125	0.125	.125	0.125	0.125
Pulse Rate (Hz)	400	400	400	400	400	400
Capacitance (μF)	30	30	30	30	30	30
Voltage (V)	140	200	140	140	150	120
Step Rate (Hz)	340	340	340	300	300	300
Swing	4	4	4	4	4	4
Rotate Increment	4	4	4	4	4	4
Direction	CCW	CCW	CCW	CCW	CCW	CCW
Interval	8	8	8	8	8	8
Shielding Gas	Argon	Argon	Argon	Argon	Argon	Argon
Shielding Gas Flow Rate (CFH)	35	35	35	35	35	35

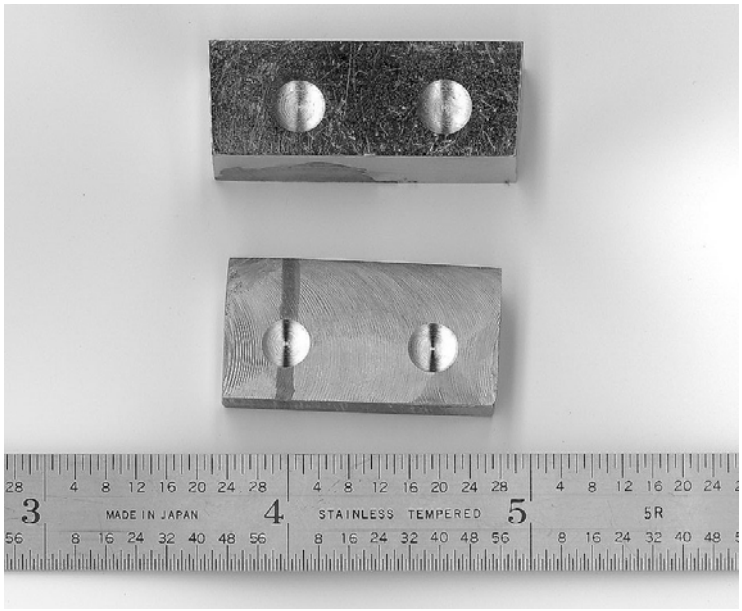

Figure 5-15 Test Samples Used for ESD Process Parameter Optimization for the M1A1 Helical Gear Shaft Repair. Top Block is Chrome-plated, Bottom Block is Uncoated AISI 9310 Steel

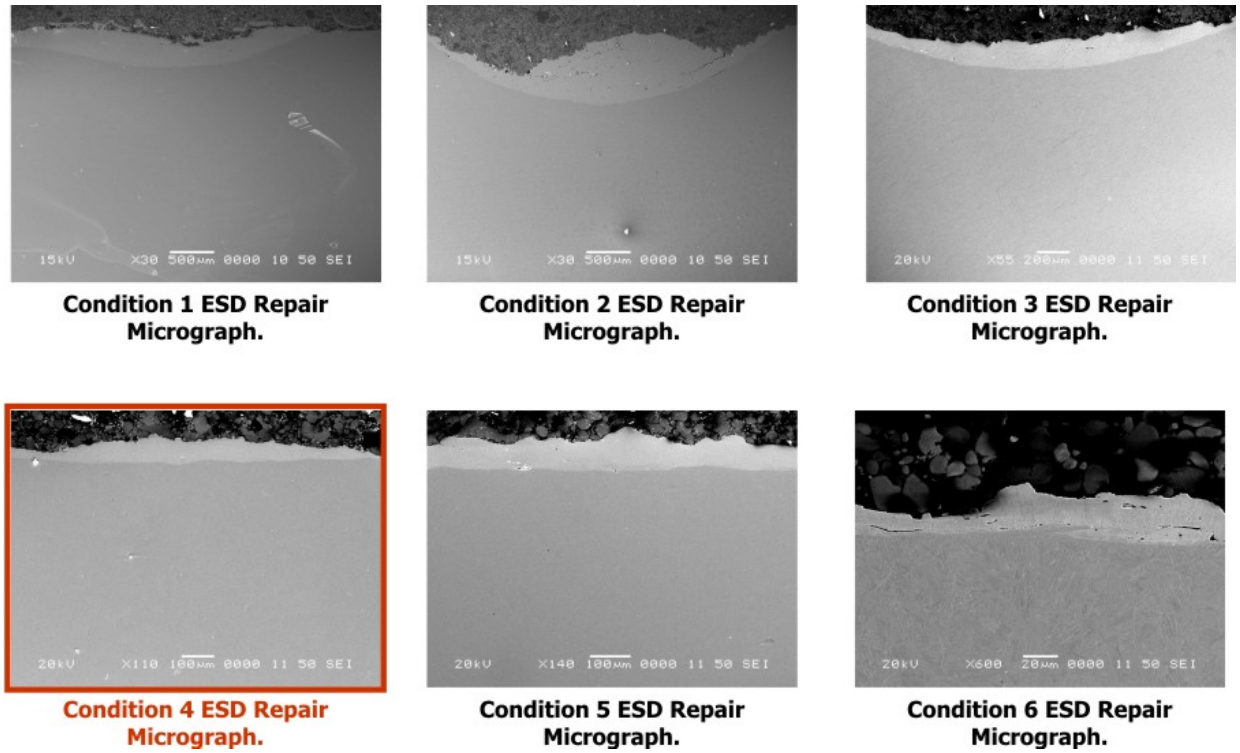

Figure 5-16 SEM Micrographs of ESD Deposits Using Different Conditions as Specified in Table 5-3

The parameters indicated in Condition 4 were chosen to be used for the repair of the helical gear shaft. These parameters were chosen for the uniformity and density of the coating, the clean interface between the coating and substrate, and the lack of voids and intergranular sites. Figure 5-17 shows an optical macrograph of two ESD-filled defects, as well as an unfilled defect, while Figure 5-18 includes an SEM micrograph of the surface of Condition 4. Figure 5-19 shows an SEM micrograph of a cross section of a Condition 4 deposit.

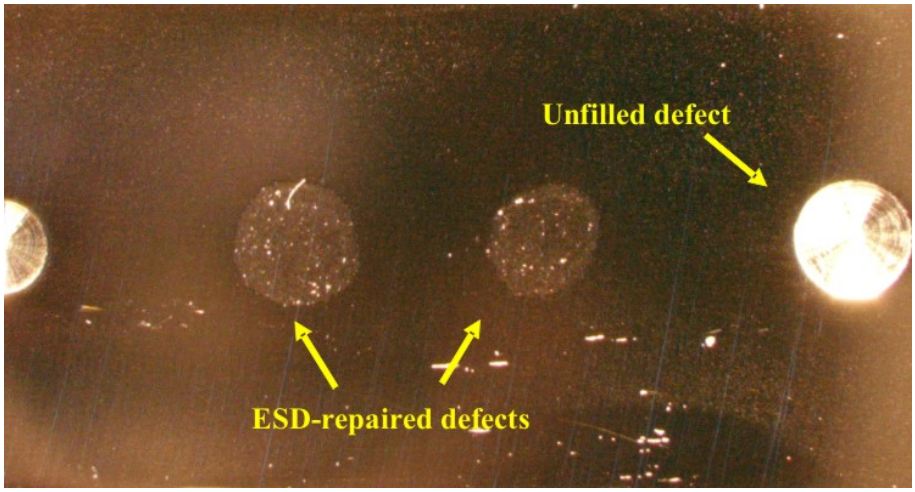

Figure 5-17 Optical Macrograph Showing Two ESD-filled Defects and One Unfilled Defect

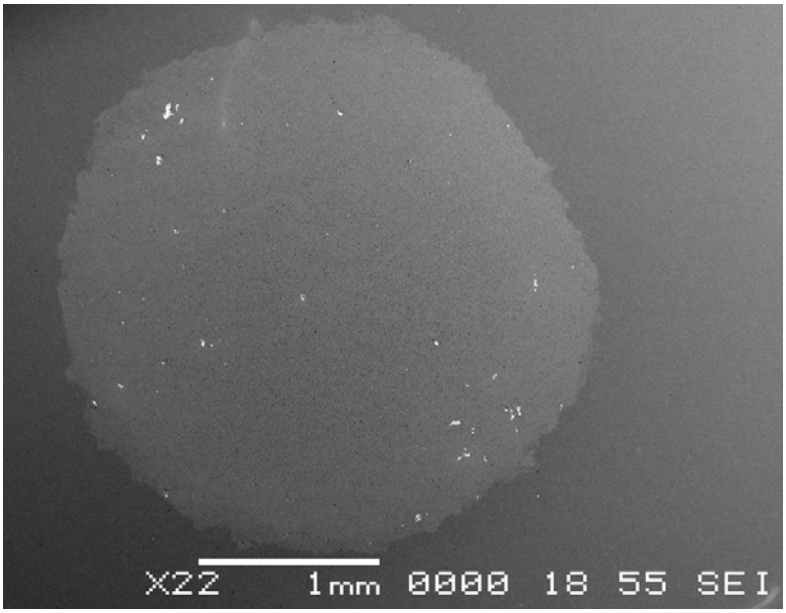

Figure 5-18 SEM Micrograph of the Surface of Condition 4 after ESD Repair

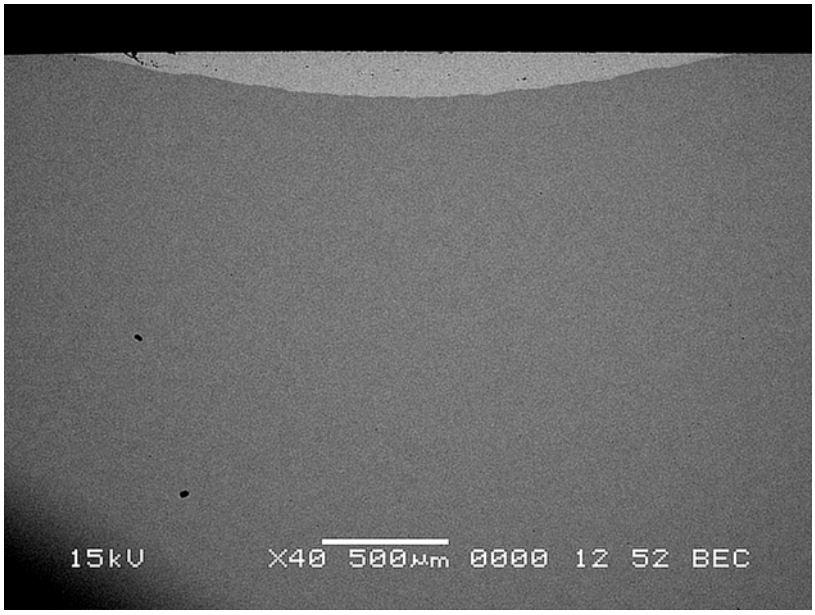

Figure 5-19 SEM Micrograph of a Cross-Section of an ESD Deposit Using Parameteres of Condition 4

Once these optimized parameters were established, defects on actual helical gear shafts were repaired utilizing ESD as shown in Figure 5-20.

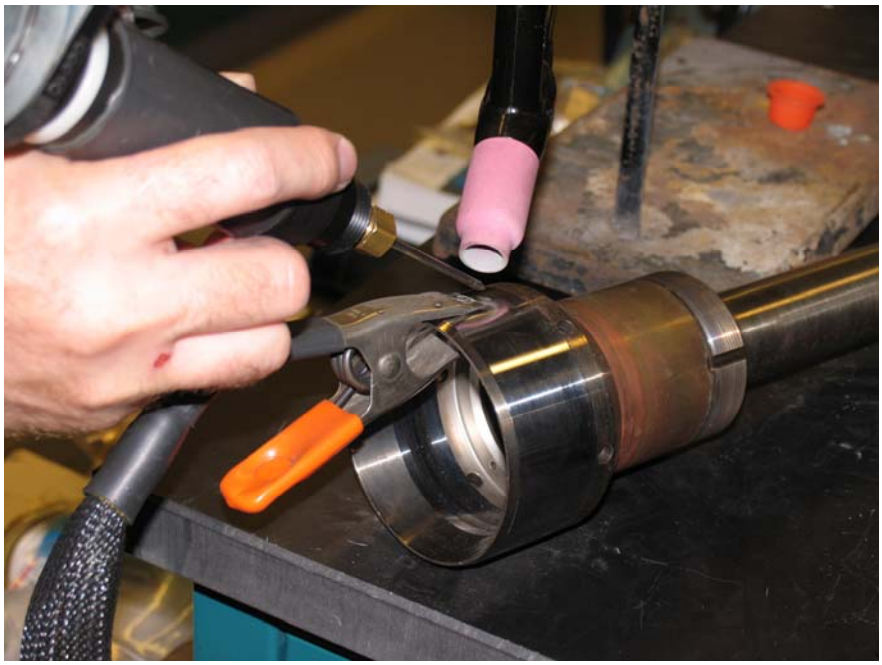

Figure 5-20 ESD Repair Being Performed at ARL on an Actual Helical Gear Shaft Containing Defects

Inspection criteria for the repair of the helical gear shaft include visual inspection, measurement of dimensional conformance and surface finish. In addition, a liquid penetrant inspection will be required to verify that there are no surface defects that could affect performance.

Engineering approval for application of ESD to repair the helical gear shaft is dependent on the results of testing ESD-repaired gear shafts in an AGT-1500 Engine Test Stand for 100 hours. This test is scheduled for the second half of 2006. In anticipation of approval of this repair procedure, a draft Reclamation Procedure has been developed and this is provided in Appendix B.

5.4. Summary and Conclusions

An ESD repair has been qualified and implemented at ANAD for the M1A1 cannon cradle, with a formal Reclamation Procedure established. To date, nine cradles have been repaired, with six additional cradles scheduled for repair in 2006. Substantial cost savings as well as increased readiness for the M1A1 tanks are expected to be realized by implementation of this procedure.

ESD repairs on M1A1 helical gear shafts have been demonstrated, although full qualification is subject to successful completion of a 100-hour engine test. Since this involves repair of hard chrome plate, special care must be taken to ensure that the "halo effect" is not generated which results in near-surface defects near the interface between the ESD material and hard chrome.

Additional components at ANAD have been selected for possible ESD repair including the M88/M60 roadwheel arm spindle, the M198 recoil rod and the M1A1 converter shaft.

This page intentionally left blank.

6. Application of ESD on Ship/Submarine Components

6.1. Background

Corrosion and wear of shipboard components exposed to seawater environments are a continual maintenance burden for the U.S. Navy. In many cases the components are quite large and repair involves removing them from the ship or submarine, which is time-consuming and costly. Quite often the corroded or worn areas are in localized areas on the components representing a very small fraction of the total surface area on the component.

An example of this is steering and diving control rods on Navy submarines. Figure 6-1 shows one of these control rods in service and Figure 6-2 shows one of the rods subsequent to removal. These rods are fabricated from Alloy K500, a precipitation-hardened nickel-copper alloy with a nominal composition of 63Ni-30Cu-2.5Al-2Fe-1.5Mn (Ti, Si, and C at less than 1%). During service, these rods are subject to wear and corrosion pitting as indicated in Figure 6-3. Generally, the surface damage is limited to small areas on the rods.

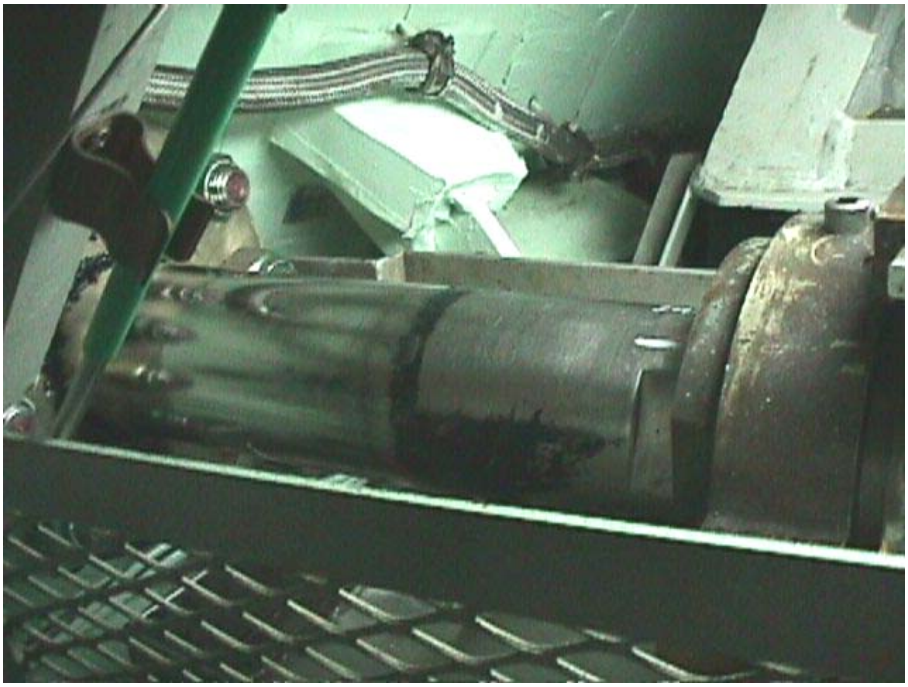

Figure 6-1 Steering/Diving Control Rod in service

Another problem area is crevice corrosion in seawater piping systems fabricated from Alloy 625, which is highly resistant to localized corrosion except in tight crevices. This type of corrosion is often encountered in components such as flanges and valves. As with the control rods, the damage is usually localized but current repairs require that the components be removed from the submarine and overhauled at a repair facility or replaced.

Figure 6-3 Steering/Diving Control Rod Subsequent to Removal From Submarine

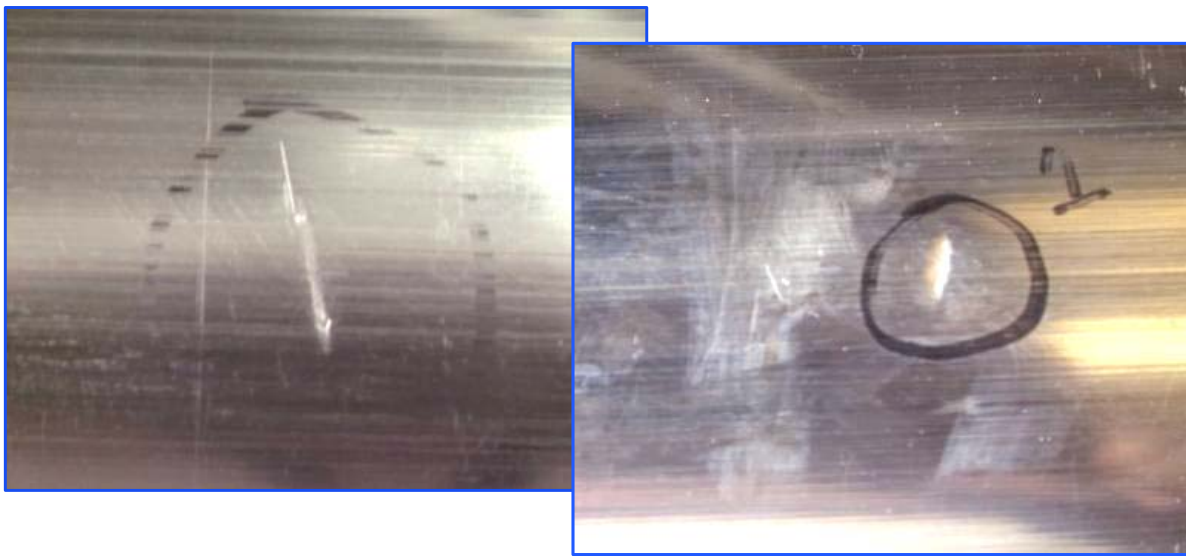

Figure 6-2 Examples of damage on Steering/Diving Control Rod Sustained in Service

Electrospark deposition was considered to potentially be an ideal technology that could be utilized for repair of the localized damage on these types of components. This was not only because ESD could deposit coatings in small areas with a metallurgical bond to the base material but also because of its portability which would enable an ESD system to be brought onboard a ship or submarine to effect repairs in situ without having to remove the damaged component. This would provide substantial cost savings as well as significantly reduce turnaround times for repair.

The Naval Surface Warfare Center Carderock Division (NSWCCD) under sponsorship from the Office of Naval Research (ONR) and ESTCP, conducted materials studies and component demonstrations in order to validate the ESD process for repair of ship and submarine components. The following sections describe the work that was performed and the results that were obtained.

6.2. ESD Deposition on Alloy K500 – Materials Studies

Electrospark depositions were performed using equipment located at NSWCCD (shown in Figure 6-4), which was acquired from ASAP, Inc. Initially nitrogen was used as a cover gas to prevent oxidation of the deposited material but this was later changed to argon. Figure 6-5 shows application of an ESD coating to a test coupon with a low-power microscope positioned to examine the deposit and the image displayed on a monitor.

Figure 6-4 ESD Equipment Located at NSWCCD Used for Materials Studies

ESD coatings of Alloy 400 were deposited onto one surface each of 1" x 1" x 0.25"-thick flat plate Alloy K500 specimens for GM9540P cyclic corrosion and electrochemical potential measurements. The chemical composition of Alloy 400 is very similar to that of K500. Additionally, a 1"-wide strip of ESD Alloy 400 was deposited onto 2" x 3" Alloy 400 sheet specimens for bend testing. For all of these tests, the ESD coatings were evaluated in the as-deposited condition.

Figure 6-5 Application of ESD Coating to Test Coupon

Table 6-1 indicates the two different sets of ESD parameters that were used for these studies, designated HFA and HFC. One pass of an ESD deposit was made by starting at the top of a test plate and proceeding downward, with slightly overlapping lines of deposit from the previous one until the entire test plate was covered. A second pass was made in a 90 degree orientation from the first pass. A lattice pattern deposit of coating material was made by alternating passes between a 0 degree and 90 degree orientation.

Table 6-1 ESD Parameters for Deposition of Alloy 400 Onto K500 Test Coupons

ESD Coating	*Nominal Composition*	*Specimen Identification*	*ESD Coating Parameters*		
			Pulse Rate (Hz)	*Capacitance (µF)*	*Voltage (V)*
Alloy 400	63Ni-28Cu-2Fe-2Mn	HFA	700 (4 passes), 1000 (2 passes)	30 (4 passes), 10 (2 passes)	100 (4 passes), 150 (2 passes)
		HFC	400 (4 passes), 700 (2 passes)	30 (6 passes)	180 (4 passes), 100 (2 passes)

6.2.1.Bend Testing

Bend testing was conducted on four ESD Alloy 400 sheet specimens in accordance with MIL-STD-1687 by bending approximately 180 degrees around a 0.5”-diameter rod. Two of the sheet specimens utilized the ESD parameters designated in Table 6-1 as HFA, while the remaining two sheet specimens were prepared by the parameters designated as HFC. The ESD coating was located on the tensile side of the bend. The bend specimens

were visually examined for flaking, delamination, or gross cracking of the coating due to bending. Small hairline cracks or alligatoring of the coating in the vicinity of the bend were permissible. This military standard test is required for qualification of thermal spray coatings and was considered relevant to the ESD coatings.

Due to the metallurgical bond formed between the ESD coating and the substrate material, the bend test results were excellent. Bend specimens which utilized both the HFA and HFC deposition parameters performed equally well. No flaking, delamination, or cracking of the ESD coating was evident in the vicinity of the bend. Figure 6-6 shows the condition of a representative ESD Alloy 400 coated sheet specimen both before and after the bend test.

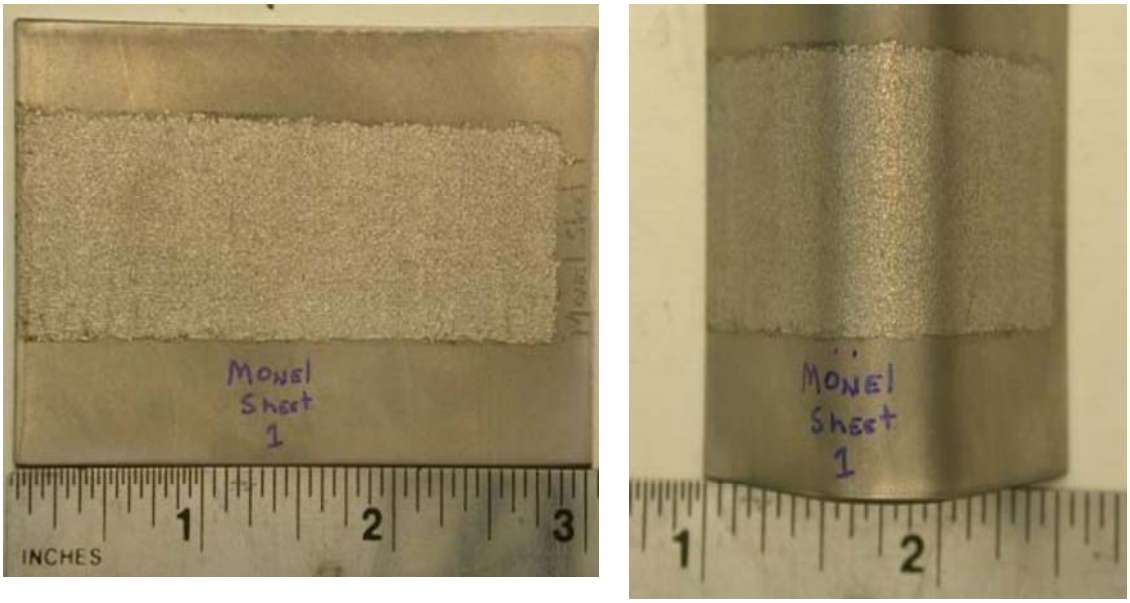

Figure 6-6 ESD Alloy 400 Coated Sheet Specimen Before (left) and After (right) Bend Testing per MIL-STD-1687

6.2.2. Corrosion Potential Measurements

Electrical leads were attached to four ESD coated specimens, and specimens were then immersed in aerated ASTM D1141 ocean water [11] for 120 days. Corrosion potential (E_{corr}) measurements were made versus a silver/silver chloride (Ag/AgCl) reference electrode on individual specimens periodically throughout the exposure.

Corrosion potential measurements as a function of time are recorded in Figure 6-7 for the ESD Alloy 400 coated specimens with specimen codes HFA and HFC. As seen in this figure, the potential data was similar between all four of the specimens and was stable with time. The average E_{corr} for these specimens measured approximately -0.040 volts (V) vs. Ag/AgCl. This E_{corr} is within the typical range of E_{corr} values reported for wrought Alloy 400 (-0.02 to –0.10 V vs. Ag/AgCl) [12], indicating that the electrospark deposited coating is comparable in terms of seawater corrosion behavior to conventional wrought material.

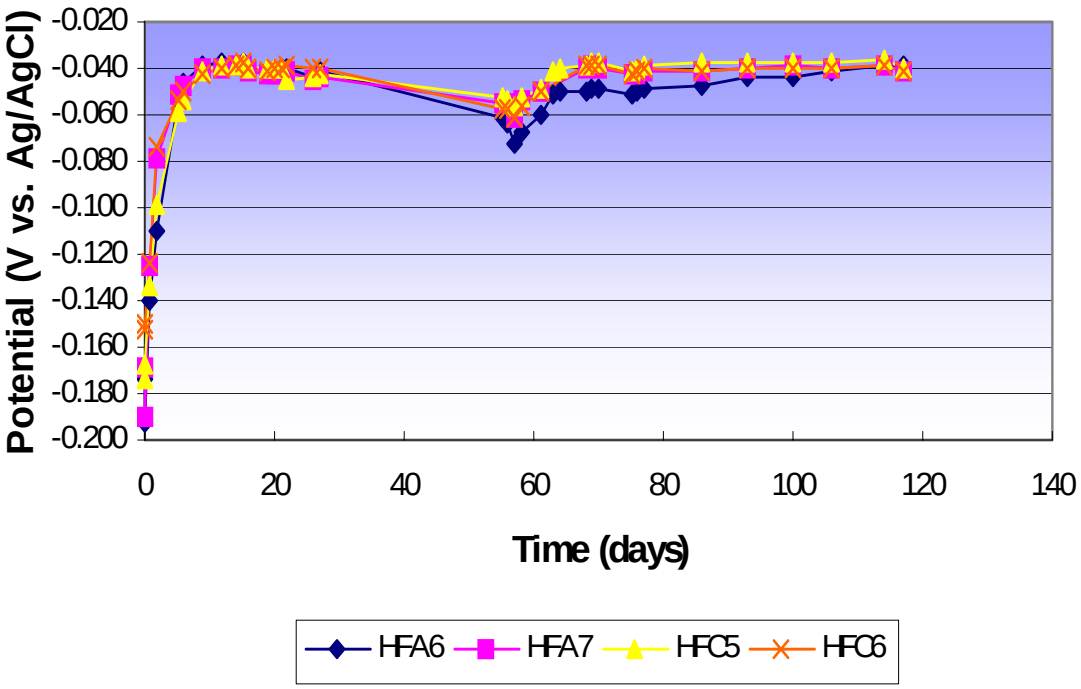

Figure 6-7 Corrosion Potential Data for ESD Alloy 400 Deposited Onto K500 Specimens

6.2.3.GM9540P Cyclic Corrosion Testing

ESD coated specimens were positioned on a non-metallic rack in the GM9540P accelerated test cabinet and exposed for 80 cycles (80 days). This exposure consists of a combination of cyclic conditions including salt mist, ambient exposure, high humidity exposure, and elevated temperatures. Specifics of the test cycle and solution are described in Table 6-2. During the exposure, specimens were visually inspected periodically without removing them from the test cabinet. After testing, specimens were removed from the cabinet, fresh water rinsed, air dried and photographed.

After 80 cycles in the GM9540P cabinet, four of the eight ESD Alloy 400 specimens exhibited corrosion on their surfaces with the attack concentrated predominantly at the edges of the specimens. The corrosion initiated within 30 cycles of exposure in the GM9540P cabinet. Metallographic evaluation of the corroded specimens is required to determine the cause and extent of the observed corrosion, although Alloys 400 and K500 have a known susceptibility to localized corrosion in marine conditions [12,13]. Figure 6-8 shows a representative specimen before and after testing, highlighting the typical degree of corrosion present.

Table 6-2 24 Hour Cycle for GM9540P Accelerated Corrosion Test

Exposure	*Time (hrs)*	*Procedure*
Ambient Soak	0	*Salt solution mist for 30 seconds followed by ambient exposure (13-28 ºC (55-82 ºF))
	1.5	*Salt solution mist for 30 seconds followed by ambient exposure (13-28 ºC (55-82 ºF))
	3	*Salt solution mist for 30 seconds followed by ambient exposure (13-28 ºC (55-82 ºF))
	4.5	*Salt solution mist for 30 seconds followed by ambient exposure (13-28 ºC (55-82 ºF))
Wet Soak	8-16	8 hour high humidity exposure (49 ± 0.5 ºC (120 ± 1 ºF) 100% RH) including 55 minute ramp to wet conditions
Dry Soak	16-24	8 hour elevated dry exposure (60 ± 0.5 ºC (140 ± 1 ºF) <30% RH) including 175 minute ramp to dry conditions

*Salt solution mist consists of 1.25% solution containing 0.9% sodium chloride, 0.1% calcium chloride, and 0.25% sodium bicarbonate.

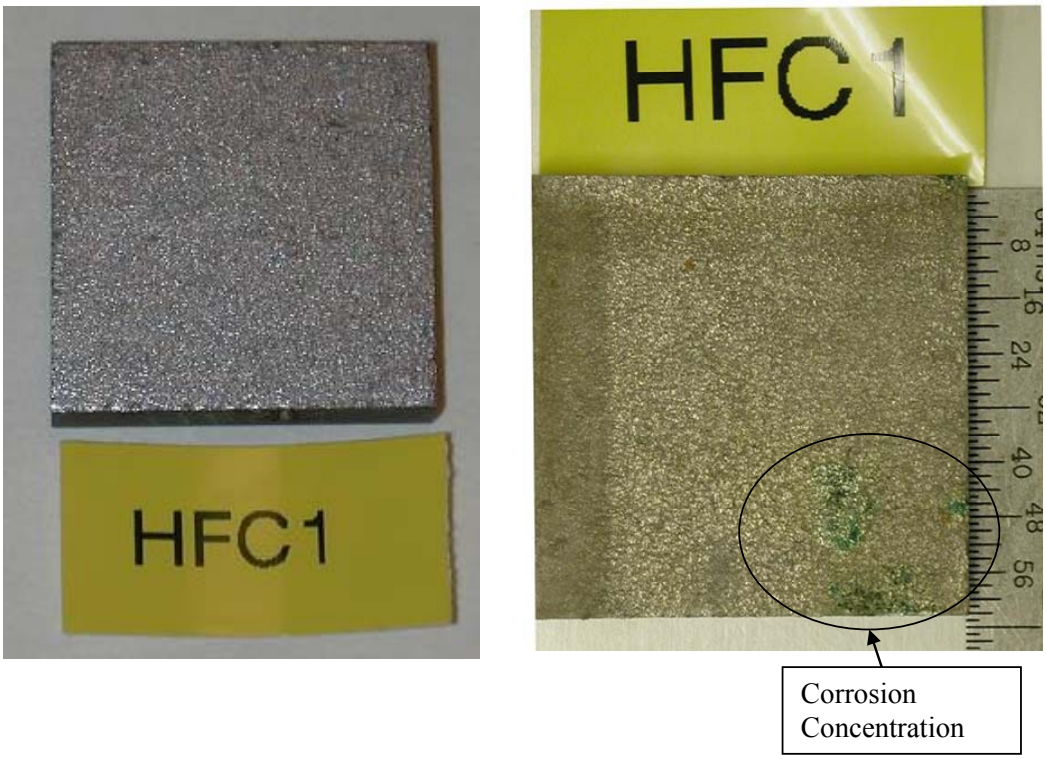

Figure 6-8 ESD Alloy 400 Deposited on K500 Specimen Before (left) and After (right) 80 Cycles in GM9540P Test Cabinet

6.3. ESD on Alloy K500 - Component Demonstration

As discussed previously, Alloy K500 steering/diving control rods were identified as components that would benefit from a successful ESD repair. To assess the viability of the ESD process, a demonstration repair was performed on a surplus Alloy K500 control rod containing small defects with depths ranging from 0.003" to 0.017". Four defects on the rod were selected, and the ESD repair was accomplished in accordance with a draft process instruction developed at NSWCCD. The repair utilized the following ESD coating parameters to deposit Alloy 400 on the K500 component: pulse rate = 400 Hz, capacitance = 30 μF, voltage = 180 V, and current = 4.3 A. After the repair, the defect area was final sanded using 600-grit silicon carbide paper to blend in with the surrounding area. Photographs of these defects were made before and after the repair, and electrodischarge machining was then used to remove sections containing the four selected areas. Sections #2 and #4 were metallographically evaluated, while sections #1 and #3 were immersed in aerated ASTM D1141 ocean water for 127 days.

Figure 6-9 shows the condition of sections #1 and #4 before and after the ESD repair was accomplished. Macroscopically, the ESD repair areas looked pristine and appeared to resemble the original, as-fabricated rod condition. Metallographic evaluation, however, identified a substantial number of voids and microcracks within the ESD coating. Figure 6-10 shows a metallographic cross-section through ESD repair section #4 with voids and microcracks present at the ESD coating-substrate interface. Sections #1 and #3 are shown in Figure 6-11 after being immersed in quiescent ocean water. Corrosion products are evident in the vicinity of the ESD repair area. These products initiated within approximately two months after being immersed. The presence of corrosion products within the repair area suggests that localized corrosion is ongoing. Evidently, the voids and microcracks present within the deposited ESD coating were interconnected, allowing seawater ingress upon immersion.

Corrosion of these repair areas identified a concern for using this process to repair narrow groove defects in seawater components. The ESD method requires direct electrical contact between the consumable electrode being deposited and the substrate material. The electrode must contact the base of the defect area in order to the deposit the ESD coating there. In narrow groove repairs, this is very difficult and the electrode often touches the sides of the defect first, causing a bridging effect with a void at the base of the defect. Hollowing out the defect area prior to ESD to lessen the narrow groove will improve the likelihood that the ESD coating electrode will contact the base rather than the sides.

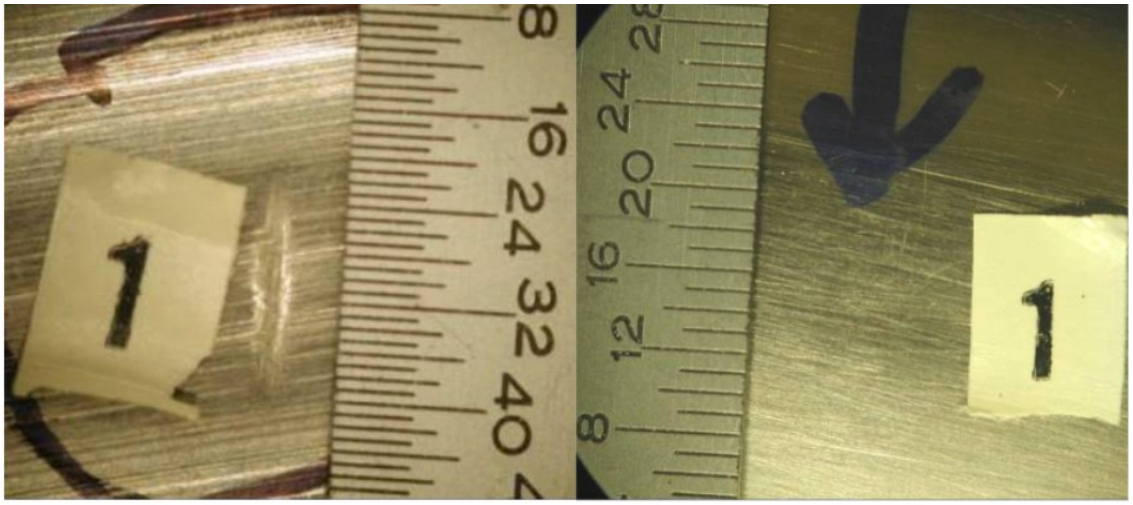

(a) Before ESD Repair After ESD Repair

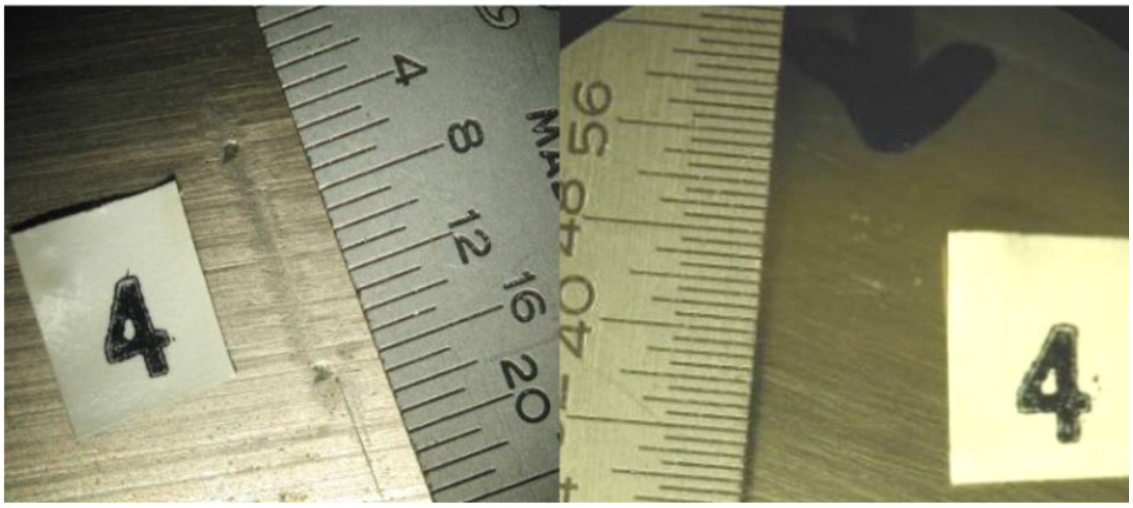

(b) Before ESD Repair After ESD Repair

Figure 6-9 ESD Sections (a) #1 and (b) #4 from Alloy K500 Rod Before and After ESD Repair

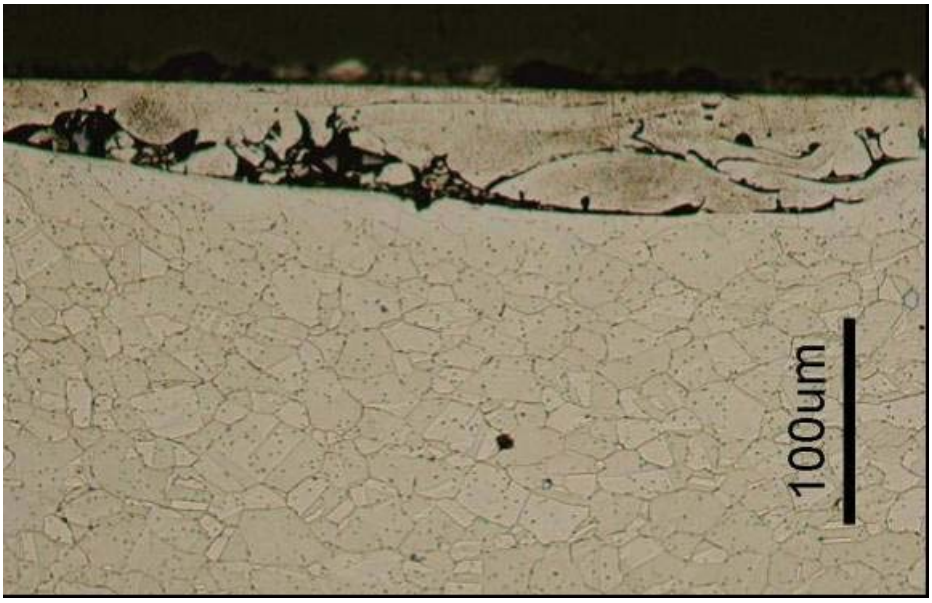

Figure 6-10 Metallographic Cross-Section through ESD Repair Section #4 from Alloy K500 Rod

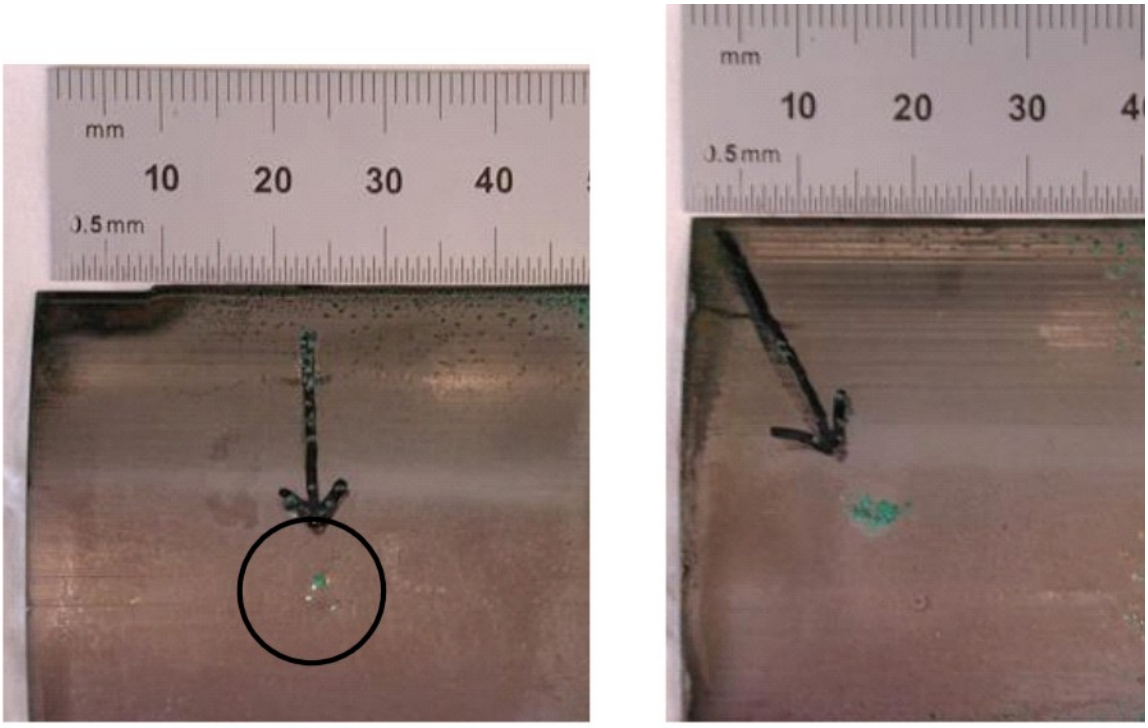

Repair Section #1 **Repair Section #3**

Figure 6-11 ESD Repair Sections #1 and #3 from Alloy K500 Rod After 127 Days Immersion in Aerated ASTM D1141 Ocean Water

Subsequent discussions with personnel from ASAP, Inc., manufacturer of the ESD equipment, identified additional areas for improving the technique used in electrospark depositing Alloy 400 on the K500 component. Training instruction was provided by ASAP to NSWCCD personnel, and the following adjustments were made to the ESD process: (1) slower electrode traversing speed over the surface of the repair, (2) increased argon cover flow to 25 cfm with a fanned tube to allow the argon to flow over a wider area, (3) ESD deposit confined to one direction only, (4) square tip rather than a pointed tip geometry utilized for the coating electrode, (5) increased frequency for cleaning the coating electrode with a diamond wheel during the repair, and (6) altered ESD coating parameters set at frequency = 500 Hz, capacitance = 50 μF, voltage = 100 V, and current = 5 A. ESD repairs were performed using the above modifications on an Alloy K500 flat plate containing simulated defect areas. The coating electrode utilized was a 0.125”-diameter Alloy 400 weld rod, and the defects were excavated to an approximate 0.023 – 0.025” depth by 0.250” width. All repair areas were then ground and polished to a 400-grit silicon carbide finish. Fluorescent penetrant inspection (FPI) was performed on the completed repair areas. Minimal bleed-out was noted, presumably indicating the presence of small voids at the surface. Metallographic cross-sections were taken through the repair areas, and a representative photomicrograph is included in Figure 6-12. The metallography showed significant improvement in the quality of the ESD coating.

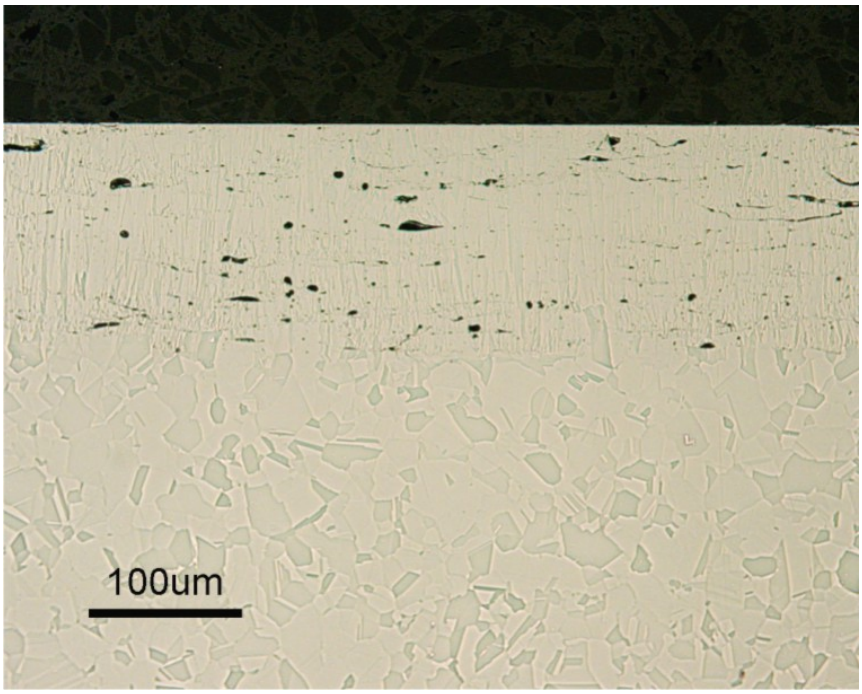

Figure 6-12 Metallographic Cross Section Through Alloy K500 Flat Plate with Simulated Defect Repaired by ESD of Alloy 400 Using Optimized Parameters

6.4. ESD Deposition on Alloy 625 – Materials Studies

As previously indicated, Alloy 625 seawater components were identified as good candidates for ESD repair. Alloy 625 has a known susceptibility to crevice corrosion in seawater; consequently, crevice damaged areas such as O-ring sealing surfaces can potentially be repaired by ESD application of more crevice-corrosion-resistant nickel-chromium-molybdenum (Ni-Cr-Mo) alloys on Alloy 625 surfaces.

For these materials studies, Alloys 59, 686 and C276 were deposited using ESD onto Alloy 625 test specimens. Table 6-3 provides the composition of the deposited alloys and the ESD deposition parameters.

Table 6-3 Coating Compositions and Deposition Parameters for ESD Deposition Onto Alloy 625 Test Specimens

			ESD Coating Parameters		
ESD Coating	***UNS Designation***	***Nominal Composition***	***Pulse Rate (Hz)***	***Capacitance (µF)***	***Voltage (V)***
Alloy 59	N06059	Ni-22Cr-15Mo-1Fe	700 (6 passes), 1000 (2 passes)	30 (6 passes), 10 (2 passes)	100 (6 passes), 150 (2 passes)
Alloy 686	N06686	Ni-21Cr-16Mo-4W-5Fe	400 (6 passes), 600 (2 passes)	30 (6 passes), 10 (2 passes)	100 (6 passes), 140 (2 passes)
Alloy C276	N10276	Ni-15Cr-16Mo-4W-5Fe-2Co	700 (6 passes), 1000 (2 passes)	30 (6 passes), 10 (2 passes)	100 (6 passes), 150 (2 passes)

Figure 6-13 shows cross-section metallography of an Alloy C276 deposit onto a flat Alloy 625 test specimen. In general, the porosity of the deposits was low and there was excellent adhesion to the base material. Similar type microstructures were obtained for deposition of Alloy 686 and Alloy 59.

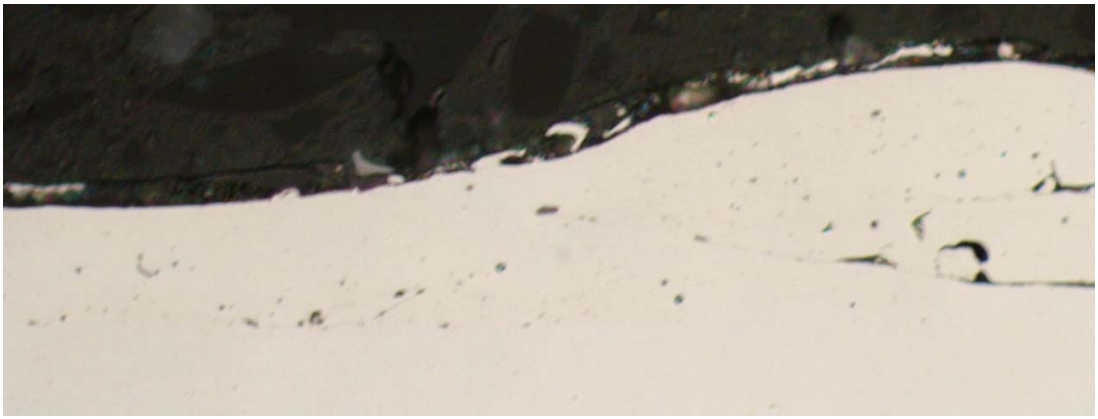

Figure 6-13 Cross-section Metallograph of ESD Deposit of Alloy C276 onto an Alloy 625 Test Specimen

6.4.1.Microhardness Measurements

A series of microhardness measurements were made in different locations in cross-section on an ESD Alloy C276 coating and these were compared to values obtained on flat Alloy 625 plates. The results are shown in Figure 6-14 which indicate that, within statistical uncertainty, the hardness of the C276 deposits was the same as for conventional wrought Alloy 625.

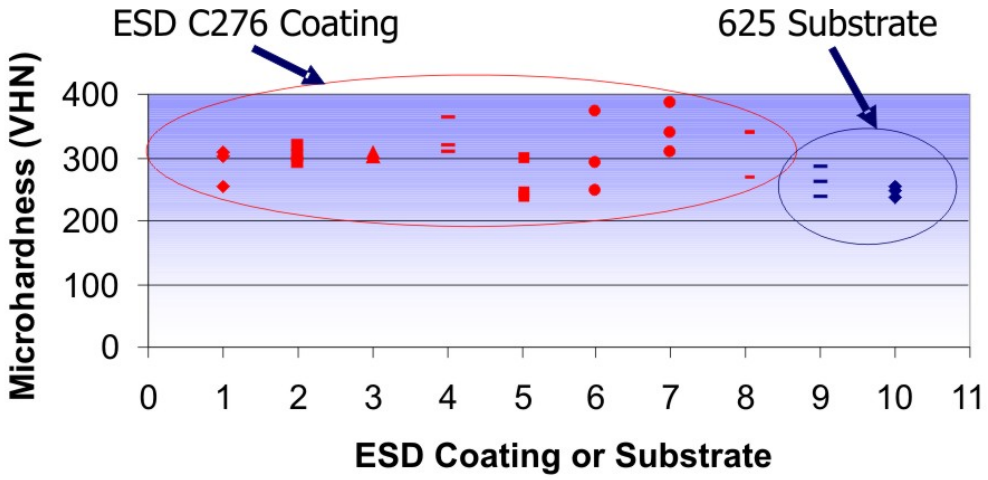

Figure 6-14 Microhardness Values for ESD C276 Coating Deposited Onto an Alloy 625 Substrate and for Bulk Alloy 625

6.4.2.Crevice Corrosion Tests

Metal-to-non-metal crevice testing was conducted on Alloy 625 plate specimens containing ESD coatings of Alloy 59, 686, and C276 within the crevice area. Control specimens of wrought Alloy 59, 686, C276, and 625 were also included in the crevice tests. Triplicate assemblies of ESD coatings and controls were exposed for 180 days in ambient temperature, quiescent, filtered natural seawater at the LaQue Center for Corrosion Technology in Wrightsville Beach, NC. Specimens were visually inspected in-situ on a periodic basis during the test exposure for evidence of crevice corrosion initiation. Corrosion potential measurements were also made periodically on the crevice specimens versus a saturated calomel reference electrode (SCE).

Each crevice assembly consisted of 4 x 6 in. (10.2 x 15.2 cm) wrought Alloy 625 plates with two polytetrafluoroethylene (PTFE) disks attached to the front and backsides and secured with insulated titanium fasteners as illustrated in Figure 6-15. For the Alloy 625 plates with ESD coatings, the Ni-Cr-Mo alloys were electrospark deposited within an approximate 2”-diameter area in the center of each side of the specimen as shown in Figure 6-16. The PTFE crevice-former disks completely covered this area so that an assessment of the crevice corrosion resistance of the ESD coating could be made. Each crevice assembly was uniformly tightened to a torque level of 75 in-lbs (8.5 Nm). Prior to assembly, the specimens were brushed with a pumice-detergent mixture, water rinsed,

acetone degreased, and then air dried. This crevice test assembly has been utilized in previous Navy investigations, and additional details of the testing can be found in reference [14]. Figure 6-17 provides a photograph of a representative test specimen with the crevice assembly configuration and Figure 6-18 shows the assemblies immersed in the seawater container.

After testing, specimens were removed from the exposure tank and rinsed with tap water, photographed, and then disassembled. Specimens were then dipped in room temperature 30% nitric acid, brush cleaned with detergent, water rinsed, acetone dipped, and air dried. Susceptibility to crevice corrosion was characterized in terms of time to initiation (as assessed by visual inspection) and maximum depth of attack within the crevice area.

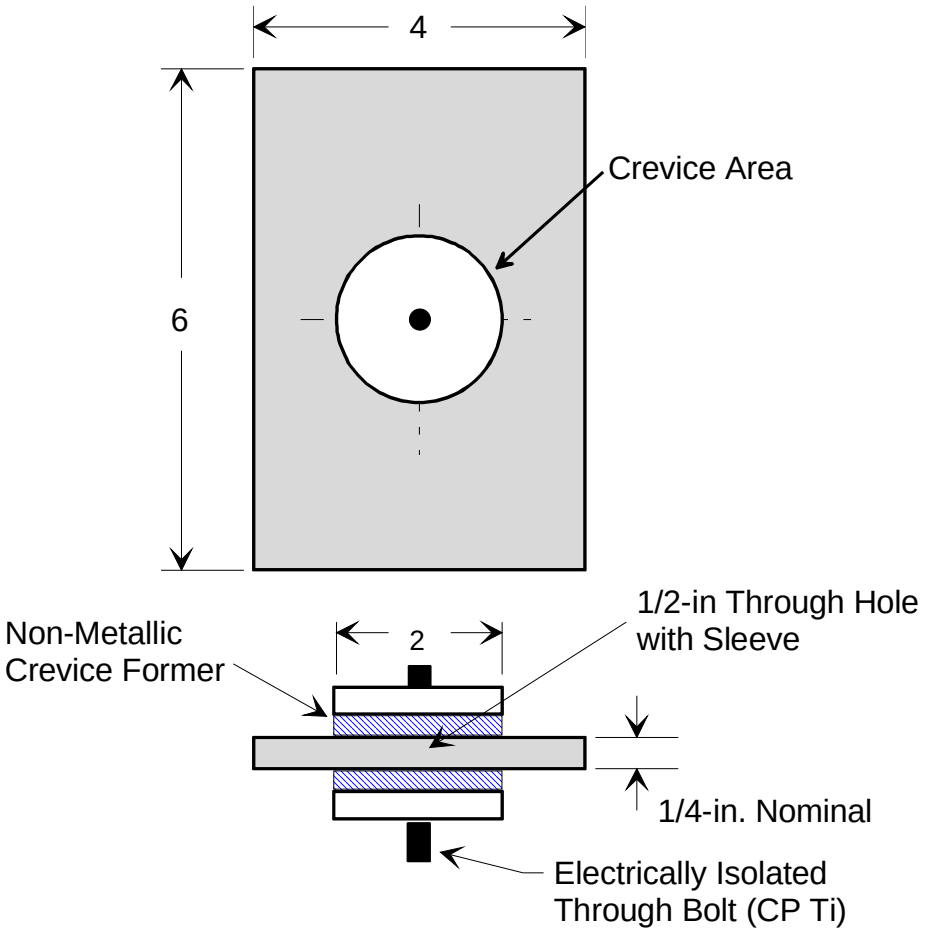

Figure 6-15 Schematic of the Crevice Corrosion Test Assembly

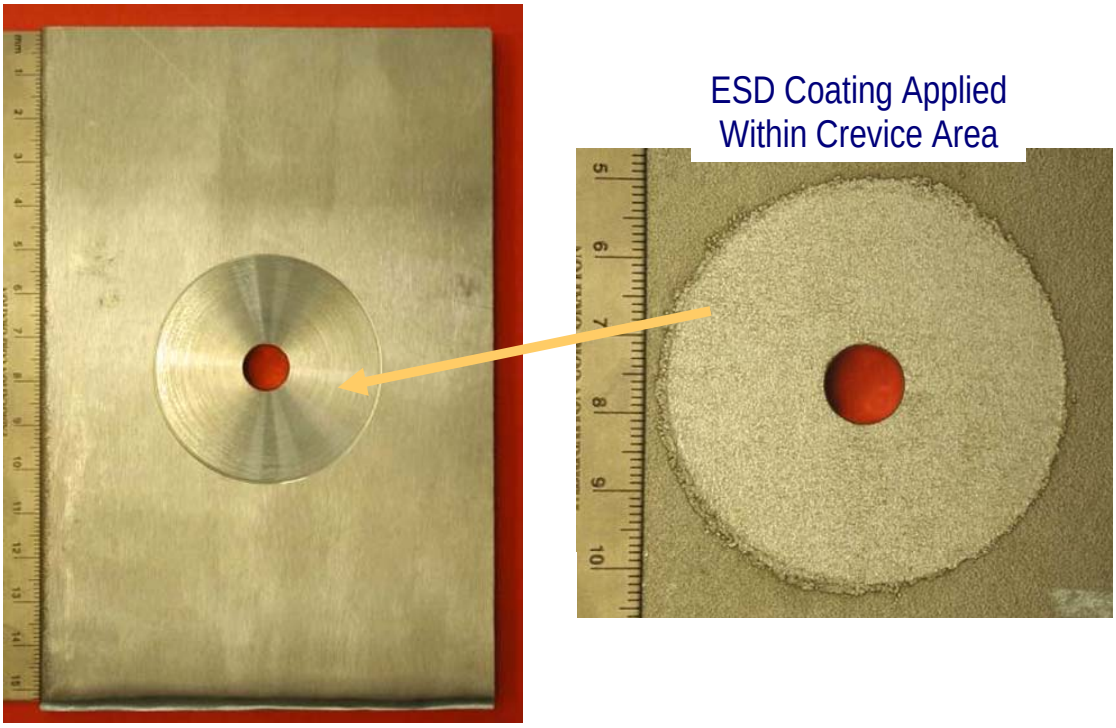

Figure 6-16 Photograph of Alloy C276 Coating Deposited in Crevice Area on Alloy 625 Test Specimen

Figure 6-17 Crevice Corrosion Specimen Assembly Prior to Testing

Figure 6-18 Crevice Corrosion Test Assemblies Immersed in Seawater

Test results for the crevice evaluation of ESD coated and control Ni-Cr-Mo alloys are included in Table 6-4. Corrosion potential measurements made on the test specimens as a function of time are reported in Figure 6-19. The seawater temperature during the 180-day test ranged from 43–88 ºF, with a mean temperature of 61 ºF.

Within the first three days of testing, nine of the 21 specimens developed surface rust. As the test period progressed, most of the rust sloughed off and settled on the floor of the seawater test tank. The surface rust was presumably due to iron contamination present on the specimen surfaces at the onset of testing.

After 180 days' exposure, ESD coated Alloys 686 and 59 and control specimens of Alloy 625, 59, 686, and C276 composition were highly resistant to crevice corrosion. No evidence of attack was noted on any of these specimens. The only specimens to exhibit crevice susceptibility were the ESD coated Alloy C276 specimens. Crevice corrosion initiated on the surfaces of each of the triplicate specimens between 9 and 14 days' exposure, based on the presence of corrosion products at the crevice sites. The extent of corrosion products accumulated at these sites increased with time through 45 days' exposure and then remained stable through the end of the exposure period. Upon disassembly at the conclusion of the testing, all six ESD C276 crevice sites had initiated

crevice attack, with a maximum depth of attack reported at 0.005 in. (0.013 mm). Figure 6-20 highlights the extent of corrosion found on these crevice specimens after 180 days. Crevice corrosion testing performed previously [15] on Alloy 625 plate specimens with ESD coatings of Alloy C276 and 59 were highly resistant to crevice attack in seawater after 183 days. The crevice corrosion exhibited by the ESD C276 specimens reported herein after only 9-14 days suggests that the as-deposited electrospark coatings contained interconnected voids and/or microcracks which led to the crevice corrosion. The initiation of corrosion on these ESD coated specimens after minimal immersion time highlights a need for non-destructive evaluation (NDE) techniques to insure adequate quality coatings.

Table 6-4 Crevice Corrosion Results for Three Ni-Cr-Mo ESD Coatings and Uncoated Controls Immersed in Quiescent, Natural Seawater for 180 Days

Substrate	ESD Coating	*Specimen A*			*Specimen B*			*Specimen C*		
		# of Initiated Sites (max 2)	*Time to Initiation (days)*	*Max. Depth of Attack in.*	*# of Initiated Sites (max 2)*	*Time to Initiation (days)*	*Max. Depth of Attack In)*	*# of Initiated Sites (max 2)*	*Time to Initiation (days)*	*Max. Depth of Attack In)*
625	**None**	**0**	**---**	**0**	**0**	**---**	**0**	**0**	**---**	**0**
686	**None**	**0**	**---**	**0**	**0**	**---**	**0**	**0**	**---**	**0**
C276	**None**	**0**	**---**	**0**	**0**	**---**	**0**	**0**	**---**	**0**
59	**None**	**0**	**---**	**0**	**0**	**---**	**0**	**0**	**---**	**0**
625	**686**	**0**	**---**	**0**	**0**	**---**	**0**	**0**	**---**	**0**
625	**C276**	**2**	**9-14**	**0.005**	**2**	**9-14**	**0.005**	**2**	**9-14**	**0.002**
625	**59**	**0**	**---**	**0**	**0**	**---**	**0**	**0**	**---**	**0**

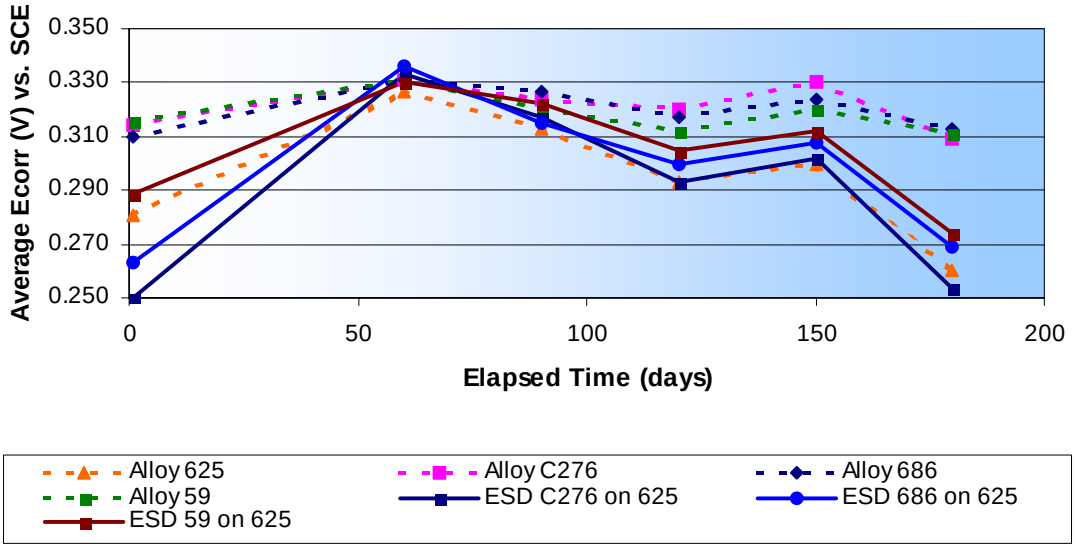

Figure 6-19 Corrosion Potential Versus Time Measurements Made on ESD-Coated and Ni-Cr-Mo Alloy Control Crevice Corrosion Test Specimens

The E_{corr} data (Figure 6-19) showed variations in potentials between the ESD coated and control specimens. The wrought Alloy 59, C276, and 686 controls remained fairly stable throughout the 180 days, staying within an E_{corr} range of approximately +0.310 to +0.330 V versus SCE. The ESD coated Alloy 59, C276, and 686 specimens demonstrated larger shifts in potential with time. These specimens had E_{corr} values ranging from +0.250 to +0.330 V versus SCE. The wrought Alloy 625 control specimens averaged E_{corr} values within the same trend as noted for the ESD coated specimens.

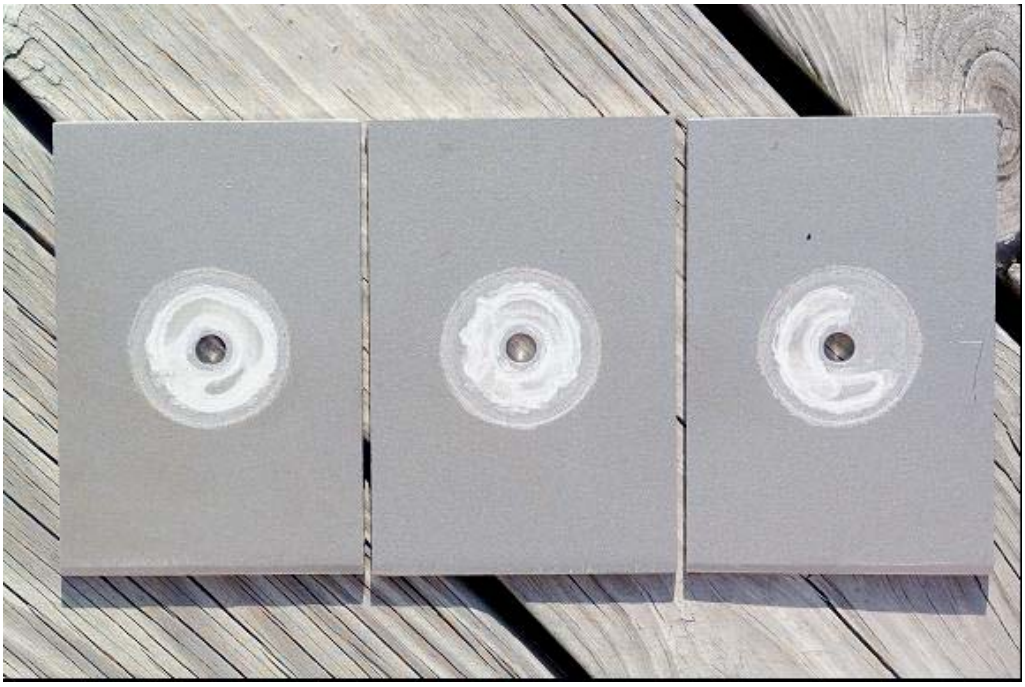

Figure 6-20 ESD Alloy C276 Coated Alloy 625 Specimens After 180 Days Immersion in Natural Seawater

6.5. Summary and Conclusions

A laboratory assessment of the electrospark deposition process for repairing Navy components was performed. Although corrosion was noted within narrow groove repair areas on the ESD coated Alloy K500 component, subsequent simulated defect specimens showed that good quality coatings can be deposited using this method. Additionally, on Alloy 625 surfaces there were apparent inconsistencies in coating quality among ESD coated Ni-Cr-Mo alloys based on the good crevice resistance noted for ESD Alloys 59 and 686 and the crevice susceptibility found on the ESD Alloy C276 specimens after immersion in natural seawater for 180 and 365 days. The ESD process appears feasible for repair of Alloys K500 and 625 Navy components; however, additional evaluation of electrospark deposition procedures and NDE methods are required to ensure consistent and optimum coating quality.

7. Cost Benefit Analysis

7.1. Background and Introduction

The PEWG fosters implementation of environmentally acceptable materials and technologies in turbine engine production, operation, and maintenance processes. The technology transfer process often involves capital investment decisions, which are typically based on an assessment of both the environmental and potential cost benefits of implemented alternatives. As a critical piece of the complete business case, a cost/benefit analysis (CBA) aids the decision making process by providing in-depth analysis of applicable costs and associated benefits of identified alternatives.

This section analyzes and quantifies the costs and benefits associated with implementing electrospark deposition (ESD) at Oklahoma City Air Logistics Center (OC-ALC) instead of repairing parts using present technologies or shipping off-site for repair. This analysis was accomplished by conducting a CBA using the Environmental Cost Analysis Methodology (ECAM) [16] and was funded by the PEWG. The ECAM was developed by Concurrent Technologies Corporation (CTC), through the National Defense Center for Environmental Excellence (NDCEE), in cooperation with Coopers & Lybrand LLP to provide a consistent methodology to quantify and evaluate environmental costs and benefits. The ECAM has been validated at Army, Navy and Air Force facilities for a variety of environmental technologies.

7.2. Technical Approach

7.2.1. Cost Benefit Analysis Scope

This CBA evaluates the cost impact of implementing an alternative process under consideration at a specific facility. This analysis considers the feasibility of using ESD on the following three aircraft engine components:

TF33 No. 5 Bearing Housing

TF39 Compressor Rear Shaft

F100 10-12 Stator Segment

Each of the components evaluated in this analysis has a different baseline repair process that is conducted at a different facility. These components and their baseline processes are listed in Table 7-1. The TF33 No. 5 Bearing Housing repair is done at OC-ALC. The F100 10-12 Stator Segment is repaired at the original equipment manufacturer (OEM) and the TF39 Compressor Rear Shaft at a commercial repair facility. The names of the repair facilities are not given due to sensitivity of operational data. Baseline data was collected at the repair facility for the TF39 Compressor Rear Shaft. This level of detail for the baseline processes was not available for the other components. The OEM which repairs the F100 10-12 Stator Segment provided total repair cost (billed to the government) per segment and OC-ALC provided repair costs per housing for the TF33 No. 5 Bearing Housing. These baseline costs were compared to the estimated process costs for the proposed alternative, ESD, which would be realized upon implementation of

this alternative process at OC-ALC. All alternative costs were provided by ASAP, Inc, the company that commercially developed the technology.

Table 7-1 Baseline Processes and Components

Component	Baseline Process
TF33 No. 5 Bearing Housing repair	Grind and Weld
TF39 Compressor Rear Shaft repair	Chromium Electroplate
F100 10-12 Stator Segment repair	Remove and Weld

The results of this CBA are calculated financial indicators that measure the cost impact noted above - implementation of this identified alternative at this specific facility. Project costs such as those associated with qualification testing of the process are not included in these financial indicators. However, these costs are included in the rough order of magnitude Return on Investment (ROI) calculations described in Section 7.7 (Project Return on Investment).

7.2.2. Cost Benefit Analysis Methodology

As part of this CBA, data collection and financial analyses were performed in accordance with the ECAM Handbook, dated March 29, 1999. To estimate the potential financial benefits of this project, the expected labor and material flow diagrams associated with baseline and alternative processes were established. Using the process flow diagrams, data collection forms were developed to collect information on the baseline and alternative processes.

Capital investments for the alternative process were identified and estimated. Where available and applicable, the following costs were captured for the alternative process:

- Design
- Equipment
- Software Purchase/Development
- Site preparation
- Construction/Installation
- Startup/Training
- Documentation
- Annual Maintenance

Capital investments to update the baseline processes if implementation did not occur were included where applicable. Disposal and salvage costs for replaced equipment were included if considered substantial.

Annual maintenance and operating costs were also included in this analysis as were any periodic maintenance costs. Where available and applicable, the following types of information related to the baseline process were collected; data related to the alternative process were estimated:

- Process Flow
- Labor Requirements
- Material Usage
- Utility Usage
- Equipment Maintenance Costs
- Waste Management and Disposal Costs
- Personal Protective Equipment (PPE) Costs
- Effect on Regulatory Compliance
- Effect on Support Facility Operations
- Effect on Providing and Administering Training
- Effect on Operating and Maintaining Equipment and Facilities
- Other Related Cost Impacts

Baseline process data were collected through a site visit and follow-on data collection via telephone and email. Where data were not available, they were assumed based on engineering judgment. Alternative process data was obtained from the technology developer, ASAP, Inc. Data collection is an integral aspect to the economic analysis process since it is highly dependent on the quality of the data collected. Inaccurate or insufficient data will result in an inadequate analysis. Therefore, the accuracy of this analysis is highly dependent on the information provided by the facilities and process developer.

Once the data was collected, a Level I and Level II ECAM analysis were conducted to evaluate the impact of implementation of the project. A Level I analysis identifies and assigns direct costs. A Level II analysis identifies and assigns indirect costs incurred by carrying out facility environmental activities supporting a process. A Level III analysis, which provides guidance on identifying, quantifying, and assigning other non-environmental support and overhead costs, was not deemed necessary for this analysis. The study period used for this analysis is 15 years. These costs were used to calculate performance measures that indicate the financial viability of this project. Additional detail on these performance measures and how they are calculated is given in Section 7.6 (Cost Analysis).

7.2.3.Cost Benefit Analysis Parameters and Assumptions

This analysis evaluates a known baseline against the implementation of an alternative. Set parameters are used to provide analysis boundaries and to ensure consistency between cost benefit analyses. To complete this analysis, it is necessary to make assumptions due to the inability to obtain all data. This could be due to the lack of availability of the data or the cost-effectiveness of data collection. An example of the former is that often utilities are not metered at each piece of equipment and must be estimated for the particular process under consideration. In addition, since the alternative has not yet been implemented many variables are unknown and can only be estimated.

Much of the data will be consistent between both the baseline and alternative processes. Examples of this may include utility and labor rates, production rates and disposal costs. Unless indicated otherwise, a burdened labor rate of $80 per hour and a production of 250 days per year were used for this analysis. Specific information for each repair process is

given in subsequent sections of this report.

7.3. Baseline Process

7.3.1.Process Description, Data and Assumptions

A site visit to OC-ALC was performed on June 28 and 29, 2005 to collect data on the baseline processes. During the site visit, interviews were held with process engineers, inventory control staff, and other employees throughout the facility. The information gathered during the site visit was supplemented with additional correspondence following the visit. A site visit to the TF39 Compressor Rear Shaft repair facility was conducted in November 2004 under a separate initiative.

7.3.1.1. TF33 No. 5 Bearing Housing Repair

In the past, OC-ALC repaired this component using a weld repair process that involves grinding and weld repairing the worn area. General repair instructions have been issued, but OC-ALC has been unable to identify a process, material, tool, or procedure to consistently produce the required polish on the mating surfaces of the splines. Presently, OC-ALC is not repairing this component, but purchasing replacements. This analysis compares the estimated cost of repairing the components at OC-ALC under the present repair procedure to repairing using ESD. Two alternative cases have also been considered. The first assumes that the average repair requires that 6 of the eighteen lugs on each housing needs to be repaired. The second case assumes that all 18 lugs need to be repaired. Table 7-2 gives the annual production rate and the details on the cases evaluated for this analysis.

Table 7-2 TF33 No. 5 Bearing Housing Repair

TF33 Bearing Housing Repairs	
Average Annual Production Needs	84 housings
Case 1	6 repaired lugs per housing
Case 2	18 repaired lugs per housing

7.3.1.2. TF39 Compressor Rear Shaft Repair

The TF39 gas turbine engine Compressor Rear Shafts are repaired using chromium electroplating; the repair process is done at a repair facility. Repairs include restoring journal diameters and repairing worn shoulders and surface chips. As stated previously, the data for this repair was collected during a site visit to the repair facility on November of 2004 under another initiative. The average number of repairs conducted for this component is given in Table 7-3 below.

Table 7-3 Chrome Plating Repairs on TF39 Gas Turbine Engine Compressor Rear Shaft

Surface	Annual Repair Rate
Journal Diameters	20 shafts per year
Shoulders	6 shafts per year
Surface Chips	5 shafts per year

7.3.1.3. F100 10-12 Stator segment repair

This component is repaired by shipping to the OEM for repair. The repair involves cutting off the three hooks on the segment and re-welding on new hooks. Table 7-4 gives the annual production for this repair.

Table 7-4 F100 10-12 Stator Segment Repairs

F100 10-12 Stator Segment Repairs	
Average Annual Repairs	34 segments

7.3.2. Capital Costs

Continuing operation of the baseline processes will not require any equipment upgrades or additional capital expenditures during the study period.

7.3.3. Operating Costs

This section provides a summary of annual labor, material, utility, and waste disposal costs for each of the baseline processes.

7.3.3.1. TF33 No. 5 Bearing Housing Repair

Baseline operating costs for the TF33 No. 5 Bearing Housing repair are based on reported annual repair quantities and repair costs provided by OC-ALC. As OC-ALC does not track these cost by number of lugs repaired, this baseline cost is an average and does not depend on the number of lugs repaired per housing. These estimated repair costs are shown in Table 7-5.

Table 7-5 Annual Operating Costs for TF33 Bearing Housing Repair Baseline Process

Resource	**Annual Costs**
OC-ALC Repair Costs	$3,563 per housing
TOTAL ANNUAL REPAIR COSTS	**$299,300**

7.3.3.2. TF39 Compressor Rear Shaft Repair

Hard chrome is applied to aircraft components to restore dimensions on worn or repaired parts. For repair of TF39 Compressor Rear Shafts that have been subjected to wear, the damaged area is machined and then to restore dimensional tolerance, a 0.010”-0.015”-thick coating is deposited via chromium electroplating, which is then machined down to a final thickness of 0.003” to 0.010”. The current chrome plating process at the repair facility includes three chrome-plating tanks and one stripping tank. To prepare parts for plating, several activities are performed including masking, stripping, peening and blasting. Masking typically consists of the use of tape and plating wax. Post-processing steps included de-masking, cleaning, baking, grinding, and inspection. The baseline process flow diagram for the current hard chrome electroplating process at the repair facility is provided in Figure 7-1.

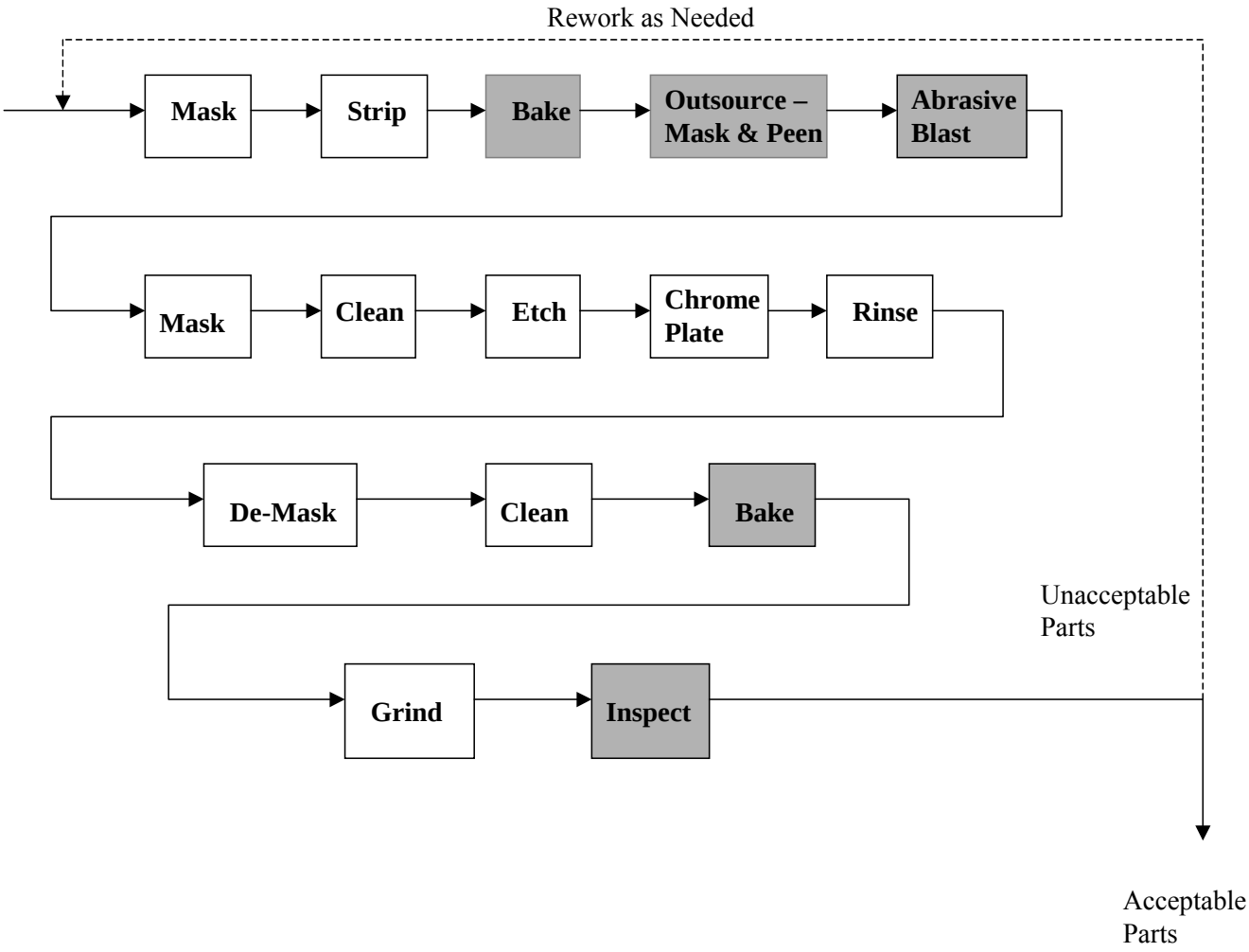

Figure 7-1 Baseline Chromium Plating Process for the TF39 Compressor Rear Shaft

Baseline process costs for the TF39 Compressor Rear Shaft are estimated based on total plating costs at the repair facility. Chromium plating represents approximately 5% of the plating conducted at the repair facility. The TF39 Compressor Rear Shaft represents approximately 5% of the chromium plating conducted at the repair facility. To capture plating costs for this analysis, total chromium plating costs were estimated based on data received from the repair facility and extracted from various plating CBAs conducted at other DoD facilities. These estimated costs were allocated based on the type of repair. For material, utility and waste costs, total plating costs for each repair were estimated based on the surface area plated during each repair. For labor and personal protective equipment, repair costs were estimated based on the total plating cycles required for that repair as this is related to the total employees necessary for each repair. Costs for four of the process steps (bake, peen, abrasive blast and inspection), shown as shaded in Figure 7-1, were not captured for this analysis. Since the parts evaluated for this analysis represent such a small portion of those parts baked, it is expected that the cost to run the bake ovens will not diminish appreciably with implementation of the alternative process. It is also expected that peening, blasting, and inspection will continue after alternative implementation. Since no change is expected with implementation for any of these

process costs, they were not included in this analysis.

The general data and assumptions related to baseline processing of the TF39 components are indicated in Table 7-6. Baseline cost allocations by cost item (e.g. labor, materials) are summarized in Table 7-7.

Table 7-6 General Data and Assumptions Related to Baseline Processing of the TF39 Components

GENERAL DATA/ASSUMPTIONS			
Description	**Value**	**Units**	**Source**
Labor Rates (burdened):			
Composite, subcontractor	80	$/hr	Site Visit
Composite, 1st level prime contractor	150	$/hr	Composite rate used for DoD CBAs
Labor Hours:			
Number of chrome plating employees	3	employees	Site Visit
Shift length	8	hr/shift	Site Visit
Number of shifts per day	1	shifts/day	Site Visit
Number of operating Days/yr	5	days/week	Site Visit
Number of operating Hours/yr	2080	hrs/yr	Calculated
Utilities			
Electric	$ 0.0600	$/kWH	Estimated based on previous CBAs
Production			
Annual components overhauled	20	parts/year	Site Visit
Annual components with chips	5	parts/year	Site Visit
Annual components with shoulders needing plated	30%	percent of overhauled	Site Visit
Surface area of journals	165	sq inches	Site Visit
Surface area of shoulders (each)	5	sq inches	Site Visit
Number of shoulders	2		Site Visit
% of chrome plated parts that are TF39	5%	percentage	Site Visit
% of total plating that is chrome	5%	percentage	Site Visit

Table 7-7 Baseline Cost Allocations By Cost Item for Repair of TF39 Compressor Rear Shaft

Baseline Process-Specific Data/Assumptions: Chromium Electroplating					
Description	**Value**	**Unit**	**Value**	**Unit**	**Source**
CAPITAL COSTS	None				Repair Facility
OPERATING COSTS					
Labor Hours					
Plating labor	312	hours/year			Calculated from facility data
Fixturing labor	negl.				Repair Facility
Lab analysis labor	no change				Estimated based on previous plating CBAs
Scrubber maintenance	captured elsewhere				Captured in total scrubber costs
Net shape grinding	8	hours/plating cycle			Repair Facility
Stripping time	24	hours to strip			Repair Facility
Stripping labor	0.5	monitor frequency	0.05	hours/ monitor	Repair Facility
Materials					
Anodes	500	$/2 year			Repair Facility
Fixturing	150	$/yr			Repair Facility
Chromic acid	66.31	lbs/year	231	$/lb	Quantity based on previous CBAs, cost collected during site visit
Sulfuric acid	275	gallons/year	13	$/gallon	Quantity based on previous CBAs, cost collected during site visit
Hydrofluoric Acid	275	gallons/year	120	$/drum (55 gallons)	Quantity based on previous CBAs, cost collected during site visit
Liquid Maskant	129.22	$/year			Estimated based on previous plating CBAs
Tape, lead and PVC	6.42	rolls	30	$/roll	Quantity based on previous CBAs, cost collected during site visit
Alkaline deruster	500	lbs/tank	1	$/lb	Repair Facility
Hydrochloric acid	330	gallons/yr	1.49	$/gallon	Repair Facility
Wastes					
Anode disposal	0	recycled			Repair Facility
Spent plating bath	0	never replaced	700	$/drum	Repair Facility
Plating tank sludge	2	times/year	525	$/drum	Repair Facility
Fixturing			200	$/year	Repair Facility
Drum wax			275	$/year	Repair Facility
Chrome filter waste	4	times/year	525	$/drum	Repair Facility
Hydrochloric acid	330	gallons/yr	400	$/drum	Repair Facility

Table 7-7 continued

Utilities					
Water, includes wastewater disposal	7411.687296	$/year			Estimated based on previous plating CBAs
Electricity - tanks	1031.235295	kWHr/yr			Estimated based on previous plating CBAs
Electricity - ovens	still will operate - no change				Repair Facility
Electricity - scrubber	captured elsewhere				Captured in total scrubber costs
EHS					
Air sampling and analysis	no change				Estimate
Haz waste accumulations sites	no change				Estimate
labor to maintain sites	no change				Estimate
weekly inspections	no change				Estimate
Addressing safety problems	no change				Estimate
PPE					
Safety glasses	1	pair/yr/operator	20	$/pair	ASAP
Gloves	2	pair/yr/operator	5	$/pair	ASAP
Coveralls	1	operator/yr	4.5	$/pair	OSHA document
SCRUBBER COSTS	24100	$/year in 1993	30160	$/2004	OSHA document; Inflation websites
BASELINE COST ALLOCATIONS (BY REPAIR)					
Surface area of journals	3300	sq inches/year			Calculated
Surface area of chip	825	sq inches/year			Calculated
Surface area of shoulders	60	sq inches/year			Calculated
Total Annual Surface Area	4185	sq inches/year			Calculated
Material Resources ratio based on surface area (journal/shaft)	0.79				Calculated
Material Resources ratio based on surface area (shoulders/shaft)	0.01				Calculated
Material Resources ratio based on surface area (chip journal/shaft)	0.20				Calculated
Plating operations	37				Calculated
Journals	20				Calculated
Shoulders	12				Calculated
Chips	5				Calculated
Labor ratio based on plating operations - journal	0.54				Calculated
Labor ratio based on plating operations - shoulder	0.32				Calculated
Labor ratio based on plating operations - chips	0.14				Calculated

Table 7-8 provides a summary of the annual operating costs for the baseline process repairs at the facility. It is important to note that these costs represent only those expected to be impacted by the implementation of ESD; total processing costs are in fact higher.

Table 7-8 Annual Operating Costs for TF39 Compressor Rear Shaft Repair Baseline Process at Repair Facility

Resource	Total TF39 Repair Costs	Total Journal Repair Costs	Total Chip Repair Costs	Total Shoulder Repair Costs
Labor	$75,640	$42,962	$10,741	$21,937
Materials	$20,731	$16,347	$4,087	$297
Utilities	$7,474	$5,893	$1,473	$107
Waste Disposal	$2,581	$2,035	$509	$37
EHS	$1,309	$707	$177	$424
TOTAL ANNUAL OPERATING COSTS	**$107,734**	**$67,945**	**$16,986**	**$22,803**

Note: These costs represent only those costs that are expected to be impacted by the implementation of ESD; total processing costs are higher.

7.3.3.3. F100 10-12 Stator segment repair

Baseline operating costs for the F100 10-12 Stator Segment Repair are based on reported annual repair quantities and repair costs provided by the repair facility. These operating costs are shown in Table 7-9.

Table 7-9 Annual Operating Costs for F100 10-12 Stator Segment Repair Baseline Process at OEM

Resource	Annual Costs
OEM Repair Charge	$1,148 per segment
TOTAL ANNUAL REPAIR COSTS	**$ 39,000**

7.4. Alternative Process

7.4.1. Process Description

The ESD process begins with excavation of the area to be repaired. This is done mechanically with grinding type processes. The excavated area and those areas directly adjacent to the area being repaired by ESD are then cleaned with an abrasive pad and isopropyl alcohol. The electrode is then used to conduct the ESD repair. After completion of the ESD repair, a surface-finishing step may be required. The process flow diagram for this process is given in Figure 7-2.

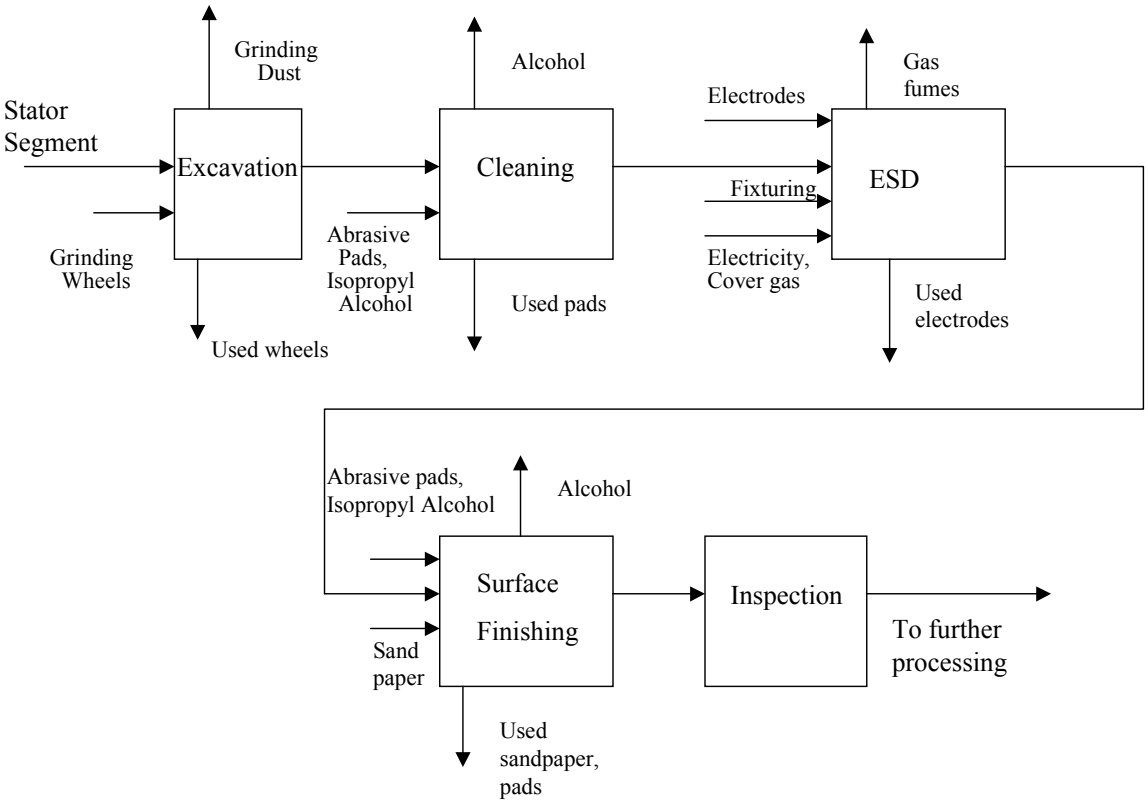

Figure 7-2 Alternative Process Flow Diagram

7.4.2.Data and Assumptions

Data collection forms were submitted to the technology developer to gather information relating to the alternative process for each repair. In addition, follow on phone interviews were held to clarify information. The baseline production data was used to estimate the costs associated with implementing the alternative process for the same production of each repair.

Table 7-10, Table 7-11 and Table 7-12 provide the data and assumptions used for the alternative analysis using ESD to repair the components for the TF33 No. 5 Bearing Housing, TF39 Compressor Rear Shaft and the F100 10-12 Stator Segment, respectively.

Table 7-10 Data and Assumptions Used for Analysis of Implementation of ESD Repair on TF33 No. 5 Bearing Housing

MODULE:	ESD			
Module-Specific Data/Assumptions:				
CAPTIAL COSTS				
Equipment				
ASAP Power Supply	1.00	ea	$ 49,000.00	ea
ESD Workstation	1.00	ea	$ 3,840.00	ea
Other				
Repair Documentation (one time charge)	8	hr	$ 80.00	$/hr
OPERATING COSTS				
Labor	**Value**	**Unit**		
Operators	1	operator/workstation		
Operator Training	12.0	hrs/operator/yr	$ 80.00	$/hr
Operator Qualification	6.0	hrs/operator/yr	burdened composite labor rate	
Operator Qualification - metallography	3.0	hrs/operator/yr	burdened composite labor rate	
Equipment Calibration	150.0	$/calibration	burdened composite labor rate	
Calibration Schedule	2.0	calibrations per year		
Process				
Excavation	0.5	hrs/lug	burdened composite labor rate	
Cleaning	0.1	hrs/lug	burdened composite labor rate	
Masking	0.0	hrs/lug	burdened composite labor rate	
Grounding	0.0	hrs/lug	burdened composite labor rate	
ESD	2.0	hrs/lug	burdened composite labor rate	
Inspection	0.3	hrs/lug	burdened composite labor rate	
Handling	0.0	hrs/lug	burdened composite labor rate	
Total Process Labor	2.9	hrs/lug	burdened composite labor rate	
Subcontracted Labor				
Surface Finishing (subcon)			$ 150.00	$/housing
Utilities				
Electricity	$ 0.50	$/lug		
Argon Gas	75	cubic feet/lug	$ 0.24	$/cu ft
Materials				
Grinding wheels	10	wheel/housing	$ 1.00	$/wheel
Abrasive pads	1	pad/lug	$ 1.00	$/pad
Lugs	6	lugs/housing		
Electrode, 410 ss rod	2	oz/lug	$ 1.13	$/oz
Holding and rotating fixture	1	fixture	$2,500	$/fixture
Inspection Materials			$ 2.00	$/lug
Total Process Materials				
EHS COSTS				
Record keeping	no change			$/hr
Grinding dust	negligible			
PPE				
Safety glasses	1	pair/yr/operator	$ 20.00	$/pair
Gloves	6	pair/yr/operator	$ 5.00	$/pair
Hearing protection	1	pair/day/operator	$ 0.05	$/pair
Dust mask	1	mask/day/operator	$ 2.25	$/mask
Total PPE			$ 625.00	$/operator/yr

Table 7-11 Data and Assumptions Used for Analysis of Implementation of ESD Repair on TF39 Compressor Rear Shaft

MODULE: ESD

Repair-Specific Data/Assumptions:	Chip Repair using ESD			
Description	**Value**	**Unit**	**Value**	**Unit**
CAPTIAL COSTS				
Equipment				
ASAP Power Supply	1.00	each	31,675.00	ea
ESD Workstation	1.00	each	3,480.00	ea
Other				
Repair Documentation (one time charge)	4.00	hr	150.00	$/hr
OPERATING COSTS				
Labor Hours				
Operators	1.00	operator/workstation		
Operator Training	8.00	hrs/operator/yr	150.00	$/hr
Operator Qualification	7.00	hrs/operator/yr	burdened composite labor rate	
Equipment Calibration	1.00	hrs/workstation/yr	burdened composite labor rate	
Process				
Excavation	0.5	hrs/chip	150.0	
Cleaning	0.1	hrs/chip	150.0	
Masking	0.0	hrs/chip	150.0	
Grounding	0.0	hrs/chip	150.0	
ESD	0.5	hrs/chip	150.0	
Inspection	0.5	hrs/chip	150.0	
Handling	2.0	hrs/chip	150.0	
Total Process Labor	3.6	hrs/chip	150.0	
Subcontracted Labor				
Surface Finishing (subcon)	4.0	hrs/chip		
Utilities				
Electricity	0.5	$/chip		
Argon Gas	15.0	cu ft/chip	0.2	$/cu ft
Materials				
Grinding wheels (1.25" carbide grinding burr)	1.0	wheel/chip	6.3	$/wheel
Abrasive pads	1.0	pad/chip	1.0	$/pad
Electrode, IN 718 rod	1.0	oz/chip	1.3	$/oz
Inspection Materials			1.5	$/chip
Total Process Materials			10.0	$/chip
EHS COSTS				
Record keeping	no change	hrs/chip	150.0	$/hr
PPE				
Safety glasses	1.0	pair/yr/operator	20.0	$/pair
Gloves	6.0	pair/yr/operator	5.0	$/pair
Hearing protection	1.0	pair/day/operator	0.1	$/pair
Dust mask	1.0	mask/day/operator	2.3	$/mask
Total PPE			$ 61.50	$/operator/yr

Table 7-11 continued

MODULE **ESD**

Repair-Specific Data/Assumptions:	**Shoulder Repair using ESD**			
Description	**Value**	**Unit**	**Value**	**Unit**
CAPTIAL COSTS				
Equipment				
ASAP Power Supply	1.00	ea	49000	ea
ESD Workstation	1.00	ea	3840	ea
Other				
Repair Documentation (one time charge)	4.00	hr	0	$/hr
OPERATING COSTS				
Labor				
Operators	1.00	operator/workstation		
Operator Training	8.00	hrs/operator/yr	0	$/hr
Operator Qualification	7.00	hrs/operator/yr	burdened composite labor rate	
Equipment Calibration	1.00	hrs/workstation/yr	burdened composite labor rate	
Process				
Excavation	0.00	hrs/shaft	150	$/hr
Cleaning	0.10	hrs/shaft	150	$/hr
Masking	0.00	hrs/shaft	150	$/hr
Grounding	0.00	hrs/shaft	150	$/hr
ESD	12.00	hrs/shaft	150	$/hr
Inspection	1.00	hrs/shaft	150	$/hr
Handling	0.00	hrs/shaft	150	$/hr
Total Process Labor	13.10	hrs/shaft	150	$/hr
Subcontracted Labor				
Surface Finishing (subcon)	8.00	hours/shaft		
Utilities				
Electricity	0.75	$/shaft		
Argon Gas	360.00	cu ft/shaft	0.24	$/cu ft
Materials				
Grinding wheels (1.25" carbide grinding burr)	NA			
Abrasive pads	2.00	pad/shaft	1	$/pad
Electrode, IN 718 rod	10.00	oz/shaft	1.38	$/oz
Inspection Materials			1.5	$/shaft
Total Process Materials			17.3	$/shaft
EHS COSTS				
Record keeping	no change	hrs/shaft	0	$/hr
PPE				
Safety glasses	1.00	pair/yr/operator	20	$/pair
Gloves	6.00	pair/yr/operator	5	$/pair
Hearing protection	1.00	pair/day/operator	0.05	$/pair
Dust mask	1.00	mask/day/operator	2.25	$/mask
Total PPE			77.6	$/operator/yr

Table 7-12 Data and Assumptions Used for Analysis of Implementation of ESD Repair on F100 10-12 Stator Segment

MODULE:	**ESD**			
Module-Specific Data/Assumptions:				
CAPTIAL COSTS				
Equipment				
ASAP Power Supply	1.00	ea	$ 49,000.00	ea
ESD Workstation	1.00	ea	$ 3,840.00	ea
Other				
Repair Documentation (one time charge)	8	hr	$ 80.00	$/hr
OPERATING COSTS				
Labor	**Value**	**Unit**		
Operators	1	operator/workstation		
Operator Training	8.0	hrs/operator/yr	$ 80.00	$/hr
Operator Qualification	4.0	hrs/operator/yr	burdened composite labor rate	
Operator Qualification - metallography	3.0	hrs/operator/yr	burdened composite labor rate	
Equipment Calibration	1.0	hrs/workstation/yr	burdened composite labor rate	
Calibration Schedule	2.0	calibrations per year		
Process				
Excavation	0.5	hrs/segment	burdened composite labor rate	
Cleaning	0.1	hrs/segment	burdened composite labor rate	
Masking	0.0	hrs/segment	burdened composite labor rate	
Grounding	0.0	hrs/segment	burdened composite labor rate	
ESD	8.0	hrs/segment	burdened composite labor rate	
Inspection	0.5	hrs/segment	burdened composite labor rate	
Handling	0.5	hrs/segment	burdened composite labor rate	
Total Process Labor	9.6	hrs/segment	burdened composite labor rate	
Subcontracted Labor				
Surface Finishing (subcon)			$ 150.00	$/segment
Utilities				
Electricity	$ 0.50	$/segment		
Argon Gas	180	cu ft/segment	$ 0.24	$/cu ft
Materials				
Grinding wheels	1	wheel/segment	$ 1.00	$/wheel
Abrasive pads	3	pad/segment	$ 1.00	$/pad
Electrode, IN 718 rod	3	oz/segment	$ 1.25	$/oz
Inspection Materials			$ 2.00	$/segment
Total Process Materials			$ 9.75	$/segment
EHS COSTS				
Record keeping	no change			$/hr
Grinding dust	negligible			
PPE				
Safety glasses	1	pair/yr/operator	$ 20.00	$/pair
Gloves	6	pair/yr/operator	$ 5.00	$/pair
Hearing protection	1	pair/day/operator	$ 0.05	$/pair
Dust mask	1	mask/day/operator	$ 2.25	$/mask
Total PPE			$ 625.00	$/operator/yr

7.4.3. Capital Costs

Implementing the alternative process will require equipment and capital expenditures. Each repair process will require a separate ESD unit; however, the capital expenditures for each repair will be the same. Table 7-13 below summarizes these expected capital costs.

Table 7-13 Capital Costs for Alternative Process

Capital Costs	
Equipment	$ 52,840
Documentation	$ 640
Total	**$ 53,480**

7.4.4. Operating Costs

Table 7-14, Table 7-15 and Table 7-16 provide summaries of the operating costs that include annual labor, material, utility, and waste disposal costs for the ESD alternative repair process for the TF33 No. 5 Bearing Housing, TF39 Compressor Rear Shaft and F100 10-12 Stator Segment, respectively.

Table 7-14 Annual Operating Costs for TF33 No. 5 Bearing Housing Repair Using ESD Process

Resource	Annual Costs
Labor	$ $131,508
Materials	$ 3,491
Utilities	$ 9,324
Waste Disposal	$ 0
Environmental Management	$ 625
TOTAL ANNUAL OPERATING COSTS	**$ 144,948**

Table 7-15 Annual Operating Costs for TF39 Compressor Rear Shaft Repair using ESD Process

Resource	Annual Costs
Labor	$24,730
Materials	$154
Utilities	$543
Waste Disposal	$0
Environmental Management	$139
TOTAL ANNUAL OPERATING COSTS	**$25,566**

Table 7-16 Annual Operating Costs for F100 10-12 Stator Segment Repair using ESD Process

Resource	Annual Costs
Labor	$ $6,460
Materials	($332)
Utilities	($1,486)
Waste Disposal	$ 0
Environmental Management	($625)
TOTAL ANNUAL OPERATING COSTS	**$ 4,018**

7.5. Implementation Benefits

This analysis estimated the cost impact associated with implementation of ESD in place of various baseline repair processes. Most savings are expected to be a result of the replacement of chromium electroplating. This includes a savings in labor, materials, waste disposal and environmental, safety and health costs. Implementation of ESD for repair of the TF33 No. 5 Bearing Housing is expected to reducing repair costs only if a percentage of the number of lugs needs to be repaired. Implementation of ESD for the F100 10-12 Stator Segment is expected to show a slight decrease in annual operating costs.

7.6. Cost Analysis

7.6.1. Description of Analysis and Indicators

This CBA was performed using the Pollution Prevention Financial Analysis and Cost Evaluation System (P2/FINANCE) software. The P2/FINANCE software generates financial indicators that describe the expected performance of a capital investment. A brief explanation on interpreting these financial indicators is provided, as are the results of the financial analyses for the implementation of the alternative process at OC-ALC.

To measure the financial viability of this project, three performance measures for investment opportunities were used: net present value (NPV), internal rate of return (IRR), and payback period. The NPV is the difference between capital investments and the present value of future annual cost benefits associated with the alternatives. The IRR is the discount rate at which NPV is equal to zero. The payback period is the time period required to recover all of the capital investment with future savings.

These financial indicators account for the time value of money, and discount the future capital investments or annual cost benefits to the current year. A 2.7% discount rate was used for this financial evaluation, which is consistent with the Office of Management and Budget (OMB) Circular Number A-94 and the ECAM. This circular provides specific

guidance on the discount rates to be applied in any analysis used to support Government decisions to initiate, renew, or expand programs or projects which would result in a series of measurable benefits or costs extending for three or more years into the future.

Guidelines for these performance measures are listed in Table 7-17.

Table 7-17 Summary of Investment Criteria

Criteria	Recommendations/Conclusions
NPV > 0	Investment return acceptable
NPV < 0	Investment return not acceptable
Highest NPV	Maximum value to the facility
IRR > discount rate	Project return acceptable
IRR < discount rate	Project return not acceptable
Shortest payback period	Fastest investment recovery and lowest risk

7.6.2.Results

The costs given above in the report were entered into the P2/FINANCE software and financial indicators were calculated. The results are provided in Table 7-18, Table 7-19, Table 7-20 and Table 7-21.

Table 7-18 Results of Financial Evaluation for TF33 No. 5 Bearing Housing Repair: Case 1: 6 Lugs Repaired

Financial Indicator	5-year	10-year	15-year
Net Present Value	$ 655,421	$1,272,267	$1,815,285
Internal Rate of Return	288.2%	288.5%	288.5%
Discounted Payback	0.36 years		

Table 7-19 Results of Financial Evaluation for TF33 No. 5 Bearing Housing Repair: Case 2: 12 Lugs Repaired

Financial Indicator	5-year	10-year	15-year
Net Present Value	($535,437)	($960,927)	($1,330,247)
Internal Rate of Return	N/A	N/A	N/A
Discounted Payback	N/A		

Numbers that appear in parenthesis are negative

N/A: Not applicable – could not be calculated as ROI was not realized

Table 7-20 Results of Financial Evaluation for TF39 Compressor Rear Shaft Repair

Financial Indicator	5-year	10-year	15-year
Net Present Value	$10,461	$64,774	$113,693
Internal Rate of Return	9.3%	22.4%	24.9%
Discounted Payback	4.16 years		

Table 7-21 Results of Financial Evaluation for F100 10-12 Stator Segment repair

Financial Indicator	5-year	10-year	15-year
Net Present Value	($36,719)	($23,667)	($10,864)
Internal Rate of Return	N/A	N/A	N/A
Discounted Payback	N/A		

N/A: Not applicable – could not be calculated as ROI was not realized

7.7. Project Return on Investment

This CBA quantifies the savings or costs of alternative implementation at a specific facility. These results can be used to assist in the objective to implement environmentally acceptable materials and technologies in various production, operation, and maintenance processes. The technology transfer process often involves capital investment decisions, which are typically based on an assessment of both the environmental and potential cost benefits of implemented alternatives. To measure the full benefit derived from alternative implementation, it is necessary to determine the full benefit for the entire DOD propulsion industrial base. To assist in making this measurement, a rough order of magnitude ROI calculation is provided. The ROI is a measure of the financial impact of this project on the propulsion industrial base. This is an initial ROI, calculated during the implementation of the project, and should be periodically updated at various milestones over the life of the project.

The project ROI was calculated using the actual budgeted project costs. This project cost includes all monies budgeted for the various tasks of the project such as identifying potential alternatives, developing a joint test protocol and any testing deemed necessary to validate the alternatives. As OC-ALC is the only facility repairing the engines that use these parts, the results from this CBA were used as total savings and the ratio of total savings to total costs was calculated as the ROI. For this calculation, Case 1 for the bearing hosing was used (i.e., routine repair of 6 lugs is required). Results for the project ROI are shown in Table 7-22.

Table 7-22 Project Return on Investment

Alternative	Total Project Costs (a)	Estimated Average Annual Savings (b)	Return On Investment (Years) (a)/(b)
ESD	$1,153,000	$175,417	7.49 years

7.8. Summary and Recommendations

This analysis estimated the annual operating costs associated with implementation of ESD in place of various baseline repair processes. Implementing ESD in place of chromium electroplating had the most benefits. This includes a savings in labor,

materials, waste disposal and environmental, safety and health costs. Implementation of ESD for weld repair of the TF33 No. 5 Bearing Housing and the F100 10-12 Stator Segment is expected to show a slight decrease in annual operating costs. This analysis indicated that using ESD to repair 6 or fewer lugs on the housing (Case 1) is less expensive then the present repair procedure. However, if all 18 lugs need repair (Case 2), then the present repair procedure is more cost effective than ESD. The 15-year NPV for the TF33 No. 5 Bearing Housing is $1.8 million for Case 1 and ($1.3) million for Case 2.

The break-even point for ESD is 12 or fewer lugs per housing needing repair. However, OC-ALC has been unable to identify a sufficient repair procedure. Implementing ESD is therefore dependent on whether OC-ALC feels that it is a better option than purchasing new components.

For the TF39 compressor rear shaft, the 15-year NPV is $113,700 with a 4.2-year payback period. Although implementing ESD for the F100 10-12 Stator Segment is expected to result in a $4,000 per year savings, the capital expenditures would not be recouped within the 15-year study period. Therefore, the 15-year NPV is negative: ($10,900).

To measure the full benefit derived from ESD implementation, it is necessary to determine the benefit for the entire PEWG propulsion industrial base. In this case, the industrial base is limited to OC-ALC, as it is the only facility overhauling the engines that use these parts. To assist in quantifying this, a rough order of magnitude ROI calculation was done using the project costs. These project costs include all monies budgeted for the various tasks of the project, such as identifying potential alternative and any testing deemed necessary to validate the alternatives. For this calculation, Case 1 for the bearing hosing was used (i.e., 6 lugs needing repair). The time period expected to obtain a full ROI for the ESD project costs of $1.1 million would be 7.5 years.

This analysis indicated that implementation of ESD in place of chromium electroplating would have significant environmental benefits; sufficient data on the other repair processes was not available to quantify any potential environmental benefits. ESD has been shown to have financial benefits when implemented in place of existing repair processes; however each repair needs to be evaluated separately to determine if ESD is economically feasible.

8. Evaluation of PNNL technologies

During the course of the dem/val program Pacific Northwest National Lab (PNNL) asked ASAP to evaluate three technologies developed by PNNL and designed to improve the quality of ESD deposits applied with ASAP's ESD equipment:

1. "Force control with audible feedback" – This technology was designed improve the consistency of manual deposits by providing an audible signal to the operator to indicate when the pressure applied to the applicator head (and hence between the head and substrate) was in the ideal range. This was expected primarily to be useful in training an operator to maintain a constant force during manual application of ESD.
2. "Force control for an automated system" – This technology was designed to improve ESD coating quality and deposition rate for automated ESD applications.
3. "Surface Sifter (SuSi)" – This was an acoustic technology designed by PNNL to be used in conjunction with the ESD process for improvement in ESD quality, specifically the reduction of cracks in crack-prone ESD deposits.

8.1. Test matrix

To perform these evaluations, a series of tests was conducted (Table 8-1), each subsequent test leveraging the information obtained in the previous test. Portland State University (PSU) was placed under contract to ASAP to prepare metallurgical specimens and perform evaluation of the ESD quality.

Table 8-1. PNNL technology test matrix.

	Operator Skill		Force Control				SuSi			# of Coupons		
Test #	skilled	untrained	audible feedback	no audible feedback	automated force control	old force control (washers)	with SuSi	no SuSi	To take place at:	7473 on 301 SS	Stellite 6 on 410 SS	4043 AL on 6061 Al
1	x		x					x	ASAP	3	3	3
2	x			x				x	ASAP	3	3	3
3		x	x					x	ASAP	3	3	3
4		x		x				x	ASAP	3	3	3
5	x		x					x	PNNL	3	3	3
6	x			x				x	PNNL	3	3	3
7		x	x					x	PNNL	3	3	3
8		x		x				x	PNNL	3	3	3
9	x				x			x	PNNL	3	3	3
10	x					x		x	PNNL	3	3	3
11	x				x		x		PNNL	3	3	3
12	x					x	x		PNNL	3	3	3
13	x		x				x		PNNL	3	3	3
14	x			x			x		PNNL	3	3	3
15		x	x				x		PNNL	3	3	3
16		x		x			x		PNNL	3	3	3
									Total	**48**	**48**	**48**

Three identical coupons were prepared for every condition in this evaluation project. The purpose of repeating these coupons was to establish the amount of scatter typical in the

data accumulated. Table 8-1 shows all the deposition rate data. Scatter within identical conditions is determined by the vertical spacing between data points. With the exception of one data point, very little scatter is detected.

The anomalous data point represents a coupon that was started repeatedly because of a malfunction in the torch rotation.

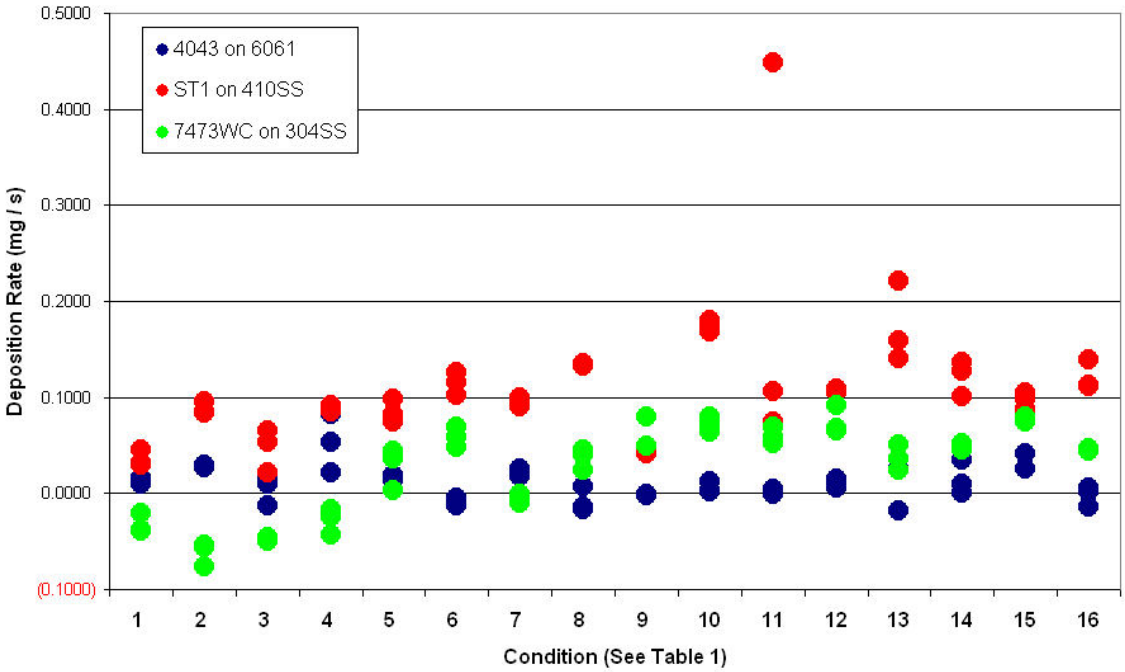

Figure 8-1 Scatter in Deposition Rate Data

8.2. Audible feedback control

For manual ESD operation PNNL developed a force control tool (Figure 8-2) that measured the ESD current through the applicator on the assumption that it was related to the force and hence to the deposit quality. The tool was designed to emit a series of audible tones reflecting the force of the electrode being applied to a substrate by an operator in a manual application. A high tone indicates too much force; a low tone indicates not enough force. This technology was expected to be a tool for an untrained ESD technician to develop the tactile sense of the optimum force required to achieve the highest ESD quality. This tool may also serve as a quality assurance tool. The objective was to evaluate this Audible Feedback Control technology to determine if it functioned as designed and was of value as an operator training tool.

8.2.1. Test Methodology

Evaluations were made by a combination of measurements to establish quantitative performance and operator surveys to establish user value.

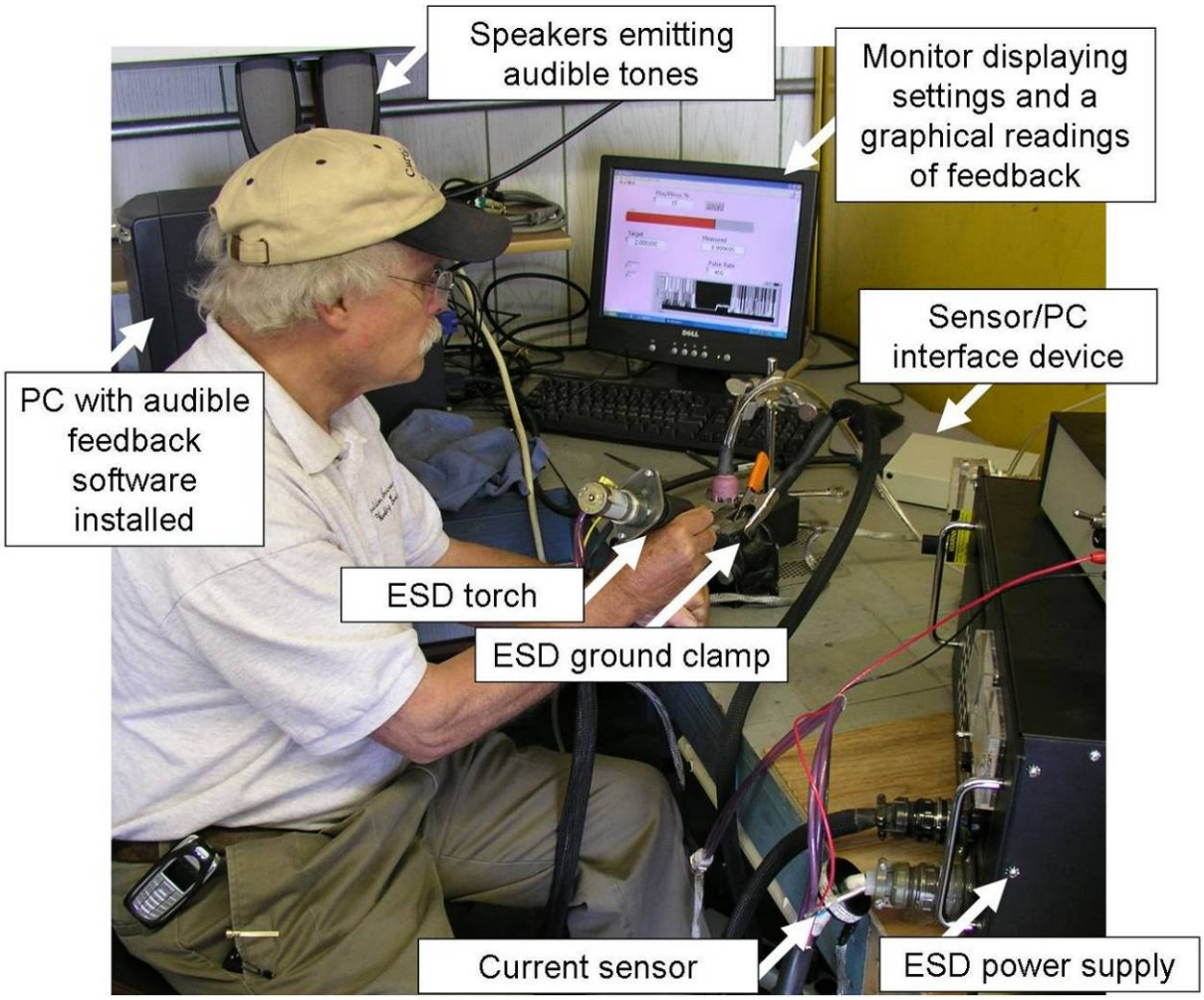

Figure 8-2. Audible Feedback Force Control

Three electrode/substrate combinations were explored, as presented in Table 8-2. The electrode material identified as 7473 is ASAP's proprietary composition of tungsten carbide/tantalum carbide/cobalt, developed for wear and corrosion resistance. The three combinations were selected to demonstrate the value of the Audible Feedback Force Control tool, as well as serve as the baseline information for the remaining tasks outlined in this project.

Table 8-2. Electrode materials and geometry.

Electrode Material	Electrode Geometry	Substrate Material	Coupon Geometry
7473	0.190" dia. rod	304 Stainless Steel	1½" x ½", 5/32" thick
Stellite 1	0.200" dia. rod	410 Stainless Steel	1½" x ½", 1/8" thick
4043 Al	0.125" dia. rod	6061 Aluminum	1½" x ½", 1/8" thick

8.2.1.1. Test Set Up and Parameters Established at ASAP

Initially, an experienced ASAP operator applied coatings to coupons and, through an iterative process involving metallographic examination, identified equipment parameter settings that produced reasonably thick coatings yet still exhibited non-optimal qualities such as porosity and cracking. This low baseline was chosen to allow for marked improvement to the deposit. Had a baseline of parameters been chosen that already produced a good deposit, there would have been little or no room for improvement and as a result would have made the determination of efficacy that much more difficult to discern. The parameters used are presented in Table 8-3.

Table 8-3. ESD test parameters for audible feedback control.

	7473 Carbide on 304 SS	Stellite 1 on 410 SS	4043Al on 6061Al
Frequency (Hz)	400	400	400
Capacitance (μF)	30	30	30
Short Circuit Voltage (V)	175	140	160
Short Circuit Current (A)	4.0	3.0	3.5

The skilled operator applied three patches of ESD coatings on coupons according to the test matrix, keeping track of deposition time to the nearest second.

8.2.1.2. Coupons Prepared at PNNL - First Iteration

While a skilled operator was actively applying ESD to the surface, to establish a 'target' current, the force applied to the coupon was measured via a digital scale. It was noted that the optimum force applied while applying ESD to both the 304 SS and 410 SS was approximately 100 grams. Due to poor ergonomics, the scale was not used under the 6061Al coupons. The target currents for each material combination were established (Table 8-4) and were used for both the manually and automatically applied ESD.

All manually applied ESD coatings were completed by both the skilled operator and the untrained operator.

Table 8-4. Target current for audible feedback - PNNL, first iteration.

Electrode / Substrate	Target Current (A)
7473 / 304 SS	1.95±15%
Stellite 1 / 410 SS	1.90±15%
4043Al / 6061Al	2.25±15%

8.2.1.3. Coupons Prepared at PNNL- Second Iteration

On processing the Audible Feedback Force Control coupons at PNNL for iteration 2, it was found that the target current for Stellite 1 on 410 SS previously determined by the skilled operator, and employed to make deposits in the first iteration, was now too high to work properly. The operator could exert enough force to extinguish the spark without receiving a signal that the target force was reached. New target currents were established for all three material combinations. A digital scale was placed under the work piece and the software monitored to determine a new target current. The targets currents for this set of coupons are presented in Table 8-5.

Table 8-5 Target Current for Audible Feedback – Second Iteration at PNNL

Electrode / Substrate	Target Current (A)
7473 / 304 SS	1.95±15%
Stellite 1 / 410 SS	1.60±15%
4043Al / 6061Al	2.20±15%

8.2.1.4. Coupons Prepared at ASAP

Even though the equipment was the same, the target currents used for the Audible Feedback Force Control system at PNNL were found to be too high to be used at ASAP.

New target currents were established by performing the ESD process on a coupon mounted on a digital scale and using a target force of 100 grams for the stainless steel substrates and 52 grams for the aluminum. The target currents are presented in Table 8-6.

Table 8-6 Target Current for Audible Feedback at ASAP

Electrode / Substrate	Target Current (A)
7473 / 304 SS	1.35±15%
Stellite 1 / 410 SS	1.00±15%
4043Al / 6061Al	1.50±15%

The completed coupons were weighed to provide data for the deposition rate calculations.

8.2.2. Results

8.2.2.1. Summary of survey comments

The operator survey forms were reviewed and a general consensus summarized.

Ease of use of the equipment: All four surveyed operators found the system easy to use, after a short period of time. All were able to maintain a constant force, as indicated by the (relative) silence of either a high or a low tone. However set-up wa rather difficult since it required two people; one applying ESD while watching an electronic scale placed under the coupon to be sure that a constant force was being used and another watching the sensor readings on the computer screen and adjusting the target current value to an approximation of the apparent current being sensed by the system.

Reliability of the equipment: All four operators found the equipment lacking in performance and repeatability. All reported one significant flaw in the technology: At times, the high and low tones would emit even when the ESD equipment was not operating.

Another issue was the inability to repeat the process. The target currents established at PNNL for manually applied ESD were approximately 50% higher than the target currents established at ASAP despite all other parameters being held constant. Similarly, the target currents for the manually applied ESD at PNNL and automation applied ESD at PNNL were different even though the same ESD parameters were used.

Value as an operator tool: All four surveyed operators felt that this technology would be beneficial in training. The improvement in training would come from:

- Shortening the time required to train a novice through intuitive reinforcement
- Easier for the trainer to listen to tones rather than focus on the arcing.

However, this claim was made with the caveat that the performance of the technology would require improvement before effectively using it as a training tool.

Equipment performance: The surveyed operators felt that the equipment did perform as stated in regards to the feedback. Higher forces produced a high tone, and lower forces produced a low tone. However, there was poor correlation between force and current target.

The most critical issue was the inability to repeat the ESD process with the same target current. The target current was established by applying the optimum force to the coupons (or workpiece) and then recording the target current displayed on the Audible Feedback Force Control software user screen. This method assumes that initially the optimum force is determined via traditional ESD process development methods unrelated to the Audible Feedback Force Control technology. The recorded target current can then be documented and used in process specification documents as an equipment parameter, just like other distinct parameters such as voltage or capacitance.

As shown in Table 8-7, the target currents used at ASAP were significantly lower that those used at PNNL and also varied across the same equipment at PNNL from iteration to iteration. Thus probe current is not a good control parameter.

Table 8-7 Variation in Target Current

Electrode / Substrate	Target Current (A) 1st Iteration at PNNL	Target Current (A) 2nd Iteration at PNNL	Target Current (A) At ASAP
7473 / 304 SS	1.95±15%	1.95±15%	1.35±15%
Stellite 1 / 410 SS	1.90±15%	1.60±15%	1.00±15%
4043Al / 6061Al	2.25±15%	2.20±15%	1.50±15%

8.2.2.2. Audible Feedback Force Control vs. the traditional manual application of ESD.

One objective of the evaluation for the Audible Feedback Force Control technology was to establish whether or not this technology contributed to improved quality in ESD deposits. To determine this, ASAP performed visual evaluation by comparing the micrographs (both 50X and 500X) of the coupons made with this technology to those made without. The evaluator did not know which groups of photomicrographs were made with the technology and which were not. The effect was rated with values ranging from -2 to +2 and called "relative quality". The following graphs (Figure 8-3 through Figure 8-7) present the effect the technology had on thickness, uniformity, porosity and cracking.

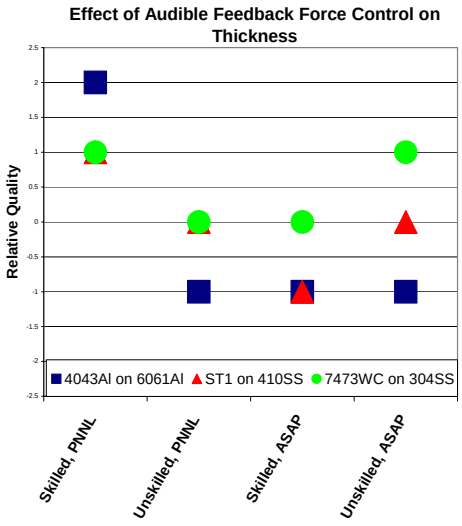

Figure 8-3 Effect on Thickness

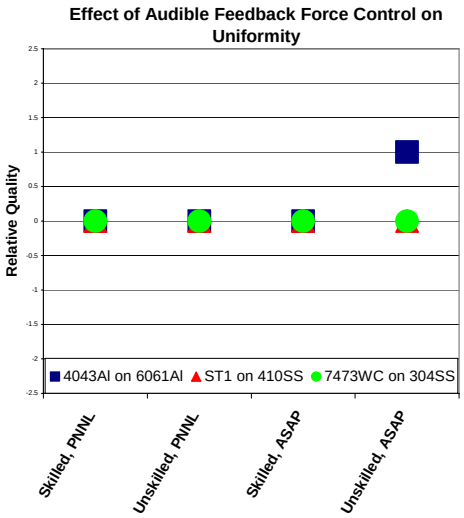

Figure 8-4 Effect on Uniformity

Based on thickness, the effect the Audible Feedback Force Control technology had was an improvement when applying 7473 on 304 SS. However, based on the data presented, the technology generally had an adverse effect for the 4043 on 6061 aluminum. The effect for Stellite 1 on 410 SS was inconclusive. Coupons prepared at PNNL showed an improvement, while those prepared at ASAP showed deterioration.

Based on uniformity, since most of the data points are zero, employing the Audible Feedback Force Control technology does not appear to have any effect.

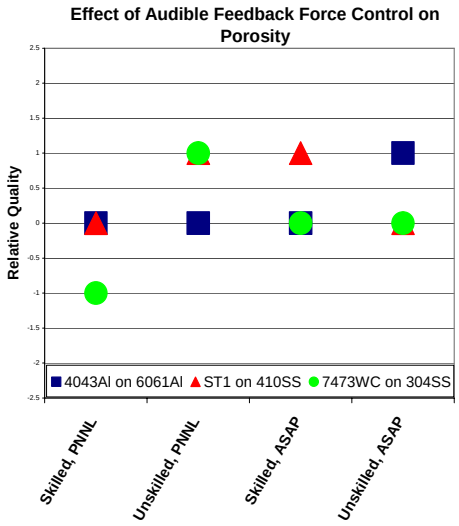

Figure 8-5 Effect on Porosity

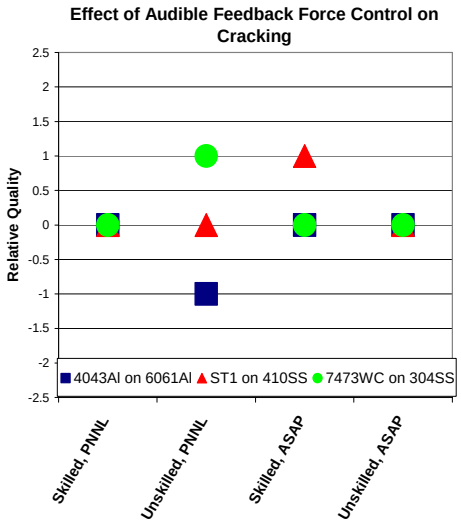

Figure 8-6 Effect on Cracking

Based on porosity, the effect the technology had was an improvement when applying Stellite 1 on 410 SS. Furthermore, employing the technology does not appear to have any significant effect for the 4043 on 6061 aluminum. The effect to the 7473 on 304 SS was inconclusive. Coupons prepared at PNNL showed both an improvement and deterioration, while those prepared at ASAP showed no effect.

Based on cracking, the technology had a slightly favorable effect on the 7473 on 304 SS and the Stellite 1 on 410 SS and a slightly adverse effect on the 4043 on 6061 aluminum.

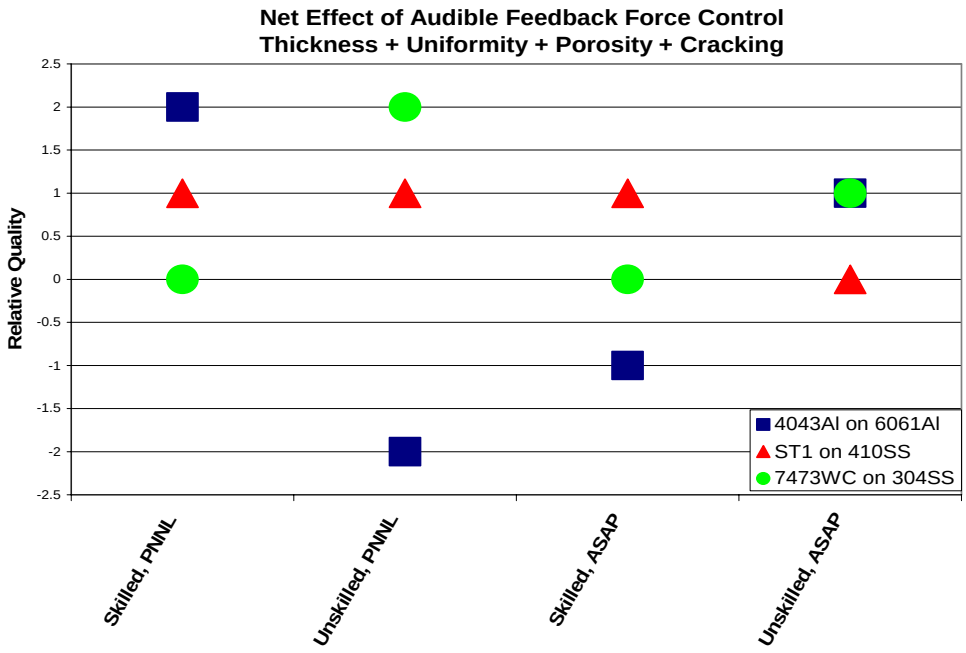

Figure 8-7 Net Effect of Using Audible Feedback Force Control

When combining the effect of employing this technology on all the properties studied (thickness, uniformity, porosity and cracking), the net effect for Stellite 1 on 410 SS was clearly an improvement. The effect for 7473 on 304 SS was also positive. The effect for 4043 on 6061 aluminum was inconclusive. Note, the combination of these properties

was strictly a summation of effects, not a value-weighted assessment.

8.2.2.3. Deposition Rate with and without the Audible Feedback Force Control Technology

For 4043 on 6061 aluminum, the Audible

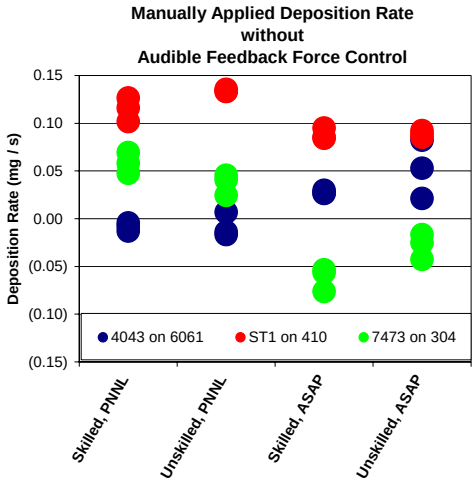

Figure 8-8 Deposition Rate without AFFCT

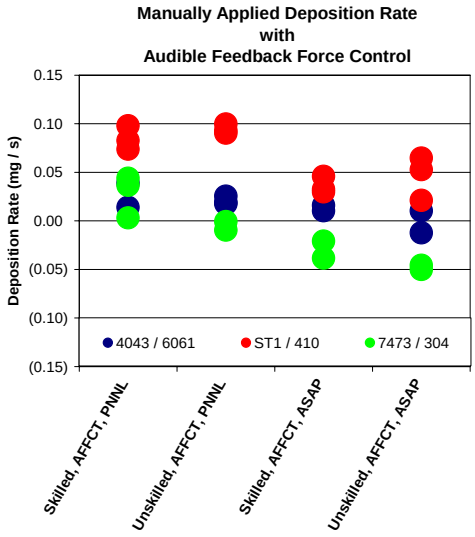

Figure 8-9 Deposition Rate with AFFCT

Feedback Force Control technology had a positive effect on deposition rate. For Stellite 1 on 410 SS and 7473 on 304 SS the technology had a negative effect on deposition rate. If all three material combinations are considered simultaneously, deposition rate seemed to decline slightly when using the Audible Feedback Force Control technology.

There is a correlation between deposit quality and speed. As the deposition rate decreases the quality of the deposit increases. For example the effect of the Audible Feedback Force Control technology was to increase the deposition rate of the aluminum but a decrease in the deposit quality was seen. Conversely the deposition rates of the other two materials decreased when the Audible Feedback Force Control technology was applied but their quality increased. This inverse effect has been noted numerous times in experimental work at ASAP on a number of different materials.

8.2.3. Conclusions on the Audible Feedback Force Control Technology

After evaluating the Audible Feedback Force Control technology developed by PNNL, ASAP has drawn the conclusion that this technology does appear to be a potential tool for integration with ASAP's existing ESD equipment. However, ASAP clearly has concerns about the reliability of the technology and feels that additional work is required before feeling comfortable in endorsing this product.

ASAP felt the equipment was easy to use, based on operator surveys. The data demonstrated an improvement in the overall quality of the ESD, based on thickness,

uniformity, porosity and cracking. The data demonstrated a slight decrease in deposition rate, although, for evaluation of this technology the focus was on training and quality, not deposition rate.

Serious concerns remain with the reliability and maturity of the Audible Feedback Force Control technology. Primarily, they are the phenomenon of a transient tone whether applying ESD or not, and the inability to repeat the ESD process with the same target current. This means that target current is a poor choice for a control parameter.

8.3. Force control for automatic ESD

Automation of the ESD process has proven, in ASAP's previous testing, to result in higher quality and more consistent deposited material, when compared to manual ESD application. One of the disadvantages to automating ESD is the loss of the tactile sense of pressure. To attain a consistent, high quality ESD deposit, applied via an automated system, a method of controlling the force of the electrode to the substrate must be employed. During the last seven years, many force control devices, integrated with ESD equipment, have been developed. These include mechanical springs, manually adding or removing weight, natural gravity solutions and pneumatic devices. Each of the force control devices has demonstrated an improvement in deposit quality and production rates. However, a more advanced and repeatable solution was still sought.

PNNL developed an approach to force control for an automated ESD system (Figure 8-10). This Automated Force Control technology employs the same technology as the Audible Feedback Force Control discussed above, but rather than generating an audible tone, it generates a signal to the "z" axis of an xyz coordinated table. This technology may demonstrate improvement in ESD quality and deposition rate for automated ESD applications.

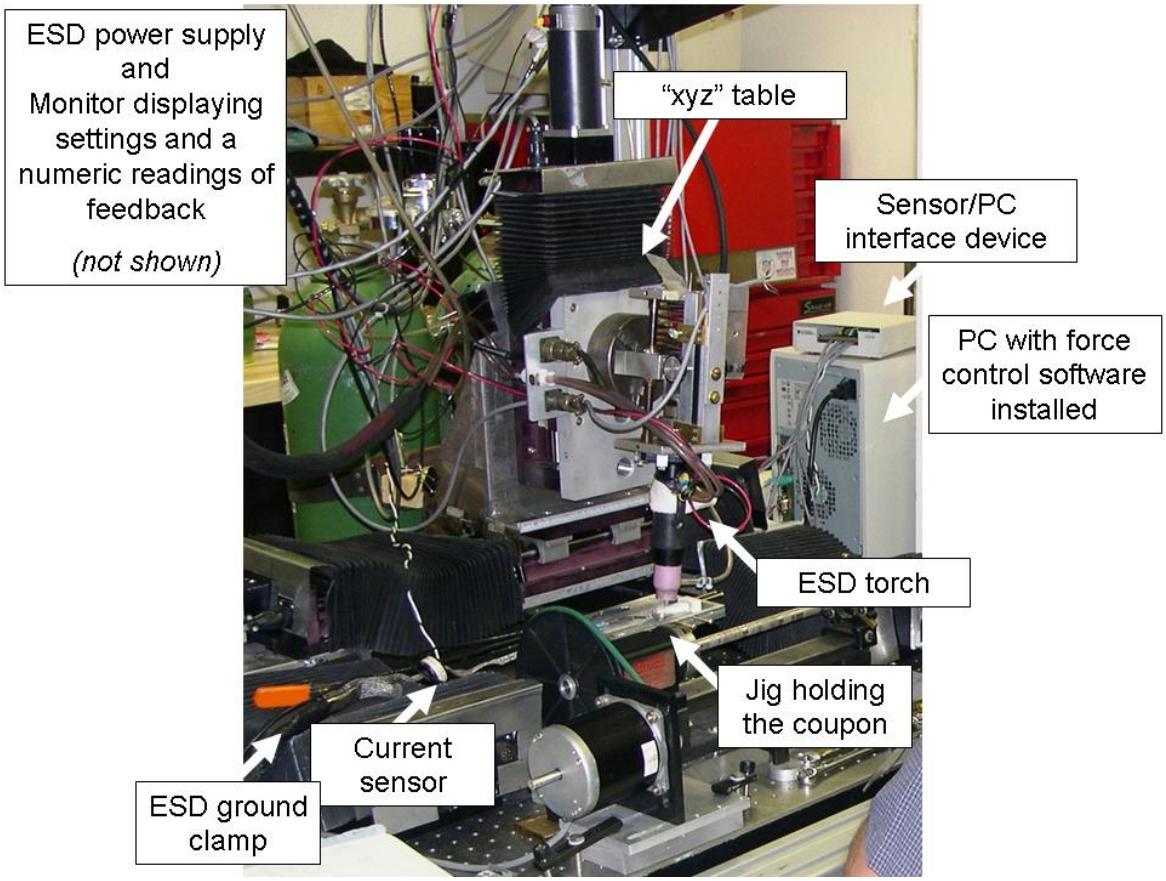

Figure 8-10 Automated Force Control

8.3.1. Test Methodology

To determine the value of the Automated Force Control technology, two tests were conducted. The test matrix explored ESD with and without the Automated Force Control. This test was conducted at PNNL with PNNL's xyz table.

The same three electrode/substrate combinations as presented in Table 4-1 were used in this phase of the project. Data generated in the initial tasks of this project (evaluation of the Audible Feedback Force Control) was leveraged as baseline data for this task. The test matrix included the traditional mechanical force control method (spring and manually added weights) and the new Automated Force Control technology.

Concurrent with preparing the coupons for the Audible Feedback Force Control, ASAP and PNNL personnel prepared coupons to evaluate the Automated Force Control technology. The evaluation began with the traditional mechanical force control (spring and weights). Based on deposition tests a target weight of 100 grams was chosen for both the 7473 carbide on 304 SS and the Stellite 1 on 410 SS, and 52 gm for the 4043Al on 6061Al. The values established for the automated force control current are shown in Table 8-8.

Table 8-8 Target Current for Automated Force Control

Electrode / Substrate	Target Current (A)
7473 / 304 SS	1.90±15%
Stellite 1 / 410 SS	1.80±15%
4043Al / 6061Al	2.20±15%

8.3.2.Results

8.3.2.1. Summary of survey comments

The operator survey forms were reviewed and a general consensus summarized.

Ease of use of the equipment: None of those surveyed found the system to be user friendly or easy to use, although one found the user interface to be clear and simple to understand. Those surveyed emphasized the observation that this system requiring considerable operator involvement.

Reliability of the equipment: Those surveyed found the equipment lacking in performance and reliability. The technology required constant adjustment and operator intervention to maintain the target currents and prevent extreme and erratic motion on the z axis. The system frequently required stopping and restarting, resulting in several coupons that could not be used. One survey reported four breakdown situations: one related to the ESD torch; one related to z motion (z axis did not respond to computer commands), and two "run-away" conditions where the torch ran into the substrate.

Equipment performance: Those surveyed felt that the equipment did not perform as designed in regards to maintaining constant force by monitoring current. Automated Force Control out-performed neither the traditional mechanical method of force control nor the manual method.

Other comments and observations: A scale was not incorporated into this evaluation, because, according to PNNL personnel, it would have provided an unstable work platform. Therefore the only method of ascertaining that a constant force was maintained was observing a constant target current (and customary visual and audible observations).

As in the evaluation of the Audible Feedback Force Control technology, the inability to repeat the ESD process with the same target current was again observed in the evaluation of Automated Force Control. As shown in Table 8-9, the target currents used for Automated Force Control differed substantially from those used in evaluating the Audible Feedback Force Control.

8.3.2.2. Automated Force Control technology vs. traditional mechanical force control

Table 8-9 Variation in Target Current, including Automated Force Control

Electrode/Substrate	Target Current (A) 1st Iteration at PNNL	Target Current (A) 2nd Iteration at PNNL	Target Current (A) At ASAP	Target Current (A) At PNNL
	Audible Feedback Force Control			Automated Force Control
7473 / 304 SS	1.95±15%	1.95±15%	1.35±15%	1.90±15%
Stellite 1 / 410 SS	1.90±15%	1.60±15%	1.00±15%	1.80±15%
4043Al / 6061Al	2.25±15%	2.20±15%	1.50±15%	2.20±15%

ASAP compared micrographs (both 50X and 500X) of the coupons made with the Automated Force Control technology to those made with standard mechanical force control. The effect was rated with values ranging from -2 to +2 and called "relative quality". Figure 8-11 presents the effect the technology had on thickness, uniformity, porosity and cracking, as well as the net effect.

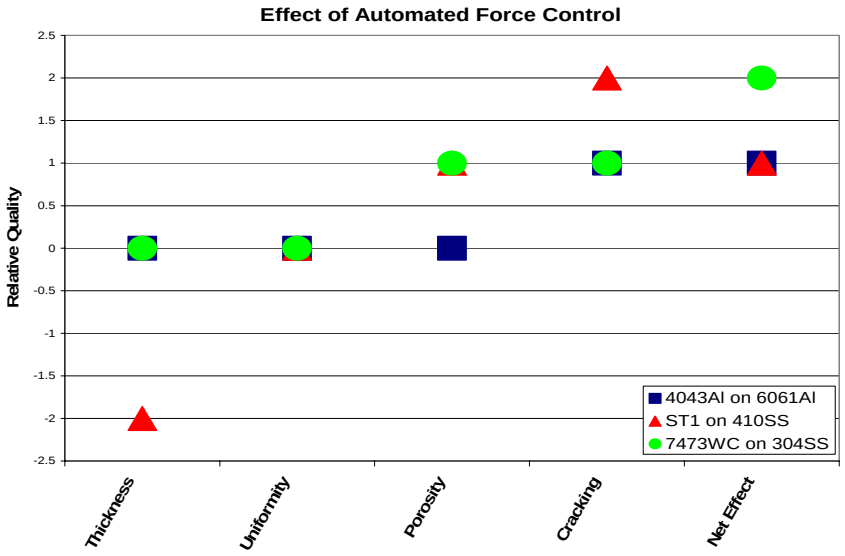

Figure 8-11 Effect of Using Automated Force Control

Based on thickness, the Automated Force Control technology had no effect when applying 7473 on 304 SS and 4043 on 6061 aluminum. However, based on the data presented, the technology seemed to have an adverse effect for the Stellite 1 on 410 SS.

Based on uniformity, since all of the data points are zero, employing the Automated Force Control technology does not appear to have any effect.

Based on porosity, the effect of the technology was an improvement when applying Stellite 1 on 410 SS and 7473 on 304 SS. Employing the technology does not appear to have any significant effect for the 4043 on 6061 aluminum.

Based on cracking, the technology had a favorable effect on all material combinations, especially for the Stellite 1 on 410 SS. From past experience, ASAP has seen deposit quality increases as deposit thickness decreases in crack prone materials such as Stellite.

When combining the effect of employing this technology on all the properties studied (thickness, uniformity, porosity and cracking), the net effect was positive for all materials. Note, the combination of these properties was strictly a summation of effects, not a value-weighted assessment.

8.3.2.3. Deposition Rate and Automated Force Control technology

The deposition rate using the traditional mechanical force control method (weights and spring, Figure 8-12 points on the left) was compared to the deposition rate using the Automated Force Control technology (points on the right).

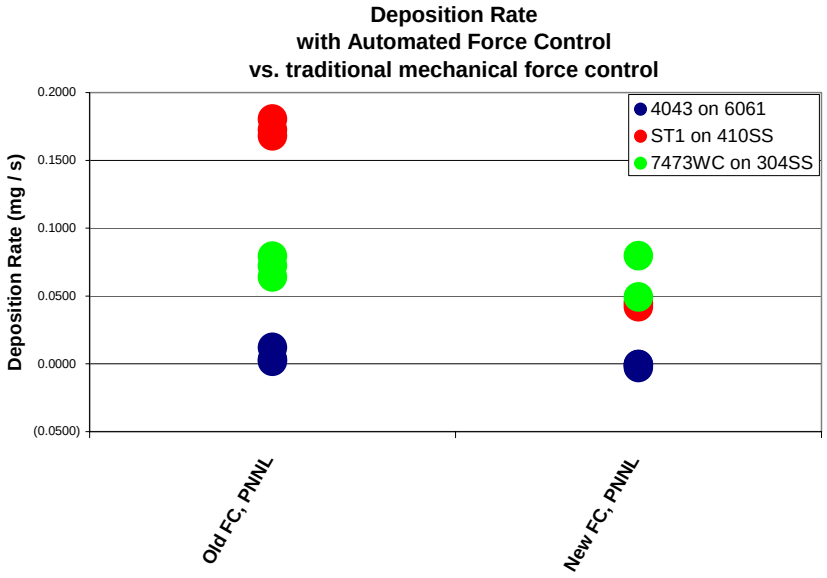

Figure 8-12 Deposition Rate with and without Automated Force Control

The plot of deposition rates comparing the two force controls for automated ESD application showed a very significant decrease in deposition rate for the Stellite 1 on 410 SS deposit. The deposition rates of the other two material combinations also decreased with the application of the Automated Force Control system but the decrease is fairly small. This data confirmed the information shown on the quality chart for thickness and uniformity.

8.3.3. Conclusions on the Automated Force Control technology

After evaluating the Automated Force Control technology developed by PNNL, ASAP has drawn the conclusion that this technology, in its current state of development, is not ready for integration with ASAP's existing ESD equipment.

In general, the data demonstrated slight to no improvement in the overall quality of the ESD, based on thickness, uniformity, and porosity. The data demonstrated that the technology had a favorable effect on reducing cracking for all material combinations. The data demonstrated a decrease in deposition rate, especially for the Stellite 1 on 410 SS deposit. Automated Force Control did not out-perform the traditional mechanical method of force control.

Serious concerns remain with the reliability and maturity of the Automated Force Control technology. Primarily, they are the inability to repeat the ESD process with the same target currents, the inability to maintain a constant force and the need for constant operator intervention.

8.4. Surface sifting

PNNL has developed a process that could be used during ESD application that may demonstrate an improvement in the ESD quality, specifically the reduction of cracks in crack-prone ESD deposits. PNNL refers to this technology as Surface Sifter (SuSi). SuSi is a process that introduces ultrasonic vibration to the substrate during the ESD coating process (Figure 8-13).

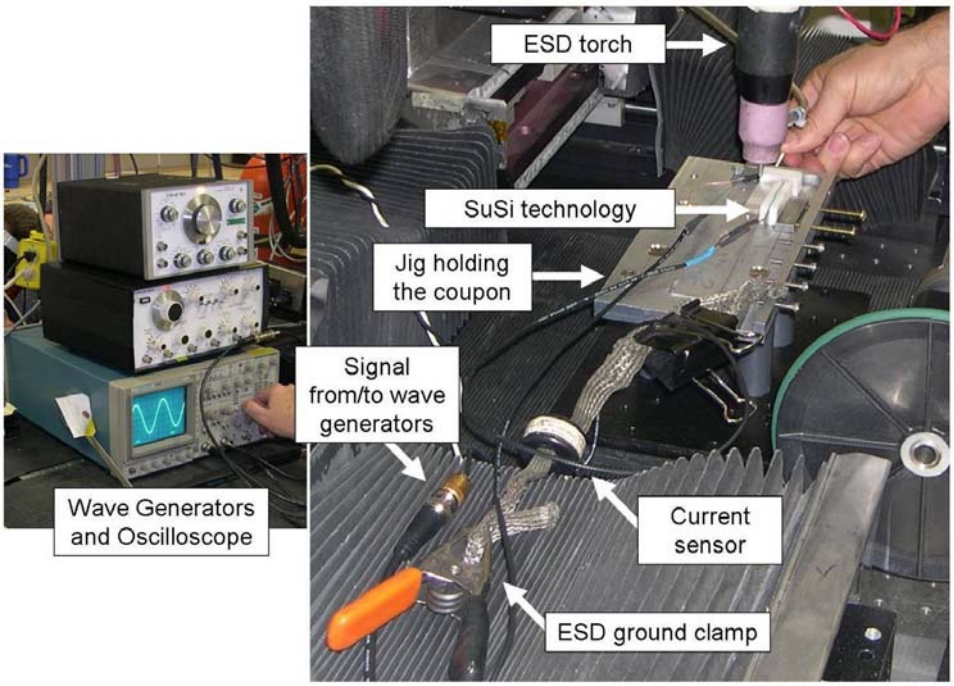

Figure 8-13 Surface Sifter (SuSi)

8.4.1. Test Methodology

To determine the value of the SuSi technology, six tests were conducted. The test matrix explored ESD with and without the SuSi process, with and without the Audible Feedback Force Control technology and with and without the Automated Force Control Technology. The same three electrode/substrate combinations presented in Table 4-1 were explored. Data generated in the initial tasks of this project (evaluation of both the Audible Feedback Force Control and Automated Force Control) was leveraged as baseline data for this task. Coupons and electrodes procured for the initial tasks of this project were used for this phase of the project.

8.4.1.1. Coupons Prepared at PNNL

The xyz table enabled with the traditional mechanical force control (spring and weight) was the first system used to evaluate the SuSi technology. SuSi was next used on the xyz table employing the Automated Force Control technology. Lastly SuSi was used on manually processed coupons made by both the skilled and untrained operators both with and without Audible Feedback Force Control.

SuSi consisted of two transducers firmly clamped against the coupons and at 90° to each other. The transducers were electrically isolated from the coupon and the clamp. The transducers were driven by two Wavetek signal generators, models 144 and 148A. Tuning of the transducers was accomplished by adjusting both the clamping force and the signal frequency on each transducer. While tuning SuSi, one of the transducers was being “driven”, the other, with the use of an oscilloscope, was being used to “listen” for the signal being sent into the coupon. When ESD was being applied, both transducers were being driven.

For this series of tests, the driving transducer was tuned (avoiding harmonics and even multiples of frequencies) to generate the highest amplitude signal in the listening transducer. Each coupon was tuned and amplitudes and period data were recorded.

The final weights of all of the coupons were measured and recorded at ASAP. This information was used to calculate the deposition rate of the deposits. The coupons were then sent to PSU for metallurgical specimen preparation and evaluation.

8.4.1.2. Metallurgical Specimen Preparation

The 410 SS and 304 SS specimens were photographed in the as-polished condition. The 6061Al specimens were lightly etched to highlight the deposit structures. Differential Interference Contrast (DIC) was employed on specimens where it was difficult to resolve the ESD with brightfield lighting, especially the 304 SS samples. Each specimen was photographed at magnifications of 50 and 500 times.

8.4.2.Results

8.4.2.1. Summary of Operator survey comments

The operator survey forms were reviewed and a general consensus summarized.

Ease of use of the equipment: According to the surveys, the equipment was difficult to use. SuSi set up was time consuming (5 to 10 minutes for each coupon) for two reasons; one, the time required to clamp each coupon and the crystals and together, and two, the time required to re-tune the signal generators for each coupon. The delicate nature of the crystals and the fine lead wires further complicated the set up.

Reliability of the equipment: Once the coupon and the crystals were clamped into place and the signal established, the equipment was reliable in that it did not break down or change over time during ESD application. However, three times during set up the wire leads broke and on one occasion a crystal broke.

Equipment performance: The equipment was intended to reduce cracks in crack prone ESD deposits via the introduction of ultrasonic vibrations. As there were no observable visual or audible indicators, it was not possible to determine whether or not the coupon was being vibrated.

Other comments and observations: In its current state of development, ASAP questions the practicality of using this technology on any geometry other than a small flat coupon.

8.4.2.2. The effect of using SuSi during the application of ESD.

The objective of the evaluation of SuSi was to determine if it improves ESD deposit quality, specifically by reducing cracks in crack-prone ESD deposits. To determine this, ASAP performed a visual evaluation by comparing the micrographs (both 50X and 500X) of the coupons made with SuSi to those made without SuSi. The effect was rated with values ranging from -2 to +2 and called "relative quality". Figure 8-14 through Figure 8-17 show the effect of SuSi technology on thickness, uniformity, porosity and cracking.

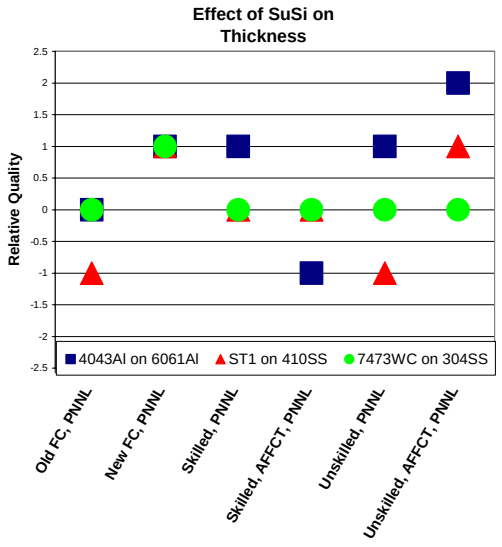

Figure 8-14 Effect on Thickness

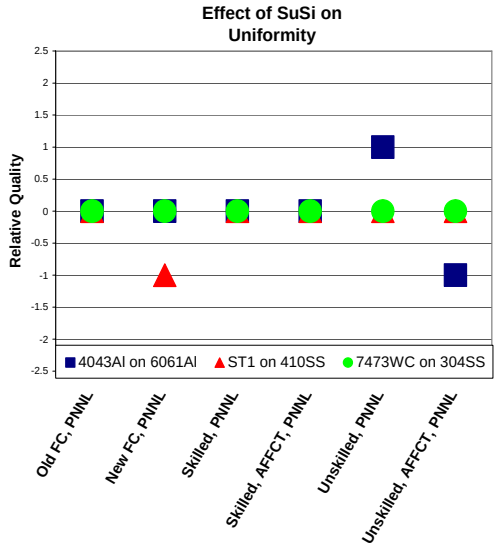

Figure 8-15 Effect on Uniformity

Based on thickness, SuSi resulted in an improvement of the 4043 on 6061 aluminum deposit. SuSi had virtually no effect for the 7473 on 304 SS deposit. For the Stellite 1 on 410 SS deposit, the results were mixed and inconclusive.

Based on uniformity, the effect of SuSi was insignificant, as all but three (out of 18) data points were zero.

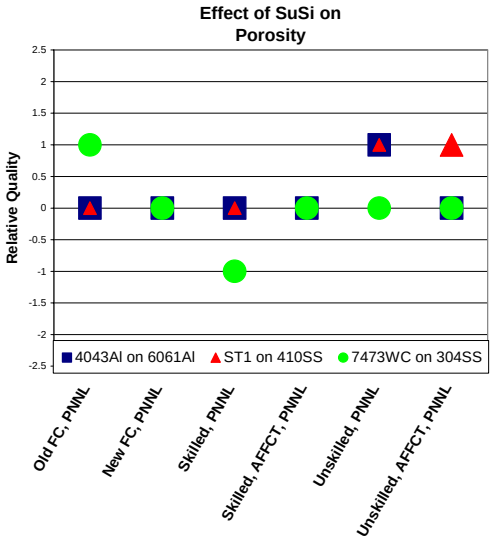

Figure 8-16 Effect on Porosity

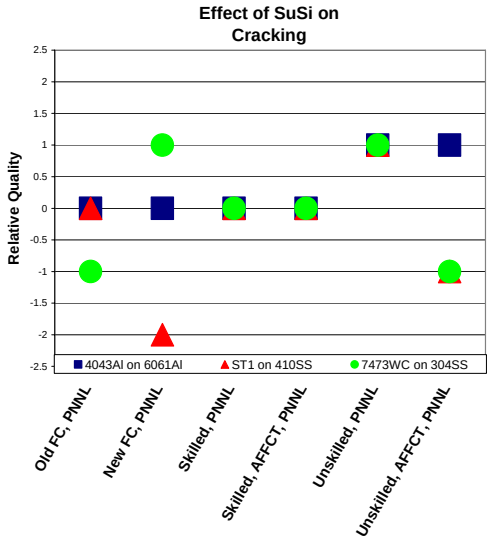

Figure 8-17 Effect on Cracking

Based on porosity, SuSi technology had a slightly positive effect for Stellite 1 on 410 SS and 4043 on 6061 aluminum deposits. The effect for 7473 on 304 SS deposit was negligible. When all three materials were considered together, SuSi had a slightly positive net influence on the porosity of the deposits.

Based on cracking, SuSi had a slight positive effect for 4043 on 6061 aluminum deposits. The effect for 7473 on 304 SS and Stellite 1 on 410 SS was scattered and inconclusive. Considering all materials together, the net effect on cracking in the deposits was inconclusive.

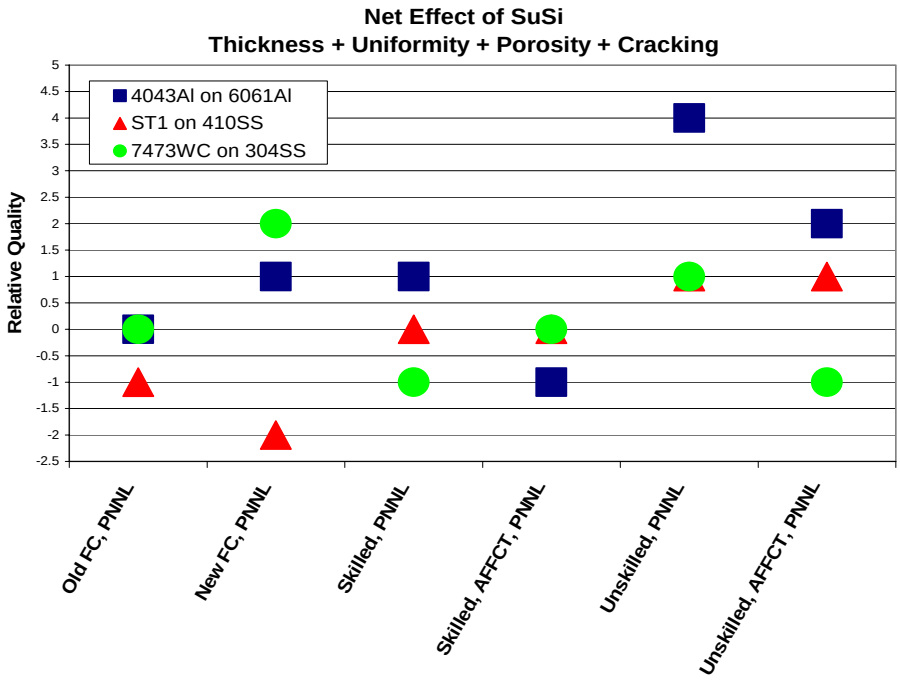

Figure 8-18 Net Effect of Using Automated Force Control

When combining all the properties studied (thickness, uniformity, porosity and cracking), the net effect of employing SuSi for 4043 on 6061 aluminum was positive. The results for the other two materials were inconclusive. Note, the combination of these properties was strictly a summation of effects, not a value-weighted assessment.

8.4.2.3. Deposition Rate with and without SuSi

In order to evaluate any improvements in deposition rate by using SuSi, two graphs (Figure 8-19 and Figure 8-20) were constructed. By comparing the two graphs, side by side, an assessment of the change in deposition rate was made.

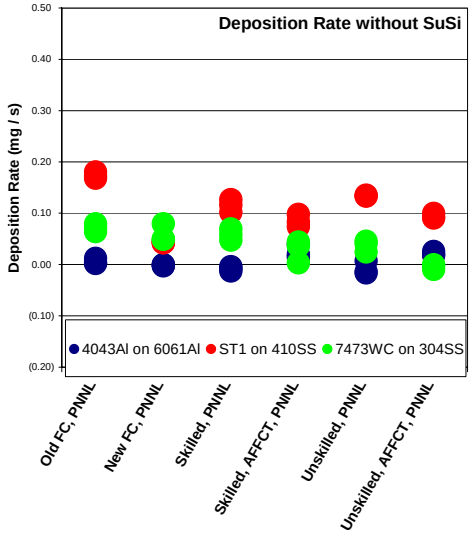

Figure 8-19 Deposition Rate without SuSi

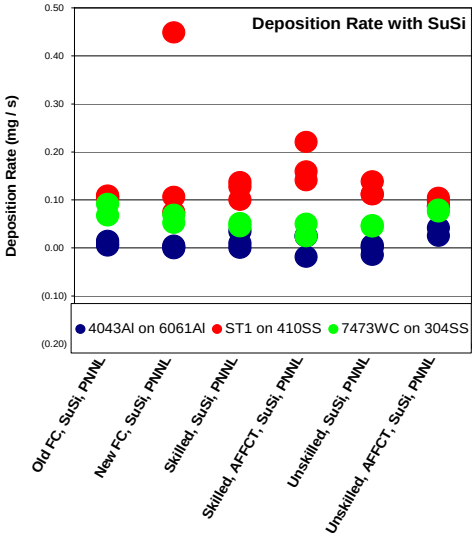

Figure 8-20 Deposition Rate with SuSi

For 4043 on 6061 aluminum, the SuSi technology had virtually no effect on deposition rate. For Stellite 1 on 410 SS and 7473 on 304 SS the technology had a somewhat positive effect on deposition rate.

Unlike the results of the Audible Feedback Force Control evaluation and the previous experience of ASAP, there was little correlation between deposition rate and quality. For example, the Stellite 1 on 410 SS and 7473 on 304 SS both showed an improvement in deposition rate. However the quality of the Stellite 1 on 410 SS was reduced; the quality of 7473 on 304 SS was improved. SuSi had no effect on the deposition rate of the 4043 on 6061 aluminum but the quality of the aluminum deposit was improved.

8.4.3. Conclusions on the SuSi technology

After evaluating the SuSi technology developed by PNNL, ASAP drew the conclusion that this technology, in its current state of development, is not ready for integration with ASAP's existing ESD equipment.

The data demonstrated a slight increase in deposition rate, although the focus of the evaluation of this technology was on quality (reducing cracks in crack-prone deposits), not deposition rate.

When evaluating the effect SuSi had for any given material (for example 4043 on 6061 aluminum), regardless of how it was applied, one conclusion was reached. The data demonstrated that SuSi had a slight positive effect for aluminum deposits. The effect for the other two materials was inconclusive. The data demonstrated some improvement in the overall quality of the ESD deposits and suggests that this technology may be useful in reducing cracks in crack-prone materials. However, ASAP has concerns regarding the maturity of this technology and feels that additional work is required.

ASAP felt that considerably more testing needed to be performed to determine how this technology may be best applied. However, even before additional tests are conducted, matters regarding ease of use and robustness must be resolved.

This page intentionally left blank.

9. Implementation

In addition to being widely used for repair of dies, molds and industrial tooling, ESD is already used commercially in a number of applications relevant to the aerospace industry:

4. Single crystal turbine blade for two gas turbine engines (FAA approved repair)
5. Second stage gas turbine blade sulfidation corrosion repair (DER repair)
6. Helicopter flap restraint for main rotor (DER approved repair).

9.1. ESD Performance

The process development and testing done in this program clearly show that high quality ESD materials can be used for dimensional reclamation and can provide performance similar to that of the original material.

- If the deposition parameters are correctly chosen, ESD coatings can reduce fatigue below what would result from excavating the damage and using no fill (or presumably a low strength fill such as epoxy) – i.e. they can restore some, but not all, of the original strength of the material.
- Whether the ESD coating is as hard and wear resistant as the parent material depends on how the alloy must be heat treated. Some heat treatments may be approximated by the deposition and quenching of the ESD alloy, but others cannot. For many materials the hardness and wear of the ESD is essentially that of the parent material.
- In general the corrosion performance of ESD alloys is similar to that of the parent, provided the material is deposited without high porosity into which fluids can penetrate.

9.2. Advantages and Drawbacks

For depot repair ESD has a number of obvious advantages:

- The process is easy to learn and can be carried out by depot artisans with a minimum of additional training.
- The equipment is inexpensive and highly portable. Thus it can be used shipboard or at operational bases to carry out repairs of reasonable quality, often without the need to remove items from the system. This has a large potential for cost savings in vehicles, ships, submarines and support equipment (including aircraft support).
- The process is clean, with no significant effluent or waste.
- ESD is a good way to repair damage in a small area of a large component, and as such it has been shown to be able to repair damaged chrome without the need for stripping and replating, for a significant ESOH saving.

All of these advantages make it ideal for use both for depot repair and operational maintenance. As this program has demonstrated, however, the process also has certain drawbacks that inhibit depot use, especially in aerospace overhaul and repair:

- In common with most other widely used welding techniques, the technology is

usually manual, making it difficult to ensure a high level of control. A robot can be employed, but this makes the process more expensive and cumbersome, and eliminates the advantage of portability.

- The quality of the interface and the ESD layer is variable, especially in terms of porosity and discontinuities.
- The combination of interface voids and tensile stress in the ESD layer is a concern for aerospace engineers, because of the possible impact on fatigue. This inhibits its specification for repair of rotating GTE components.
- When repairing chrome plating, there is a tendency to form a "halo" of voids and discontinuities around the repaired area at the ESD/chrome plating interface.

Ultrasonic impact treatment has been shown to have a very positive effect on the structure of ESD coatings. However, it is seen by aerospace engineers as a crude process that would need to be carefully evaluated and characterized before being applied to aerospace components (although one might argue that it is no more crude than shot peening or low plasticity burnishing). Furthermore, it cannot be used in conjunction with manual ESD, or in areas that are not readily accessible. This means that in general the ESD material must function adequately by itself. This is especially true if it is to be readily employed by depot artisans in D- and O-level maintenance.

9.3. Cost/Benefit Analysis

The cost-benefit analysis carried out for ESD showed that it is very cost-effective for small areas but not for large areas because of its slow deposition rate. This is clearly seen in the analysis of the TF33 #5 bearing housing, where the repair is highly cost-effective for repairing a few lugs on each component, but not for more extensive repairs. The cost analysis model findings are borne out by the application to gun cradles at ANAD, where the component can be reclaimed by repairing a few small corroded areas on a large diameter.

Significant improvements in ESOH compliance could also be obtained by using ESD to repair limited areas on large chromed components, rather than stripping, repairing and rechroming.

9.4. Implementation at Repair Depots

The Oklahoma City ALC was the lead demonstration overhaul facility with work also being done at NSWC Carderock and Anniston Army Depot. Each of these locations was equipped with an ESD system from ASAP.

Vehicles – Anniston Army Depot

The process has already been qualified and put into production at ANAD, and its use there appears likely to grow as depot personnel become more acquainted with the process.

- The first qualified repair is the repair of corrosion pits in the Abrams gun cradle. This repair is now in regular use, successfully repairing about one cradle per month, for an annual saving of about $300,000. Although this component would

otherwise be condemned rather than stripped, repaired and rechromed, it demonstrates the use of ESD as a chrome repair. It is also important to note that the repair was developed by depot engineers and artisans with very little input from outside. This illustrates that ESD could be a very powerful tool for depot use in reclaiming components that would otherwise be condemned.

- The second repair at ANAD is repair of pitted areas in an M1A1 turbine engine helical gear shaft. The ESD repair appears to work very well, and again, the repair is made on a chrome plated area without the need to strip and replate the chrome. It is likely to be approved if a repaired shaft passes a 100 hour engine test. This repair illustrates the important point that ESD can be used for repair of rotating GTE components, provided they are not flight-critical. Thus, while Tinker AFB would not be able to use such a repair without extensive (and very expensive) validation and qualification testing, it can be introduced for vehicle (and presumably also for ship and stationary) gas turbines with far greater ease.

Vehicle repair appears to be one of the best applications for the technology, since the risks are lowest. Potential applications include:

- Worn or corroded components where the repair area is small and the replacement cost is high, or where the item is no longer manufactured.
- Hydraulic actuators, which are used on a large number of Army earth moving and loading machinery, and which tend to become corroded and pitted.
- Diesel and turbine engine components for vehicles.
- Turbine engine components for stationary (power) turbines.

Ships and submarines – Carderock

The technology has shown itself to be promising, but there are some issues that must be solved if it is to be a viable repair option:

- A primary issue in development work at Carderock was the halo of porosity created around the repair location. ASAP has now developed methods that appear to minimize, and perhaps completely eliminate, this problem.
- One of the ESD Monel alloys (C276) suffered severe crevice corrosion, although the others (Alloys 59 and 686) performed essentially as well as bulk Monel. It is not clear whether this was a result of severe interface porosity or of the ESD alloy having a greater sensitivity.

Carderock concluded that ESD has promise, but that a significant amount of work is needed to develop the technology to ensure consistently high quality repairs.

Although the Carderock work left a number of questions unanswered, there would appear to be a high potential for application in ships and submarines where the area to be repaired is small, or even where it is large, but where the component cannot be removed for repair without the expenditure of very high cost and time. Examples include:

- Hydraulic, power, drive, pump and propeller shafts in submarines, where removal and repair is difficult and expensive. In most cases the ability to effect repairs in cramped spaces with the component in place would appear to be particularly

applicable to ships and submarines. As with vehicles, qualification should be much easier than with aircraft.

- Aircraft carrier steam plants, valves, etc.
- Valves and other components in shipboard systems, especially where these items must be repaired at sea.

For at-sea repairs, ESD has the advantage that applying it is a skill easily acquired and the equipment takes up minimal space.

In order to be used in marine applications the coating methods must be perfected for Monels and similar corrosion-resistant materials. It will be especially important to demonstrate that repairs can be made using ESD alloys that are resistant to crevice corrosion and that can be deposited with good quality (low porosity) interfaces.

Aircraft GTEs – OC-ALC

The reason for designating OC-ALC, the Air Force Engine Repair Depot as the primary location was that Rolls Royce had implemented the technology for repair of non-rotating engine components that were mis-machined or otherwise damaged in manufacture. The reason for Rolls' use of ESD only on non-rotating components was concern over the possibility of cracking and of a fatigue debit that the process was seen to have produced in their original testing. Seeing the success at Rolls, the other OEMs and OC-ALC were very interested in its possibilities.

Repairs were developed and demonstrated for several components:

1. Bearing housing for dimensional restoration of the #5 bearing – TF33 engine
2. Compressor rear shaft repair – TF39 engine
3. Repair of 10-12 stator segment – F100 engine.

Of these the #5 bearing housing is the only one that has been qualified at this point. The TO has been modified to permit this repair, which had a very high cost-benefit if the extent of repair was limited.

The primary barrier to the use of the technology for aircraft GTE repairs is the very high cost of qualification and testing followed by the extensive paperwork required for TO changes and OEM acceptance. GTE repairs must be accepted both by the depot and the OEM, and the cost of the time and paperwork alone is the major cost component. If an engine test is required, the cost can be well in excess of $1 million, making a change practicable only if testing can be piggy-backed onto existing engine tests. In addition, OEM acceptance depends very strongly on whether ESD is defined as a coating, not a weld, since acceptance and qualification of a weld method is much more difficult.

It has been repeatedly emphasized that the easiest way to gain acceptance and adoption of the technology for Air Force GTE repair is through the MRB system. Whenever a component cannot be repaired by standard TO methods, the component is evaluated by a Materials Review Board (MRB) engineer to determine if a repair can be made or if the component must be condemned. In order to use it MRB engineers must be aware of the capability of the technology, and see it as a method they can draw on for repairs where there are no other qualified repairs already specified in the TO.

Another aircraft-related area in which ESD could probably contribute is the repair of corrosion and wear damage on aircraft ground support equipment, such as generators, compressors, bomb and missile loading systems, and the many other vehicles and equipment items needed to support land- and carrier-based flight operations.

9.5. Conclusions

ESD technology can make a clear impact on clean repairs in vehicles, support equipment, ships and submarines at D-, I and O-level. The equipment is very simple to use, training requirements are minimal, and repairs can be developed by local engineers and artisans (the repairs at ANAD required very little development, which was done by base personnel). The technology is ideal for corrosion repair where the demands on the material are relatively simple (no high stresses or high fatigue), and where the areas to be repaired are small. Very common components such as hydraulic actuators on vehicles are obvious potential applications where ESD can provide a much better repair than the typical epoxies and other methods in use today. Many of these components are chrome plated and an ESD repair will allow them to continue functioning at close to their original performance, minimizing the number of strip and repair (and chrome plating) cycles that these items will go through in their lives. Aircraft GTEs should be considered as a long-term application since they have proved to be the most difficult area in which to use this technology. It is most cost-effective when used to isolated damage or corrosion on large or expensive components.

This page intentionally left blank.

10. References

1. Technology Demonstration Plan, "Electrospark Deposition for Localized Repair of Gas Turbine Engine Components," issued by DOD Environmental Security Technology Certification Program, February 2005
2. Navy/Industry Task Group Report, "Impact of Anticipated OSHA Hexavalent Chromium Worker Exposure Standard on Navy Manufacturing and Repair Operations," October 25, 1995
3. H. S. Rawdon, in discussion of paper by Bain, Transactions of the AIME, v.79, p. 37 (1924)
4. N. C. Welsh , "Frictional Heating and Its Influence on the Wear of Steel," J. Applied Physics, v 28, p. 960 (1957)
5. R. N. Johnson, "Coatings for Fast Breeder Reactor Components," Thin Solid Films, v. 118, p. 31 (1984)
6. K. Natesan, "HighTemperature Corrosion in Coal Gasification Systems," Corrosion, v. 41, p. 646 (1985)
7. R. N. Johnson and G. L Sheldon, "Advances in the Electrospark Deposition Coating Process," J. Vac. Sci. Technol., v. A4, p. 2740 (1986)
8. S. W. Borenstein, J. Kelley and D. Boone, "Evaluation of Coatings to Reduce Erosion and Corrosion-Related Problems," Proceedings of the 1991 International Joint Power Generation Conference, ASEM, v. 13, p. 177 (1991)
9. J. E. Kelley and R. M. Kaufman, "Surface Modifications Resistant to Erosion, Abrasion, Galling and Corrosion by Pulse Fusion Alloying," Proceedings of the Materials for Resource Recovery and Transport Conference, Metallurgical Society of CIM, p. 355 (1998)
10. G. E. P. Box and D. W. Behnken, "Some New Three-Level Designs for the Study of Quantitative Variables," Technometrics, v. 2, p. 455 (1960)
11. ASTM D1141, "Standard Practice for the Preparation of Substitute Ocean Water," American Society for Testing and Materials, West Conshohocken, PA, 2003
12. J. A. Beavers, *Corrosion of Metals in Marine Environments*, Metals and Ceramics Information Center, Columbus, OH, p. 5-9, 1986
13. J. R. Davis, ed., *Metals Handbook, Volume 13, Corrosion*, ASM International, Metals Park, OH, p. 653, 1987
14. D. M. Aylor et al., "Corrosion-Resistant Seawater Valves," Proceedings of the Tri-Service Corrosion Conference, Myrtle Beach, SC, November 1999
15. D. M. Aylor et al., "Electrospark Deposited Coating Technology for Naval Applications," Paper #213, National Association of Corrosion Engineers Conference, 2003

16. “Environmental Cost Analysis Methodology (ECAM) Handbook,” Environmental Security Technology Certification Program (ESTCP) Validation Tasks, Contract No. DAAA21-93-C-0046, Task No. 098, CDRL No. A013, Concurrent Technologies Corporation, Johnstown, PA, January 7, 1999

11. Points of Contact

NAME	ORGANIZATION	CONTACT INFORMATION	ROLE IN PROJECT
Bruce Sartwell	Naval Research Lab Code 6170 Washington DC 20375	Ph: 202-767-0722 Fax: 202-767-3321 Email: bruce.sartwell@nrl.navy.mil	ESTCP Project Manager
Larry McCarty and Norma Price	Advanced Surfaces and Processes, Inc. 85 North 26th Ave. Cornelius, OR 97113	Ph: 503-640-4072 Fax: 503-640-8070 Email: larry.mccarty@advanced-surfaces.com	ESD process and equipment development
Vic Champagne	Army Research Lab AMSRL-WM-MD Aberdeen Proving Ground, MD 21005	Ph: 410-306-0822 Fax: 410-306-0806 Email: vchampag@arl.army.mil	Army applications
Denise Aylor	Naval Surface Warfare Center – Carderock Division 9500 MacArthur Blvd West Bethesda, MD 20817	Ph: 301-227-5136 Fax: 301-227-5548 Email: denise.aylor@navy.mil	Navy ship and submarine applications
Keith Legg	Rowan Technology Group	Ph: 847-680-9420 Fax: 847-680-9682 Email: klegg@rowantechnology.com	Materials testing coordination

APPENDIX A

M1A1 CRADLE
RECLAMATION PROCEDURE

RECLAMATION PROCEDURE – M1A1 Cannon Cradle

ANNISTON ARMY DEPOT
PROCESS MANAGEMENT DIVISION

NUMBER: PMD 03-39 (REV 1)	**PAGE** 1 **OF** 4 **PAGE**		**DATE:** 25 June 2003
NOUN: Cradle	**NSN:** 1015-01-262-8613		**P/N:** 9377202
	UNIT PRICE: $24,636.00		
END ITEM: M1A1	**ESTIMATED RECLAMATION COST:**		
	MANHOURS: 9	@ $76.50	= $ 688.50
	MATERIALS:		= 10.00
PREPARED BY: Ivey		**TOTAL**	= $ 698.50

REMARKS: Suggestion AMVA030051

PURPOSE: To repair pits in the 13.254”+ .003” ID of Cradle, P/N 9377202. The pits to be repaired are those that still remain after the cradle ID is ground the maximum amount allowed during the preparation phase of the ID chrome plating reclamation procedure found in DMWR 9-2350-264-2.

NOTES:

1. Disassembly, cleaning, and assembly to be IAW DMWR 9-2350-264-2.

2. Cradle must meet all other requirements of DMWR 9-2350-264-2 prior to becoming a candidate for repair using this procedure.

3. **IMPORTANT**-Repair only the pits that are in “Zone AR” and the .380” wide area of the ID between “Zone AR” and the end of the cradle (See Drawing 9377202). Pits in “Zone AT” of the ID are not to be repaired using this procedure.

4. Pits larger than .375”Ø x .050” cannot be repaired using this procedure.

5. No more than 10 pits may be repaired using this procedure.

6. This procedure has been successfully accomplished at ANAD (See attached photos).

1. **EQUIPMENT**:
a. As required by DMWR 9-2350-264-2.

b. Electro-Spark Deposition (ESD) Equipment as manufactured by Advanced Surfaces and Processes, Inc., or equal. http://www.advanced-surfaces.com/

c. Hand-held, high-speed grinder w/grinding tool and wire brush.

d. ID Grinder.

RECLAMATION PROCEDURE – M1A1 Cannon Cradle

ANNISTON ARMY DEPOT
PROCESS MANAGEMENT DIVISION

2. **MATERIAL**:

a. As required by DMWR 9-2350-264-2.

b. Vapor degreaser.

c. Inconel 718 bare electrode (.125″ Diameter x 4″ long).

3. **PROCEDURE:**

a. Clean cradle using vapor degreaser.

b. Using hand-held grinder w/wire brush, remove corrosion from pit.

c. Using hand-held grinder w/grinding tool, break the sharp edges of the pit. If possible, maintain a width to depth ratio of 10:1 minimum to 20:1. The finish on the excavated defect should be in the 32-64 rms range for best ESD results.

d. All excavated areas and areas immediately adjacent to areas to be ESD repaired should be aggressively rubbed with a suitable medium grade abrasive pad followed by an isopropyl alcohol wash using a clean, lint-free cloth. If ESD repairs are not made within 24 hours after cleaning, it is recommended that the area to be ESD repaired be re-cleaned using the method described in this paragraph.

e. Grounding: All components requiring ESD repair must be properly grounded. The grounding clamp should be placed on an area of the part not designated to receive ESD and must be tightly clamped to prevent arcing between the ground clamp and the component. Place ground clamp as close to ESD work zone as practicable.

f. Electrode Selection and Installation: A .125″ diameter electrode shall be used for this repair, of either composition listed in paragraph 2c. The electrode selected should be evaluated for straightness as excessive run out will cause poor ESD. Electrode tip shall resemble a rounded cone geometry (shaped using Dremel® or similar tool), and shall stick out from torch by approximately 1-inch. The process of reshaping and cleaning the electrode tip will be done extensively during the ESD repair process as the electrode is consumed.

g. Cover Gas: Shielding the ESD area with a cover gas is recommended whenever possible. For this procedure, argon gas with a flow rate of 35 CFH worked effectively.

h. Electrode Rotational Speed and Stroke: An electrode rotation speed of approximately 1200 rpm is generally prescribed for affecting ESD repairs. The stroke utilized when repairing may include one or more of the following: 1) climbing only, 2) cutting only, 3) combination of cutting and climbing, 4) circular or semi-circular, and 5) zigzag.

RECLAMATION PROCEDURE – M1A1 Cannon Cradle

ANNISTON ARMY DEPOT
PROCESS MANAGEMENT DIVISION

i. Using the ESD Equipment with the rotating torch (ASAP Model AH-98-MKIDD), the following settings/parameters and the electrode listed in paragraph 2c, fill the pit to .005” - .010” above the parent material surface. This will ensure complete cleanup during grinding.

- Pulse Rate – 580 Hz
- Capacitance – 20 mfd
- Voltage – 100 volts
- Shielding gas – Argon
- Shielding gas flowrate – 35 SCFH

j. Using ID grinder, grind ID to prepare for chroming IAW DMWR 9-2350-264-2.
k. Chrome plate and finish grind ID IAW DMWR 9-2350-264-2.

4. **INSPECTION**:

Characteristic Requisite	Method of Inspection
Serviceability	Visually (10X Microscope)
No blistering, peeling, cracking allowed.	
Dimensional	Measure
IAW DMWR 9-2350-264-2	
Surface Finish	Measure
	IAW DMWR 9-2350-264-2

RECLAMATION PROCEDURE – M1A1 Cannon Cradle

ANNISTON ARMY DEPOT
PROCESS MANAGEMENT DIVISION

NUMBER: PMD 03-39 (REV 1)	**PAGE** 4 **OF** 4 **PAGE**	**DATE:** 25 June 2003

PITS PREPARED FOR ESD REPAIR

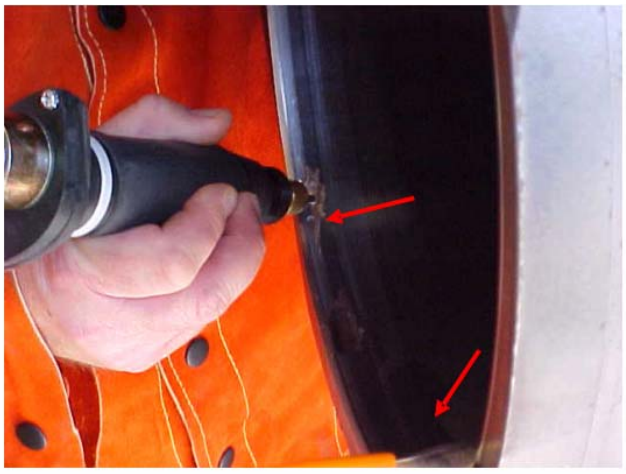

REPAIR PROCESS

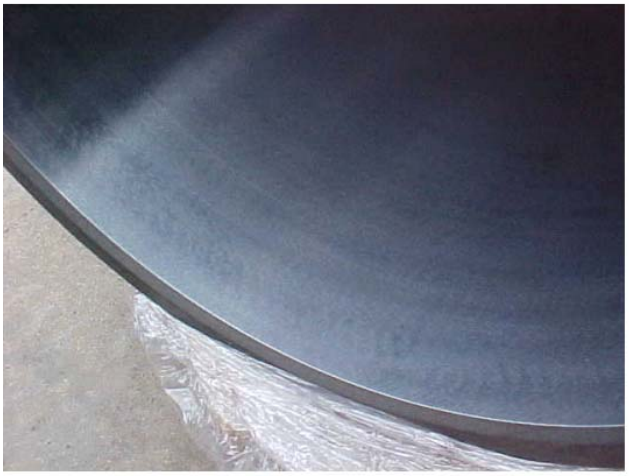

AFTER ESD REPAIR, CHROME PLATING, AND FINISH GRINDING

SIOAN FORM 750-127-E, Rev 12 Mar 97
(RPLS SDSAN Form 1002)

APPENDIX B

M1A1 HELICAL (SUN) GEAR RECLAMATION PROCEDURE

RECLAMATION PROCEDURE–M1A1 Helical(Sun)Gearshaft

ANNISTON ARMY DEPOT
PROCESS MANAGEMENT DIVISION

NUMBER:	**PAGE** 1 **OF** 6 **PAGES**	**DATE:** January 11, 2006	
NOUN: helical gear	**NSN:**	**P/N:** 12284387	
	UNIT PRICE: $2,195.00		
END ITEM: M1A1	**ESTIMATED RECLAMATION COST:**		
	MANHOURS: 8	@ $76.50	= $ 612.00
	MATERIALS:		= $ 30.00
PREPARED BY:		**TOTAL**	= $ 642.00
REMARKS:			

PURPOSE: To repair pits and wear marks which extend through the chrome plating to the base metal in the 3.5005”+ .0005” OD of helical gearshaft, P/N 12284387.

NOTES:

1. Disassembly, cleaning, and assembly to be IAW NMWR 9-2835-255-5.

2. Gearshaft must meet all other requirements of NMWR 9-2835-255-5 prior to becoming a candidate for repair using this procedure.

3. **IMPORTANT**- Repair only corrosion pits and wear marks that are in “Zone 7” (See Drawing 12284387). Wear marks larger than 0.375” wide cannot be repaired using this procedure.

4. Pits larger than .375”Ø x .050” deep cannot be repaired using this procedure. Wear marks larger than .375” wide cannot be repaired using this procedure.

5. No more than 3 flaws may be repaired using this procedure.

6. This procedure has been successfully accomplished at ARL (See attached photos).

1. **EQUIPMENT**:

a. As required by NMWR 9-2835-255-5.

b. Electro-Spark Deposition (ESD) Equipment as manufactured by Advanced Surfaces and Processes, Inc., or equal (http://www.advanced-surfaces.com/)

c. Hand-held, high-speed grinder w/grinding tool and wire brush.

RECLAMATION PROCEDURE – M1A1 Helical(Sun)Gearshaft

ANNISTON ARMY DEPOT
PROCESS MANAGEMENT DIVISION

2. **MATERIAL**:

a. As required by NMWR 9-2835-255-5.

b. Vapor degreaser.

c. Inconel 718 bare electrode (.125" Diameter x 4" long).

3. **PROCEDURE:**

a. Machine the 3.500 to 3.501 inch diameter (NMWR 9-2835-255-5, Figure G-2) removing the existing chrome plating down to the base metal.

b. Measure machined diameter. If diameter is 3.490 inches or more, gearshaft may be reclaimed. If diameter is less than 3.490 inches, discard gearshaft.

c. Use steel shot (NMWR 9-2835-255-5, item 26, Appx. C) at a peening intensity of 8 to 10A with a minimum coverage of 150% and shot peen area to be sprayed IAW AMS-S-13165. Mask features not to be chrome plated.

d. Clean gearshaft using vapor degreaser.

e. Using hand-held Dremel® tool (or equivalent), remove corrosion from pit.

f. Using hand-held Dremel® tool (or equivalent), break the sharp edges of the pit or wear mark. If possible, maintain a width to depth ratio of 10:1 minimum to 20:1. The finish on the excavated defect should be in the 32-64 rms range for best ESD results.

g. All excavated areas and areas immediately adjacent to areas to be ESD repaired should be aggressively rubbed with a suitable medium grade abrasive pad followed by an isopropyl alcohol wash using a clean, lint-free cloth. If ESD repairs are not made within 24 hours after cleaning, it is recommended that the area to be ESD repaired be re-cleaned using the method described in this paragraph.

h. Grounding: All components requiring ESD repair must be properly grounded. The grounding clamp should be placed on an area of the part not designated to receive ESD and must be tightly clamped to prevent arcing between the ground clamp and the component. Place ground clamp as close to ESD work zone as practicable.

i. Electrode Selection and Installation: A .125" diameter electrode shall be used for this repair, of either composition listed in paragraph 2c. The electrode selected should be evaluated for straightness as excessive run out will cause poor ESD. Electrode tip shall resemble a rounded cone geometry (shaped using Dremmel® or similar tool), and shall stick out from torch by approximately 1-inch. The process of reshaping and cleaning the electrode tip will be done extensively during the ESD repair process as the electrode is consumed.

j. Cover Gas: Shielding the ESD area with a cover gas is recommended whenever possible. For this procedure, argon gas with a flow rate of 35 CFH worked effectively.

k. Electrode Rotational Speed and Stroke: An electrode rotation speed of approximately 1200 rpm is generally prescribed for affecting ESD repairs. The stroke utilized when repairing may include one or more of the following: 1) climbing only, 2) cutting only, 3) combination of cutting and climbing, 4) circular or semi-circular, and 5) zigzag.

l. Using the ESD Equipment with the rotating torch (ASAP Model AH-98-MKIDD), the following settings/parameters and the electrode listed in paragraph 2c, fill the pit or wear mark to .005” - .010” above the parent material surface. This will ensure complete cleanup during grinding.

- Pulse Rate – 400 Hz
- Capacitance – 30 mfd
- Voltage – 140 volts
- Shielding gas – Argon
- Shielding gas flowrate – 35 SCFH

m. Finish grind OD IAW Eng. Dwg. 12284387.
n. Chrome plate gearshaft diameter in accordance with NMWR 9-2835-255-5 (Paragraph D.14, Appendix D) to exceed final diameter requirements shown on Figure G-2. Minimum chrome thickness must be 0.002 inch after final machining.
o. Place plated gearshaft in oven (IAW NMWR 9-2835-255-5; Paragraph 2.1) heated to 265 ± 10ºF for five (5) hours. Remove from oven. Machine chrome plated surface to meet dimensional and finish requirements shown in NMWR 9-2835-255-5 (Figure G-2). Chrome thickness after final machining must be from 0.002 to 0.005 inch.
p. Inspect gearshaft IAW NMWR 9-2835-255-5 (OIP-12284368/12284387, Table 4-6).
q. Inspect chrome plating IAW NMWR 9-2835-255-5 (Paragraph D.13, Appendix D).
r. Balance gearshaft IAW NMWR 9-2835-255-5 (Appendix L).

RECLAMATION PROCEDURE – M1A1 Helical(Sun)Gearshaft

ANNISTON ARMY DEPOT
PROCESS MANAGEMENT DIVISION

NUMBER:	**PAGE** 4 **OF** 6 **PAGES**	**DATE:** January 11, 2006

4. **INSPECTION**:

Characteristic Requisite	Method of Inspection
Serviceability	Visually (10X Microscope)
No blistering, peeling, or cracking allowed.	
Liquid Penetrant Inspection	IAW Eng. Dwg. 12284387
Dimensional	Measure
IAW Eng. Dwg. 12284387	
Surface Finish	Measure
	IAW Eng. Dwg. 12284387

SIOAN FORM 750-127-E, Rev 12 Mar 97
(RPLS SDSAN Form 1002)

RECLAMATION PROCEDURE–M1A1 Helical(Sun)Gearshaft

ANNISTON ARMY DEPOT
PROCESS MANAGEMENT DIVISION

NUMBER:	PAGE 5 OF 6 PAGES	DATE: January 11, 2006

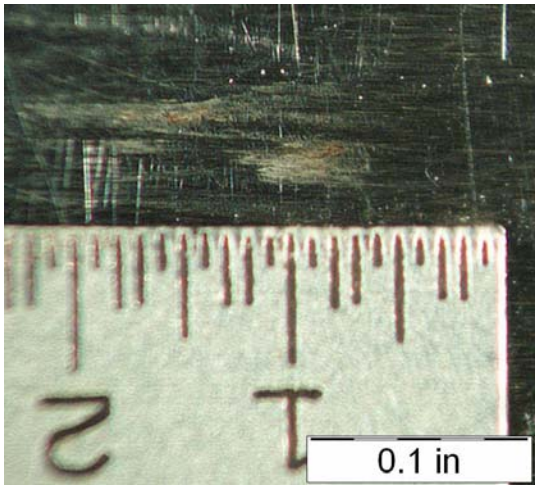

CORROSION PIT FOR ESD REPAIR

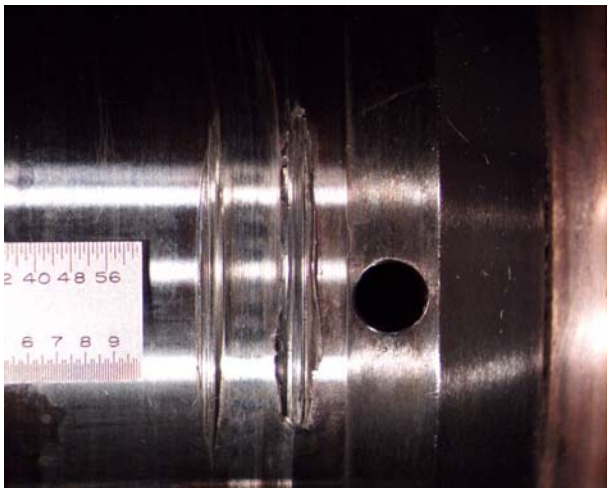

WEAR MARK FOR ESD REPAIR

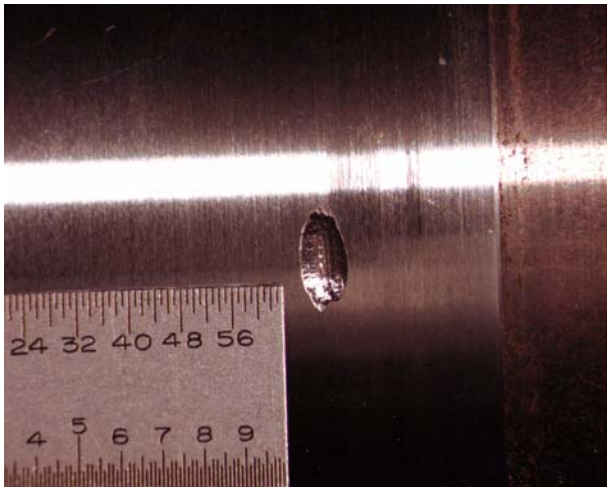

CORROSION PIT PREPARED FOR ESD

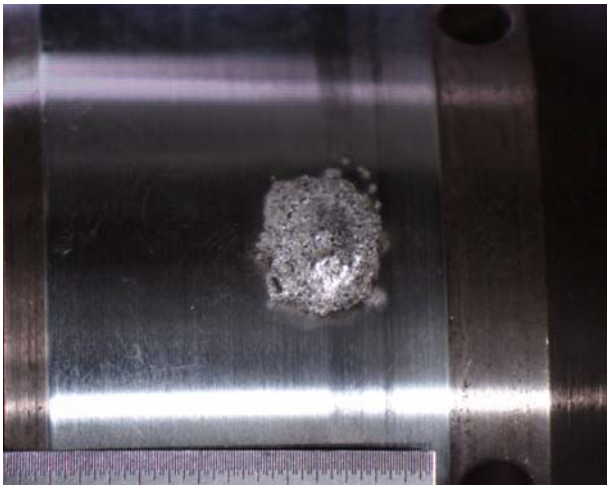

CORROSION PIT FILLED IN BY ESD

SIOAN FORM 750-127-E, Rev 12 Mar 97
(RPLS SDSAN Form 1002)

RECLAMATION PROCEDURE – M1A1 Helical(Sun)Gearshaft

ANNISTON ARMY DEPOT
PROCESS MANAGEMENT DIVISION

NUMBER:	**PAGE** 6 **OF** 6 **PAGES**	**DATE:** January 11, 2006

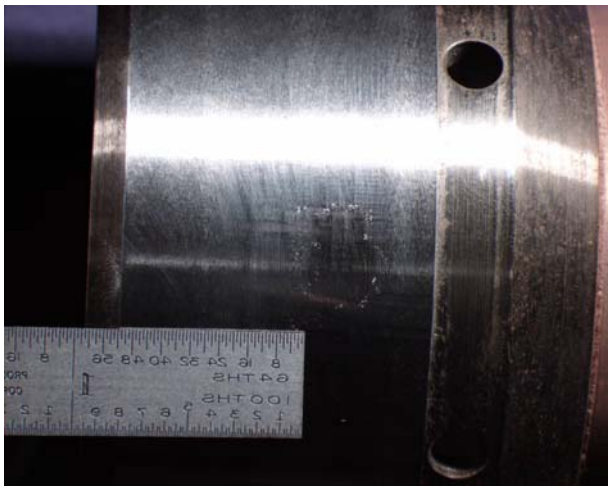

CORROSION PIT AFTER ESD REPAIR AND FINISH GRINDING

SIOAN FORM 750-127-E, Rev 12 Mar 97
(RPLS SDSAN Form 1002)